# LATE QUATERNARY PALEOCEANOGRAPHY OF THE GREAT AUSTRALIAN BIGHT:

## A Geochemical and Sedimentological Study of Cool-Water Carbonates ODP Leg 182, Site 1127

Miriam S. Andres

2002
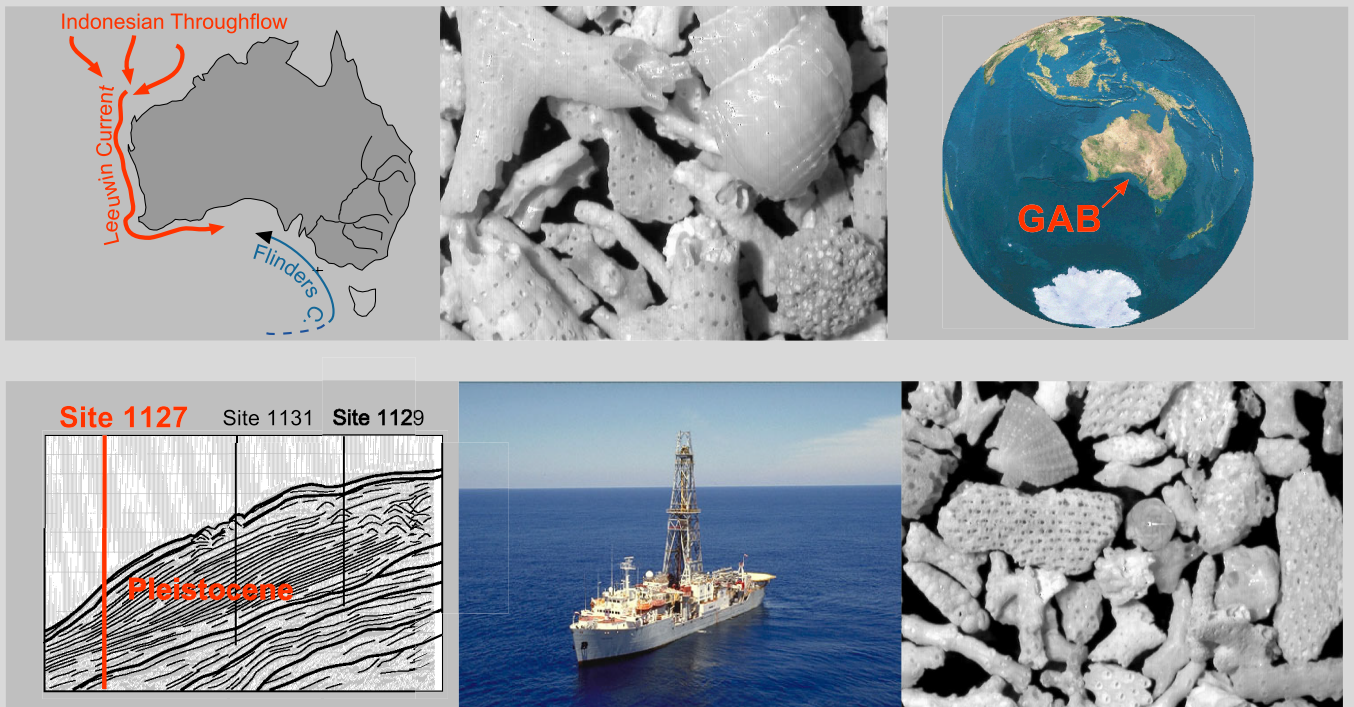
Diss. ETH No. 14831

LATE QUATERNARY PALEOCEANOGRAPHY OF THE
GREAT AUSTRALIAN BIGHT:
A Geochemical and Sedimentological Study of Cool-Water
Carbonates, ODP Leg 182, Site 1127

A dissertation submitted to the
SWISS FEDERAL INSTITUTE OF TECHNOLOGY ZURICH
for the degree of
DOCTOR OF NATURAL SCIENCES

Presented by
MIRIAM S. ANDRES
Dipl Geol., University of Zurich
Born August 4, 1972
Citizen of Aetingen, Solothurn

Accepted on the recommendation of:

| | |
|---|---|
| Prof. Dr. Judith A. McKenzie | Referee |
| PD Dr. Stefano M. Bernasconi | Co-referee |
| Prof. Dr. Thomas Stocker | Co-referee |
| Dr. Daniel Ariztegui | Co-referee |

Zurich, 2002

## ABSTRACT

The thesis aims at identifying paleoceanographic and paleoclimatic change in the temperate-water realm of the Great Australian Bight (GAB). It shows that changes are reflected in the sedimentary succession of cool-water carbonates and that these sediments contain chemical, physical and biological signatures to assess them. Furthermore, these changes are correlated to regional and global changes with respect to timing and amplitude. To accomplish these aims, a detailed, high-resolution geochemical and sedimentological study was undertaken using proxy records developed from a 450-m long marine sediment record spanning the last 850,000 years, which was recovered at Site 1127 during ODP Leg 182, on the (GAB).

The GAB, a wide, cool-water carbonate dominated, ramp-type shelf, directly faces the Southern Ocean. Due to the high-energy environment, the biogenic carbonate sediments are swept seaward where they accumulate on the shelf edge and slope. The modern oceanography is influenced by the warm, oligotrophic water of the Leeuwin Current, which flows around the tip of southwest Australia, and by the cooler, nutrient-rich waters of the Southern Ocean entering the Bight from the east as the Flinders Current.

The importance of the Southern Ocean within the global climate system has been shown in Late Quaternary studies. Yet, long and continuous records from the southern mid-to-high latitudes of the ocean are sparse. This region is ideally suited to contribute an appropriate record for the following reasons: (1) its mid-latitude, Southern Hemisphere location is far removed from Northern Hemisphere melt-water pulsing, but also at some distance to the Antarctic ice-sheet influence, (2) sedimentation rates form the basis for high-resolution studies, (3) abundant planktonic foraminifera provide a detailed chronology, (4) sea-level fluctuations have a large impact on continental margin evolution, and (5) the continental proximity allows to link terrestrial and open ocean setting.

The stratigraphy, based on a $^{14}$C-dated chronology for the last 50 ka and on correlated $\delta^{18}$O fluctuations in the remainder of the record, identifies the last 21 glacial-interglacial cycles. Thus, variations in carbonate mineralogy, sand-fraction percentages and Natural Gamma Ray measurements reflect the response of the neritic shelf community to sea-level rise and fall over the last 850 ka. During the last 250 ka (MIS 1-6), bryozoan mound growth is prolific during nutrient-rich glacial conditions, but absent during warm Leeuwin Current-influenced interglacials. The less pronounced mid-Pleistocene glacial-interglacial fluctuations (MIS 7 to 21) are explained by a generally northerly position of the Subtropical Convergence Zone but also during interglacials, which prevents Leeuwin Current flow into the GAB region. Site 1127 record not only represents the longest continuous record of paleoceanographic change in the sparsely documented southern mid-latitude region but also links open-ocean changes onto the continental margin of cool-water carbonate deposition.

A high-resolution $\delta^{18}$O record and $^{14}$C-chronology records in unprecedented detail changes in paleoceanography and margin evolution of the last glacial cycle. The initial step-wise warming during the LGM to Holocene transition is interrupted by two rapid cold reversals, which are $^{14}$C-dated from 13.1 to 12.3 and 12.3 to 11.1 thousand years before present and separated by a brief but significant warming. The timing and nature of these two cold reversals correlates overall to the recently proposed Oceanic Cold Reversal observed in the mid-latitude Indian Ocean. The second, more intense, abrupt cooling, although smaller in amplitude, resembles and is synchronous with the Younger Dryas Chronozone as evidenced in the Northern Hemisphere.

Bulk sedimentary iron abundance data together with the $\delta^{18}$O record document oceanographic, hydrologic and atmospheric circulation changes affecting the southern Australia and adjacent GAB during the last 20,000 years. Interpreted as SST and dust proxy records, the 10-m sequence shows the dramatic change from the cold, dry and windy LGM to the wet and warm Early Holocene and document the aridification and increased climate variability due to ENSO during the Late Holocene.

## ZUSAMMENFASSUNG

Die vorgelegte Doktorarbeit befasst sich mit der Identifizierung von paläozeanographischen und klimatischen Veränderungen in den kalten Wassermassen der Grossen Australischen Bucht (GAB). Sind solche Veränderungen in der sedimentären Sequenz von Kaltwasserkarbonaten archiviert, und beinhalten die Sedimente chemische, physikalische und biologische Signaturen um solche zu identifizieren? Des weiteren, falls die Veränderungen archiviert sind, wie korrelieren sie zu regionalen und globalen Veränderungen, vor allem bezüglich Gleichzeitigkeit und Ausmass? Um diese Fragen zu beantworten, befasste sich diese geochemische und sedimentologische Studie mit der detaillierten und hochauflösenden Analyse des Sedimentkerns 1127. Dieser bis zu 850 000 Jahre (850 ka) zurückreichender, 450 m langer Kern wurde auf der 182. Forschungsfahrt des Internationalen Tiefseebohrprogramms (ODP) gebohrt.

Die GAB ist gekennzeichnet durch einen weiten, leicht geneigten Kontinentschelf am nördlichen Rand des Südozeans. Starke Strömungen transportieren das biogen produzierte Karbonat den Schelf hinunter und lagern es am Kontinentalrand und -abhang ab. Die heutige Ozeanographie wird stark von den warmen, nährstoffarmen Wassermassen des Leeuwin Stroms beeinflusst, welcher um die südwestliche Spitze Australiens fliesst. Des weiteren wird das Gebiet von den kälteren, nährstofffreichen Wassermassen des von Ostern her fliessenden Flinders Stroms beeinflusst.

Die wichtige Rolle des Südozeans im globalen Klimasystem, wurde in Studien des Spätquartärs gezeigt. Doch bis heute, existieren nur wenige, lange und kontinuiertliche Archive aus den mittleren und hohen Breiten der Südhemisphäre. Aus folgenden Gründen eignet sich ein Archiv aus dieser Region besonders: (1) die mittleren Breiten der Südhemisphäre liegen weit entfernt von den Schmelzwassereinträgen der Nordhemisphäre und in grosser Distanz zum Antarktischen Eisschild, (2) hohe Sedimentationsraten ermöglichen hochauflösende Studien, (3) planktonische Foraminiferen bilden die Grundlage einer detailierten Chronologie, (4) Meeresspiegelschwankungen haben einen grossen Einfluss auf die Evolution eines Kontinentalrandes, und (5) die Nähe des Australischen Kontinents ermöglicht die Verbindung von terrestrischen und marinen Archiven.

Anhand der Sauerstoffisotopenstratigraphie wurden die letzten 21 glazial-interglazialen Zyklen identifiziert. Variationen in der Karbonatmineralogie, Sandfraktion und Messungen der natürlichen Gammastrahlung spiegeln die Reaktion der neritischen Schelfgemeinschaft auf Meeresspiegelschwankungen der letzten 850 ka wieder. Während den letzten 250 ka (MIS 1-6), wuchsen Bryozoenhügel unter nährstofffreichen Glazialbedingungen, während sie in den warmen, vom Leeuwin Strom beeinflussten Interglaziale wieder verschwanden. Die weniger deutlichen mittel-Pleistozänen glazial-interglazialen Schwankungen (MIS 7 to 21) können durch eine nördlichere Position der Subtropischen Konvergenzzone erklärt werden, welche den Einfluss des Leeuwin Stromes in die GAB verhinderte. Der Kern 1127 repräsentiert nicht nur das längste, kontinuierlichste Archiv in dieser zu wenig untersuchten Gegend, sondern verbindet zusätzlich die ozeanischen Veränderungen mit den Veränderungen auf dem von Kaltwasserkarbonaten dominiertem Kontinentalrand.

Ein weiterer Teil der Studie befasst sich mit der jüngten geologischen und ozeanographischen Geschichte der GAB. Der hochauflösende $\delta^{18}O$ Datensatz und die $^{14}C$-Chronologie zeigen im Detail die Veränderungen der Paleozeanographie und des Kontinentalrandes während des letzten glazialen Zyklusses, vor 20 000 Jahren bis heute. Die anfänglich stufenweise Erwärmung während des Übergangs von der letzten Eiszeit ins Holozän in Kern 1127 wird von zwei abrupten Kälteeinbrüchen unterbrochen (datiert 13.1 bis 12.3 und 12.3 bis 11.1 ka). Die zeitlich Abfolge und die Eigenschaften dieser Kälteeinbrüche korrelierten mit dem Ozeanischem Kälteeinbruch aus den mittleren Breiten des Indischen Ozeans. Die zweite, stärkere Abkühlung, obwohl kleiner in der Amplitude, ähnelt und ist zeitgleich mit der Jüngeren Dryzas Chronozone der Nordhemisphäre.

Die hochauflösende Sequenz von Kaltwasserkarbonaten aus der GAB erweist sich als exzellentes Archiv der paläozeanographischen und klimatischen Veränderungen des Spätquatärs.

# 1   INTRODUCTION

Complex large and small-scale patterns of atmospheric and oceanic circulation and their interaction control heat distribution and global circulation but also explain much of the variability observed in the climatic record. Understanding this variability arising from external forcing, i.e. changes in the earth's orbital parameters or variations of solar irradiation, internal oscillations and feedback mechanisms, apart from the increasing effect of anthropogenic influence, is an intense field of research and debate. Numerous and diverse approaches are taken to detect past, understand current and predict future climate variability and change. Paleoclimatologists and paleoceanographers study the past oceanic and atmospheric part of the climate system prior to the instrumental record. Instrumental measurements only span a very small fraction of the Earth's long climatic history and are, therefore, insufficient in providing us with a long-term perspective of climate evolution and variability. Climatologists and oceanographers use modern synoptic observational data from space, air, land and water, in addition to the instrumental record to understand today's climatic system. The use of numerical modeling, especially coupled ocean-atmosphere models contribute to our understanding of the physical mechanisms determining ocean-atmosphere dynamics beyond the limits of analytical methods (Böning and Semtner, 2001; Wood and O'Brien, 2001). Numerical models further can be used to forecast variability or, when set to past boundary conditions, help understand modes and mechanisms of paleoclimate change.

The reconstruction of past climatic changes is possible if it can be shown that signals preserved in geological archives, such as marine sediments, tree-rings, lake sediments, corals, speleotherms, ice cores etc., truthfully preserve paleoclimatic and/or –oceanographic variations. For the development of a detailed and reliable paleorecord, accurate direct dating or correlation of discrete intervals with other records is necessary for the conversion of the measured record into the time domain. The paleorecords can be compared to other paleorecords in a local to regional context and its global significance evaluated. It is only then, and best in combination with other paleorecords and numerical models that hypothesized causes and underlying mechanisms of climate change can be tested and, if rejected, alternatives proposed.

This thesis aims to identify paleoceanographic and paleoclimatic change in the temperate-water realm of the Great Australian Bight. It proposes to determine if such changes are reflected in the sedimentary succession of cool-water carbonates and if these sediments contain chemical, physical and biological signatures to assess these. Furthermore, if such changes are recorded, do they correlate to regional and global changes with respect to timing and amplitude? To accomplish these aims, a detailed, high-resolution geochemical study of sediments from ODP Site 1127 was undertaken.

## 1.1 Identifying Paleoceanograhic Change Through Proxy Records

Marine sediments preserve a wealth of information for the reconstruction of ocean and climate history in the form of their microfossil assemblage, organic matter, elemental and isotopic composition of fossils or other sediment components. Additionally, their depositional architecture, sediment accumulation rates, colour, and physical properties provide us with abundant information on conditions during the time of deposition. Often, however, the desired information cannot directly be deduced from the sedimentary archive but has to be interpreted via parameters that are closely related to the desired parameter. In paleo-reconstructions, short for paleoceanographic, -climatic, -ecological, and –environmental reconstructions, the problem is solved by using *proxy variables*. They stand in for desired but unobservable variables such as temperature, salinity, productivity, wind speed, oxygen content, etc. The concept of *proxy variables*, short *proxy*, is based on chemicals and physical laws, relating proxy with targeted parameter, for example, between the oxygen isotopic composition of calcite, and global ice volume and temperature. Although several proxies were used in this study, the temperature proxy record is the main focus.

### 1.1.1 The Use of Oxygen Isotopes as Temperature Proxy in Paleoceanography

The temperature distribution in the surface-ocean is undoubtedly one of the most important single parameters in paleoceanographic reconstructions. The distribution of sea-surface temperature (SST) not only provides us with information on ocean circulation, but also, to a large extent explains biogeography and productivity patterns. This study makes use of the oxygen isotopic composition of calcite precipitated in the bulk sediment and marine microfossils, such as foraminifera, as a proxy for temperature.

The oxygen isotopic composition of calcite is primarily a function of the isotopic composition and temperature of the water in which the calcite is produced (Epstein et al., 1953). Glacial-interglacial changes in the $\delta^{18}O$ of planktonic foraminifera, thus, record changes in the $\delta^{18}O$ of seawater associated with the growth and decay of glaciers, as well as local changes in temperature and/or salinity (Emiliani, 1955, 1966; Shackleton, 1967). From the last glaciation to present, the $\delta^{18}O$ change attributable to ice volume was estimated to be 1.2‰ (Fairbanks, 1989). Most recent studies by Schrag et al. (2002) on the isotopic composition of pore fluids, however, estimate a global average change in $\delta^{18}O$ of seawater of $1.0 \pm 0.1$‰. Therefore, if we subtract the ice volume effect from the total glacial-interglacial $\delta^{18}O$ change in foraminifera, the residual value should represent the SST change with local changes in hydrography (salinity). A 0.22‰ change in $\delta^{18}O$ transfers approximately to a 1.0°C change in temperature (Epstein and Mayeda, 1953; Schrag et al., 2002).

## 1.2    Dating, Chronology and Stratigraphy

Reconstruction of long-term paleoceanographic and paleoclimatic change and identification of rapid warming and cold reversals in marine sediments have less significance until they are converted from a depth into time scale. Stratigraphy deals with the age relation of the deposited sediments and applies the simple law of superposition (Steno 1669), which states that, in an undeformed sequence, sediments at the bottom are older than the overlying younger ones. In order to access change on a global scale, sediments of the same age have to be stratigraphically correlated. Marine sediments are correlated using a number of different methods, i.e. lithostratigraphy, biostratigraphy, magnetostratigraphy and chronostratigraphy. Often the combination of different stratigraphies forms the basis of a reliable age model. This study uses the correlation method of oxygen isotope stratigraphy supported by bio- and magnetostratigrahy for the Late Pleistocene time period. Sediments deposited during the last ~45,000 years before present are absolutely dated using the radiocarbon method.

### 1.2.1    Oxygen Isotope Stratigraphy

Oxygen isotope stratigraphy is widely applied in marine geology and a powerful tool to correlate marine sediments. Oxygen possesses three stable isotopes, a common 'light' $^{16}O$ isotope and the rare 'heavy' $^{17}O$ and $^{18}O$ isotopes. Isotope measurements generally determine the ratio of $^{18}O$ to $^{16}O$. In the hydrologic cycle, $^{16}O$ is preferentially enriched in the water vapour during evaporation (Urey, 1947). Seawater is thus enriched in the heavier $^{18}O$ isotope compared to meteoric waters, and this difference forms the basis of oxygen isotope stratigraphy (Emiliani, 1955). Ice-sheets lock up enormous amounts of $^{16}O$-enriched freshwater and the remaining ocean water is thus progressively enriched in $^{18}O$ as ice-sheets grow during glaciation. Marine microfossils, such as foraminifera, precipitating their calcite shells in glacial-age water will, therefore, incorporate its 'heavy, glacial' isotopic signal. Conversely, an interglacial or warm time period is characterized by 'light' or lower oxygen isotope values.

The pioneering work of Emiliani, using oxygen isotopes in the study of deep sea cores, was followed by numerous studies across the ocean basins and sedimentary settings, all confirming that the oxygen isotopic composition of foraminifera oscillates in response to Pleistocene glacial-interglacial fluctuations. Their distinct cyclicity and amplitude, which is fairly regular over the last 1 million years and globally recognizable, has led to the assignment of isotopic stage numbers (Emiliani, 1955; Emiliani and Milliman, 1966). Marine isotopic stages (MIS) number alternating interglacial and glacial episodes, with odd numbers representing interglacials and even numbers glacials beginning with the present interglacial being MIS 1. A global isotope stratigraphy composed of stacked oxygen isotope records termed the SPECMAP stack (Imbrie et al., 1984) is used as a reference for oxygen isotope stratigraphy (Shackleton and Opdyke, 1973). Important aspects of oxygen isotope stratigraphy are that the events are globally synchronous and globally distributed and, therefore, ideally suited for the comparison and correlation to other time scales, i.e. magneto- and/or biostratigraphy. Furthermore, calcareous microfossils are abundantly found in all oceans and, in combination with the technical

advancement of mass spectrometry, have made this method a standard correlation tool in paleoceanography and marine geology.

### 1.2.2    The Use of Radiocarbon Dating in Chronostratigraphy

In addition to establishing relative time scales by the correlation of events as described above, it is also possible to obtain absolute ages for events in the geologic past. The radiocarbon dating or $^{14}$C dating method is probably the most widely used absolute dating method in young marine sediments. The method is based on the principle that the instable or radiogenic isotope $^{14}$C decays with a fixed rate or half-life of 5730 years (Arnold and Libby, 1949). $^{14}$C, produced in the atmosphere by interactions of cosmic-ray produced neutrons and $^{14}$N, is oxidized to carbon dioxide ($CO_2$). It is then incorporated into the calcite shell of calcareous marine microfossils or organic matter. Upon their demise, $^{14}$C-uptake ceases and the $^{14}$C activity decreases according to the decay law.

There are several problems inherent to the radiocarbon method that should be kept in mind, especially when using the very convenient internet-based programs (CALIB.html) where $^{14}$C-ages are converted to calendar ages by simply pressing the 'enter-button'. The method is limited to samples younger than ~ 55,000 years because after 10 half-lives the $^{14}$C concentration drops below detection levels. Variations in the atmospheric production of $^{14}$C, due to changing solar activity (Stuiver et al., 1991) or variations of the earth's magnetic field (Geyh and Schleicher, 1990), cause significant deviations between the radiocarbon age and the true calendar age. The comparison of counted tree-ring ages and $^{14}$C dates on the same tree-ring sample or Uranium-series and $^{14}$C dates on the same coral (Bard, 1998) or counted and $^{14}$C dated varves of lake sediments (Hajdas, 1993; Kitagawa and van der Plicht, 1998) all show that radiocarbon ages are systematically too old. This phenomena has to be accounted for when converting the $^{14}$C age to the calendar age. Furthermore, radiocarbon-dated marine sediments have to be corrected for their 'reservoir age', which is the difference between atmospheric $CO_2$ and surface-dissolved inorganic carbon (Geyh and Schleicher, 1990).  The reservoir of inorganic carbon ($CO_2$) dissolved in ocean water masses, is much larger than the atmospheric reservoir making these waters older than the atmosphere by ~ 400 years. Furthermore, ages dated around 10,000 radiocarbon years before present are affected by a number of '$^{14}$C plateaux' (Ammann and Lotter, 1989). A large influx of $^{14}$C-depleted carbon from the oceans, combined with a decrease in the rate of $^{14}$C production at the top of the atmosphere, gives an 'age plateau' such that the same $^{14}$C age covers a wide span of real time, about 1,000 years.

The discussion on interhemispheric climate linking, the synchrony or asynchrony of events especially during the transition from the last glacial to the Holocene, is tightly coupled to that of radiocarbon dating. In order to compare and correlate marine sedimentary records with those from the polar ice-cores and the terrestrial realm, a common age scale, of calendar years BP is necessary. This work makes extensive use of this method in order to assess the timing of paleo-change recorded in sediments deposited in the Great Australian Bight compared to regional and global records.

## 1.3    Late Quaternary Paleo-Change in the Southern Hemisphere

Today's mid- to high-latitude Southern Hemisphere is dominated by the Southern Ocean and Antarctica, with only a small amount of landmass, southern South-America, the tip of southern Africa and southern Australia, reaching beyond 30° latitude. Compared to the small landmass and the vastness of the Southern Ocean, a disproportional amount of paleorecords derive from the terrestrial environment. The reason for this bias certainly lies in the easy access to lakes, bogs, moraines, and speleotherms, even in remote areas, compared to the organization of large drilling campaigns needed to reach the marine sedimentary environment of the continental shelf and deep sea or the Antarctic ice cap. Thanks to international deep-sea drilling initiatives such as DSDP, ODP and IMAGES, paleo-change, as observed and preserved in the marine record, is now available, although spatial distribution is still insufficient. Furthermore, deep-sea records from the Southern Ocean are marked by low sedimentation rates and often lack calcareous sediments, an ideal marine archive of oceanographic change. Yet, unravelling the younger climatic history of Antarctica preserved in its thick ice-cap has undoubtedly catapulted our knowledge and thinking about climate change into a new dimension and, when compared to the Greenland ice-cores, forms the basis of understanding interhemispheric climate linkage.

This study, based on a marine sedimentary core from the Great Australian Bight, directly facing the Southern Ocean, poses the question if paleoceanographic and paleoclimatic change, known to have influenced the deep Southern Hemisphere, is recorded on the southern Australian margin. In this context, paleoceaongraphic and paleoclimatic change in the Southern Ocean, Antarctic ice and southern terrestrial realm is briefly introduced.

### 1.3.1    The Southern Ocean

The strong eastward flow of the Antarctic Circumpolar Current (ACC) and it associated frontal systems, driven by the strong westerly winds, is the dominant feature in the Southern Ocean. The absence of land barriers in the high-latitude Southern Ocean, a prerequisite for the ACC, has a far-reaching influence on the dynamics of currents in this region, as well as on global ocean circulation and climate (Rintoul et al., 2001).
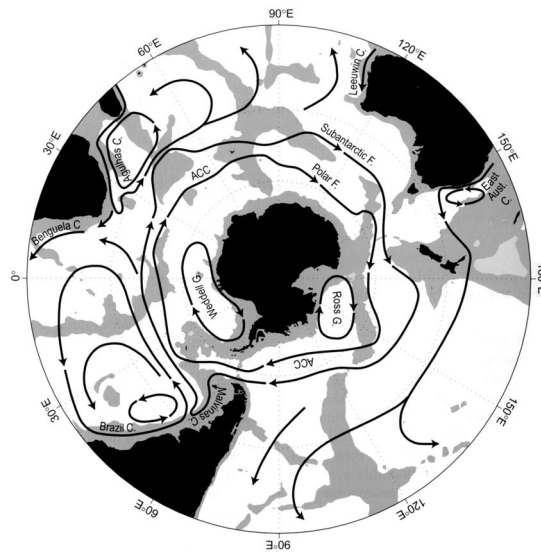
*Figure 1.1.* Schematic map of the major currents in the Southern Hemisphere south of 20 °S. Depths shallower than 3500 m are shaded. The Antarctic Circumpolar Current (ACC) is bounded by two important oceanic frontal systems, the Subantarctic Front (SAF) and the Polar Front (PF). Taken from Rintoul et al. (2001)

The ACC connects each of the major ocean basins, thus, permitting global overturning circulation, which in turn dominates the global transport of heat, fresh-water and other properties influencing the climate (Schmitz, 1996b). In the context of interhemispheric climate linkage, it is important to mention that from the North Atlantic, the southward-flowing western boundary current transports North Atlantic Deep Water (NADW) to the Southern Ocean. The NADW joins lower Circumpolar Deep Water (CDW) in the Southern Ocean from where it is transported eastward as part of the ACC (Schmitz, 1996a). To the north, the ACC is bounded by two major oceanic fronts, the Subantarctic Front (SAF) and Polar Front (PF) and even further north the Subtropical Front (Belkin and Gordon, 1996).
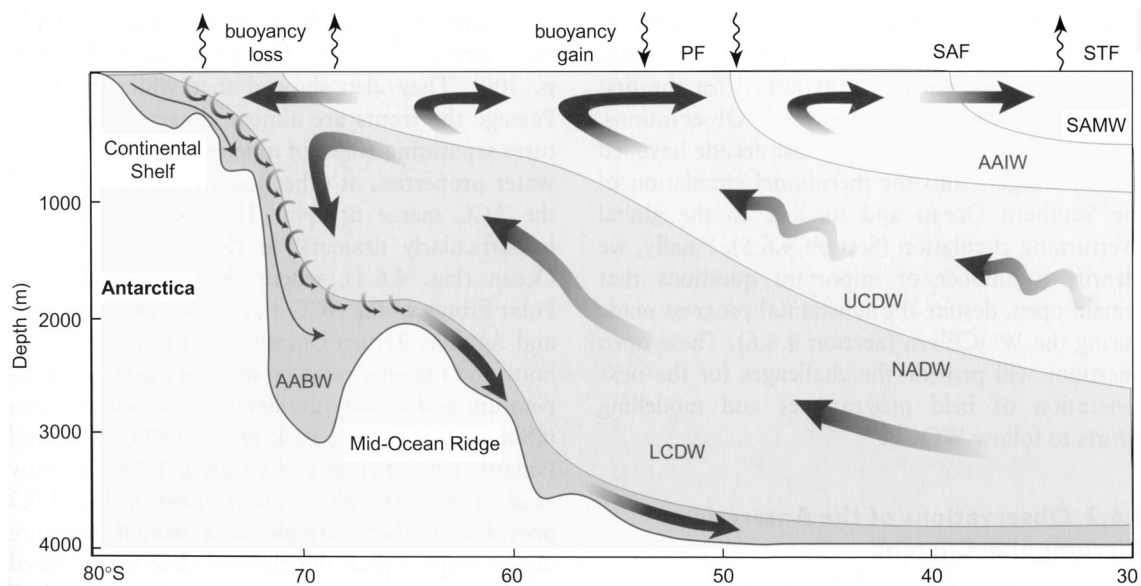
**Figure 1.2.** *A schematic view of the meridional overturning in the Southern Ocean. Upwelling North Atlantic Deep Water (NADW) mixes with Lower and Upper Circumpolar Deep Water (LCDW, UCDW) Surface waters are primarily the result of northward Ekman transport beneath the strong westerly winds and interaction with UCDW. Near the Antarctic continent, the waters are dominated by the formation and sinking of dense Antarctic Bottom Water (AABW). Taken from Rintoul et al. (2001).*

Late Pleistocene climatic change, on glacial-interglacial time-scales, was impressively demonstrated by the work of Hays et al. (1976) on two cores from the Southern Indian Ocean (Hays et al., 1976). Their reconstructions showed that much of the observed variance is concentrated at frequencies coinciding with those predicted by orbital or Milankovitch forcing, i.e. precession, eccentricity, and obliquity at 19,000-21,000, 41,000, and 100,000 year periods, respectively. This work provided the first strong evidence that the Earth's orbital parameters and the effect on incoming solar radiation play an important role in causing glacial-interglacial variations. Numerous studies in various geographic locations and different proxy records have subsequently confirmed this pattern. Although the external causes are identified, the mechanism linking the insolation changes to climatic and oceanographic changes are unclear. Research and discussion centers around the question of how the relatively small insolation changes have such a large effect on the growth and demise of ice sheets on a 100,000-year periodicity. Thermohaline circulation plays a major role in driving glacial-interglacial change (Imbrie et al., 1992). During glacials, the decreased summer insolation, results in a general cooling of the high northern latitude atmosphere and surface-ocean, reducing evaporation and increasing snowfall and sea-ice cover. The glacial Southern Ocean is characterized by extensive sea-ice growth around Antarctica, and the northward displacement of the ACC, associated frontal systems and the westerly wind belt. Reduced thermohaline circulation and NADW flux to the Southern Hemisphere is thought

to be compensated for by an increased Antarctic water flux to the north (Charles et al., 1996; Ninnemann, 2002).

The transition from the last glacial to the Holocene is marked by several climatic swings. Although the ocean circulation is often viewed as slow and passive, it tends to react strongly and rapidly to only minor changes. This is impressively illustrated in the North Atlantic by the instability of the thermohaline circulation to increased fresh-water input from melting ice-sheets, as proposed to have happened during the Younger Dryas Chronozone (Fairbanks, 1989), and as observed in paleorecords (Keigwin et al., 1994) and model simulations (Manabe and Stouffer, 1997; Rahmstorf and Willebrand, 1995). The identification and timing of paleoceanographic change during the last deglaciation, occurring on millennial to submillenial or even centennial time scales, in the Southern Ocean is a controversial and heavily debated topic. The main reason for the controversy lies in the scarcity of marine records with sufficient resolution, chronology and reliable proxy records to assess paleoceanographic change on these short time scales (Bard et al., 1997; Sarntheim et al., 2000). Furthermore, the comparison of the few high-resolution marine records from the Southern Ocean (Alley and Clark, 1999) with representative northern and southern deglaciation records suggests no uniform response (Alley, 2000; Bender, 1998). Yet, knowledge of the spatial distribution and relative timing is important for our understanding of the location of the driving force, i.e. polar versus tropical regions, but also in identifying the underlying mechanism and feedbacks. This also provides the boundary conditions for numerical models and the physical understanding of ocean-atmosphere interaction expressed in the concept of the 'bipolar sea-saw' (Broecker, 1998; Stocker, 1998). The seesaw effect implies that changes in the ocean circulation mirror freshwater impacts, i.e. a response of the deep-ocean currents to an increase in the deep-water production in one hemisphere, is equivalent to a decrease in the opposite hemisphere.

### 1.3.2   Antarctic Ice Cores

Annual snow accumulation on the ice sheets of Antarctica form the basis of a continuous and high-resolution climate archive. A wide range of different proxy-records have been developed from the ice, and particles and gas bubbles that are trapped inside the ice. They provide information on local climate (precipitation, air temperature), regional (e.g. wind-blown dust, sea-salt), and global (composition of atmosphere, solar variability) conditions (Alley, 2000). It is, however, their atmospheric gas record that has most impacted paleoclimatology and changed the view of interhemispheric climate linking (White and Steig, 1998). Atmospheric gases, such as methane, mix so rapidly between the hemispheres that changes in their concentrations are essentially globally synchronous (Blunier and Brook, 2001). Significant methane fluctuations in the Antarctic ice cores, therefore, must coincide with fluctuations in the Northern Hemisphere Greenland ice cores, and, thus, allow for the development of a common timescale. Uncertainties remain due to fact that the age of the ice does not equal the age of the gas in which is trapped (Schwander et al., 2001).

To date, seven Antarctic ice cores spanning more than 1000 years have been recovered from ice sheets and domes of Antarctica. The Vostok ice core from East Antarctica spans the past four glacial-interglacial cycles and provides the longest ice-core record to date (Petit et al., 1997; Petit et al., 1999). Variations in the deuterium record, a proxy for air temperature, correlates to the SPECMAP $\delta^{18}O$ record of continental ice volume change. The dust record confirms that glacials are times of increased continental aridity, dust mobilization and transport. Furthermore, the good correlation of the concentration of greenhouse gases ($CO_2$ and $CH_4$) with temperature indicates that they may have contributed to glacial-interglacial change by amplifying orbital forcing (Petit et al., 1999).

Ice-core records from Byrd, Dome C, and Taylor Dome provide further abundant and diverse paleoclimatic information, especially providing detailed and high-resolution coverage of the last glacial-interglacial cycle. Of particular interest is the step-wise nature of the last deglaciation, where the warming trend was interrupted by a cooling event, with an estimated surface temperatures decrease of ~3-4°C at Vostok station (Jouzel et al., 1995; Mayewski et al., 1996). Termed the Antarctic Cold Reversal (ACR), it provoked much discussion when compared with the rapid cooling of the Younger Dryas (YD) event observed in the Northern Hemisphere. The synchronisation of Antarctic and Greenland ice cores via the methane record proved that the YD cooling follows that of the ACR by at least 1,800 years (Blunier et al., 1997). Although the ice core from Taylor Dome shares the main features of the Vostok record, $\delta^{18}O$ fluctuations are more abrupt and of larger amplitude than at Vostok or Byrd. Interestingly, the warm interstadials of the last glacial correlate well to the Greenland GISP2 ice core record. The 'North Atlantic' character of the Taylor Dome record is partly explained by its oceanic proximity and the direct influence of thermohaline circulation (Grootes et al., 2001).

Detailed deuterium excess measurements on an ice core from Dome C (Stenni et al., 2001) are interpreted as SST cooling at the moisture source for Dome C precipitation. Termed the Oceanic Cold Reversal, it spans the time of Northern Hemisphere cooling and it remains to be determined if this is not the Southern Hemisphere's expression to change in the Northern Hemisphere (Steig, 2001).

### 1.3.3 The Southern Continents

Terrestrial paleoclimatic reconstruction of the southern mid- to high-latitudes is restricted to the relatively small landmass of South America, Australia, New Zealand and Antarctic compared to the large oceanic area surrounding them. Apart from South America, there is no land between 40°S and Antarctica. Western coasts are characterized by major cold, equatorward flowing currents with the notable exception of the Leeuwin Current in Australia, whereas warm currents prevail on the eastern continental margins. Extremely cold winter air temperatures over Antarctica leads to much steeper temperature gradients over the Southern compared to the Northern Hemisphere, which in turn tends to produce much stronger and more persistent zonal winds, particularly in the zone of the mid-latitude Westerlies (Hobbs et al., 1998).

The bulk of paleoclimatic reconstructions for the Late Quaternary period, concentrate on the last 20,000 years, with particular emphasis on the last glacial maximum, the deglacional transition and

Holocene climatic optimum. Just as in the marine realm, Late Pleistocene glacial-interglacial cyclicity has dominated the terrestrial environment, as evidenced in the few available long terrestrial records, that have been reported, i.e. rainfall variation in the 200,000 year old Pretoria Salt Pan (Partridge et al., 1997), or fluctuating lake levels and vegetation in Australian lake records of Lynch's Crater (250,000 years) and Lake George (350, 000 years) (Kershaw, 1989).

The last glacial maximum (LGM), ~18,000 years before present, is by far the best-documented glacial interval. Although the local and regional expression of the LGM might be different, the climate of the southern continents during the LGM was generally cold, dry and windy. Temperature estimates range from 5°C lower in Southern Africa (Lindesay, 1998), with a decrease of up to 10°C in the Australian interior (Miller et al., 1997). Wide-scale aridity is evidence in low lake levels and episodes of major dune building. Glacier advances are reported from the Andes, south-east Australian highlands, Tasmania, and the New Zealand Alps. Continental shelves were exposed due to lowered sea-level, and, due to the northward displacement of the Westerlies, the areas were affected by higher wind-speed regimes.

The last deglaciation and associated cold reversals are well documented in numerous Southern Hemisphere paleorecords, yet there is still considerable uncertainty in the nature, exact timing, rate and magnitude of these rapid changes in comparison to Northern Hemisphere changes, such as the Younger Dryas Chronozone (YDC) dated between 12.7 and 11.5 ka BP. The comparison of records suggests that the terrestrial response to changes in the ocean-atmosphere system is not uniform. In South America, pollen records from southern Chile (Moreno et al., 2001) and lake sediments from Argentina (Ariztegui et al., 1997) indicate cooling events quasi-synchronous to Northern Hemisphere cooling during the Younger Dryas Chronozone. Lake sediments in southern Chile (Bennett et al., 2000), however, indicate that there was no cooling equivalent to the YDC. A cooling observed from Patagonian pollen studies by (Markgraf, 1993) can be explained with local effects. In New Zealand, the case is similar. Moraine deposits are interpreted as glacier advancement in response to cooling, which dates synchronous to the YDC cooling (Denton and Hendy, 1994), but pollen records from only 300 km north of the evidenced glacier advance (Singer et al., 1998) indicate that there was no significant temperature decrease in this time period. A significant cooling event, although predating the YDC by 600 radiocarbon years is evidenced by a fine-resolution pollen record from the northern part of New Zealand, further adding to the controversy (Newnham, 2000). Paleorecords in phase with Northern Hemisphere cooling are explained by an atmospheric circulation change, and, if the record indicates no, little or asynchronous change, then the absence or lag is attributed to slow oceanic thermohaline circulation (Peteet, 1995).

The long-held recognition that the Holocene time period is one of climate stability is rapidly changing as high-resolution paleorecords indicate substantial and possibly global climate variations, which are small when compared to variations during the last deglaciation but fundamental for our understanding of the most recent climatic history. The Holocene Climatic Optimum (~9000-6000 years BP.) is marked by a global decline in air temperatures (Steig, 1999), but increasing greenhouse gas

concentrations (Indermühle et al., 1999). In the temperate latitudes, some areas, i.e. southern Africa, document mid-Holocene aridity followed by cooler and wetter conditions, whereas others document the opposite. Paleobotanical and lake-level data from Australia indicate increasing aridity after 5000 years BP. This pattern is explained by the displacement of the rain-bearing mid-latitude Westerlies in South Africa and South Australia (Harrison and Dodson, 1993; Lindesay, 1998). The current sparse und punctuated picture needs further high-resolution archives in order to understand the spatial and temporal characteristics of mid-Holocene change.

Weather and climate anomalies referred to as the El Niño/Southern Oscillation (ENSO), constitute the largest single-source of interannual variability on a global scale. The wide-ranging and severe effects observed in the southern continents today, i.e. the loss of crops due to drought or flooding, and the impact on commercial fisheries due to changing ocean conditions, has led paleoclimatatologist to search for paleo-records of ENSO variability in the past (Nicholls, 1992). The generally more stable climate in the Early Holocene and absence of comparable precipitation patterns (Schulmeister and Lees, 1995) indicate either a much-reduced amplitude of ENSO variability or a change in the extratropical expression of ENSO (McGlone et al., 1992). Recent studies (Koutavas et al., 2002; Stott et al., 2002) have shown evidence for the existence of a long-term El Niño-like pattern during the last glacial cycle, whereas changing conditions during the mid-Holocene are linked to a La Niña-like pattern.

## 1.4   General Aims and Objectives of Thesis

In this study, the general approach of paleo-reconstruction is applied to the marine sedimentary archive of ODP Site 1127 on the Great Australian Bight. It's mid-latitude location, directly facing the Southern Ocean, makes the Site a potentially key archive for the study of Southern Hemisphere paleoceanographic and paleoclimatic change. Because the recovered sedimentary archive represents the first long Late Pleistocene record of cool-water carbonates, initial research addressed the following fundamental questions:

### Stratigraphic integrity

Site 1127 is located in the high-energy environment of the continental shelf edge and, although continuous and high recovery characterizes the core from Hole 1127B, the question remained if sediments were deposited in continuous stratigraphic order or if sediment reworking and slumping resulting in a disturbed and incomplete record.

### Sedimenatary expression of change

How are changes reflected in the sedimentary succession of cool-water carbonates, and do their sediments contain chemical, physical and biological signatures to assess these? Furthermore, if

changes are recognized, how do these correlate to regional and global changes with respect to timing and amplitude?

Two time intervals are focused to address these questions: 1) The last glacial-interglacial transition and Holocene spanning the last 20,000 years and 2) the Late Pleistocene covering the last 780,000 years. Each time interval in itself then contains a set of more specific questions:

*Glacial-interglacial transition*

The warming trend from the LGM to the Holocene is not uniform but marked by cold reversals. Timing, amplitude and extent of deglaciation is insufficiently documented. The existence, spatial distribution and relative timing of cold reversals such as for example the Younger Dryas Chronozone or the Oceanic Cold Reversals remain controversial in Southern Hemisphere paleorecords. How is the deglaciation expressed in sediments from the Great Australian Bight? Can cool-water carbonates preserve the evidence of rapid climate change, and, if yes, how does it correlate to global evidence for rapid climate change?

**Holocene**

Increasing evidence shows that the mid-Holocene time period is characterized by profound oceanic and atmospheric change, yet changes are very small when compared to the LGM-Holocene transition. Is this much smaller and 'subtle' change archived on the continental margin setting Site 1127 and potentially confirm mid-Holocene changes evidenced by terrestrial records?

**Late Pleistocene**

Late Pleistocene climate is dominated by glacial-interglacial cyclicity. What is the effect of sea-level rise and fall on a carbonate ramp compared to a carbonate platform setting? How does glacial-interglacial cyclicity from the continental shelf margin compare to global records like SPECMAP, which are based on records from the pelagic realm.

**Leeuwin Current**

The Leeuwin Current carries warm waters into the Great Australian Bight. Studies have shown that the Leeuwin Current was weaker or absent during the last glacial period and the Southern Ocean waters prevailed on the shelf. Is this pattern recorded in previous glacial periods of the Late Pleistocene?

**Continental-open ocean link**

Sediments deposited in the Great Australian Bight comprise benthic and planktonic bioclastic carbonate. Analysis of the planktonic components provides information of the upper, open-ocean

conditions, whereas the benthic bioassemblage reflects the bottom shelf conditions. Global open-ocean changes can, therefore, be linked to the continental margin in order to assess margin response to climate change.

## 1.5   Outline of Thesis

The results are divided into three topical parts each of which contains three chapters. Chapters partly represent discrete papers, which are either published, submitted or in preparation.

### *Part I - Introduction*

Chapter 1 summarizes the scientific background that led to this study and presents the general objectives and aims of the work.

Chapter 2 introduces the reader to the study area of southern Australia and the Great Australian Bight, in particular discussing the geographic and geologic setting.  In order to understand the developed paleorecord through time, the current oceanographic and climatic regimes are summarized before discussing the paleoceanographic and paleoclimatic interpretation. The Great Australian Bight is the largest area of cool-water carbonate deposition today. Its characteristics and unusual features are presented shortly and contrasted to tropical counterparts. The last part of this chapter introduces Ocean Drilling Program Leg 182, the drilling campaign that led to the recovery of the sedimentary archive of Site 1127. The analysis of Site 1127 samples form the basis of all data presented in this work.

Chapter 3 gives an overview and shortly discusses the methods used in the thesis.

### *Part II - Last glacial to Holocene Transition*

Part II, containing Chapters 4 to 6, concentrates on the most recent geologic, oceanographic and climatic history, that of the last glacial to Holocene time period, spanning the last 20,000 years before present. A radiocarbon-based chronology allows the comparison with other regional and global data sets.

Chapter 4 focuses on Termination I, the deglaciational period between the Last Glacial Maximum and the Holocene. The high-resolution and well-dated Site 1127 record from 18,000 to 10,000 years before present indicates step-wise warming and a rapid cold reversal that occurs synchronous to the Younger Dryas Chronozone. In comparison to Northern and Southern Hemisphere records, magnitude and timing of the Site 1127 cold reversals are assessed.

In Chapter 5, high-resolution oxygen isotopes and bulk iron abundances document in detail changes in sea-surface temperatures, sea-level rise and the hydrological cycle on the southern Australian margin for the last 18,000 years before present. Oxygen isotopes of planktonic foraminifera are used as a

proxy for sea-surface temperatures, whereas the bulk sedimentary iron is interpreted as a proxy for dust transported into the study area via the wind. The dry cold glacial is followed by step-wise sea-level rise and warming. Warm and wet conditions are inferred for the Early to Middle Holocene, followed by a trend towards dry and warm conditions in the Late Holocene. This record represents the first high-resolution marine record spanning the last glacial cycle and the results support the vegetational and hydrologic changes inferred not only from Australian terrestrial records but also from New Zealand.

Chapter 6 discusses sedimentary characteristics and changes from the last glacial to Holocene time period. Small-sized foraminifera and reduced diversity characterize the last glacial compared to the following interglacial. Unusually high sedimentation rates, the occurrence of benthic foraminifera Uvigerina spp in large numbers and depleted bulk nitrogen isotopes identify the Early Holocene as an especially productive time period.

## *Part III - The Late Pleistocene Period*

Part III containing Chapters 7 to 9 discusses the Late Pleistocene, approximately 800,000 year long record of Site 1127, and evaluates the stratigraphy and response to glacial-interglacial cyclicity.

Chapter 7 evaluates the potential of constructing an oxygen and carbon isotope stratigraphy for the late Pleistocene based on bulk and fine-fraction (<38 μm) sediment samples. The comparison of the oxygen isotope data with the classic SPECMAP curve indicates an overall good correlation, although the magnitude is smaller than expected from global pelagic records and might be due to the neritic-dominated sediment composition of Site 1127. The study indicates that an isotope stratigraphy based on planktonic and benthic foraminifera is needed to fully evaluate the response of cool-water carbonates deposited on a margin setting to global ice-volume fluctuations, and hence, associated sea-level variations.

Chapter 8 documents the development of an isotope stratigraphy based on planktonic and benthic oxygen isotopes. The stratigraphic analysis is additionally supported by simultaneous changing variations in carbonate mineralogy and Natural Gamma Ray from downhole logging. Together, these data form the basis for the age model. The isotope sea-level record links the continental margin setting to the deep ocean, pelagic record. Changes in carbonate mineralogy, Natural Gamma Ray log and further physical properties are used to estimate the effects of Late Pleistocene sea-level change on a cool-water carbonate ramp.

Chapter 9 summarizes the main conclusions of the thesis and their implications. The outlook suggests ideas for new and ongoing research. In particular, paleoceanographic studies on continental margins, so far poorly developed, can provide high-resolution archives in key-locations.

## References

Alley, R. B. (2000). Ice-core evidence of abrupt climate change. *Proceedings of the National Academy of Sciences* **97,** 1331-1334.

Alley, R. B., and Clark, P. U. (1999). The Deglaciation of the Northern Hemisphere: A Global Perspective. *Annual Reviews Earth and Planetary Sciences* **27,** 149-182.

Ammann, B., and Lotter, A. (1989). Late-glacial radiocarbon and palynostratigraphy on the Swiss Plateau. *Boreas* **18,** 109-126.

Ariztegui, D., Bianchi, M. M., Masaferro, J., Lafargue, E., and Niessen, F. (1997). Interhemispheric synchrony of Late-glacial climatic instability as recorded in proglacial Lake Mascardi, Argentina. *Journal of Quaternary Science* **12,** 333-338.

Arnold, J. R., and Libby, W. F. (1949). Age determination by radiocarbon content: checks with samples of known age. *Science* **110,** 678-680.

Bard, E. (1998). Geochemical and geophysical implications of the radiocarbon calibration. *Geochimica et Cosmochimica Acta* **62,** 2025-2038.

Bard, E., Rostek, F., and Sonzogni, C. (1997). Interhemispheric synchrony of the last deglaciation inferred from alkenone palaeothermometry. *Nature* **385**.

Belkin, I. M., and Gordon, A. L. (1996). Souther Ocean Fronts from Greenwich Meridian to Tasmania. *Journal of Geophysics* **101,** 3675-3696.

Bender, M. (1998). Interhemispheric phasing of millenial-duration of climate events during the last 100ka. *In* "AGU Chapman conference - Mechanisms of Millenial-Scale Global Climate Change. Abstracts with program p. 10.", pp. 10.

Bennett, K. D., Haberle, S. G., and Lumley, S. H. (2000). The Last Glacial-Holocene Transition in Southern Chile. *Science* **290,** 325-328.

Blunier, T., and Brook, E. J. (2001). Timing of Millenial-Scale Climate Change in Antarctica and Greenland During the Last Glacial Period. *Science* **291,** 109-112.

Blunier, T., Schwander, J., Stauffer, B., Stocker, T. F., Dällenbach, A., Indermühle, A., Tschumi, Chappellaz, J., Raynaud, D., and Barnola, J.-M. (1997). Timing of the Antarctic Cold Reversal and the atmospheric CO2 increase with respect to the Younger Dryas event. *Geophysical Research Letters* **24,** 2683-2686.

Böning, C. W., and Semtner, A. J. (2001). High-resolution modelling of the thermohaline and wind-driven circulation. *In* "Ocean Circulation and Climate." (G. Siedler, J. Church, and J. Gould, Eds.), pp. 693. International Geophysics Series. Academic Press, London.

Broecker, W. S. (1998). Paleocean circulation during the last deglaciation: A bipolar seesaw?,. *Paleoceanography* **13,** 119-121.

Charles, C. D., Lynch-Stieglitz, J., Ninnemann, U. S., and Fairbanks, R. G. (1996). Climate connections between the hemisphere recealed by deep sea sediment core/ice core correlations. *Earth and Planetary Science Letters* **142,** 19-27.

Denton, G. H., and Hendy, C. H. (1994). Younger Dryas Age Advance of Franz Josef Glacier in the Southern Alps of New Zealand. *Science* **264,** 1434-1437.

Emiliani, C. (1955). Pleistocene temperatures. *Journal of Geology* **63,** 538-578.

Emiliani, C., and Milliman, J. D. (1966). Deep-sea sediments and their geologic record. *Earth-Science Reviews* **1,** 105-132.

Epstein, S., and Mayeda, T. (1953). Variations of the O18 content of waters from natural sources. *Geochimica et Cosmochimica Acta* **4,** 213-224.

Fairbanks, R. G. (1989). A 17,000-year glacio-eustatic sea lovel record: influence of glacial melting rates on the Younger Dryas event and deep-ocean circulation. *Nature* **342,** 637-642.

Geyh, M. A., and Schleicher, H. (1990). "Absolute age determination: physical and chemical dating methods and their application." Springer, Berlin.

Grootes, P. M., Steig, E. J., Stuiver, M., Waddington, E. D., and Morse, D. L. (2001). The Taylor Dome Antarctic 18O Record and Globally Synchronous Changes in Climate. *Quaternary Research* **56,** 289-298.

Hajdas, I. (1993). "Extension  of the radiocarbon calibration curve by AMS dating of laminated sediments of lake Soppensee and lake Holzmaar, ETH Nr. 10157.", ETH-Zurich.

Harrison, S. P., and Dodson, J. (1993). Climates of Australia and New Guinea since 18,000 yr B.P. *In* "Global Climates since the Last Glacial Maximum." (J. Wright, J.E., J. E. Kutzbach, T. Webb III, W. F. Ruddiman, F. A. Street-Perrott, and P. J. Bartlein, Eds.), pp. 265-293. University of Minnesota Press, Minneapolis.

Hays, J. D., Imbrie, J., and Shackleton, N. J. (1976). Variations in the earth´s orbit: pacemaker of the ice ages. *Science* **194,** 1121-1132.

Hobbs, J., Lindesay, J., and Bridgman, H. (1998). Introduction: a Southern Hemisphere Overview. *In* "Climates of the Southern Continents." (J. Hobbs, J. Lindesay, and H. Bridgman, Eds.), pp. 297. John Wiley & Sons Ltd, Chichester.

Imbrie, J., Boyle, E. A., Clemens, S. C., Duffy, A., Howard, W. R., Kukla, G., Kutzbach, J. E., Martinson, D. G., McIntyre, A., Mix, A. C., Molfino, B., Morley, J. J., Peterson, L. C., Pisias, N. G., Prell, W. L., Raymo, M. E., Shackleton, N., and Toggweiler, J. R. (1992). On the structure and origin of major glaciation cycles, 1, Linear response to Milankovitch forcing. *Paleoceanography* **7**.

Imbrie, J., Hays, J. D., Martinson, D. G., McIntyre, A., Mix, A. C., Morley, J. J., Pisias, N. G., Prell, W. L., and Shackleton, N. J. (1984). The orbital theory of Pleistocene climate: support from a revised chronology of the marine d18O record. *In* "Milankovitch and Climate, Part 1." (A. J. Berger, J. Imbrie, J. D. Hays, G. Kukla, and B. Saltzman, Eds.), pp. 269-305. Dordrecht: Riedel Publishing Co.

Indermühle, A., Stocker, T. F., Joos, F., Fischer, H., Smith, H. J., Wahlen, M., Deck, B., Mastroianni, D., Tschumi, J., Blunier, T., Meyer, R., and Stauffer, B. (1999). Holocene carbon-cycle dynamics based on CO2 trapped in ice at Taylor Dome, Antarctica. *Nature* **3398,** 121.

Jouzel, J., Vaikmae, R., Martin, M., Duclos, Y., Stievenard, M., Lorius, C., and Toots, M. (1995). The two-step shape and timing of the last deglaciation in Antarctica. *Climate Dynamics*, 151-161.

Keigwin, L. D., Curry, W. B., Lehmann, S. J., and Johnsen, S. (1994). The role of the deep ocean in North Atlantic climate change between 70 and 130 kyr ago. *Nature* **371,** 323-325.

Kershaw, A. P. (1989). Was there a 'Great Australian Arid Period'? *Search* **20,** 89-92.

Kitagawa, H., and van der Plicht, J. (1998). Atmospheric Radiocarbon Calibration to 45,000 yr B.P.: Late Glacial Fluctuations and Cosmogenic Isotope Production. *Science* **279,** 1187-1190.

Koutavas, A., Lynch-Stieglitz, J., Marchitto, T. M., and Sachs, J. P. (2002). El Niño-like pattern in ice age tropical Pacific sea surface temperature. *Science* **297,** 226-229.

Lindesay, J. (1998). Past climates of Southern Africa. *In* "Climates of the Southern Continents." (J. Hobbs, J. Lindesay, and H. Bridgman, Eds.), pp. 297. John Wiley & Sons Ltd, Chichester.

Manabe, S., and Stouffer, R. J. (1997). Coupled ocean-atmosphere model response to freshwater input: Comparison to Younger Dryas event. *Paleoceanography* **12,** 321-336.

Markgraf, V. (1993). Younger Dryas in southernmost South America - an update. *Quaternary Science Reviews* **12,** 351-355.

Mayewski, P. A., Twickler, M. S., Whitlow, S. I., Meeker, L. D., Yang, Q., Thomas, J., Kreutz, K., Grootes, P. M., Morse, D. L., Steig, E. J., Waddington, E. D., Saltzman, E. S., Whung, P.-Y., and Taylor, K. C. (1996). Climate changes during the last deglaciation in Antarctica. *Science* **272,** 1636-1638.

McGlone, M. S., Kershaw, A. P., and Markgraf, V. (1992). El Niño/Southern Oscillation climatic variability in Australasian and South American paleoenvironmental records. *In* "El Niño: Historical and Paleoclimatic Aspects of the Southern Ocean Oscillation." (H. F. Diaz, and V. Markgraf, Eds.), pp. 435-462. Cambridge University Press, Cambridge.

Miller, G. H., Magee, J. W., and Jull, A. J. T. (1997). Low-latitude glacial cooling in the Southern Hemisphere from amino-acid racemization in emu eggshells. *Nature* **385,** 241-244.

Moreno, P. I., Jacobson Jr, G. L., Lowell, T. V., and Denton, G. H. (2001). Interhemispheric climate links revealed by the late-glacial cooling episode in southern Chile. *Nature* **409,** 804-808.

Newnham, R. M., and Lowe, D. J. (2000). Fine-resolution pollen record of late-glacial climate reversal from New Zealand. *Geololy* **28,** 759-762.

Nicholls, N. (1992). Historical El Niño/Southern Oscillation variability in the Australasian region. *In* "El Niño: Historical and Paleoclimatic Aspects of the Southern Oscillation." (H. F. Diaz, and V. Markgraf, Eds.), pp. 151-173. Cambridge University Press, Cambridge.

Partridge, T. C., deMenocal, P., Lorentz, S. A., Paiker, M. J., and Vogel, J. C. (1997). Orbital forcing of climate over South Africa: a 200,000 year rainfall record from the Pretoria Saltpan. *Quaternary Science Reviews* **16**.

Peteet, D. (1995). Global Younger Dryas. *Quaternary International* **28,** 93-104.

Petit, J.-R., Basile, I., Leruyuet, A., Raynaud, D., Lorius, C., Jouzel, J., Stievenard, M., Lipenkov, V. Y., Barkov, N. I., Kudrayashov, B. B., Davis, M., Saltzman, B., and Kotlyakov, M. (1997). Four climate cycles in Vostok ice core. *Nature* **387,** 359-360.

Petit, J. R., Jouzel, J., Raynaud, D., Barkov, N. I., Basile, I., Bender, M., Chappellaz, J., Davis, M., Delaygue, G., Delmotte, M., Kotlyakov, M., Legrand, M., Lipenkov, V. Y., Lorius, C., Pépin, L., Ritz, C., Saltzman, E., and Stievenard, M. (1999). Climate and atmospheric history of the past 420000 years from the Vostok ice core, Antarctica. *Nature* **399,** 429-436.

Rahmstorf, S., and Willebrand, J. (1995). The role of temperature feedback in stabilising the thermohaline circulation. *Journal of Physical Oceanography* **25,** 787-805.

Rintoul, S. R., Hughes, C. W., and Olbers, D. (2001). The Antarctic Circumpolar Current system. *In* "Ocean Circulation and Climate." (G. Siedler, J. Church, and J. Gould, Eds.). International Geophysics Series. Academic Press, London.

Sarntheim, M., Kennett, J. P., Chappel, J., Crowley, T., Curry, W. B., Duplessy, J. C., Grootes, P., Hendy, I. L., Laj, C., Negendank, J., Schulz, M., Shackleton, N. J., Voelker, A., Zolitschka, B., and al., e. (2000). Exploring Late Pleistocene climate variations. *Eos, Transactions, American Geophysical Union* **81,** 625, 629-630.

Schmitz, W. J. (1996a). On the World Ocean Circulation, Vol I: Some Global Features/North Atlantic Circulation, pp. 141. Woods Hole Oceanographic Institution, Technical Report, WHOI-96-03.

Schmitz, W. J. (1996b). On the World Ocean Circulation, Vol II: The Pacific and Indian Oceans / A Gobal Update, pp. 237. Woods Hole Oceanographic Institution, Technical Report, WHOI-96-08.

Schrag, D. P., Adkins, J. F., McIntyre, K., Alexander, J. L., Hodell, D. A., Charles, C. D., and McManus, J. F. (2002). The oxygen isotopic composition of seawater during the Last Glacial Maximum. *Quaternary Science Reviews* **21,** 331-342.

Schulmeister, J., and Lees, B. G. (1995). Pollen evidence from tropical Australia for the onset of an ENSO-dominated climate at c. 4000 BP. *The Holocene* **5,** 10-18.

Schwander, J., Jouzel, J., Hammer, C. U., Petit, J.-R., Udisti, R., and Wolff, E. (2001). A tentative chronology for the EPICA Dome Concordia ice core. *Geophysical Research Letters* **28,** 4243-4246.

Shackleton, N. J., and Opdyke, N. D. (1973). Oxygen isotope and paleomagnetic stratigraphy of equatorial Pacific core V28-238: oxygen isotope temperatures and ice volumes on a $10^5$ year and $10^6$ year scale. *Quaternary Research* **3,** 39-55.

Singer, C., Shulmeister, J., and McLea, B. (1998). Evidence Against a Significant Younger Dryas Cooling Event in New Zealand. *Science* **281,** 812-814.

Steig, E. J. (1999). Mid-Holocene Climate Change. *Science* **286,** 1485-1487.

Steig, E. J. (2001). No Two Latitudes Alike. *Science* **293,** 2015-2016.

Stenni, B., Masson-Delmotte, V., Johnsen, S., Jouzel, J., Longinelli, A., Monnin, E., Röthlisberger, R., and Selmo, E. (2001). An Oceanic Cold Reversal During the Last Deglaciation. *Science* **293,** 2074-2077.

Stocker, T. F. (1998). The seesaw effect. *Science* **282,** 61-62.

Stott, L. D., Poulsen, C., Lund, S., and Thunell, R. C. (2002). Super ENSO and Global Climate Oscillations at Millennial Time Scales. *Science* **297,** 222-226.

Stuiver, M., Braziunas, T. F., Becker, B., and Kromer, B. (1991). Climatic, solar, oceanic and geomagnetic influences on late-glacial and Holocene atmospheric $^{14}C/^{12}C$ change. *Quaternary Research* **35,** 35-65.

Urey, H. C. (1947). The thermodynamic properties of isotopic substances. *Journal of the Chemical Society London*, 562-581.

White, J. W. C., and Steig, E. J. (1998). Timing is everything in the game of two hemispheres. *Nature* **394,** 717-718.

Wood, R. A., and O'Brien, F. O. (2001). Coupled ocean-atmosphere models. *In* "Ocean Circulation and Climate." (G. Siedler, J. Church, and J. Gould, Eds.), pp. 693. nternational Geophysics Series. Academic Press, London.

# 2   THE GREAT AUSTRALIAN BIGHT

## 2.1   Study Area

### 2.1.1   Great Australian Bight

The Great Australian Bight (GAB) forms the central embayment of Australia's southern continental margin, located between 124-134°E and 32-34°S (Fig. 2.1). Unlike most other modern carbonate platforms its latitude-parallel location does not cross any oceanographic and climatic belts (James et al., 2001). To the northwest it is bounded by Archean and Paleoproterozoic crystalline rocks of the Yilgarn Craton and to the east by Paleoproterozoic rocks of the Gawler Craton. The coastline to the north is characterized by the shear sea-cliffs cutting into the cool-water carbonate limestones of the Eucla Group of Eocene to Middle Miocene age (James and Bone, 1994). The Nullarbor Plain, a flat, treeless, cavernous karst landscape, extends northward from these cliffs into the arid hinterland (Fig. 2.2 and 2.3). No rivers drain the area into the Bight. Whereas the eastern (James et al., 1997; James et al., 1992; Li et al., 1996) and to a lesser extent the western (Feary and James, 1995; Li et al., 1999) GAB region are well studied, the central GAB shelf is virtually undocumented (James et al., 2001). Most studies here focused on the Holocene to sub-recent sediment and facies distribution. In this context, ODP Leg 182 drilling results not only fill in this central GAB gap but also provide the first continuous subsurface information of the underlying Cenozoic carbonate succession.
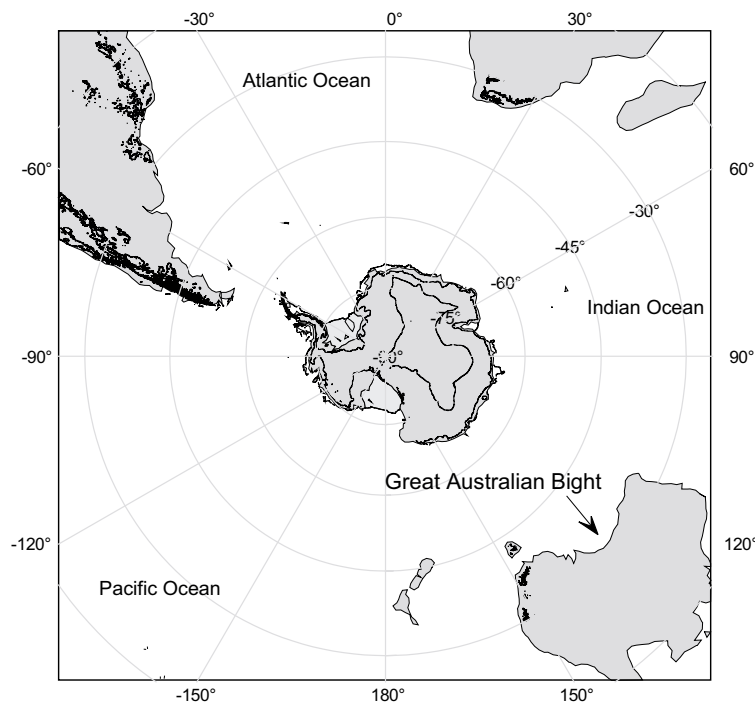


**Figure 2.1.** *Location of the Great Australian Bight from a Southern Hemisphere perspective.*

### 2.1.2    Geologic Setting, Tectonic Framework and Seismic Stratigraphy

The divergent, passive continental margin of southern Australia formed during the protracted period of extension and rifting that led to the separation of Australia and Antarctica in the Cretaceous. It evolved during the subsequent northward drift of the Australian continent throughout the Cenozoic (Stagg et al., 1989; Willcox & Stagg, 1990; Veevers et al., 1990). The onset of faster spreading in the middle Eocene coincides with the establishment of fully marine conditions and initiation of carbonate sedimentation, which has continued until the present (Bein & Taylor, 1981; Stagg et al, 1990).

The geology of the region is dominated by the underlying and inland extension of the GAB basin (Fig. 2.2) (Stagg et al., 1989). The basement consists of Precambrian granitic rocks and metasediments (Fig. 2.3), similar to those exposed onshore (Bein & Taylor, 1981). The shelf is underlain by several deep sub-basins filled with up to 12 km of mostly Cretaceous terrigeneous clastic sediment. (Wilcox et al., 1988; Davies et al., 1989). In 1990 an exploratory off-shore well, Jerboa 1 was drilled by the Japan National Oil Company (Fig. 2.2). It penetrated 1738 m into the Cenozoic and Cretaceous sedimentary succession before ending in basement rocks. Results of the dry well provide useful information on the Cretaceous stratigraphy and depositional history of the GAB. Unfortunately, only the bottommost 145 m of Tertiary section was actually recovered. Thus, until, Leg 182 there was no information available on the younger sediments (Bein & Taylor, 1981). Geohistory analysis of the Jerboa-1 well has indicated minimal Tertiary subsidence (Hegarty et al., 1988), making the GAB region a particularly stable continental margin.
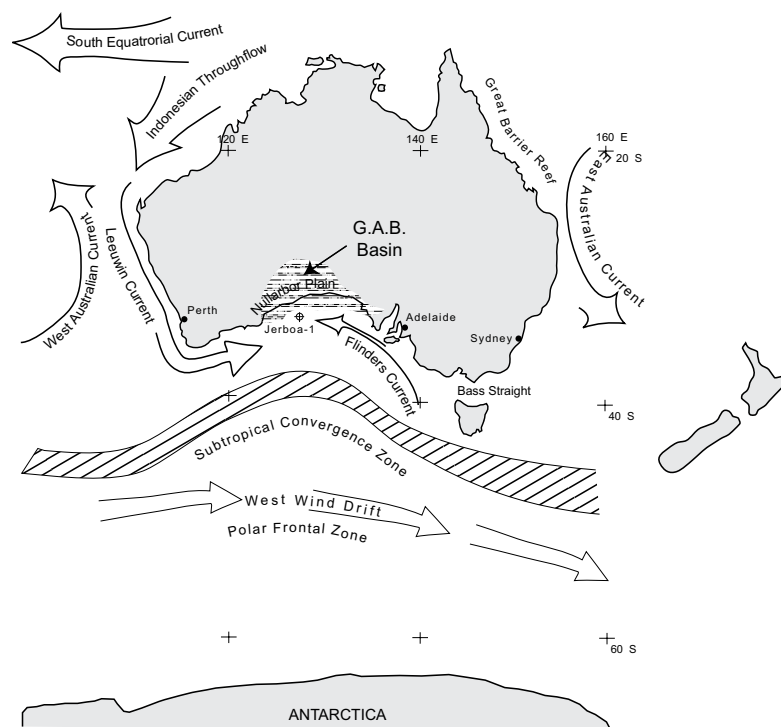


***Figure 2.2.*** *Schematic overview of Australia: general oceanographic setting and the location Cenozoic of the Great Australian Bight basin.*

A number of seismic surveys, and especially those in preparation for ODP Leg 182 drilling provided information on the Tertiary and Quaternary development of the GAB. Feary & James (1995) interpreted ~5500 km of seismic reflection data in the western-GAB which indicate that the 700-m thick Cenozoic section off the Eucla basin was largely deposited as a prograding cool-water carbonate ramp (Fig. 2.3). Of interest to this work are Sequences 1 & 2, that are indicated in the schematic and interpreted seismic image of Fig. 2.3. Sequence 1 is interpreted as a thin aggradational Holocene drape and forms the basis of the work presented in Part II of the thesis. Sequence 2 is characterized by a thick, prominent sigmoidal sequence that thins out towards the shore and is thickest beneath the present-day shelf edge. During the deposition of Sequence 2, widespread development of broad, low relief, biogenic (bryozoan) mounds sitting on the shelf and upper slope within Sequence 2 occurred. Sequence 2 is the focus of part III of the thesis.
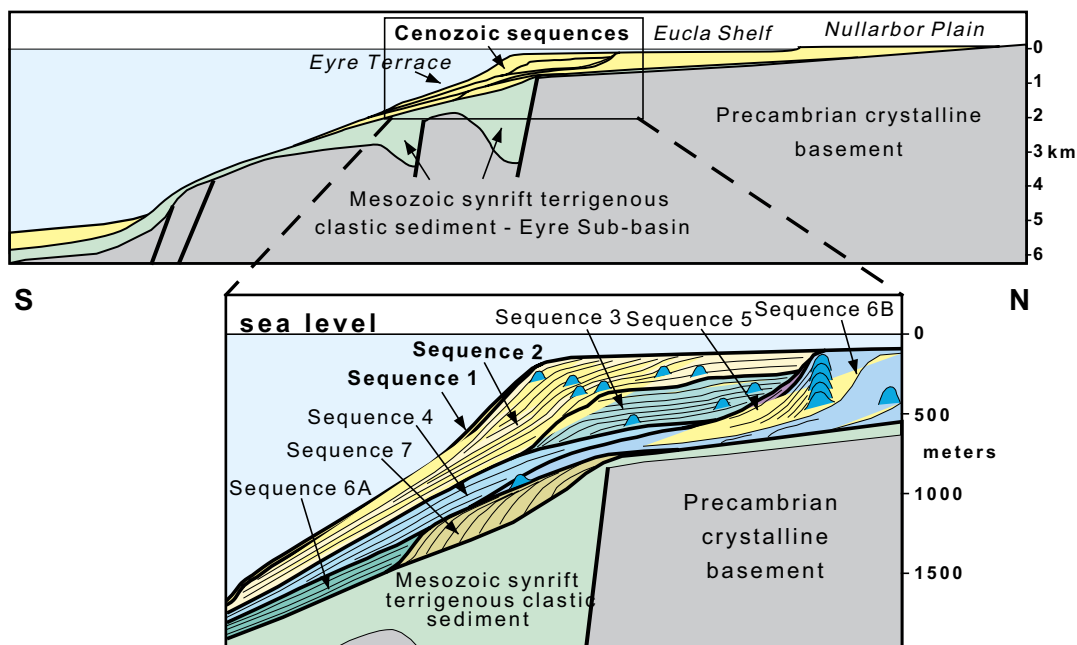


**Figure 2.3.** *Distribution of Cenozoic sequences. Schematic north-south section from the Nullabor plain (onshore) across the Eyre Terrace (longitude 128°E). Seven Cenozoic sequences interpreted from seismic data were identified. Mesozoic syn-rift to early post-rift siliciclastic sequences and Precambrian crystalline basement underlie the shelf. Note the distribution of biogenic mounds within many Cenozoic sequences. Vertical scales are approximate. (Taken from ODP Leg 182 Scientific Prospectus).*

### 2.1.3  Oceanography

The modern shelf is an unusually wide (150 to 200 km), gently south-ward sloping surface, which directly faces the cold Southern Ocean. High (>2.5 m) modal deep-water wave heights and long period (> 12 s) swell waves are a common feature and wavelengths of 200 m have been reported (Short and

Hesp, 1982). Along most of southern Australia the tidal range is less than 2 m (Murray-Wallace and Belperio, 1991). The south-west north-east directed wave action is the result of large storms originating north of Antarctica. The Subtropical Convergence Zone is located ~500 km to the south, although towards the Bight and weakening at the same time (Fig. 2.2 and 2.4a). The modern oceanography is influenced by two main water masses the Leeuwin Current and Southern Ocean waters, although the setting is made more complex by a third watermass, the Flinders Current, whose dynamics are not fully understood (for further discussion see (Herzfeld, 1997; James et al., 2001; Rochford, 1986)).

*The Leeuwin Current*

The Leeuwin Current (Fig. 2.2 and 2.4a) is a comparatively warm, low-salitnity flow carrying nutrient-depleted topical Indian Ocean waters south along the coast of Western Australia (Rochford, 1984; Rochford, 1986). It rounds Cape Leeuwin to become a W-E directed flow into the GAB, with significant local offshelf eddies (Cresswell, 1991). Annual mean transport is estimated at 3-5 Sv, with average current velocities of 0.1-0.2 m/s (Tomczak and Godfrey, 1994). This south-flowing eastern boundary current is unique in the Southern Hemisphere (Morgan & Wells, 1991), since it overcomes the equatorward wind-stress. The flow appears to be driven by a steric sea-level slope of 0.33 m from 20°S to 32°S. It has been suggested that the cause of the poleward downslope is the flow from the Pacific via the Indonesian Throughflow into the Indian Ocean north of Western Australia (Pickard and Emery, 1990; Tomczak and Godfrey, 1994). When entering the Bight, the east-flowing, narrow (<100 km), shallow (<200 m) shelf water is comparatively warm in the west, on average 21°C (19°C in winter) and in the east 17°C (15°C in winter) (Legeckis and Cresswell, 1981; Pearce and Walker, 1991). Surface nutrient levels are very low for inorganic phosphate (0.02-0.06 mg-atom/l), being the lowest measured in the Indian and Southern Ocean (Rochford, 1986). In comparison, the continental shelf waters off Southern and Western Australia are warmer in winter than the corresponding regions off southern Africa and Chile in summer. These conditions have produced a marine biota in which many tropical and subtropical marine organisms have their most southerly record (Li et al., 1999; Maxwell and Cresswell, 1981; Pearce and Walker, 1991). The Leeuwin Current varies seasonally, flowing strongest during the autumn and winter months (April to September) and weakest during the summer months (October to March). This can also be verified by the lowered surface salinities (35.7 - 35.5‰) during times of strong winter-flow (Cresswell and Golding, 1980; Herzfeld, 1997). On an interannual scale, El Niño-Southern Oscillations affect the Leeuwin Current. In 'normal' (non-ENSO) years, coastal sea levels are relatively high, and the resulting cross-shelf sea-level slope implies that the southward alongshore flow of the Leeuwin Current is strong. During El Niño years, however, coastal sea levels fall, due to lowered pressure gradient between the Pacific Warm Pool and the Southern Ocean, weakening the Leeuwin Current (Pearce and Phillips, 1988). This observation is additionally confirmed by hydrographic data indicating that El Niño periods are associated with generally cooler and more saline conditions on the shelf, confirming weaker southward transport of

tropical waters. This, on the other hand, has consequences for the larvae distribution and settlement of the rock lobster, the most valuable single-species fishery in Australia (Caputi et al., 1996).

## *The Flinders Current*

Knowledge of the off-shelf, sub-surface and adjacent deep ocean circulation is based on a few modelling studies and even fewer observations (Middleton and Cirano, 2002). The existence of westward directed transport and it's possible importance to the circulation along Australia's southern shelves was first noted in the analysis of Bye (1983), who used annual mean wind stress curl and an analytical model to show that a westward flowing boundary current should exist off the shelf south of Australia (Fig. 2.2 and 2.4a). The existence of the flow, named the Flinders Current (Bye, 1972), was supported by subsequent hydrographic data (Hufford et al., 1997). Waters originate from a large wind-driven anticyclonic gyre, the northern arm of which intensifies, first moving northward and then flowing westward as the Flinders Current, an undercurrent beneath the Leeuwin Current (Bye, 1971; Bye, 1972). Bringing cold (~10°C) and nutrient rich waters it can move onto the shelf when the Leeuwin Current weakens (James et al., 2001).

## *Southern Ocean Waters*

The Southern Ocean or west wind drift waters invade the shelf from a southwesterly direction, bringing cold and even less saline waters into the GAB region (Fig. 2.4a) (Rochford, 1986). The Subtropical Front, a major oceanic front, defined by the 12°C isotherm at 150 m water depth, marks the southern limit of GAB-influencing circulation (Belkin and Gordon, 1996). South of Australia, the Subtropical Front is found to bend strongly northward, weakening at the same time (Fig. 2.4a). Two deep meridional ocean transects south of Australia, as part of the World Ocean Circulation Experiment, found the Subtropical Front 39°S in the west (120°E) and about 220 km further north in the east (132°E) (Schodlok et al., 1997), indicating that it comes closer to the south Australian continent than previously thought. Temperatures at the surface range from 12.7-14.8°C and at 200 m depth from 9.9-11.9°C, with salinity ranges from 34-35‰. Subantarctic Mode Water characterizes the intermediate water mass down to a 600 m water depth at 120°E (Schodlok et al., 1997), which is significantly deeper than the reported 400 m water depths at 135°E (Patterson and Whitworth, 1990).
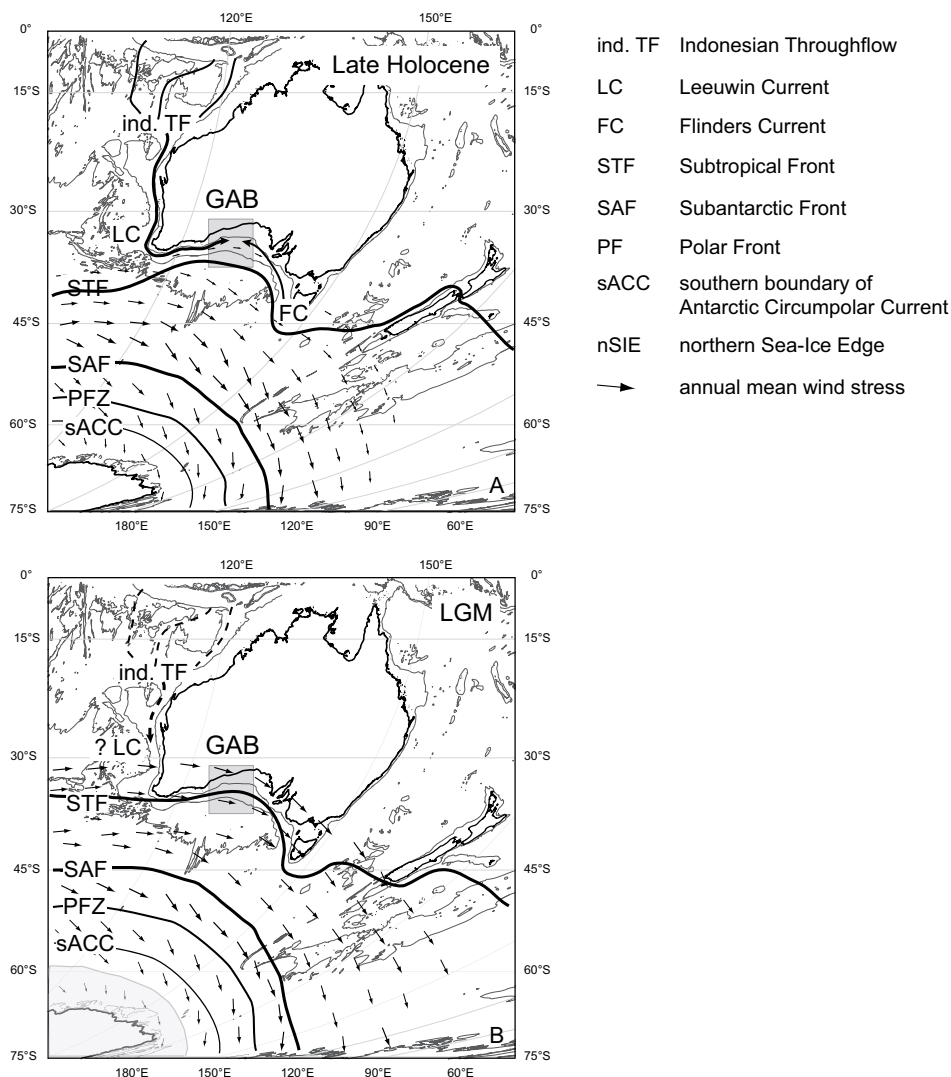
***Figure 2.4.*** *Schematic comparison of paleoceanographic setting for the (A) Late Holocene and (B) Last Glacial Maximum. Note the growth of Antarctic sea ice and the northward expansion of the oceanic fronts and wind regime during the last glacial time period. The flow of the Leeuwin Current (LC) is weaker or even absent (B).*

### 2.1.4   Paleoceanography

The interaction among water masses, currents and oceanic fronts not only produces a unique marine biota but also has also significantly influenced the paleontological, paleoecological and sedimentological record through time. McGowran et al. (1997) reviewed and discussed the overall biogeographic impact of the Leeuwin Current over the past 40 Ma, proposing its first occurrence in the late middle Eocene and episodic flow in the later Palaeogene and Neogene. A small, middle-Miocene barrier reef, interpreted from seismic data (Fig. 2.3), was used as evidence for a warm-water flow at that time (Feary and James, 1995). The late Quaternary paleoceanography is dominated by glacial-interglacial fluctuations and the GAB foraminiferal record indicates a strong Leeuwin Current flow during the Holocene and last interglacial with a weakening or complete shut-down during glacials due

to a northward shift of the Subtropical Frontal Zone (Fig. 2.4) (Almond et al., 1993; Li et al., 1999). Glacial/interglacial temperature and productivity cycles are evident from benthic oxygen and carbon isotope data (Holbourn et al., 2002) and this study. During and immediately after the last glacial lowstand, the combination of lowered sealevel, weakened Leeuwin Current and increased upwelling probably led to an enhanced carbon flux to the seafloor that favoured prolific bryozoan growth and mound formation (Holbourn et al., 2002; James et al., 2000). Due to lowered sea-level during the last glacial maximum both Tasmania and New Guinea were joined to the Australian mainland and ocean currents were deflected with the loss of the throughways in the region of the Bass and Torres Straits. Fluctuations in the position of the Subtropical Front south of Australia, based on the assemblage-change of calcareous nannoplankton (Findlay and Flores, 2000), led to poleward movement during interglacials and equatorward during glacials (Fig. 2.4b).

Australia is an ideal location for the reconstruction of eustatic sea-level since it is far removed from Northern Hemisphere ice-sheets and melt-water pulsing and, thus, less influenced by glacio-hydro-isostatic effects. During the last interglacial (~125 ka) sea-level was 2 m above present sea-level (Murray-Wallace and Belperio 1991).  Data from the Bonaparte Gulf off northwestern Australia indicate that sea-level was 120 lower than present and suggest an initial sea-level rise at 19 ka, followed by 2000 to 3000 years of much slower melting before the onset of the main deglaciation (Yokoyama et al. 2000). Evidence for rapid sea-level rise at 14 ka and during the Younger Dryas cold period is not unequivocal and currently based on a few records only (Fleming et al., 1998). A recent study on the spatial and temporal variability in the Holocene sea-level record of the southern Australian coastline indicates a greater than average rate of Early Holocene rise of ~10 mm/year from 10,000 to 6,400 radiocarbon years BP (Belperio et al., 2002).

## 2.1.5   Climate

The Mediterranean-type climate of southwest to southeast Australia is characterized by hot dry summers and mild wet winters. The major controlling factor of these seasonal changes is the descending air of the subtropical belt of high pressure and divergence and its latitudinal migration across Australia (Fig. 2.5). During summer, the subtropical high-pressure belt at it's southernmost position (37-38°S), bringing hot dry weather to the south by traveling anticyclones (Fig. 2.5a, b). In winter, the belt is sufficiently far north (29-32°S) (Pittock, 1973) that the southern part of the continent comes under the influence of the Westerlies (Fig. 2.5c, d). These circulation changes result in distinct seasonal rainfall distribution patterns. The summer-dominating anticyclones bring dry and hot air, and only the troughs in-between draw in moist-maritime northwesterly airflows bringing occasional summer rain to the east coast and southeastern highlands. Predominantly, the mean annual rainfall occurs in winter with amounts ranging between 30 to 90 cm (Specht, 1969) associated with the low-pressure systems of the Westerlies. Tasmania's southerly location lies within the rain-bearing Westerlies throughout the year.

The seasonally migrating subtropical high-pressure belt not only affects rainfall but also wind direction and strength as illustrated in the comparison of winter and summer wind regimes. During summer the southerly position of the belt results in the counter-clockwise circulation of the winds around the highs with winds coming from a southeast to easterly direction for the majority of summer. Winter winds dominantly blow from the west to northwest and are the strongest of the year.

The El Niño-Southern Oscillations (ENSO) has a major effect on the modern climate of Australia, amplifying interannual variability, imposing temporal weather patterns causing widespread drought and heavy rainfall episodes (Nicholls, 1992). In southern Australia the central and eastern regions are most affected by ENSO variability. During El Niño events, the migrating subtropical high-pressure belt is intensified by the breakdown in the Walker Circulation. As a result the rain-bearing Westerlies are deflected to the south leading to reduced rainfall and drought (McGowan et al., 2000; Whetton, 1997). The Walker Circulation is a pattern of zonal flows over the equator across the Pacific. The strength and direction of the circulation are measured by the difference between sea-level pressures at Papeete (Tahit, 17°S) and Darwin (northern Australia, 12°S), 8500 km away. During El Niño it weakens and is displaced to the East.

Summer
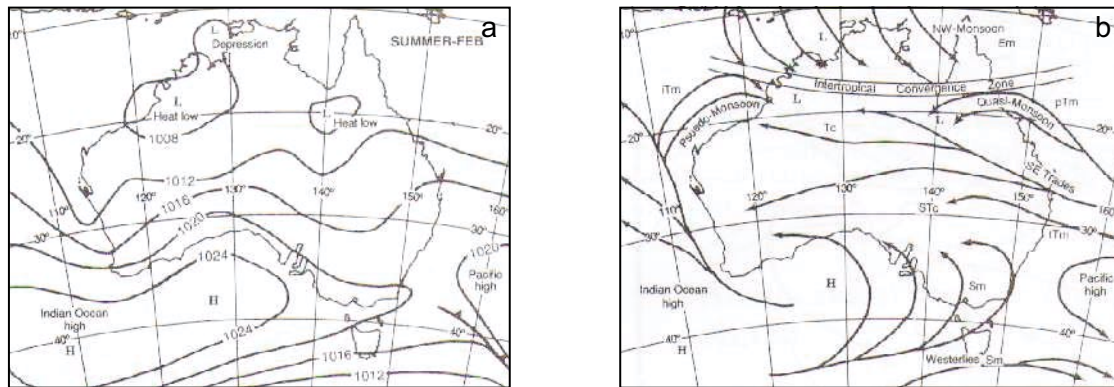


Winter
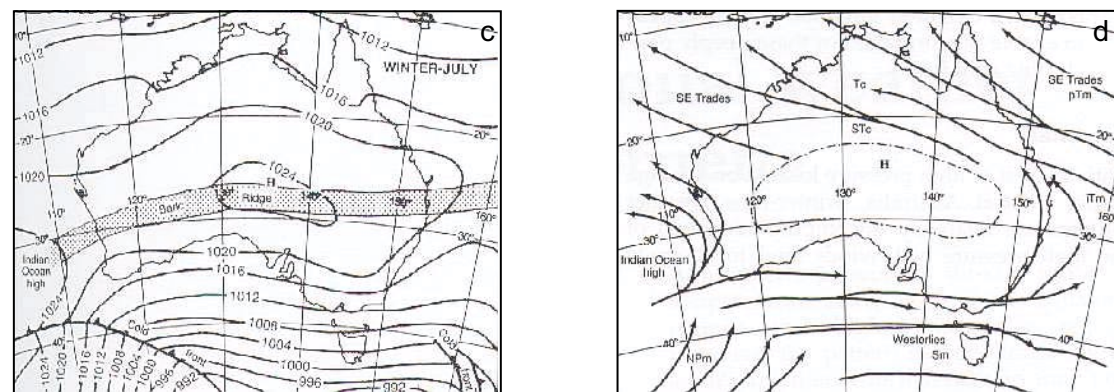


***Figure 2.5.*** *Synoptic chart of Australia illustrating typical summer and winter pressure distribution (a,c) and wind patterns (b,d) (modified after van Hazel, 2001). Note the presence of the high-pressure cell over the Great Australian Bight (a) in summer. During winter the subtropical high-pressure belt moves north (b) and the southern Australian margin comes under the influence of rain-bearing Westerlies (d).*

## 2.1.6    Paleoclimate

Paleoclimatic change of terrestrial southern Australia is well documented for the late Quaternary (Kershaw et al., 2000). Especially, lake records from southeastern and to a lesser extent southwestern Australia provide a wealth of information on hydrological and vegetational change through the reconstruction of lake-levels and pollen assemblages (Harrison and Dodson, 1993). Further data come from moraines left by glacier advances (Barrows et al., 2001), temperature estimates inferred from emu eggshell amino-acid racemization (Miller et al., 1997), and windiness as evidence by paleodune activity (Zheng et al., 2002).

### Late Pleistocene

Paleoclimatic records extending back into the Late or even Middle Pleistocene are rare but the maar lakes of the southeast Australian province Victoria have provided a few long lacustrine records. The record of Pejark Marsh, although discontinuous, reaches back ~1 Ma (Wagstaff et al., 2001), whereas the records of Lake Terang, probably cover the last 450 ka (Kershaw, 1995) and that of Lake Wangoom the last 200 ka (Harle et al., 1999). Late Pleistocene vegetation and climatic change in western Tasmania is recorded in the 125 ka record of Lake Selina (Colhoun et al., 1999). In summary, all of these records indicate clear changes in moisture levels in concert with glacial/interglacial cyclicity. Interglacial periods are generally moister and the vegetations responds with forest growth, in contrast to glacial periods that are dominated by dry steppe and woodland.

Reliable chronologies beyond the limits of radiocarbon dating are of concern when studying paleorecords older than the last glacial maximum. Additionally, last glacial aridity often reduced or even stopped sediment deposition, limiting fossil preservation and thereby preventing the development of a well-dated, multiproxy chronology.

### Last Glacial Maximum

Sea surface temperature estimates for the last glacial maximum, around 18,000 years BP indicate a 2-4°C decrease in SST (Anderson et al., 1989; Thunell et al., 1994) with up to a 9°C decrease for the continental interior (Miller et al., 1997). Wide-scale aridity is evidenced in lower lake-levels at nearly all investigated southern Australia sites (Harrison and Dodson, 1993), near-absence of swamp or bog communities (Kershaw, 1995) and the growth of extensive steppe areas (Kershaw et al., 1986). Small glaciers covered the Snowy Mountains of the southeastern highlands and their moraines document glacier advances (Barrows et al., 2001). The annual frequency of dust-storm events is proposed to have increased by up to 50% compared to today due to increased windiness (McTainsh and Lynch, 1996), which coincides with the last major dune-building phase that occurred between 25 and 13 ka, reaching a maximum between 20 and 16 ka (Wasson, 1984; Wasson, 1986; Zheng et al., 2002). Quartz and clay distribution maps off the coast of eastern Australia and the Tasman Sea (Thiede, 1979) indicate that rates of deposition during the last glacial maximum were significantly higher compared to the Holocene. Furthermore, calcareous dust, eroded from the exposed GAB shelf, is found in SE Australian soils (McTainsh, 1989).

In summary, compared to today, climate during the LGM was drier, cooler and windier and this pattern of paleoenvironmental change is explained with the poleward displacement of the subtropical high-pressure belt. This in turn pushes the Westerlies southward and deprives southern Australia of winter rain. Drier conditions in Tasmania indicate that the southerly displacement was sufficient to exclude Tasmania from year-round westerly influence with forest reconstructions from southern Argentina placing the Westerlies to south of the 41° latitude (Markgraf, 1987). The zone of Southern-Hemisphere Westerlies was probably also contracted due to the southward displacement of the subtropical high-pressure belt in the north and the expansion of the Antarctic high in the south

(Rognon and Williams, 1977). Model results confirm the poleward displacement in response to steeper latitudinal and temperature gradients caused by the extension of Antarctic sea ice (Kutzbach, 1986).

### LGM-Early Holocene Transition

The effect of deglaciation and global warming was only felt in southern Australian paleorecords by ~ 16 ka when temperature estimates for the continental interior document rapid warming (Miller et al., 1997), which correlates well with the last glacier advance of ~16,8 ka (Barrows et al. 2001). The cold steppe vegetation was gradually replaced by sclerophyll forest between 15 and 10 ka (Kershaw et al., 1991). Low lake levels during most of the deglaciation, however, indicate that wide-scale aridity persisted over most of Australia until ~12 ka (Harrison and Dodson, 1993). After 12 ka, a gradual transition to wetter conditions was first observed in Tasmania where lake levels were rising around 11 ka, reaching coastal southeastern Australia by ~10 ka. This pattern reflects the gradual northward shift of the southern margin of the subtropical high-pressure belt and associated Westerlies. Wide-scale and long-lasting aridity is undoubtedly well documented in the lake records, but, unfortunately, it results in an incomplete or at best low-resolution paleoenvironmental record spanning the glacial to Holocene transition, such as the Tower Hill record reaching back to the last glacial maximum (D'Costa et al., 1989).

### Early Holocene

The Early Holocene is characterized by a generally wetter environment, as evidenced by high lake levels and vegetation, indicating that moister and/or warmer conditions developed across the region after 12 ka. The trend to wetter conditions culminated at 7 ka (Harrison and Dodson, 1993) in southeastern Australia, correlating with the high-lake event documented in two recent paleorecords from the understudied area of southwestern Australia (Zheng et al., 2002). The equatorward displacement of the subtropical high-pressure belt from its present position, allowing for the year-round influence of the Westerlies can explain the observed pattern (Harrison and Dodson, 1993).

### Late Holocene

Climatic conditions after ~7 ka became drier in southwestern and coastal southeastern Australia as observed in the gradually declining lake levels towards the present (Harrison and Dodson 1993). In southwestern Australia, the termination of the high-lake event in the middle Holocene is followed by the reactivation of widespread eolian activity (Zheng et al., 2002). The intensification of the subtropical high-pressure belt over Australia is considered the cause for the increasing aridity of southern Australia after ~5 ka (Schulmeister, 1999). Further, increased El Nino variability and its effect on the most recent paleoclimate history of tropical Australia has been studied (Schulmeister and Lees, 1995), and most likely also affected the southern part of the continent.

## 2.2   Cool-Water Carbonates

Cool-water carbonates represent a major component of sedimentary geology. Carbonate research, however, has long concentrated on warm-water tropical settings because reefs and carbonate platforms are considered to be potential reservoirs for oil and gas. In contrast, cool-water carbonates have been less studied (James et al., 1997) and, only in recent years the carbonate research community has turned its focus from of the tropics higher latitudes and cooler water. Although, the expression cool-water carbonates is used in this work, these sediments have also been termed temperate carbonates (Lees and Buller, 1972), non-tropical carbonates (Nelson et al., 1988), and extratropical carbonates (McGowran et al., 1997).

The modern continental margin of southern Australia is the largest cool-water carbonate depositional realm on Earth today. The Ocean Drilling Program (ODP) conducted the first drilling campaign into a cool-water carbonate environment from October to December 1998 during ODP Leg 182 (Fig. 2.8). A series of 9 sites were cored with the recovery of sediments representing the first offshore Eocene to modern succession of cool-water carbonates to be studied.

### 2.2.1   Historical Remarks

The fact that cool-water carbonates have been neglected for so long has astonished authors, such as Chave (1967) who indicated that these carbonates could form at all latitudes, regardless of water temperature, as long as terrigeneous clastic sediment input was low. Lees and Buller (1972) followed by Lees (1975) discussed the distribution of grain types, the role of salinity and temperature and, thus, put the distinct cool-water carbonate setting into an oceanographic perspective. Cool-water carbonates were identified and primarily studied in the Southern Hemisphere, particularly in New Zealand (Carter, 1975), Australia (Connolly and van der Borch, 1967; Wass et al., 1970; Marshall and Davies, 1978) and South Africa (Siesser, 1971). A symposium on cool-water carbonates held in 1986 resulted in a surge of studies around the world, emphasizing the south-facing shelves in southern Australia. A number of papers were collected in a special publication on cool-water carbonates (James and Clarke, 1997). These studies have since been complemented by research resulting from new data sets generated in preparation for ODP Leg 182. Feary and James (1995 and 1998) reported on major advances in the seismic stratigraphy and geologic evolution of the Cenozoic cool-water Eucla platform and Cenozoic biogenic mounds in the Eucla basin, whereas Li et al. (1999) summarized the foraminiferal biofacies on the southern shelf and their paleoceanographic significance. The newest and probably the most integrated and multi-proxy results stem from the results of Leg 182 in a series of published and forthcoming papers.

### 2.2.2   What are Cool-Water Carbonates?

A cool-water bio-assemblage is composed of molluscs, foraminifers, echinoderms, bryozoans, barnacles, ostracods, sponges, worms, ahermatypic corals and coralline algae (Fig. 2.6). Cool or temperate assemblages commonly mantle continental margins in the mid to high latitudes, where sea

water temperatures barely rise above 20°C. How they are distinguished from their warm-water counterpart is a question that Lees and Buller (1972) attempted to answer by analyzing numerous carbonate sands and gravels from shelves less than 100 m depth situated between 60°N and 60°S in latitude. They proposed the term *Foramol Association* in contrast to the *Chlorozoan Association* for the warm-water carbonates. In contrast, nutrients are thought to have an important influence for the *Foramol Association* that thrive and accumulate when they are abundant.

In the most complete description of the cool-water depositional realm, James (1997) presents a set of new definitions, which more accurately reflects modern thinking on carbonate sedimentation patterns and is useful for the interpretation of the ancient record. The term *Chlorozoan* is replaced by the *Photozoan Association* indicating shallow, warm-water benthic calcareous communities and emphasizes the light-dependant nature of the bio-assemblage. The term Foramol, inadequate as the combination of two taxa, is replaced by the term *Heterozoan Association* (greek: heteros = other/different). In warm water, the *Heterozoan* Association can be characteristic of environments located beneath the photic zone. Therefore, the *Heterozoan* Association does not necessarily mean the sediments that originate from a cool-water environment, but all cool-water carbonates are always *Heterozoan*.
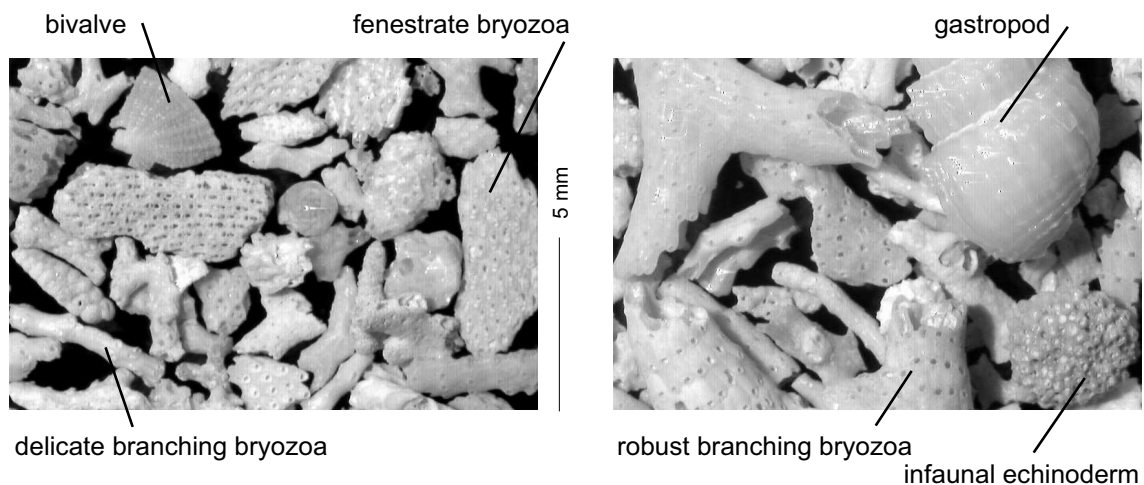


**Figure 2.6.** *Light-microscope photographs of a typical cool-water carbonate assemblage washed over a 355 μm sieve. Note skeletal nature of the coarse fraction and the diverse bryozoan fauna.*

### 2.2.3    Cool-Water Carbonates Versus Tropical Carbonates

Temperature, undoubtedly characterizes the main difference between cool-water and tropical carbonates. However, a number of further factors add to the difference that are briefly discussed below and schematically summarized in Fig. 2.7.

*Temperature.* Lees and Buller (1972) were the first to contrast modern temperate-water and warm-water shelf carbonates. They noted that the water temperature is a significant environmental factor and

estimated a minimum temperature of 14-15°C for the development of temperate-water carbonates. For tropical carbonates and the growth of coral reefs, the widely acknowledged minimum temperature, sustained over a longer period of time, is 18°C (Veron, 1995). A minimum of 14-15°C and a maximum of 18-19°C in temperature range are observed in the Great Australian Bight (Legeckis and Cresswell, 1981).

*Global distribution.* The effect of temperature greatly influences the global distribution of tropical and cool-water or temperate carbonates. Tropical carbonates are classically found in a belt between 30° northern and southern latitude although warm ocean currents (i.e. Eastern Australian Current, Kuroshio, and Gulf Stream) and warm marginal seas (i.e. Red Sea) slightly modify the distribution. Cool-water carbonates are dominantly found beyond 30°, in mid-latitude settings of the subtropics. They are limited polewards by sub-polar carbonates that accumulate in regions of seasonal ice, but their assemblage differs not much from those found in the temperate realms (Heinrich et al., 1997). Cold ocean currents, however, allow for their dispersal equatorward just as warm ocean currents allow for their growth poleward.

*Biologic Assemblage.* The main difference in the bio-assemblage is the lack of hermatypic (reef-building) corals and calcareous green algae in the cool-water carbonate assemblage. Most other organisms are found in both assemblages, although, the amount and species diversity varies (see James, 1997 for further discussion).

*Light.* The typical *Heterozoan Association* is dominated by benthic light-independent organisms, whereas the term *Photozoan Association* emphasizes the light-dependant nature of tropical corals and calcareous green algae.

*Nutrients.* Phototrophic corals with the help of symbionts concentrate and recycle nutrients and, thus, thrive in oligotrophic oceanographic settings (Veron 1995). In contrast, cool-water carbonates are dominantly produced by invertebrate animals, and food supply, therefore, is very important. Furthermore, their mid-to higher latitude location makes them susceptible to seasonal, annual and long-term changes in upwelling, displacement of oceanographic fronts, and surface circulation.

*Architecture.* The light-dependency of tropical and light-independency of cool-water carbonates fundamentally influences the architecture of the carbonate build-up. Coral reefs grow upward to near sea-level, resulting in the classical coral or pinnacle reef structures (e.g. Great Barrier Reef or Great Bahama Bank). Also, the back-reef lagoon on the lee-ward margin is only covered with a few metres of water. In contrast, the cool-water carbonate setting is characterized by a slightly inclined ramp and open shelves with average water depths of 100-150 m as in the case of the GAB.

*Sea-Level Change.* Sea-level rise and fall during interglacial-glacial time periods, respectively, have major consequences on the architecture of the carbonate-build-ups. During sea-level lowstand, the tropical carbonate reef or platform is exposed and the carbonate factory shuts down. The platform is characterized by non-deposition, karstification and/or erosion. In contrast, a ramp-type setting, where the area of carbonate production shifts seaward down the ramp, is generally reduced, but never ceases.

*Carbonate Mineralogy & Diagenesis*. Cool-water carbonates can be distinguished by their calcite mineralogy (Chave, 1967; Nelson et al., 1988). Low- and high-magnesium calcite are the more stable forms of calcite and it is suggested that these sediments remain largely uncemented since they lack aragonite to provide carbonate for cement precipitation (James and Choquette, 1990b). Aragonite and high-magnesium calcite are the dominant precipitates in tropical carbonates, which are is less stable and prone to early diagenetic alteration.

# Cool-Water vs. Tropical Carbonates

## Temperature

accumulate in
waters< 20° C

need growth
temperatures >18° C

## Global Distribution

mid-latitudes
 >30° N & >30° S

tropics,
between 30° N & 30° S

## Bio-assemblages

molluscs
foraminifers
echinoderms
bryozoans
barnacles
ostracods
sponges
serpulids
ahermatyic corals
coralline algae

-> light independent

hermatypic corals*
green algae*
coralline algae
foraminifers*
sponges
serpulids
echinoderms

-> light dependent
*(can) harbour
 photosymbionts

## Margin Morphology

inclined ramp

barrier reef with lagoon

150-200 km wide

~120 km wide

~100-150 m
water depth

~ 7 m
water depth

Great Australian Bight

Great Bahama Bank

## Nutrient Conditions

nutrient-rich
upwelling waters

in oligotrophic
open-ocean settings

## Carbonate Mineralogy & Diagenesis

dominated by
LMC & HMC
-> more stable,
very slow
cementation

dominated by
aragonite & HMC
-> less stable,
early cementation

*Figure 2.7. Schematic comparison of cool-water carbonates vs. tropical carbonates.*

## 2.3   ODP Leg 182

The focus of the Ocean Drilling Program (ODP) on continental margins has largely concentrated on tropical and subtropical carbonate environments. Further, carbonate margin and platform drilling has dominantly occurred in the warm-water realm. With ODP Leg 182, the first deep-sea drilling campaign into the cool-water carbonate sedimentary setting on a continental margin was undertaken. From October through December 1997, a series of 9 sites (Fig. 2.8) in water depths ranging from 200 to 3900 m recovered over 3.5 km of core, representing the first offshore Eocene to modern succession of cool-water carbonates ever drilled.

Due to its pioneering character and unprecedented nature, a wide range of drilling objectives addressed the topics of paleoceanography, carbonate sedimentation models, Southern Ocean sea-level record and the affect of sea-level fluctuation on stratigraphic packaging and early diagenesis, shallow sub-surface fluid flow, and the evolution of mid-latitude oceanic and neritic biotas. Details on the Leg 182 Objectives and Initial results are published in the initial reports Volume of Leg 182 (Feary et al., 2000).
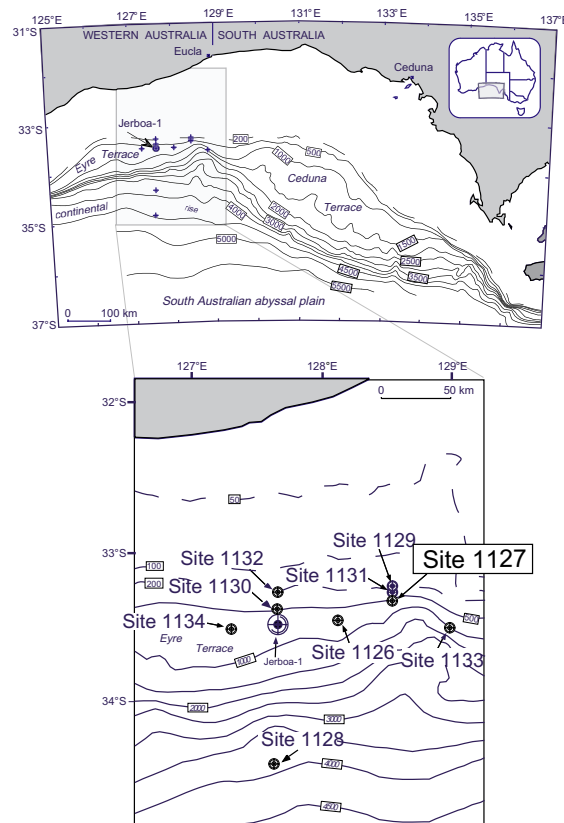


***Figure 2.8.*** *Maps showing the location of ODP Leg 182 drill sites in the western Great Australian Bight region. Site 1127, the focus of this work, is the most seaward site of the Eastern Transect (together with Sites 1131 and 1129). Jerboa-1 is an oil-exploration well drilled in 1980 and provided the only subsurface information up to the drilling of Leg 182. Figure taken from the Leg 182 Scientific Prospectus.*

### 2.3.1   Site 1127 sedimentary archive

ODP Site 1127 was chosen for this work since: 1) the sequence contains well-preserved foraminifera, a prerequisite for the development of an isotope stratigraphy, and 2) the well-recovered, thick sedimentary pile representing high sedimentation rates forms the basis for a high-resolution study. Site 1127 is the most seaward site of a three-site transect (together with Sites 1131 & 1129 forming the E-Transect) through a set of late Neogene clinoforms directly in front of the present-day shelf edge (Fig. 2.8 and 2.9). It is located in 480.6 m water depth. Drilling recovered a total 510.7 m of sediment with an average 95% recovery.

The lithology is dominated by fine-grained, intensely bioturbated, greenish gray bioclastic wackestones to packstones. Calcareous nannofossils and planktonic foraminifera indicate an extraordinarily expanded Pleistocene sequence of more than 450 m, the focus of work in Part III. Both planktonic and benthic foraminiferal assemblages are well preserved, with the latter indicating upper shelf to bathyal origin. The generally temperate-water fauna is accompanied by warm-water species at various intervals, probably reflecting a combination of global climatic fluctuations and regional paleoceanographic variations, especially considering the variable influence of the Leeuwin Current. Biostratigraphic datums indicate average sedimentation rates of 240 m/m.y. Paleomagnetic measurements revealed a long section of normal polarity down to 343.3 mbsf, which was interpreted as the Brunhes magnetic zone. Geochemical analysis of the sediment and pore fluids revealed extraordinarily high concentrations of methane and hydrogen sulfide occurring throughout the Pleistocene succession. Pore fluids are characterized by high salinities. Site 1127 did not only have higher than normal initial organic matter content but the organic material was preserved, probably as a result of the high sedimentation rates. The sediments were slightly disrupted due to the degassing making the physical properties measurements of limited stratigraphic value. Hole conditions, however, were excellent for logging permitting a number of tool strings to be run. The Formation Micro Scanner data show cycles and surfaces, which can be correlated with the conventional logs like gamma ray, sonic and resistivity. Results from Site 1127 are fully discussed in detail in the Initial Reports Volume of Leg 182 (Shipboard Scientific Party 2000).
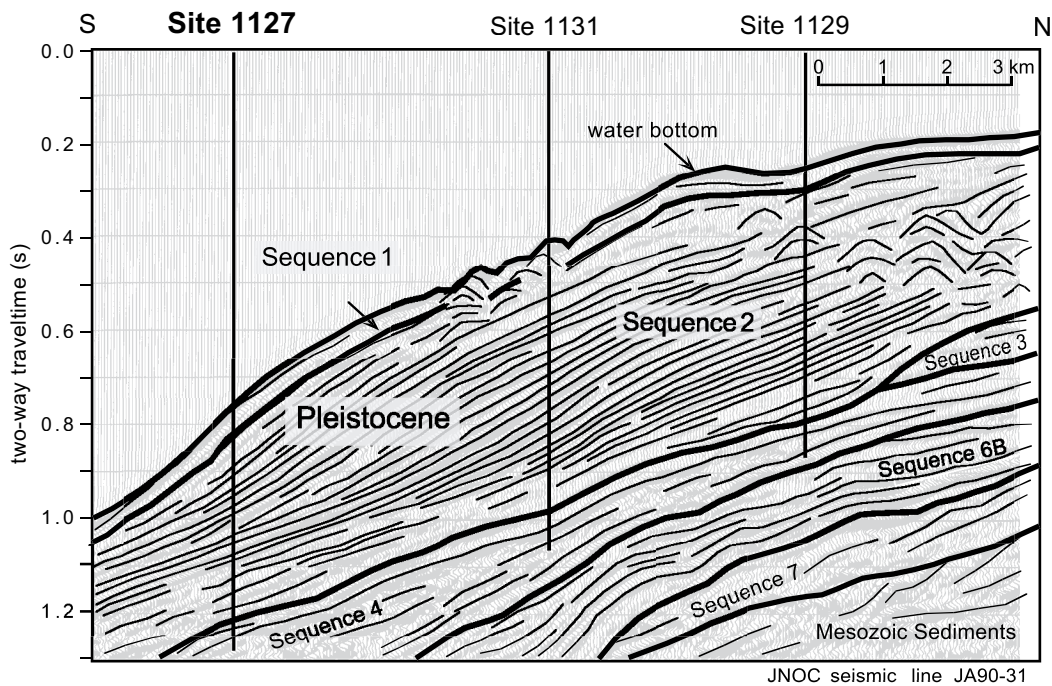
***Figure 2.9.*** *JNOC (Japan National Oil Company) seismic line for the eastern drilling transect, overlain by the three drill sites. Site 1127, located in 480 m of water depth, penetrated through a set of Late Neogene clinoforms just in front of the present-day shelf edge. Drilling recovered a total of 510.7 m of sediment with an average recovery of 95%.*

## References

Almond, D., McGowran, B., and Li, Q. (1993). Late Quaternary Foraminiferal record from the Great Australian Bight and its environmental significance. *Memoir Association Australasian Paleontologist* **15,** 417-428.

Anderson, D. M., Prell, W. L., and Barratt, N. J. (1989). Estimates of sea surface temperature in the coral sea at the last glacial maximum. *Paleoceanography* **4,** 615-627.

Barrows, T. T., Stone, J. O., Fifield, L. K., and Cresswell, R. G. (2001). Late Pleistocene Glaciation of the Kosciuszko Massif, Snowy Mountains, Australia. *Quaternary Research* **55,** 179-189.

Belkin, I. M., and Gordon, A. L. (1996). Souther Ocean Fronts from Greenwich Meridian to Tasmania. *Journal of Geophysics* **101,** 3675-3696.

Belperio, A. P., Harvey, N., and Bourman, R. P. (2002). Spatial and temporal variability in the Holocene sea-level record of the South Australian coastline. *Sedimentary Geology* **150,** 153-169.

Bye, J. A. T. (1971). Variability south of Australia. *In* "Proceedings of the International Science Symposium.", pp. 119-135, Sydney, Australia.

Bye, J. A. T. (1972). Ocean Circulation South of Australia. *In* "Antarctic Oceanology II: The Australian-New Zealand Sector." (D. E. Hays, Ed.), pp. 95-100. A.G.U. Antarctic Research Series. A.G.U. Antarctic Research Series, Washington D.C.

Bye, J. T. (1983). The General Circulation in a Dissipative Basin with Longshore Wind Stresses. *Journal of Physical Oceanography* **13,** 1553-1563.

Caputi, N., Fletcher, W. J., Pearce, A. F., and Chubb, C. F. (1996). Effect of the Leeuwin Current on the recruitment of fish andinvertebrates along the Western Australian coast. Proceedings of the International Larval Fish Conference. *Marine and Freshwater Research* **47,** 147-156.

Chave, K. E. (1967). Recent Carbonate Sediments - An Unconventional View. *American Geological Institute Council on Education in the Geological Sciences, Short Reviews* **7,** 200-204.

Colhoun, E. A., Pola, J. S., Barton, C. E., and Heijnis, H. (1999). Late Pleistocene vegetation and climate history of Lake Selina, western Tasmania. *Quaternary International* **57/58,** 5-23.

Cresswell, G. R., and Golding, T. J. (1980). Observations of a south flowing current in the south-eastern Indian Ocean. *Deep-Sea Research* **27A,** 449-466.

D'Costa, D. M., Edney, P., Kershaw, A. P., and DeDekker, P. (1989). Late Quaternary palaeoecology of Tower Hill, Victoria, Australia. *Journal of Biogeography* **16,** 461-482.

Feary, D. A., Hine, A. C., Malone, M. J., and et al. (2000). Proceedings of the Ocean Drilling Program. *In* "Proceedings of the Ocean Drilling Program, Initial Reports, 182 [CD-ROM]:." (A. C. Hine, D. A. Feary, and M. J. Malone, Eds.), Available from: Ocean Drilling Program, Texas A&M University, College Station , TX 77845-9547, USA.

Feary, D. A., and James, N. P. (1995). Cenozoic biogenic mounds and buried Miocene(?) barrier reef on a predominantly cool-water carbonate continental margin - Eucla basin, western Great Australian Bight. *Geology* **23,** 427-430.

Findlay, C. S., and Flores, J. A. (2000). Subtropical Front fluctuations south of Australia (45 09'S, 146 17'E) for the last 130 ka years based on calcareous nannoplankton. *Marine Micropaleontology* **40,** 403-416.

Fleming, K., Johnston, P., Zwartz, D., Yokoyama, Y., Lambeck, K., and Chappell, J. (1998). Refining the eustatic sea-level curve since the Last Glacial Maximum using far- and intermediate-field sites. *Earth and Planetary Science Letters* **163,** 327-342.

Harle, K. J., Kershaw, A. P., and Heijnis, H. (1999). The contributions of uranium/thorium and marine palynology to the dating of the Lake Wangoom pollen record, western plains of Victoria, Australia. *Quaternary International* **57/58,** 25-34.

Harrison, S. P., and Dodson, J. (1993). Climates of Australia and New Guinea since 18,000 yr B.P. *In* "Global Climates since the Last Glacial Maximum." (J. Wright, J.E., J. E. Kutzbach, T. Webb III, W. F. Ruddiman, F. A. Street-Perrott, and P. J. Bartlein, Eds.), pp. 265-293. University of Minnesota Press, Minneapolis.

Hegarty, K. A., Weissel, J. K., and Mutter, J. C. (1988). Subsidence history of Australia's southern margin: Constraints on basin models. *AAPG Bulletin* **72,** 615-633.

Heinrich, R., Freiwald, A., Bickert, T., and Schäfer, P. (1997). Evolution of an Arctic open-shelf carbonate platform, Spitzbergen Bank (Barents Sea). *Cool-Water Carbonates* **56,** 440.

Herzfeld, M. (1997). The annual cycle of sea surface temperature in the Great Australian Bight. *Progress in Oceanography* **39,** 1-27.

Holbourn, A. E., Kuhnt, W., and James, N. P. (2002). Late Pleistocene isotope stratigraphy and paleoceanography of the Great Australian Bight: The benthic foraminiferal record. *Plaeoceangoraphy*, 14-23.

Hufford, G. E., McCartney, M. S., and Donohue, K. A. (1997). Northern boundary current and adjacent recirculations off southwestern Australia. *Geophysical Research Letters* **24,** 2797-2800.

James, N. P., and Bone, Y. (1994). Paleoecology of Cool-water, Subtidal Cycles in Mid-Cenozoic Limestones, Eucla Platform Southern Australia. *Palaios* **9,** 457-476.

James, N. P., Bone, Y., Collins, L. B., and Kyser, T. K. (2001). Surficial Sediments of the Great Australian Bight: Facies Dynamics and Oceanography on a Vast Cool-Water Carbonate Shelf. *Journal of Sedimentary Research* **71,** 549-567.

James, N. P., Bone, Y., Hageman, S. J., Feary, D. A., and Gostin, V. A. (1997). Cool-water carbonate sedimentation during the terminal Quaternary sea-level cycle: Lincoln Shelf, Southern Australia. *In* "Cool-Water Carbonates." (N. P. James, and J. D. A. Clarke, Eds.), pp. 53-75. S.E.P.M. Special Publication.

James, N. P., Bone, Y., von der Borch, C. C., and Gostin, V. A. (1992). Modern carbonate and terrigenous clastic sediments on a cool water, high energy, mid-latitude shelf: Lacepede, southern Australia. *Sedimentology* **39,** 877-903.

James, N. P., and Choquette, P. W. (1990b). The meteoric diagenetic environment. *In* "Diagenesis." (I. A. McIlreath, and D. W. Morrow, Eds.), pp. 35-74. Geological Association of Canada, St. John's.

James, N. P., and Clarke, J. A. D. (1997). Cool-Water Carbonates. *In* "SEPM Special Publication.", pp. 440. SEPM, Tulsa.

James, N. P., Feary, D. A., Surlyk, F., Simo, J. A. T., Betzler, C., Holburn, A. E., Qianyu, L., Matsuda, H., Machiyama, H., Brooks, G. R., Andres, M. S., Hine, A. C., Malone, M. J., and Party, O. D. P. L. S. (2000). Quaternary bryozoan reef mounds in cool-water, upper slope environments: Great Australian Bight. *Geololy* **28,** 647-650.

Kershaw, A. P. (1995). Environmental change in Greater Australia. *In* "Antiquity: Transitions: Pleistocene to Holocene in Australia and Papua New Guinea." (J. Allen, and J. F. O'Connell, Eds.), pp. 656-675.

Kershaw, A. P., D'Costa, D. M., McEwan Mason, J. R., and Wagstaff, B. E. (1991). Palynological evidence for Quaternary vegetation and environments of mainland southeastern Australia. *Quaternary Science Reviews* **10,** 391-404.

Kershaw, A. P., McEwan Mason, J. R., McKenzie, G. M., Strickland, K. M., and Wagstaff, B. E. (1986). Aspects of the development of cold-adapted flora and vegetation in the Cenozoic of southeastern mainland Australia. *In* "Flora and fauna of alpine Australasia: ages and origins." (B. A. Barlow, Ed.), pp. 147-160. CSIRO, Melbourne.

Kershaw, P., Quilty, P. G., David, B., van Huet, S., and McMinn, A. (2000). Palaeobiogeography of the Quaternary of Australasia. *Memoir of the Association of Australasian Paleontologists* **23,** 471-516.

Kutzbach, J. E. (1986). The influence of changing orbital parameters and surface boundary conditions on climate simulations for the past 18,000 years. *Journal of the Atmospheric Sciences* **43,** 1726-1759.

Lees, A., and Buller, A. T. (1972). Modern temperate-water and warm-water shelf carbonate sediments contrasted. *Marine Geology* **13,** 67-73.

Legeckis, R., and Cresswell, G. R. (1981). Satellite observations of sea-surface temperature fronts off the coast of western and southern Australia. *Deep-Sea Research* **28A,** 297-306.

Li, Q., James, N. P., Bone, Y., and McGowran, B. (1999). Paleoceanographic significance of recent foraminiferal biofacies on the southern shelf of Western Australia: a preliminary study. *Paleogeography, Paleoclimatology, Paleoecology* **147,** 101-120.

Li, Q., McGowran, B., James, N. P., Bone, Y., and Cann, J. H. (1996). Mixed Foraminiferal Biofacies on the Mesotrophic, Mid-Latitude Lacepede Shelf, South Australia. *Palaios* **11,** 176-191.

Markgraf, V. (1987). Paleoenvironmental changes at the northern limit of the subantarctic Nothofacgus forest, lat 37°S, Argentina. *Quaternary Research* **28,** 119-129.

Maxwell, J. G. H., and Cresswell, G. R. (1981). Dispersal of tropical marine fauna to the Great Australian Bight by the Leeuwin Current. *Australian Journal of Marine Freshwater Research* **32,** 493-500.

McGowan, H. A., McTainsh, G. H., Zawar-Reza, P., and Sturman, A. P. (2000). Identifying regional dust transport pathways: application of kinematic trajectory modelling to a trans-Tasman case. *Earth Surface Processes and Landforms* **25,** 633-647.

McGowran, B., and al., e. (1997). Biogeographic impact of the Leeuwin Current in southern Australia since the late middle Eocene. *Paleogeography, Paleoclimatology, Paleoecology* **136,** 19-40.

McTainsh, G. H. (1989). Quaternary aeolian dust processes and sediments in the Australian region. *Quaternary Science Reviews* **8,** 235-253.

McTainsh, G. H., and Lynch, A. W. (1996). Quatitative estimates of the effect of climate change on dust storm activity in Australia during the Last Glacial Maximum. *Geomorphology* **17,** 263-271.

Middleton, J. F., and Cirano, M. (2002). A boundary Current Along Australian's Southern Shelves: the Flinders Current. *Journal of Geophysical  Research* **submitted**.

Miller, G. H., Magee, J. W., and Jull, A. J. T. (1997). Low-latitude glacial cooling in the Southern Hemisphere from amino-acid racemization in emu eggshells. *Nature* **385,** 241-244.

Murray-Wallace, C. V., and Belperio, A. P. (1991). The last interglacial shoreline in Australia - a review. *Quaternary Science Reviews* **10,** 441-461.

Nelson, C. S., Hyden, F. M., Keane, S. L., Leask, W. L., and Gordon, D. P. (1988). Application of bryozoan zoarial growth-form studies in facies analysis of non-tropical carbonate deposits in New Zealand. *Sedimentary Geology* **60,** 301-322.

Nicholls, N. (1992). Historical El Niño/Southern Oscillation variability in the Australasian region. *In* "El Niño: Historical and Paleoclimatic Aspects of the Southern Oscillation." (H. F. Diaz, and V. Markgraf, Eds.), pp. 151-173. Cambridge University Press, Cambridge.

Patterson, S., and Whitworth, I. T. (1990). Physical Oceanography. *In* "Antarctic Sector of the Pacific Ocean.", pp. 55-93. Elsevier, New York.

Pearce, A. F., and Phillips, B. F. (1988). ENSO events, the Leeuwin Current and larval recruitment of the Western Rock Lobster. *Journal du Conseil* **45,** 13-21.

Pearce, A. F., and Walker, D. I. (1991). The Leeuwin Current: an influence on the coastal climate and marine life of Western Australia. *In* "Journal of the Royal Society of Western Australia.", Perth, Western Australia.

Pickard, G. L., and Emery, W. J. (1990). "Descriptive physical oceanography: an introduction." Butterworth-Heinemann, Oxford.

Pittock, A. B. (1973). Global meridional interactions in stratosphere and troposphere. *Quaterly Journal of the Royal Meteorological Society* **99,** 424-437.

Rochford, D. J. (1984). Effect of the Leeuwin Current upon Sea Surface Temperatures off South-western Australia. *Australian Journal of Marine and Freshwater Research* **35,** 487-489.

Rochford, D. J. (1986). Seasonal Changes in the Distribution of Leeuwin Current Waters off Southern Australia. *Australian Journal of Marine and Freshwater Research* **37,** 1-10.

Rognon, P., and Williams, M. A. J. (1977). Late Quaternary climatic changes in Australia and North Africa: A preliminary interpretation. *Palaeogeoraphy, Palaeoclimatology, Palaeoecology* **21,** 285-327.

Schodlok, M., Tomczak, M., and White, N. (1997). Deep sections through the South Australian Basin and across the Australian-Antarctic Discordance. *Geophysical Research Letters* **24,** 2785-2788.

Schulmeister, J. (1999). Australasian evidence fro mid-holocene climate change implies precession control of Walker Circulation in the Pacific. *Quaternary International* **57/58,** 81-91.

Schulmeister, J., and Lees, B. G. (1995). Pollen evidence from tropical Australia for the onset of an ENSO-dominated climate at c. 4000 BP. *The Holocene* **5,** 10-18.

Shipboard Scientific Party. (2000). Site 1127, Proceedings of the Ocean Drilling Program. *In* "Proceedings of the Ocean Drilling Program, Initial Reports, 182 [CD-ROM]:." (D. A. Feary, A. C. Hine, M. J. Malone, and et al, Eds.), Available from: Ocean Drilling Program, Texas A&M University, College Station , TX 77845-9547, USA.

Short, A. D., and Hesp, P. A. (1982). Wave, beach and dune interactions in southeastern South Australia. *Marine Geology* **48,** 259-284.

Specht, R. L. (1969). A comparison of tthe sclerophyllous vegetation characteristic of Mediterranean type climates of France, California, and southern Australia. I. Structure, morphology, and succession. *Australian Journal of Botany* **17,** 227-292.

Thiede, J. (1979). Wind regimes over the late Quaternary southwest Pacific ocean. *Geology* **7,** 259-262.

Thunell, R. C., Anderson, D., Gellar, D., and Miao, Q. (1994). Sea-Surface Temperature Estimates for the Tropical Western Pacific during the Last Glaciation and Their Implications for the Pacific Warm Pool. *Quaternary Research* **41,** 255-264.

Tomczak, M., and Godfrey, S. J. (1994). "Regional Oceanography: An Introduction." Pergamon, Oxford.

Veron, J. E. N. (1995). "Corals in space and time." UNSW Press, Sydney.

Wagstaff, B. E., Kershaw, A. P., O'Sullivan, P. B., Harle, K. J., and Edwards, J. (2001). An Early to Middle Pleistocene palynological record from the volcanic crater of Pejark Marsh, Western Plains of Victoria, southeastern Australia. *Quaternary International* **83-85,** 211-232.

Wasson, R. J. (1984). Late Quaternary palaeoenvironments in the desert dunefields of Australia. *In* "Late Cainozoic Palaeoclimates of the Southern Hemisphere." (J. C. Vogel, Ed.), pp. 419-432. Balkema, Rotterdam.

Wasson, R. J. (1986). Geomorphology and Quaternary history of the Australian continental dunefields. *Geographical Review of Japan* **59,** 55-67.

Whetton, P. (1997). Floods, droughts and the Southern Oscillation. *In* "Windows on Meteorology: Australian Perspective." (E. K. Webb, Ed.), pp. 180-199. CSIRO Publishing, Australia.

Yokoyama, Y., Lambeck, K., DeDekker, P., Johnston, P., and Fifield, L. K. (2000). Timing of the Last Glacial Maximum from observed sea-level minima. *Nature* **406,** 713-716.

Zheng, H., Powell, C. M., and Zhao, H. (2002). Eolian and lacustrine evidence of late Quaternary palaeoenvironmental changes in southwestern Australia. *Global and Planetary Change* **744,** in press.

# 3  METHODS

Marine sediments contain abundant information for the reconstruction of ocean and climate history. The measurement of the isotopic composition of marine microfossils in sedimentary sequences is a well-established, standard method in paleo-studies and plays a central part in the presented work. Isotopes, however, are only one way of studying oceanographic and/or climatic change. A number of different methods were used in the thesis with the initial aim of strengthening the isotopic evidence, but the data often complicated or even contradicted the initial hypothesis. Nevertheless, I believe that only a combination of different and preferably independent methods analyzing the chemical, physical and biological signal allows one to fundamentally assess environmental change. This integrated and multiproxy approach not only forces us to think about influencing and controlling factors producing a given signal but potentially tells us something about the cause and trigger of change through time. The following chapter gives an overview and shortly discusses the methods used in the thesis.

## 3.1  Drilling Procedures & Sample Preparation

### 3.1.1  ODP Drilling and Sampling

The studied Site (Site 1127) was triple cored using the advanced hydraulic piston corer and extended core barrel corer to recover the sedimentary sequence. Cores were handled and samples taken onboard the JOIDES Resolution according to standard ODP procedures. Sample density was increased in specific intervals by additional post-cruise sampling at the ODP Gulf Coast Repository, where Leg 182 cores are stored.

### 3.1.2  Sample Handling

Sediment samples (~15 cc) were treated as follows: a small amount was separated, oven-dried (30°C) and homogenized for bulk sediment analysis. The remainder was dried and weighed, after which a small amount was set aside to be used for the fine fraction aliquot. The remainder was washed over a 63μm sieve, dried and weighed once again. Additionally, samples taken at 3-4 m intervals in the core were washed over a 38μm sieve, and the 38-63 μm fraction dried and weighed. For fine fraction (<38 μm) analysis, the small amount set aside was washed over a 38 μm sieve and the fine fraction collected beneath, sonicated and filtered over a 0.45 μm membrane filter and dried.

## 3.2  Studied Foraminifera

Planktonic and benthic foraminifera were primarily studied for their carbon and oxygen isotopic signature and only semi-quantitatively for their faunistic and ecological information. Further, planktonic foraminifera were used for absolute ^{14}C-AMS dating in the upper 30 m of the core and for their stratigraphic value in the remainder of the core.

### 3.2.1    Planktonic Foraminifera

Planktonic foraminifera dwell in the near-surface to intermediate waters of the ocean. Their oxygen isotopic composition reflects equilibrium at these varying water depths and their carbon isotopic composition is controlled by insitu productivity and respiration. Before calculating temperatures, the oxygen isotope value is corrected by the "oxygen isotope disequilibrium" which is different for every species. The studied planktonic foraminifera are illustrated in light-microscope photographs shown in Plate 1.

### *Globerinoides ruber*

The planktonic foraminiferal species *Globigerinoides ruber* (white variety) (d'Orbigny, 1839), thriving close to the sea surface, has been widely used for paleoceanographic reconstructions in tropical, subtropical and temperate latitudes. *G. ruber* has been identified as being frequent to common in the Eucla area of the GAB (Li et al., 1999; Li et al., 1996) and found throughout the core from Site 1127. Although known to migrate within or below the surface mixed layer, its surface origin in the upper 40 m of the water column makes it an ideal species to estimate surface-water carbon and oxygen isotopic values. For the calculation of sea-surface temperatures, the oxygen isotope values were corrected by a mean "oxygen isotope disequilibrium" of –0.5‰ (Niebler et al., 1999).

### *Globigerina bulloides*

The second investigated species, *Globigerina bulloides* (d'Orbigny, 1826), when occurring in abundance, characterizes upwelling settings regardless of its geographical position. It is a typical transitional species, tolerating a wide range of temperatures, from the temperate mid-latitudes to polar regions and occurring in abundance within these waters (Bé and Gilmer, 1977). For the subtropical and transitional parts of the oceans, its depth preference lies in the upper 80 m of the water column (Schiebel et al., 1997) making it useful for the reconstruction of surface water conditions. *G. bulloides* is frequent to abundant throughout the core from Site 1127. A mean "oxygen isotope disequilibrium" of +0.5‰ (Niebler et al., 1999) was used.

### *Globorotalia inflata*

*G. inflata* calcifies in a water depth between about 100 and 300 m water depth and shows a wide geographical distribution from the Subtropical Gyre to the Antarctic Zone in the Southern Hemisphere (Niebler et al., 1999). It is the dominant planktonic foraminiferal species in the Site 1127 core and allows for monospecific AMS radiocarbon dating.  Between 410 and 760 individuals were picked from the 255 to 355 µm size fraction for analysis.

*G. ruber*
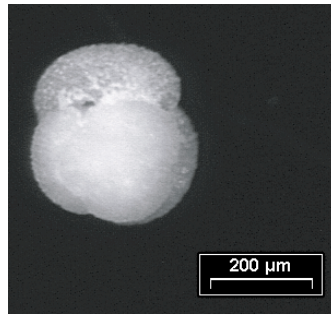


spiral side
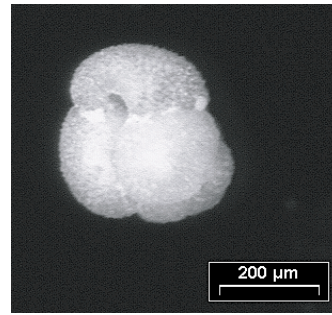
umbilical side
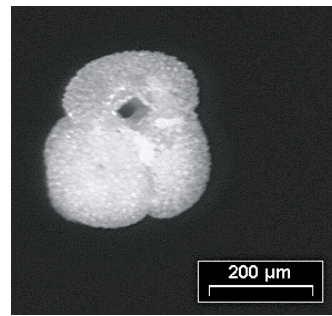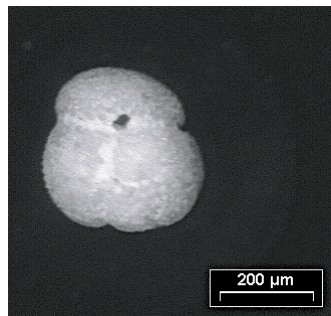


*G. bulloides*
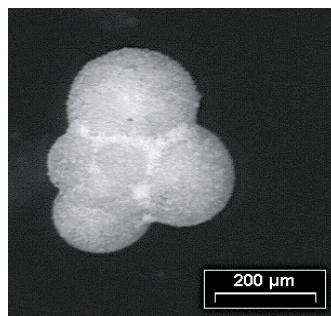


spiral side
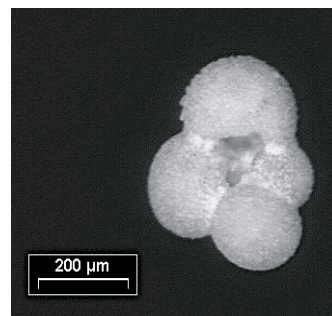
umbilical side

*G. inflata*
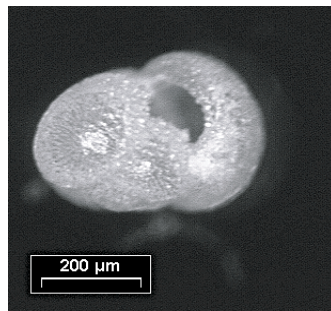


spiral side
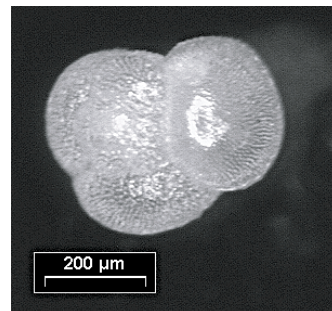
umbilical side

**Plate 3.1.** *Light-microscope photographs of typical planktonic foraminifera found in the Site 1127 sediments.*

## 3.2.2    Benthic Foraminifera

The isotopic signal of benthic foraminifera is not only the basis for Pleistocene oxygen isotope stratigraphy (Shackleton and Opdyke, 1973), but it also serves as a useful tracer of bottom water ventilation. Benthic foraminifera are a well-established proxy indicator for paleoproductivity and carbon-flux to the bottom environment (Jorissen and Rohling, 2000). The studied benthic foraminifera are illustrated in light-microscope photographs shown in Plate 2 and 3.

### *Fontbotia wuellerstorfi & Cibicidoides spp.*

*Cibicidoides wuellerstorfi* (Schwager 1866), now assigned to *Fontbotia wuellerstorfi* (Loeblich and Tappan, 1988), is described as a sessile epifaunal foraminifera and prefers hard substrates in bathyal to abyssal regions (Altenbach et al., 1999; Murray, 1986). Species of the Cibicides/Cibicidoides group live on the shelf to bathyal depths and occupy epifaunal to deep infaunal habitats (Corliss, 1991; Schiebel, 1992). Due to their epifaunal way of life, *F. wuellerstorfi* is considered free from the effects of pore-water isotopic variations. It is known to precipitate its calcite tests out of isotopic equilibrium with seawater and several authors have suggested correction factors (Graham et al., 1981; Murray, 1986). *F. wuellerstorfi* is considered to require only minor adjustment factors ($^{18}O$= 0.64‰, $^{13}C$=0.0‰) (Shackleton and Hall, 1984). Not all samples contain sufficient individuals of both *F. wuellerstorfi* and *Cibicidoides* spp for more specific analysis. They were, however, separately analyzed for their oxygen and carbon isotope compositions and compared wherever possible.

### *Uvigerina spp.*

The *Uvigerina* group consists of mainly infaunal, some epifaunal, free-living benthic foraminifera. They prefer muddy sediment and occur from shelf to bathyal regions (Lutze, 1986). When living in the sediment they, therefore, reflect the conditions of the pore water rather than the true bottom water. The pore waters are strongly influenced by the sedimentation of organic substance and the carbon isotopes used to reconstruct productivity changes. For their isotopic composition, Shackleton (1974) concluded that at temperatures above 7°C *Uvigerina* spp. secrete their tests in oxygen equilibrium with seawater in which they live. Uvigerina spp. were not present in all samples.

*F. wuellerstorfi*
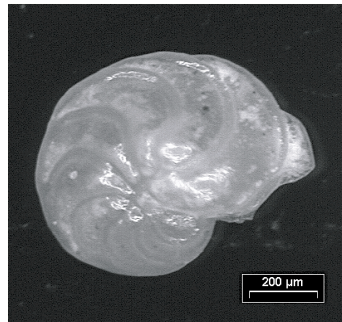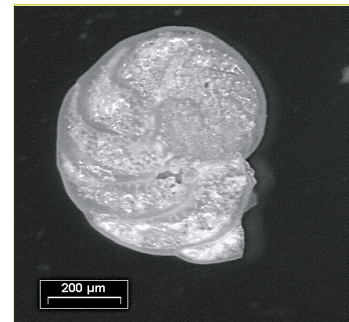


spiral side                                  umbilical side

*F. wuellerstorfi* cf.
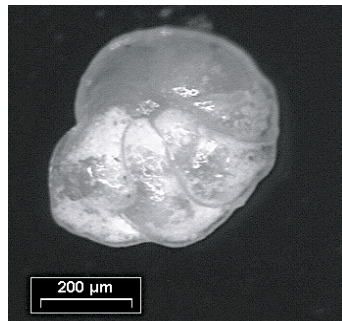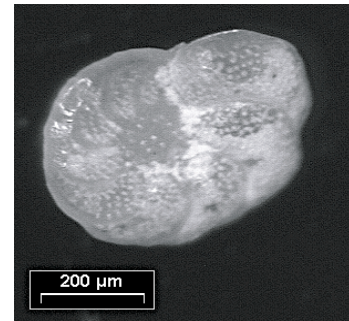


spiral side                                  umbilical side
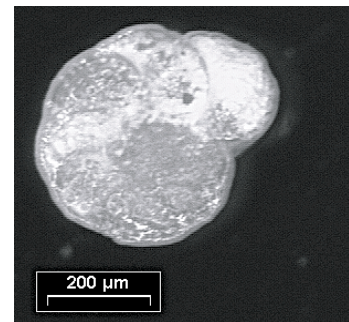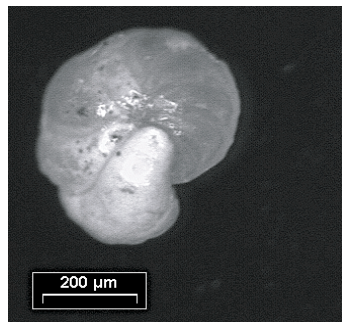


Pteropod:
*Clio convexa*
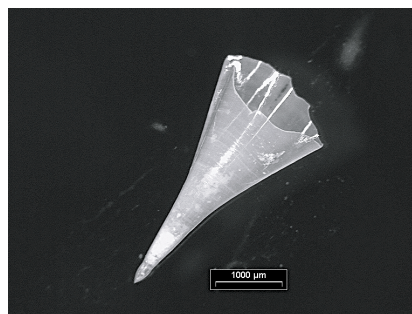


**Plate 3.2.** *Light-microscope photographs of typical benthic foraminifera and pteropods found in the Site 1127 sediments.*

## 3.3   Isotopic Analysis

### 3.3.1   Oxygen and Carbon Isotopes

All benthic and planktonic foraminifera used for stable isotopic analyses were picked from the 250-355 μm fraction. They were ultrasonically cleaned in order to remove contamination, especially of calcaraeous coccoliths and/or diagenetic overgrowths. Foraminifera picked from Site 1127B show only minor alterations up to a depth of ~350 mbsf and the continued presence of aragonitic pteropods (Plate 2) in sediments deposited during glacial intervals support this observation. Preservation decreases downcore, however, and only individuals with minor overgrowth were picked for analysis If ultrasonic treatment did not remove signs of alterations, they were discarded.

For the isotopic analysis of bulk and fine fraction, samples of approximately 0.5 mg were used. For the analysis of foraminifera, an average of 15-20 planktonic and 3-5 benthic foraminifera were placed in a metal beaker and crushed in methanol. The samples were reacted at 90°C with 100% phosphoric acid in a common acid bath according to the following reaction:

$$2H_3PO_4 + 3CaCO_3 \Leftrightarrow Ca_3(PO_4)_2 + 3H2O_{(g)} + 3CO_2$$
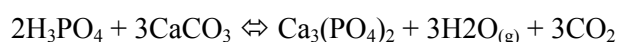
Water produced during the reaction was separated by freezing using a cold trap held at -90°C. The carbon and oxygen isotopic composition of the evolving $CO_2$-gas was then analyzed in the dual inlet VG Precision Isotope Ratio Mass Spectrometer (PRISM) at the Geological Institute, ETH Zurich, Switzerland. Isotopic compositions are expressed in the common δ notation:

$$\delta_{sample} = \{(R_{sample}/R_{standard})-1\} \times 1000$$

where R is the stable isotope ratio of the heavy to the light isotope:

$$R = {}^{18}O/{}^{16}O \text{ or } {}^{13}C/{}^{12}C$$

The isotope ratio is measured relative to the Vienna Pee Dee Belemnite carbonate standard (VPDB) and expressed in permil deviation from the standard. Instrument accuracy, as referred to an internal carbonate standard, is 0.08 ± 0.03‰ (1σ) for $\delta^{18}O$ and 0.06 ± 0.03‰ (1σ) for $\delta^{13}C$. About ten standards were measured during each run of 30 samples to determine precision for replicate analysis. Bulk and fine fraction $\delta^{18}O$ and $\delta^{13}C$ are given in Table 7.1 of Chapter 7, whereas $\delta^{18}O$ and $\delta^{13}C$ of planktonic and benthic foraminifera can be found in Appendix A1.

### 3.3.2   Nitrogen Isotopes

For nitrogen isotope analysis, approximately 30 mg of homogenized bulk sediment sample was filled into tin capsules and combusted at 1040°C in an elemental analyser (Carlo Erba NCS 2500) coupled in

continuous flow with a mass spectrometer (Fisons Optima) with standard set-up for $N_2$ gas. The large amount of $CO_2$ produced was diluted away. Isotope ratios are expressed in the common δ notation as described in section 3.3.1, where

$$R = {}^{15}N/{}^{14}N$$

The isotope ratio is expressed in permil deviations vs. atmospheric Nitrogen (AIR). Instrumental precision based on the repeated anlyses of standards $(NH_4)_2SO_4$, IAEA-N1 and IAEA-N2 is generally better 0.6‰. The data are found in Appendix A2.

## 3.4   Coulometric Analysis

Total carbon (TC) and total inorganic carbon (TIC) were measured with an UIC, Inc.™ coulometer system. For the TC-measurement, the samples were combusted at 950ºC to convert all form of carbon into $CO_2$, which was subsequently measured in the coulometer. The samples for the TIC analysis were treated with 2N $HClO_4$ to release the $CO_2$ from any carbonate minerals. Due to the slow dissolution reaction, the samples were heated during the treatment. Total organic carbon content (TOC, wt%) was calculated as difference between TC and TIC. The measurement is presented as weight % carbonate, assuming all carbonate was precipitated in the form of calcite. Data can be found in Appendix A3.

## 3.5   XRD Analysis

X-ray diffraction (XRD) measurements were performed to determine the relative percentages of high-magnesium calcite, low-magnesium calcite, aragonite, dolomite and quartz. Analytical procedures are discussed in the Explanatory Notes Chapter of the Initial Reports Volume (Feary et al., 2000). All XRD data presented here are shipboard data reported in the Proceedings of the ODP: Initial Reports Volume 182 (Feary et al., 2000).

## 3.6   NGR Logging

The Natural Gamma Radiation tool (NGR) detects the natural radioactivity of the formation. Most gamma radiation is emitted by the radioactive isotope ${}^{40}K$ and by radioactive elements in the U and Th series. Natural Gamma Radiation measurements were recorded with the Multisensor track tool (see Explanatory notes in (Feary et al., 2000) for more details). Shipboard data presented herein can be found in the Proceedings of the ODP: Initial Reports Volume 182 (Feary et al., 2000). NGR was measured every 16 cm for a 26-second period and units are in counts per second (cps). Data were smoothed using a 5-point moving average.

## 3.7   XRF Analysis

The relative abundance of seven chemical elements (K, Ca, Ti, Mn, Fe, Cu, Sr) was measured on the surface of the archive half of the core, using the X-ray fluorescence (XRF) core scanner at Bremen University (Jansen et al., 1998; Röhl and Abrams, 2000). The method is non-destructive and can, therefore, be applied to the fully intact and unsampled archive half of split sediment cores. The XRF data was collected at 1 cm intervals over a 1 $cm^3$ and 30-second count time in the upper 34.4 m of core. The data interval is increased to 1 cm from 7.43 to 8.79 mbsf. Standards with known elemental compositon are measured in regular intervals as controls. Data can be found in Appendix A4.

## 3.8   Radiocarbon Dating

Accelerator mass spectrometry (AMS) radiocarbon dating was performed on monospecific planktonic foraminifera *G. inflata* samples. Between 410 and 760 individuals were picked from the 255 to 355μm size fraction and sonicated in alcohol prior to analysis. The chemically treated samples were combusted to to $CO_2$ and the gas reduced to graphite powder. Samples were analyzed at the Swiss Federal Institute of Technology AMS Facility, ETH-Zurich (Bonani et al., 1987). Samples ranging from 0 to 24,000 years have been calibrated using the program CALIB HTML version 4.3 (http://radiocarbon.pa.qub.ac.uk/calib/) and the marine calibration dataset MARINE 98 (Stuiver and Braziunas, 1993; Stuiver et al., 1998a). The local effects, the difference ΔR (Stuiver and Braziunas, 1993) in reservoir age of the local region and the model ocean, is on average 61 ± 29 years for the GAB region (Reimer and Reimer, 2001). Samples older than 24,000 years were calibrated using the equation published by Bard (1998):

Age (cal years BP) $= -3.0126 \times 10^{-6} \times$ (Age $^{14}$C years BP)$^2$ + 1.2896 x (Age 14C years BP) – 1005

Sample information, radiocarbon dates and calibration are summarized in Table 3.1.

**Table 3.1    Radiocarbon Dates**

| Sample ID | Lab Code | Core depth (mbsf) | Weight of sample (mg CaCO$_3$) | $^{14}$C AMS Age ($^{14}$C yrs BP) | Calibrated Age (2σ, max-min range, yrs BP) | Intercepts used in Age Model (yrs BP) | Remarks |
|---|---|---|---|---|---|---|---|
| 1H-2 2-6 | ETH-24288 | 0.02 | 15.45 | 1,295 ± 55 | 913 - 657 | 760 | a, core top sample |
| 1H-2 50-55 | ETH-23893 | 2.00 | 15.3 | 6,385 ± 65 | 6,949 - 6,625 | 6,760 | a |
| 1H-3 72-75 | ETH-24289 | 3.72 | 9.54 | 8,135 ± 75 | 8,849 - 8,363 | 8,530 | a |
| 2H-1 100-103 | ETH-24364 | 6.90 | 8.95 | 9,515 ± 110 | 10,581 - 9,717 | 10,260 | a |
| 2H-2 2-7 | ETH-24363 | 7.42 | 8.95 | 9,875 ± 90 | 11,148 - 10,244 | 10,590 | a |
| 2H-2 50-55 | ETH-23922 | 7.90 | 8.5 | 10,135 ± 105 | 11,601 - 10,360 | 11,080 | a, term. YDC |
| 2H-2 101-107 | ETH-23892 | 8.41 | 14.03 | 10,930 ± 90 | 12,881 - 11,498 | 12,330 | a, onset YDC |
| 2H-2 115-119 | ETH-25860 | 8.55 | 12.66 | 11,340 ± 85 | 13,741 - 12,417 | 12,880 | a |
| 2H-2 135-139 | ETH-25861 | 8.75 | 13.68 | 11,750 ± 85 | 13,777 - 12,974 | 13,160 | a |
| 2H-3 50-55 | ETH-24290 | 9.40 | 17.18 | 14,420 ± 95 | 17,162 - 16,133 | 16,630 | a |
| 2H-3 65-69 | ETH-25862 | 9.55 | 16.97 | 14,920 ± 85 | 17,758 - 16,698 | 17,200 | a |
| 2H-3 101-106 | ETH-24355 | 9.91 | 26.5 | 24,630 ± 180 | 28,930 | | b |
| 2H-5 25-30 | ETH-24291 | 12.15 | 10.8 | 35,150 ± 480 | 40,600 | | b |
| 2H-7 3-9 | ETH-24356 | 14.93 | 12.3 | 46,180 ± 1,500 | | | c, age reversal |
| 3H-1 110-115 | ETH-24357 | 16.50 | 14.1 | 50,220 ± 2,489 | | | c, age reversal |
| 3H-5 3-8 | ETH-24362 | 21.43 | 10.6 | 41,820 ± 1,080 | 47,660 | | b |
| 4H-5 60-65 | ETH-24358 | 30.43 | 9.7 | 45,750 ± 1,560 | (51,690) | | d |

Radiocarbon dates from Site 1127, Great Australian Bight. All dates are based on monospecific samples of planktonic foraminifera *G. inflata* (>150 µm)

a: ages calibrated using CALIB program html version 4.3

b: ages calibrated using the equation of Bard (1998)

c: age reversal: data not used in age model; large sample size, high sand-fraction percentage may indicate reworking and/or mass sediment transport

d: tentative calibration

## 3.9    Sedimentation and Mass Accumulation Rates

Sedimentation rates were calculated by assuming constant sedimentation between dated horizons for the upper part of the core and between tie-points (isotopic events) of correlation with the SPECMAP time scale.

Mass accumulation rates (MAR) of bulk sediment were calculated from sedimentation rates (SR) and dry bulk density (DBD) as follows:

$$\text{MAR (g cm}^{-2}\text{ ka}^{-1}) = \text{SR (cm ka}^{-1}) \times \text{DBD (g cm}^{-3})$$

Accumulation (AR) rates for separate sediment components were calculated by multiplying its concentration (wt %) with the bulk sediment MAR:

$$\text{AR}_{component} = [\text{component}] \times \text{MAR}$$

Dry bulk density data was taken from shipboard analysis (Feary et al., 2000).

## 3.10   Age Model

Age models were developed by linearly interpolating and assuming constants sedimentation rates between dated, in the case of radiocarbon dates, or correlated, in the case of the oxygen isotope stratigraphy. The first age model is based on calibrated $^{14}$C AMS dates (Table 3.1) and the age-depth relationship plotted in Figure 3.1. The second age model (Fig. 3.2) is based on the oxygen isotopes from bulk, fine fraction, and planktonic foraminifera in correlation to the SPECMAP curve (Imbrie et al., 1984). The shipboard-identified Brunhes/Matuyama boundary (B/M) is used as basal tie-point. Further magnetostragigraphic datums (Fuller et al., 2001) and the last occurrence of the pink variety of *G. ruber* (Thompson et al., 1979) are added.  The age model based solely on the oxygen isotope stratigraphy from bulk and fine fraction data is presented in Table 7.2 of Chapter 7.
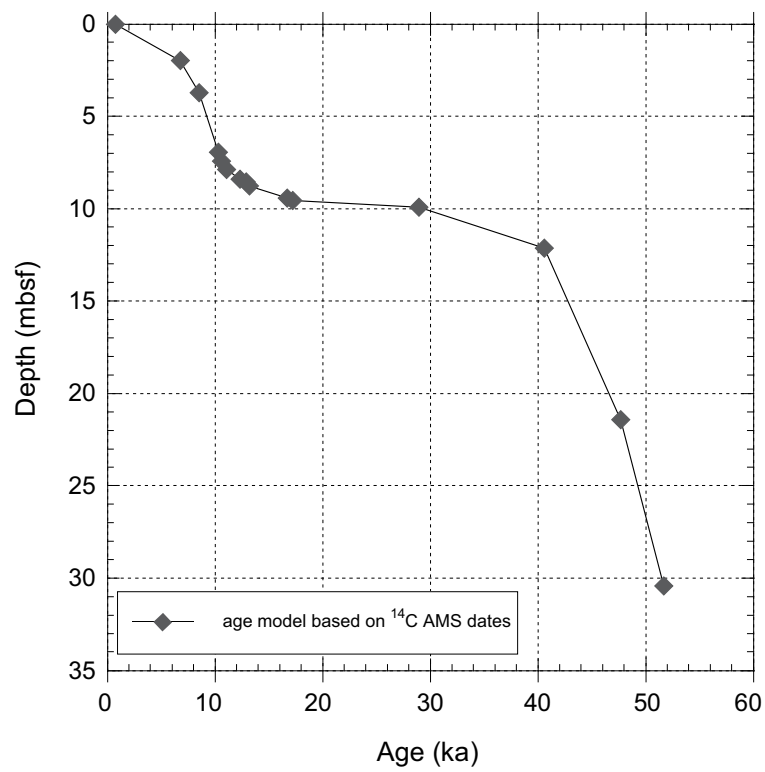
**Figure 3.1.** *Age model for the last 50 ka based on calibrated $^{14}$C-AMS dates.*
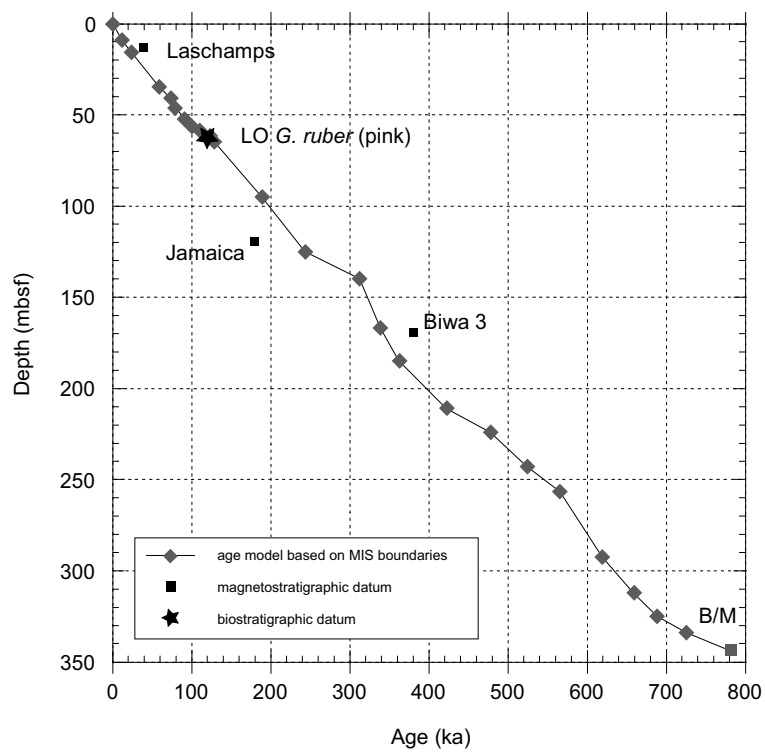


**Figure 3.2.** *Age model for the Late Pleistocene based on correlation to the SPECMAP time scale (Imbrie et al. 1984).*

# References

Altenbach, A. V., Pflaumann, U., Schiebel, R., Thies, A., Timm, S., and Trauth, M. (1999). Scaling Percentages and Distributional Patterns of Benthic Foraminifera with Flux Rates of Organic Carbon. *Journal of Foraminiferal Research* **29,** 173-185.

Bard, E. (1998). Geochemical and geophysical implications of the radiocarbon calibration. *Geochimica et Cosmochimica Acta* **62,** 2025-2038.

Bé, A. W. H., and Gilmer, R. W. (1977). An ecological, zoogeographic and taxonomic review of recent planktonic foraminifera. *In* "Oceanic Micropaleontology." (A. T. S. Ramsey, Ed.), pp. 1-100. Academic Press, New York.

Bonani, G., Beer, J., Hofmann, H., Sunal, H. A., Suter, M., Wölfi, W., Pfleiderer, C., Junghans, C., and Münnich, K. O. (1987). Fractionation, precision and accuracy in $^{14}$C and $^{13}$C measurements. *Nuclear Instruments and Methods in Physics Research* **B29,** 87-90.

Corliss, B. H. (1991). Morphology and microhabitat preferences of benthic foraminifera from the northwest Atlantic Ocean. *Marine Micropaleontology* **17,** 195-236.

d'Orbigny, A. D. (1826). Tableau méthodique de la classe des Cephalopodes. *Annales des Sciences Naturelles* **7,** 96-169, 245-314.

d'Orbigny, A. D. (1839). Voyage dans l'Amérique Méridionale. *In* "Foraminifères." (P.Bertrand, Ed.), Strasbourg.

Feary, D. A., Hine, A. C., Malone, M. J., and et al. (2000). Proceedings of the Ocean Drilling Program. *In* "Proceedings of the Ocean Drilling Program, Initial Reports, 182 [CD-ROM]:." (A. C. Hine, D. A. Feary, and M. J. Malone, Eds.), Available from: Ocean Drilling Program, Texas A&M University, College Station , TX 77845-9547, USA.

Fuller, M., Molina-Garza, R., Antretter, M., and Lichowski, F. (2001). Magnetostratigraphy of the Plio-Pleistocene Carbonate Section of the Great Australian Bight:. *Bulletin GSA Australia (submitted)*.

Graham, D. W., Corliss, B. H., Bender, M. L., and Keigwin, L. D. (1981). Carbon and oxygen isotopic disequilibria of recent deep-sea benthic foraminifera. *Marine Micropaleontology* **6,** 483-497.

Imbrie, J., Hays, J. D., Martinson, D. G., McIntyre, A., Mix, A. C., Morley, J. J., Pisias, N. G., Prell, W. L., and Shackleton, N. J. (1984). The orbital theory of Pleistocene climate: support from a revised chronology of the marine d18O record. *In* "Milankovitch and Climate, Part 1." (A. J. Berger, J. Imbrie, J. D. Hays, G. Kukla, and B. Saltzman, Eds.), pp. 269-305. Dordrecht: Riedel Publishing Co.

Jansen, J. H. F., Van der Gaast, S. J., Koster, B., and Vaars, A. J. (1998). CORTEX, a shipboard XRF-scanner for element analyses in split sediment cores. *Marine Geology* **151,** 143-153.

Jorissen, F. J., and Rohling, E. J. (2000). Foraminiferal proxies of paleoproductivity. *In* "Special Issue of Marine Micropaleontology.", pp. 131-344.

Li, Q., James, N. P., Bone, Y., and McGowran, B. (1999). Paleoceanographic significance of recent foraminiferal biofacies on the southern shelf of Western Australia: a preliminary study. *Paleogeography, Paleoclimatology, Paleoecology* **147,** 101-120.

Li, Q., McGowran, B., James, N. P., Bone, Y., and Cann, J. H. (1996). Mixed Foraminiferal Biofacies on the Mesotrophic, Mid-Latitude Lacepede Shelf, South Australia. *Palaios* **11,** 176-191.

Loeblich, A. R., Jr., and Tappan, H. (1988). "Foraminiferal genera and their classification." Van Norstrand Rheinhold Company, New York.

Lutze, G. F. (1986). Uvigerina species of the Eastern North Atlantic. *In* "Atlantic-Europena Oligocene to Recnet Uvigerina." (G. J. v. d. Zwaan, F. J. Jorissen, P. J. J. M. Verhallen, and C. H. v. Daniels, Eds.), pp. 21-46. Utrecht Micopaleontological Bulletins, Utrecht.

Murray, J. W. (1986). Living and dead Holocene foraminifera of Lyme Bay, southern England. *Journal of Foraminiferal Research*, 347-352.

Niebler, H.-S., Hubberten, H.-W., and Gersonde, R. (1999). Oxygen Isotope Values of Planktic Foraminifera: A Tool for the Reconstruction of Surface Water Stratification. *In* "Use of Proxies in Paleoceanography: Examples from the South Atlantic." (G. Fischer, and G. Wefer, Eds.), pp. 165-189. Springer Verlag, Berlin, Heidelberg.

Reimer, P. J., and Reimer, R. W. (2001). A marine reservoir correction database and on-line interface. *Radiocarbon* **43,** 461-463 with supplemental material URL:http://www.calib.org.

Röhl, U., and Abrams, L. J. (2000). High-resolution, downhole and non-destructive core measurements from Sites 999 and 1001 in the Caribbean Sea: Application to the late Paleocene thermal maximum. *Proceedings of the Ocean Drilling Program Scientific Results* **165,** 191-302.

Schiebel, R. (1992). "Recent benthic foraminifera in sediments of the shelf and upper continental slope from the Gulf of Guinea (West Africa).", Christian Albrechts Universität Kiel.

Schiebel, R., Bijma, J., and Hemleben, C. (1997). Population dynamics of the planktic foraminifer *Globigerina bulloides* from the eastern North Atlantic. *Deep Sea Research Part II* **44,** 1701-1713.

Schwager, C. (1866). Fossile Foraminiferen von Kar Nikobar - "Novara",  Expedition, 1857-1859,Geologischer Theil 2, pp. 187-268, Wien.

Shackleton, N. J., and Hall, M. A. (1984). Oxygen and carbon isotope stratigraphy of DSDP Hole 552A: Pliocene-Pleistocene glacial history. *Initial Reports DSDP* **81,** 599-610.

Shackleton, N. J., and Opdyke, N. D. (1973). Oxygen isotope and paleomagnetic stratigraphy of equatorial Pacific core V28-238: oxygen isotope temperatures and ice volumes on a $10^5$ year and $10^6$ year scale. *Quaternary Research* **3,** 39-55.

Stuiver, M., and Braziunas, T. F. (1993). Modeling atmospheric 14C influences and 14C ages of marine samples to 10,000 BC. *Radiocarbon* **35,** 137-189.

Stuiver, M., Reimer, P. J., Bard, E., Beck, J. W., Burr, G. S., Hughen, K. A., Kromer, B., McCormac, G., van der Plicht, H., and Spurk, M. (1998a). INTCAL98 Radiocarbon Age Calibration, 24,000-0 cal BP. *Radiocarbon* **40,** 1041-1083.

Thompson, P. R., Bé, A. W. H., Duplessy, J.-C., and Shackleton, N. J. (1979). Disappearance of pink-pigmented Globigerinoides ruber at 120,000 yr BOP in the Indian and Pacific Ocean. *Nature* **280,** 554-558.

# 4 ABRUPT CLIMATE OSCILLATIONS DURING THE LAST DEGLACIATION: THE GREAT AUSTRALIAN BIGHT RECORD INDICATES SYNCHRONOUS INTERHEMISPHERIC CLIMATE LINKAGE

## Abstract

The transition from the last glacial maximum to the Holocene (20,000 to 10,000 years before present) was marked by several climatic fluctuations. In contrast to Northern Hemisphere deglaciation records, which show rapid return to near-glacial conditions during the Younger Dryas Chronozone (Alley and Clark, 1999), their southern ice-core counterparts record two significant but separate cooling events: the Antarctic Cold Reversal (Jouzel et al., 1995) and the Oceanic Cold Reversal (Stenni et al., 2001). The relative timing of these two reversals compared to the northern equivalent of the Younger Dryas event is central for our understanding of interhemispheric linkages and to explain causes and mechanisms of abrupt climatic change. Apart from the Antarctic ice cores, high-resolution and well-dated paleoclimatic records from the Southern Hemisphere are sparse. Here, we report on an unprecedented high-resolution, southern mid-latitude marine archive from the Great Australian Bight. The oxygen isotope composition from planktonic foraminifera indicates two rapid cold reversals, which are ^{14}C-dated from 13.1 to 12.3 and 12.3 to 11.1 thousand years before present and separated by a brief but significant warming. The timing and nature of these two cold reversals correlates overall to the recently proposed Oceanic Cold Reversal observed in the mid-latitude Indian Ocean. The second, more intense, abrupt cooling, although smaller in amplitude, resembles and is synchronous with the Younger Dryas Chronozone as evidenced in the Northern Hemisphere.

## 4.1 Introduction

Northern and Southern Hemisphere marine, terrestrial and ice-core paleoclimate archives show evidence for abrupt climate change during the last glacial-interglacial transition, but only a few records, mostly from ice-cores, are available to determine the role of the Southern Hemisphere in global climate change. For example, the Antarctic Cold Reversal (ACR), a well-marked cooling phase starting at ~14 and lasting until ~12.5 thousand calendar years before present (ka BP), is present in most Antarctic ice cores and seems inherent to this part of the world. In contrast, the Younger Dryas Chronozone (YDC), a prominent cold reversal dated between 12.9 and 11.5 ka BP, marks the return to near-glacial conditions in the North Atlantic realm. Although a widely documented phenomena in various paleorecords and different geographic settings of the Northern Hemisphere and tropics, the mid-to-high latitude records of the YDC from the Southern Hemisphere remain controversial and inconclusive (Bennett et al., 2000; Denton and Hendy, 1994; Moreno et al., 2001; Petit et al., 1999;

Singer et al., 1998). To date and to our knowledge, no marine record from the southern mid-to-high latitudes recording variations at submillenial resolution has been published.

A recent study by Stenni et al. (2001) shows the existence of a third cooling event, the Oceanic Cold Reversal (OCR) at approximately 13.2 to 11.5 ka BP which occurs about 800 years later than the end of the ACR and continues well into the YDC. They propose that changes in the deuterium excess (*d*) in the Dome C ice core (East Antarctica) reflect a change of 0.8°C in sea-surface temperature at the moisture source for Dome C precipitation, which is located in the Indian Ocean (Fig. 4.1a). It remains to be proven, however, if the OCR could possibly represent the Southern Hemisphere's expression of the Northern Hemisphere YDC (Steig, 2001). Depending on the distribution and timing of the YDC, oceanic or atmospheric circulation has been suggested as the mechanism propagating the cooling event. Ice-sheet growth and sudden melt-water discharge have been invoked as the triggers (Alley and Clark, 1999; Fairbanks, 1989), but the underlying cause continues to be elusive. The question remains: Was the cooling during the YDC a local or a global phenomenon? Using a high-resolution oxygen isotope marine record from the Great Australian Bight, we propose to explore this question.

## 4.2   Location

The Great Australian Bight's (GAB) mid-latitude setting is ideally suited to provide an appropriate record of the last glacial-interglacial transition because: (1) it lies beyond the direct influence of Northern Hemisphere thermohaline circulation and melt-water pulsing, (2) the sedimentation rates are sufficient to allow for high-resolution studies, and (3) it is located in the source region of precipitation for Antarctic ice cores.
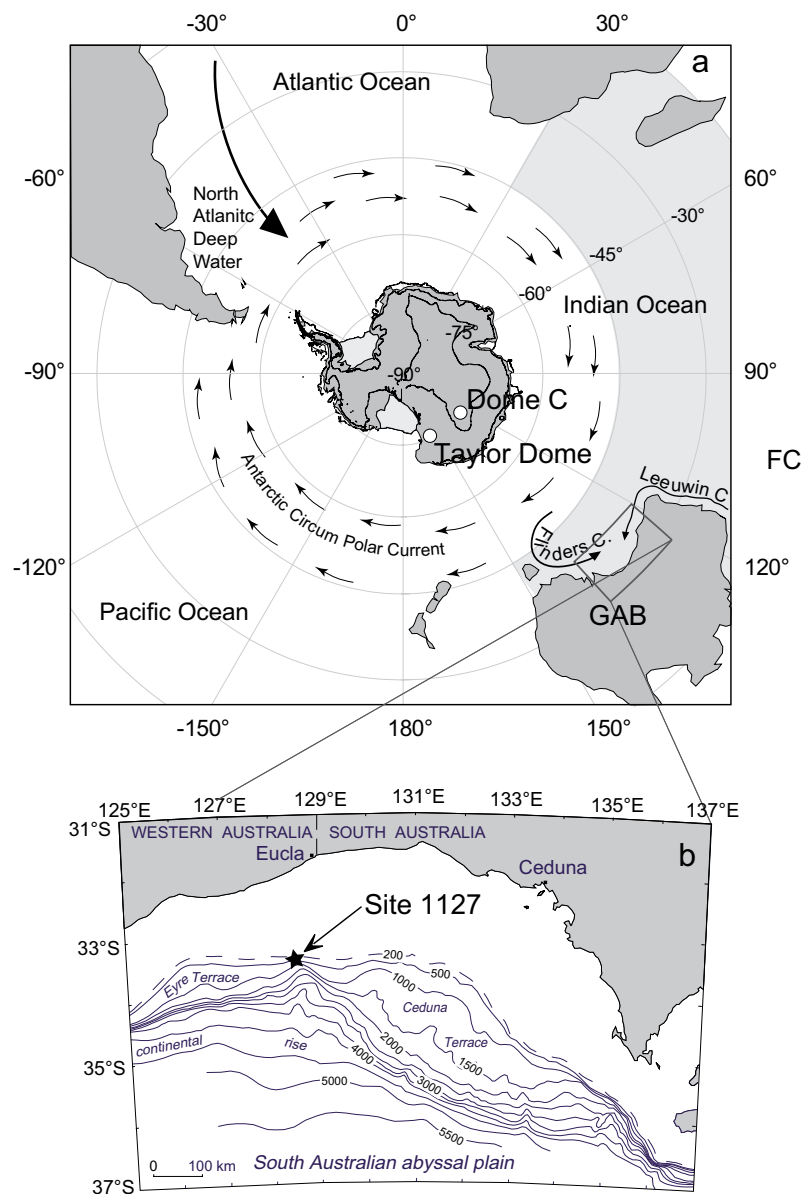
***Figure 4.1.*** *(a) Map of Southern Hemisphere showing the location of the Great Australian Bight (GAB) with respect to Antarctic ice cores from Dome C and Taylor Dome. The modern water masses influencing the region are illustrated. (b) The insert is a detailed map of the GAB continental margin off southern Australia. ODP Leg 182, Site 1127, is located immediately in front of the present day shelf edge in 480 m of water depth.*

The GAB on the continental margin of southern Australia (124-134°E, 32-34°S) is the largest cool-water carbonate depositional realm on Earth today (Feary and James, 1998) (Fig. 4.1f). Comprising a 100-150 km wide ramp-type shelf, the GAB directly opens to the Southern Ocean. It is wind and wave-swept year round and a site of abundant sediment production, but, due to the high-energy environment, most biogenic material is swept seaward where it accumulates on the shelf edge and slope (James, 1997). The sediments are fine-grained, bioclastic carbonates. The general oceanography

is influenced by Southern Ocean waters (Fig. 4.1a). They invade the shelf from a southeasterly direction via the Flinders Current, which is a large wind-driven anticylonic gyre (Bye, 1972; Hufford et al., 1997). The Leeuwin Current, a warm pole-ward directed eastern boundary current, flowing around the tip of southwestern Australia and into the GAB plays a major role in the modern oceanographic setting. In contrast, foraminiferal studies (Almond et al., 1993; Li et al., 1999) indicate that, during glacials, the Leeuwin current flow was absent or significantly weaker. Thus, with the northward migration of the Southern Ocean water masses, cooler conditions prevailed on the shelf than during interglacial times.

## 4.3   Results

Ocean Drilling Program (ODP) Leg 182, Site 1127 was drilled immediately in front of the present-day shelf edge in 480.6 m of water depth (Fig. 4.1b). Here we present a high-resolution oxygen isotopic study on sediments cored from 7 to 10 m below the seafloor in Hole 1127B, which span the last deglaciation. Age control is determined from 8 AMS radiocarbon dates on monospecific planktonic foraminifera samples (Table 4.1) (Stuiver et al., 1998a). Sample spacing is 5 cm for planktonic species *G. ruber* and 25 cm for *G. bulloides*, except over the second cold reversal where sample spacing was increased to 5 cm.  Sedimentation rates vary considerably, ranging from 23 cm/kyr at the end of the LGM and increasing to 40 cm/kyr during the transition and 160 cm/kyr in the earliest Holocene, leading to the uneven spacing of the isotopic results when plotted against time (Fig. 4.2b). Although off-shelf transport and bioturbation could potentially disturb the stratigraphic integrity, the high sedimentation rates minimize this disturbance. Based on the age integrity given by the high-resolution ^{14}C-chronology, we are confident that the sediments record a true paleoceanographic signal.

| Sample ID | Lab Code | Core depth (mbsf) | $^{14}$C AMS Age ($^{14}$C yrs BP) | | Calibrated Age (2σ, yrs BP) | |
|---|---|---|---|---|---|---|
| 2H-1 100-103 | ETH-24364 | 6.90 | 9,515 ± | 110 | 10,581 - | 9,717 |
| 2H-2 2-7 | ETH-24363 | 7.42 | 9,875 ± | 90 | 11,148 - | 10,244 |
| 2H-2 50-55 | ETH-23922 | 7.90 | 10,135 ± | 105 | 11,601 - | 10,360 |
| 2H-2 101-107 | ETH-23892 | 8.41 | 10,930 ± | 90 | 12,881 - | 11,498 |
| 2H-2 115-119 | ETH-25860 | 8.55 | 11,340 ± | 85 | 13,741 - | 12,417 |
| 2H-2 135-139 | ETH-25861 | 8.75 | 11,750 ± | 85 | 13,777 - | 12,974 |
| 2H-3 50-55 | ETH-24290 | 9.40 | 14,420 ± | 95 | 17,162 - | 16,133 |
| 2H-3 65-69 | ETH-25862 | 9.55 | 14,920 ± | 85 | 17,758 - | 16,698 |

*Table 4.1. Radiocarbon dates from Site 1127, Great Australian Bight. All dates are based on monospecific samples of planktonic foraminifera G. inflata (>150 µm). Radiocarbon measurements were obtained at the Swiss Federal Institute of Technology (ETH) AMS Facility. Ages have been calibrated using the program CALIB HTML version 4.3 (http://radiocarbon.pa.qub.ac.uk/calib/) (ΔR = 61 ± 29, Method A and the marine calibration dataset MARINE98), (Stuiver et al., 1998a).*

Deglacial warming, as observed in the oxygen isotope record of *G. ruber* (Fig. 4.2b), is initially abrupt, obtaining a temporary plateau between approximately 16.2 and 13.2 ka BP. before rapid warming returns just thereafter. The renewed warming trend, however, is then interrupted by two significant cold reversals designated CR1 and CR2. CR1 begins fairly abruptly at 13.1 ka BP and ends at 12.8 ka BP with a comparably gradual warming trend. This brief warming, culminates at ~12.3 ka BP and separates the two CR events. CR2 begins abruptly after 12.3 ka BP and ends at 11.2 ka BP, after which warming continues into the Early Holocene. Similar trends, although at a lower resolution, are seen in the isotopic record of *G. bulloides* noting that the cooling event is synchronous and just as abrupt. Assuming a 1‰ glacial-interglacial decrease in the isotopic composition of seawater (Schrag et al., 2002), a 3-4°C LGM-Holocene SST temperature increase is observed and in agreement with other records for the Southern Ocean (Stenni et al., 2001). The 0.6‰ isotopic increase at the time of CR2 represents a SST decrease of approximately 2°C.
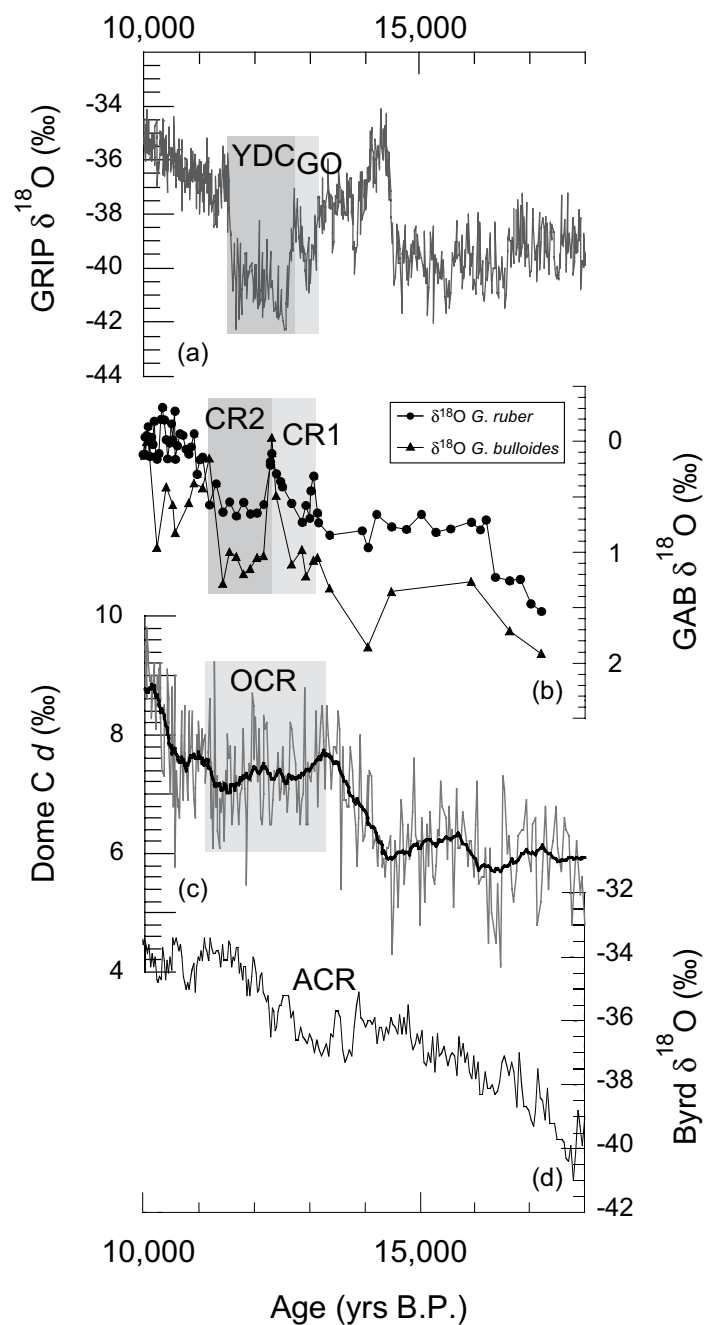
***Figure 4.2.*** *Comparison of the LGM to Holocene transition from Northern and Southern Hemisphere ice core data with GAB results. The Greenland Ice Core Project (GRIP) (a) and Byrd $\delta^{18}O$ (d) data on methane synchronized time scales (Blunier and Brook, 2001) illustrate the relative timing of the YDC and GO in the Northern Hemisphere and the ACR in the Southern Hemisphere, respectively. GAB Site 1127 $\delta^{18}O$ results (b) are plotted as a function of age, where GAB chronology is based on AMS 14C dating (Table 1), and show a double cold reversal CR1 and CR2. Antarctica Dome C deuterium excess data (c), on Dome C time scale (Schwander et al., 2001), are shown in order to compare the relative timing of OCR.*

## 4.4    Correlation of Southern Ocean and Ice Core Data

The GAB last deglaciation record is characterized by an initial stepwise warming trend, which is punctuated by 2 significant cooling events (CR1 and CR2) interrupting the overall warming. The relative timing of abrupt climatic events on a global scale is important in evaluating mechanisms driving climate change. Figure 4.2 illustrates the comparison of the GAB record to ice core data from the Northern Hemisphere, i.e. GRIP (Greenland), and from the Southern Hemisphere, i.e. Dome C and Byrd (Antarctica). In comparison with the Byrd record, we note that CR1 clearly lags the beginning of the ACR but correlates with the beginning of the OCR and, interestingly, also with the beginning of a cold reversal termed the Gerzensee-Killarney Oscillation (GO) in Europe and North America or Intra-Allerod Cold Period (IACP) in Greenland (Yu and Wright, 2001). The warming separating the two cold reversals correlates to a slight variation in the OCR curve. CR2 falls within the second part of the OCR, but, notably, its characteristic shape and abrupt beginning and ending resembles that of the YDC. Although apparently slightly lagging the YDC (12.5 to 11.5 ka BP), CR2 can be considered synchronous with YDC, within the errors of $^{14}$C dating. Furthermore, we have corrected our radiocarbon data using a reservoir effect of 400 year. We could argue that a smaller correction would be more appropriate, based on the fact that the GAB is shallow water shelf environment with vigorous mixing of the upper water column due to swell and storm activity.

The mid-latitude Indian Ocean, is the main moisture source for Dome C precipitation (Stenni et al., 2001), and the surface water of the GAB. A significant SST cooling, as inferred from the Dome C *d* excess record, should, therefore, be recorded in the $\delta^{18}O$ of planktonic foraminifera deposited in the GAB. The double-peaked cooling observed in the GAB isotopic record is, indeed, synchronous with the OCR, but, whereas Stenni et al. determined a 0.8°C decrease for the OCR, the GAB isotope event requests an initial 1-2°C cooling followed by a return to warmer conditions with a second cooling of ~2°C. Our interpretation assumes no change in the $\delta^{18}O$ of the water although we are aware that hydrologic change potentially has effected the isotope record. The OCR temperature estimates of Stenni et al. neglect the influence of relative humidity and wind changes, which the authors readily admit limits their reconstruction. Our 2°C temperature change, as recorded interpreted from the GAB isotope record, indicates that the relative humidity could have changed by up to 10-20%. As winds and/or source areas shifted, oceanic fronts were displaced pole-ward and temperature gradients flattened during the progression of the last deglaciation.

In comparison to Northern Hemisphere records, we note that CR1 intriguingly resembles the G/K or IACP oscillation, not only in the timing of the onset of the cooling (13.15 ka BP for GRIP; 13.1 ka BP for GAB) but also in the duration of the isotopic low, with 413 years from the GRIP data compared to ~407 years from the GAB data. Further, both records observe abrupt cooling followed by comparably gradual warming, which appear to occur synchronously. Differences do, however, exist. The warming separating CR1 from CR2 obviously lags the warming separating G/K from the YDC by ~400 years. In this part of the record, our age model is affected by the $^{14}$C plateau of constant age, offering a

plausible explanation for the offset. The same time lag relative to the GRIP record is also evident when correlating the onset and termination of CR2 with the YDC. Calibrated age ranges (Table 1) of the GAB record lie well within the proposed timing of the GRIP record, further supporting the notion that the apparent lag is due to the limits of the dating method. Apart from timing, the CR2-YDC comparison is even more convincing than for CR1-G/K. The character of the CR2 curve with abrupt onsets and endings, and the time of duration correlate remarkably well to the YDC.

Discussion on the existence and timing of Northern Hemisphere phenomena observed in Southern Hemisphere records often concludes with a reference to ocean circulation when interpreted as a regionally restricted event or to atmospheric circulation in order to invoke global synchronicity (Moreno et al., 2001; Denton and Hendy, 1994). Ironically, the Antarctic ice core from Taylor Dome and its 'North Atlantic' character suggest an oceanic solution for interhemispheric climate linkage (Grootes et al., 2001). Due to thermohaline circulation (THC), the slightly warmer North Atlantic Deep Water (NADW) mixes with Circum Polar Deep Water (CPDW) in the Atlantic sector of the Southern Ocean and its signature is distributed via the Antarctic Circum Polar Current (ACC). The Flinders Current (FC) (Hufford et al., 1997; Fig. 4.1a), an anti-gyral flow, south of Australia, carries waters of the ACC and associated fronts into the GAB and, therefore, links southern Australian and Southern Ocean waters. Thus, a weakening or even shut-down of the THC, as proposed for the YDC and G/K due to meltwater discharge (Fairbanks, 1989; Manabe and Stouffer, 1997), results in a significantly decreased influence of the NADW component in the CPDW and subsequent ACC. Hence, cooling in the Northern Hemisphere could occur synchronously with cooling in the Southern Hemisphere.

## 4.5    Conclusion

The evidence for cold reversals during the last deglaciation from the GAB, Dome C, and Taylor Dome archives, which are synchronous with the YDC in the Northern Hemisphere, is documented at different geographic locations and observed in three different types of proxies. Although we cannot discriminate atmospheric or oceanic circulation as the underlying mechanism propagating the cooling around the globe, we propose that the generally smaller amplitude in change and overall dampened signal favours an active oceanic role. Together, these marine and ice core records provide strong evidence that surface-ocean cooling is not regionally confined and, furthermore, that the cooling occurs synchronous with that observed from the Northern Hemisphere. In this context, ice-cores from the Antarctic interior, undoubtedly precise recorders of global atmospheric change and based on their gas record, have to be reassessed with respect to the newly emerging information from the southern mid-latitude oceans. Further high-resolution paleorecords developed in marine sequences from this region are needed to improve our current understanding of Southern Hemisphere climate change. In particular, continental margins could potentially offer high-resolution archives in key locations.

## Acknowledgements

## References

Alley, R. B., and Clark, P. U. (1999). The Deglaciation of the Northern Hemisphere: A Global Perspective. *Annual Reviews Earth and Planetary Sciences* **27,** 149-182.

Almond, D., McGowran, B., and Li, Q. (1993). Late Quaternary Foraminiferal record from the Great Australian Bight and its environmental significance. *Memoir Association Australasian Paleontologist* **15,** 417-428.

Bennett, K. D., Haberle, S. G., and Lumley, S. H. (2000). The Last Glacial-Holocene Transition in Southern Chile. *Science* **290,** 325-328.

Blunier, T., and Brook, E. J. (2001). Timing of Millenial-Scale Climate Change in Antarctica and Greenland During the Last Glacial Period. *Science* **291,** 109-112.

Bye, J. A. T. (1972). Ocean Circulation South of Australia. *In* "Antarctic Oceanology II: The Australian-New Zealand Sector." (D. E. Hays, Ed.), pp. 95-100. A.G.U. Antarctic Research Series. A.G.U. Antarctic Research Series, Washington D.C.

Denton, G. H., and Hendy, C. H. (1994). Younger Dryas Age Advance of Franz Josef Glacier in the Southern Alps of New Zealand. *Science* **264,** 1434-1437.

Fairbanks, R. G. (1989). A 17,000-year glacio-eustatic sea lovel record: influence of glacial melting rates on the Younger Dryas event and deep-ocean circulation. *Nature* **342,** 637-642.

Feary, D. A., and James, N. P. (1998). Seismic Stratigraphy and Geological Evolution of the Cenzoic, Cool-Water Eucla Platform, Great Australian Bight. *AAPG Bulletin* **82,** 792-816.

Grootes, P. M., Steig, E. J., Stuiver, M., Waddington, E. D., and Morse, D. L. (2001). The Taylor Dome Antarctic 18O Record and Globally Synchronous Changes in Climate. *Quaternary Research* **56,** 289-298.

Hufford, G. E., McCartney, M. S., and Donohue, K. A. (1997). Northern boundary current and adjacent recirculations off southwestern Australia. *Geophysical Research Letters* **24,** 2797-2800.

James, N. P. (1997). The Cool-Water Carbonate Depositional Realm. *In* "Cool-Water Carbonates." (N. P. James, and J. D. A. Clarke, Eds.), pp. 1-20. S.E.P.M. Special Publication.

Jouzel, J., Vaikmae, R., Martin, M., Duclos, Y., Stievenard, M., Lorius, C., and Toots, M. (1995). The two-step shape and timing of the last deglaciation in Antarctica. *Climate Dynamics***,** 151-161.

Li, Q., James, N. P., Bone, Y., and McGowran, B. (1999). Paleoceanographic significance of recent foraminiferal biofacies on the southern shelf of Western Australia: a preliminary study. *Paleogeography, Paleoclimatology, Paleoecology* **147,** 101-120.

Manabe, S., and Stouffer, R. J. (1997). Coupled ocean-atmosphere model response to freshwater input: Comparison to Younger Dryas event. *Paleoceanography* **12,** 321-336.

Moreno, P. I., Jacobson Jr, G. L., Lowell, T. V., and Denton, G. H. (2001). Interhemispheric climate links revealed by the late-glacial cooling episode in southern Chile. *Nature* **409,** 804-808.

Petit, J. R., Jouzel, J., Raynaud, D., Barkov, N. I., Basile, I., Bender, M., Chappellaz, J., Davis, M., Delaygue, G., Delmotte, M., Kotlyakov, M., Legrand, M., Lipenkov, V. Y., Lorius, C., Pépin, L., Ritz, C., Saltzman, E., and Stievenard, M. (1999). Climate and atmospheric history of the past 420000 years from the Vostok ice core, Antarctica. *Nature* **399,** 429-436.

Schrag, D. P., Adkins, J. F., McIntyre, K., Alexander, J. L., Hodell, D. A., Charles, C. D., and McManus, J. F. (2002). The oxygen isotopic composition of seawater during the Last Glacial Maximum. *Quaternary Science Reviews* **21,** 331-342.

Schwander, J., Jouzel, J., Hammer, C. U., Petit, J.-R., Udisti, R., and Wolff, E. (2001). A tentative chronology for the EPICA Dome Concordia ice core. *Geophysical Research Letters* **28,** 4243-4246.

Singer, C., Shulmeister, J., and McLea, B. (1998). Evidence Against a Significant Younger Dryas Cooling Event in New Zealand. *Science* **281,** 812-814.

Steig, E. J. (2001). No Two Latitudes Alike. *Science* **293,** 2015-2016.

Stenni, B., Masson-Delmotte, V., Johnsen, S., Jouzel, J., Longinelli, A., Monnin, E., Röthlisberger, R., and Selmo, E. (2001). An Oceanic Cold Reversal During the Last Deglaciation. *Science* **293,** 2074-2077.

Stuiver, M., Reimer, P. J., Bard, E., Beck, J. W., Burr, G. S., Hughen, K. A., Kromer, B., McCormac, G., van der Plicht, H., and Spurk, M. (1998a). INTCAL98 Radiocarbon Age Calibration, 24,000-0 cal BP. *Radiocarbon* **40,** 1041-1083.

Yu, Z., and Wright, J., J.E. (2001). Response of interior North America to aburpt climate oscillations in the North Atlantic region during the last deglaciation. *Earth-Science Reviews* **52,** 333-369.

# 5 HIGH-RESOLUTION PALEOCLIMATE RECORD LINKING OCEAN AND ATMOSPHERIC CIRCULATION PATTERNS FOR THE PAST 20,000 YEARS

## Abstract

High-resolution oxygen isotope and iron (Fe) abundance data from sediments cored off the southern Australian continental margin document in unprecedented detail oceanographic, hydrologic and atmospheric circulation changes occuring during the last 20,000 years. Oxygen isotope compositions record the glacial to interglacial transition in an initially stepwise manner, with a double return to cooler conditions at the end of the deglaciation, before warming continues into the Early Holocene. Changes in the isotopic values during the mid-Holocene correlate to maximum temperature estimates from terrestrial paleo-data and coincide with Holocene sea-level rise. Increased isotope variability during the Late Holocene is attributed to rapidly changing hydrologic conditions during ENSO fluctuations. The bulk sedimentary Fe record is interpreted as primarily the result of aeolian dust transport. The record could also be affected by sea-level rise at the end of the deglaciation and transgression-induced reworking during the deglaciation. The Fe abundance was lowest at the end of the glacial, when continental aridity and higher wind speeds carried the dust offshore thus bypassing the Great Australian Bight. Early Holocene high-sedimentation rates and high Fe concentrations correlate with overall wet conditions on the Southern Australian continent. We propose that high Fe concentrations reflect dust plumes entrained by pre-frontal northerly winds, with subsequent dust-scavenging precipitation depositing sediment over the Bight area. Since the mid-Holocene, ~5000 to 7000 years ago, a decrease in Fe abundance correlates with an overall trend towards drier conditions. This high-resolution geochemical study at Site 1127, on the continental shelf facing the open ocean in a mid-latitude Southern-Hemisphere location, documents in detail the Late Glacial through Holocene paleoceanographic conditions affecting the Great Australian Bight, as well as climatic changes impacting the hinterland. The combined record allows the linkage of the open-ocean and terrestrial environments in this particularly understudied region of the Southern Hemisphere.

## 5.1 Introduction

Beyond 30°S, the vast Southern Ocean dominates the Southern Hemisphere, and landmasses are relatively small. Most high-resolution and well-dated last glacial to Holocene paleoclimatic reconstructions from this region, apart from ice-cores, are predominantly based on the terrestrial environments of southern South America (Markgraf, 2001), Australia (Harrison and Dodson, 1993), and New Zealand (McGlone et al., 1993). Comparably few marine records are available (Bard et al., 1997; Charles et al., 1996) and these often lack temporal resolution and reliable chronology. Furthermore, most of these marine records are concentrated in the Atlantic sector of the Southern

Ocean and, therefore, are subject to variations of the North Atlantic Ocean. South Australian paleo-studies, dominantly from lake and peat bog settings, reconstruct the regional hydrology using lake-level fluctuations and vegetation changes derived from pollen profiles (Harrison and Dodson, 1993). Further data are based on moraines left by glacier advances (Barrows et al., 2001) and temperature estimates inferred from emu eggshell amino-acid racemization (Miller et al., 1997). As deglaciation progressed with rising temperatures, the glaciers retreated, and widespread aridity resulted in low lake-levels. It was not until the Early Holocene that lakes and peat bogs were fully established.

Here, we present a high-resolution marine paleoclimate record spanning the past 20 thousand years before present (ka BP) developed from a core recovered in the central Great Australian Bight (GAB). This region is ideally suited to contribute an appropriate record for the following reasons: (1) its mid-latitude, southern Hemisphere location is far removed from Northern Hemisphere influence, but also at some distance to the Antarctic ice-sheet influence, (2) sedimentation rates form the basis for high-resolution studies, (3) abundant planktonic foraminifera provide a detailed chronology, and (4) the continental proximity allow us to link terrestrial and open ocean setting.
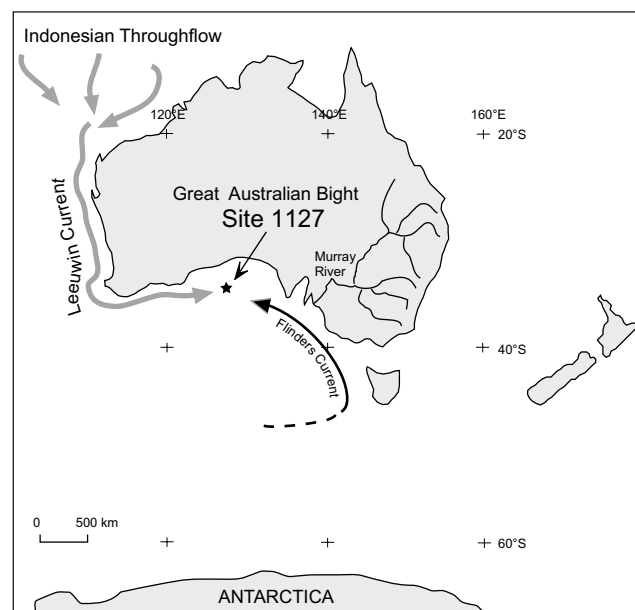


***Figure 5.1.*** *Schematic overview of Australia and general oceanographic setting of Site 1127 in the Great Australian Bight (GAB).*

The Great Australian Bight (GAB) on the continental margin of southern Australia (124-134°E, 32-34°S) is a cool-water carbonate depositional realm, being the largest of its kind on Earth today (Feary and James, 1998). Comprising a 100-150 km wide ramp-type shelf, the GAB directly opens to the Southern Ocean (Fig. 5.1). Although it is wind and wave-swept year round, it is a site of abundant sediment production, but, due to the high-energy environment, most biogenic material is swept seaward where is accumulates at the shelf edge and slope setting (James and Clarke, 1997). Ocean

Drilling Program (ODP) Leg 182, Site 1127 was drilled just in front of the present-day shelf edge in 480.6 m of water depth (Fig. 5.1). The studied interval covers the uppermost 10 m of the 510-m long core recovered at Hole 1127B, spanning the last 20 ka BP. Sediments are composed of fine-grained, bioclastic carbonates. The modern oceanography in the region is influenced by two major water masses (Fig. 5.1). The Leeuwin Current, originating in the Indonesian Throughflow, carries warm, oligotrophic waters south along the coast of Western Australia before its swings around the tip of southwestern Australia and flows into the Bight. The Southern Ocean invades the shelf from a southwesterly direction, bringing cool and nutrient-rich waters. The oceanography is further complicated by the Flinders Current, which results from a large, wind-driven anti-gyral flow carrying cold nutrient rich waters from the subtropical frontal region into the GAB (Bye, 1972; Hufford et al., 1997). The Flinders Current becomes an undercurrent to the Leeuwin Current during strong Leeuwin Current flow but it can move onto the shelf when the Leeuwin Current weakens (James et al., 2001). The interplay between the Southern Ocean water-masses and the LC on glacial-interglacial time scales has been documented in only a few studies (Almond et al., 1993; Li et al., 1999). It is suggested that, during glacials, the LC was absent or significantly weaker, and cool, Southern Ocean conditions prevailed on the shelf.

## 5.2 Results

Planktonic foraminifera species *Globingerinoides ruber* and *Globigerina bulloides* dwell in the mixed layer of the ocean. Their oxygen isotopic ratio ($\delta^{18}O$), primarily a function of the isotopic composition and temperature of the water in which the calcite is produced, is a well-established proxy for sea-surface temperature estimates. Age control is obtained by 11 AMS radiocarbon dates on monospecific planktonic foraminiferal samples converted to calendar years (Table 5.1). Sample spacing is 5 cm for *G. ruber* and 25 cm for *G. bulloides*, except over the cooling event, where spacing was increased to 5 cm. Varying sedimentation rates, ranging from 40 cm/kyr during the deglaciation, strongly increasing to 145 cm/kyr during the Early Holocene, and decreasing to 33 cm/kyr in the Late Holocene, lead to uneven spacing of the isotopic results when plotted against time. Although off-shelf transport and bioturbation can potentially disturb the stratigraphic integrity, we are confident that the high sedimentation rates overcompensates for this fact. In addition to the age integrity, early diagenesis and carbonate dissolution contribute to a sedimentary record, which provides a true paleoceanographic signal.

| Sample ID | Lab Code | Core depth (mbsf) | 14C AMS Age (14C yrs BP) | | | Calibrated Age (2σ, yrs BP) | | |
|-----------|----------|-------------------|--------|---|-----|--------|---|--------|
| 1H-2 2-6 | ETH-24288 | 0.02 | 1,295 | ± | 55 | 913 | - | 657 |
| 1H-2 50-55 | ETH-23893 | 2.00 | 6,385 | ± | 65 | 6,949 | - | 6.625 |
| 1H-3 72-75 | ETH-24289 | 3.72 | 8,135 | ± | 75 | 8,849 | - | 8,363 |
| 2H-1 100-103 | ETH-24364 | 6.90 | 9,515 | ± | 110 | 10,581 | - | 9,717 |
| 2H-2 2-7 | ETH-24363 | 7.42 | 9,875 | ± | 90 | 11,148 | - | 10,244 |
| 2H-2 50-55 | ETH-23922 | 7.90 | 10,135 | ± | 105 | 11,601 | - | 10,360 |
| 2H-2 101-107 | ETH-23892 | 8.41 | 10,930 | ± | 90 | 12,881 | - | 11,498 |
| 2H-2 115-119 | ETH-25860 | 8.55 | 11,340 | ± | 85 | 13,741 | - | 12,417 |
| 2H-2 135-139 | ETH-25861 | 8.75 | 11,750 | ± | 85 | 13,777 | - | 12,974 |
| 2H-3 50-55 | ETH-24290 | 9.40 | 14,420 | ± | 95 | 17,162 | - | 16,133 |
| 2H-3 65-69 | ETH-25862 | 9.55 | 14,920 | ± | 85 | 17.758 | - | 16,698 |

***Table 5.1.*** *Radiocarbon dates from Site 1127, Great Australian Bight. All dates are based on monospecific samples of planktonic foraminifera G. inflata (>150 μm). Radiocarbon measurements were obtained at the Swiss Federal Institute of Technology (ETH) AMS Facility. Ages have been calibrated using the program CALIB HTML version 4.3 (http://radiocarbon.pa.qub.ac.uk/calib/) (ΔR = 61 ± 29, Method A and the marine calibration dataset MARINE98), (Stuiver et al., 1998a).*

### 5.2.1   Oxygen isotope Record

In the oxygen isotope stratigraphic record of planktonic foraminifera (Fig. 5.2a), the deglaciation is characterized by an initial stepwise warming followed by two cold reversals (CR1 and CR2), before warming continues into the Holocene (see Chapter 4). A slight decrease in the oxygen isotope ratio (~0.3‰) marks the transition between Late and Early Holocene at 7.5 to 6.5 ka BP, whereas, during the last 1500 years a slight increase is again observed. Overall, $\delta^{18}O$ values decrease by 1.75‰ from the last glacial maximum (LGM) values of ~1.5‰ to average Late Holocene values of –0.25‰. Assuming a 1‰ change in glacial-interglacial isotopic composition of seawater (Schrag et al., 2002), this corresponds to a temperature increase of ~3°C. A comparable trend, although at overall lower resolution, is seen in the isotopic record of *G. bulloides*. Furthermore, *G. bulloides* plot at a near-constant offset relative to *G. ruber* of ~0.3 to 0.5‰ indicating its deeper depth habitat in the water column (Hemleben, 1989).

### 5.2.2   Bulk Sedimentary Iron Abundances

The relative abundance of bulk sedimentary iron (Fe) (Fig. 5.2b) was measured on the surface of the core archive half using the X-ray fluorescence (XRF) core scanner at Bremen University (Röhl and Abrams, 2000). Sample spacing is 1 cm in sediments older than 12.2 ka BP and 2 cm in the younger section, corresponding to a sample resolution of approximately 70 and 11 years during deglaciation and Early Holocene, respectively. The lowest Fe abundances were measured in sediments deposited

during the LGM. The mid-deglaciation is marked by increasing values from 17.2 to ~14.6 ka BP, followed by a slight decrease, and continued rising values towards the Holocene after ~13 ka BP Fe abundances during the two cold reversals as identified by the isotope stratigraphy differ. During CR1, Fe abundances are at a minimum. During the intervening warming between CR1 and CR2, the Fe abundances increase sharply, reaching an apparent plateau throughout CR2. In fact, the Fe abundance does not depict significant change during CR2, but is rather characterized by abrupt changes before and after the cooling. The earliest Early Holocene (11 to 9 ka BP) contains the highest Fe abundances, which is followed by a continuous long-term decrease up to 5 ka BP. The late Holocene is marked by low Fe abundances, comparable to those measured during limited the early deglaciation. Calculated accumulation rates indicate that the Fe signal is not an affect of increasing or decreasing sedimentation rates, resulting in a dilution or concentration of the bulk sedimentary iron respectively, as the highest concentrations are found where sediment accumulation rates are highest.
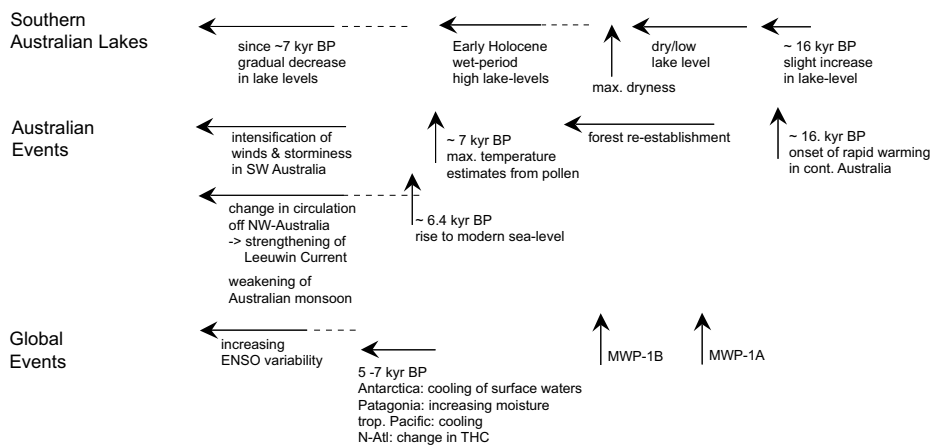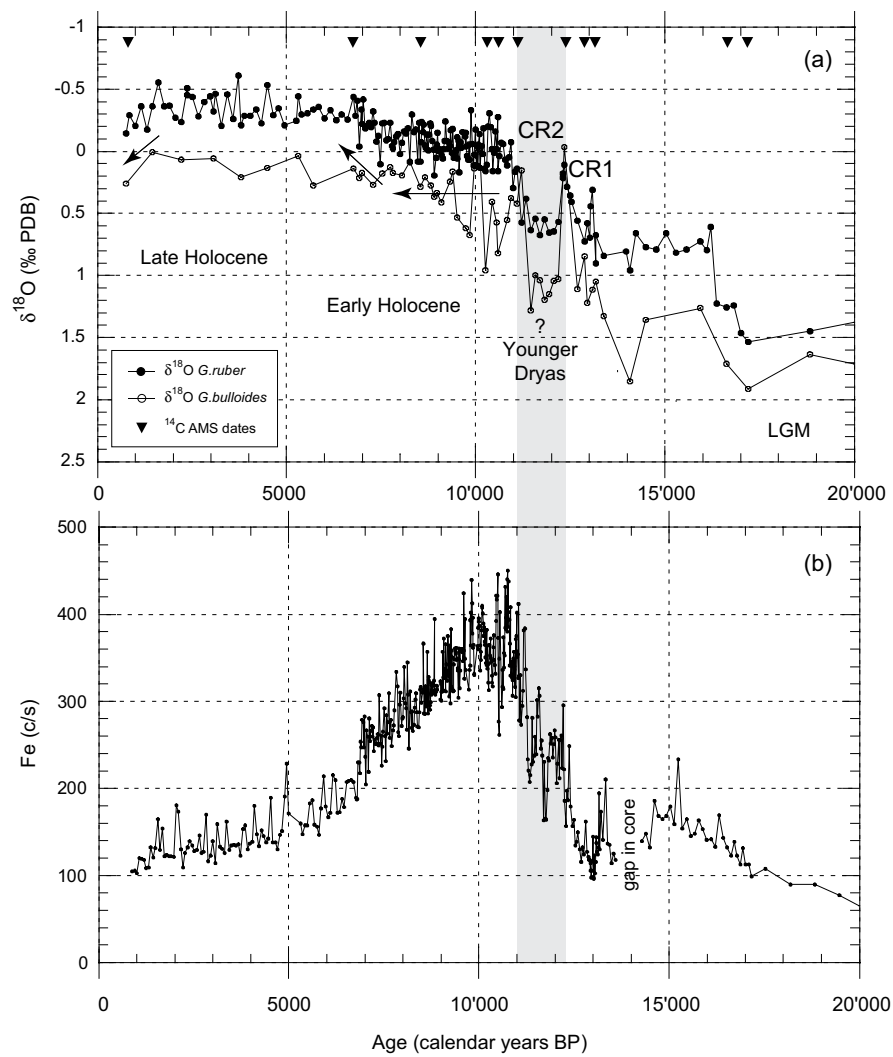
***Figure 5.2.*** *Comparison of the oxygen isotope record (a) and relative iron abundances (b) at Site 1127 for the last 20,000 years before present. The chronology is based on 11 AMS radiocarbon- dated horizons (Table 5.1). The Site 1127 record is correlated to significant events recorded in southern Australian lakes, overall in Australia and on a global scale.*

### 5.2.3   Fe-Record During the Deglaciation

Apart from increasing temperatures, marine deglaciational records, and in particular continental shelf records, were influenced by rising sea-level. During the LGM, Site 1127, located on the upper slope, was located in ~360 m of water depth (Yokoyama et al., 2000; Yokoyama et al., 2001), but large areas of the upper shelf were covered by only tens of metres of water and the inner shelf totally exposed. Sea-level rise and transgression onto the shelf resulted in reworking of older sediments and off-shelf transport influenced the slope records. The generally steady increase in Fe abundances during deglaciation, which is interrupted during cold reversals followed by abrupt increases, suggests a link to sea-level rise, and Fe content (Fleming et al., 1998) (Fig. 5.2). The initial Fe-abundance increase at ~17 ka BP corresponds to a globally observed change in the rate of sea-level rise (Fleming et al., 1998). Rapid sea-level rise as observed from coral records and proposed to be the result of large freshwater discharge (Bard et al., 1996), is not documented for meltwater pulse 1A (MWP-1A) just after 14 ka BP due to a data gap resulting from missing core taken for an interstitial water sample. MWP-1B could be associated with the sharp increase of Fe abundances and decreasing $\delta^{18}O$ values at 11.5 ka BP. Rising sea-level, therefore, may have influenced the deglaciational Fe-concentrations, but only to a limited extent. First, the high-resolution chronology over the LGM-Holocene transition, with dated horizons within a 10-20 cm interval, show no age reversal, which is evidence for minimal sediment reworking. Secondly, Early Holocene Fe abundances are three to four times higher than in the Late Holocene, and, although the mid-Holocene is marked by the last, albeit small sea-level rise to modern levels (Belperio et al., 2002), the Fe abundances decrease. In summary, the Fe-record of the GAB is affected by sea-level rise and transgression over the shelf, but other environmental parameters must be invoked to account for most of the signal. We argue that the Fe-record is in part the result of sea-level fluctuations during the last deglaciation, but overall, the record is dominated by the mechanism transporting the iron into the GAB.

## 5.3   Discussion

### 5.3.1   Fe-Transport Mechanisms

There are two possible ways of iron-transport into the GAB, either as river runoff or aeolian dust. If the Fe-record reflects regional river runoff, it would provide a measure of rainfall to the region, on the other hand, if wind-transported is the dominant mechanism, it could be interpreted as a proxy for the position and strength of winds. The modern climate in southern Australia is strongly influenced by the mean position of the subtropical high-pressure belt and annual or long-term shifts result in significant changes in regional rainfall (Pittock, 1978). On a seasonal scale (Fig. 5.3), its southerly position during the austral summer, suppresses rainfall along the southern to southwestern margin and summers are dry. In winter, its more northerly position allows for rainfall carried over the land mass by the Westerlies.

As already noted, during LGM and early deglaciation, southern Australia was cold and dry, and temperature estimates for the continental interior were up to 9°C lower before 16 ka BP (Miller et al., 1997). In contrast, after 11 kyr B.P., conditions became increasingly wetter as observed from high lake-levels and vegetation, probably representing an equatorward shift of the subtropical high-pressure belt and Westerlies (Harrison and Dodson, 1993). In this context, the simple and logical interpretation would be that the Fe-abundance record is a direct measure of rainfall and riverine input, with low Fe abundance indicating low rainfall during the LGM and high Fe abundances indicating higher precipitation during the Early Holocene. A similar interpretation was reported for Fe-abundance studies in the Cariaco Basin (Haug et al., 2001) and southern Chile (Lamy et al., 2001).

The GAB region is a pure carbonate depositional realm, with its hinterland composed of Eocene to Miocene carbonate sedimentary rocks. No rivers or paleorivers drain or have drained the immediate area (James et al., 2001), and only a few, local rivers in SW-Australia flow in a south to southwesterly direction. The Murray River, draining large parts of southeastern Australia, flows into the ocean close to Adelaide, and considering the westward flow of the Flinders Current, is a potential source of iron into the GAB area. However, even if large amounts of riverine input would reach the ocean, flocculation processes at the freshwater-saltwater interface, as well as instantaneous consumption by the biota in the nutrient-depleted shelf waters, would probably leave very little Fe available for sediments in the Bight.

A second mechanism to explain the observed Fe distribution invokes winnowing and redistribution of Fe due to ocean currents. Fe deposited on the exposed shelf during the LGM could have been reworked during sea-level rise and transgression explaining increasing and high Fe-abundances during the deglaciation and Early Holocene. Decreasing iron availability on the shelf in the Late Holocene could then explain the decreasing Fe abundances observed in the record.

///   mean position of subtropical high prressure belt (STHB)
>—→   mean position of Westerlies associated with fronts
\↘   Northerlies preceeding fronts
▒   Dust source: Western Nullabor region
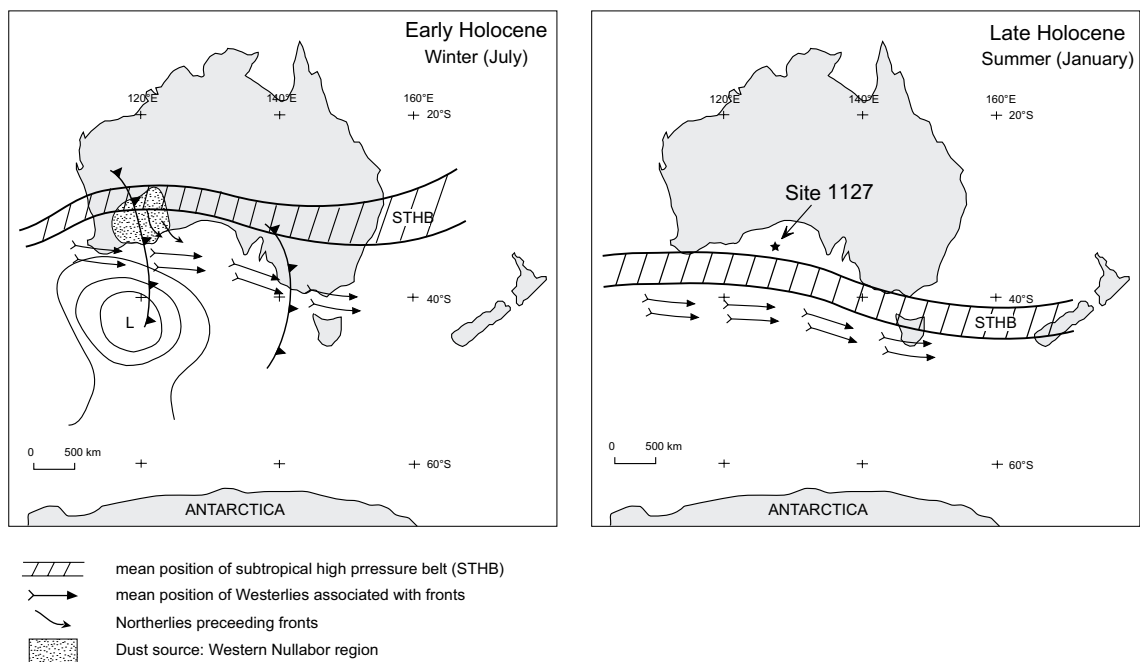
*Figure 5.3. Comparison of the Early Holocene (Winter) and Late Holocene (Summer) circulation pattern over Southern Australia. Modified after (Harrison and Dodson, 1993).*

A third possible mechanism, proposes that the iron is transported by winds and the apparent contradiction between high Fe abundances and high precipitation can be explained as follows. Cold fronts, associated with the Westerlies, rotate in a cyclonic (i.e. clockwise fashion). Before they pass over the SW Australian region, pre-frontal northerly winds entrain dust from the arid interior (Sprigg 1982). Weather systems responsible for dust entrainment and transport are also frequently responsible for large amounts of precipitation, and the scavenging effect of precipitation causes dust deposition in a very efficient and direct manner (McGowan et al., 2000). Only moderate wind-storms are needed to transport dust particles, 10-20 µm in size, over distances of ~500 km (McGowan et al., 2000). Central Australia, especially the semi-arid to arid western Nullabor region, is identified as one of the most frequent dust storm area (McTainsh and Pitblado, 1987) and the distance between the dust source and deposition area in the GAB is within 500 km.

Grain-size analysis of the non-carbonate fraction and the determination of Fe in the clay or silt fraction is necessary in order to discriminate between aeolian or riverine input and is the focus of ongoing work. For the moment, Fe-transport into the GAB area as dust is basically supported by the paleodata and, thus, our favoured working hypothesis.

### 5.3.2   South-Australian Paleoclimate Record

*Last glacial maximum (>16 ka BP)*

How do the GAB SST and dust records relate to changes observed in the marine and continental records of southern Australia over the past 18,000 years? During the LGM, the annual frequency of

dust-storm events is proposed to have increased by up to 50% (McTainsh and Lynch, 1996), in coincidence with the last major dune-building phase between 25 to 13 ka (Wasson, 1984; Wasson, 1986). Quartz and clay distribution maps off the coast of Eastern Australia and the Tasman Sea (Goldberg and Griffin, 1970; Thiede, 1979) indicate that sedimentation rates during the LGM were significantly higher compared to the Holocene and, furthermore, calcareous dust, eroded from the exposed GAB shelf, is found in SE Australian soils (McTainsh, 1989). The oceanographic setting is marked by colder SST's, up to 3-4°C as shown in the GAB $\delta^{18}O$ record, but also evidenced by the absence of warm water foraminifera (Li et al., 1999), lowered sea-level and exposed upper shelf. The Leeuwin Current was weaker, if not absent (Li et al., 1999; McGowran and al., 1997), and higher wind-speeds promoting long-shore currents and upwelling have been proposed (James et al., 2000). In summary, numerous and independent proxies indicate higher wind speeds during the LGM. Fe abundances during this period, however, are the lowest in the entire record (Fig. 5.2). We argue that, on average, higher wind-speeds and dust-plumes originating in the arid southwest were bypassing the Bight and the dust was deposited offshore western Australia, in New Zealand, as evidenced by red snow events in the Southern Alps (McGowan et al., 2000), the Southern Ocean (Griffin et al., 1968), and sub-Antarctic islands (McGowan et al., 2000). Our data are consistent with the late Pleistocene quartz sediment maps for the Tasman Sea and support Sprigg's (1982) hypothesis that the 'roaring thirties' were the dominant dust-transporting winds during the LGM. Further, Southern Hemisphere dust records from the subpolar Indian Ocean (Kent, 1982) and Vostok ice-core (Petit et al., 1999) observe the highest dust fluxes during the LGM resulting from higher wind speeds and thus further supporting our by-pass interpretation for the GAB record.

### *Deglaciation (16-10 ka BP)*

The record representing the deglaciational period was affected by sea-level rise and the little Fe deposited in the GAB area was reworked during the transgression. It is, however, noteworthy to mention the impressive correlation between a slight increase in lake-levels around 16 ka BP (Harrison and Dodson, 1993) and the slight increase in the Fe-record (Fig. 5.2) further supporting our theory of coinciding dust deposition and rainfall. The low Fe-abundances around 13 ka BP corresponds to the first cold reversal (CR1), as identified in the oxygen isotope record. Maximum continental aridity, evidenced from overall low lake levels (Harrison and Dodson, 1993) was reached only at ~12 ka BP During the second cold reversal, CR2, the Fe-abundances are marked by a double-spiked structure but with no clear CR2-wide trend. The interpretation of stagnating sea-level in light of global cooling and near-return to glacial conditions during the Younger Dryas Chronozone (YDC) is therefore reasonable (see Chapter 4). Increasing Fe-abundances, although affected by sea-level rise, can also be interpreted as a result of an increased dust transport and associated precipitation. Evidence for increasing wetness is once again found in the lake-level history of southern Australia, which indicates a gradual transition to wetter conditions after 12 ka (Harrison and Dodson, 1993).

## Holocene (<10 ka BP)

The Early Holocene in the GAB sedimentary record is marked by high Fe-abundances, high sediment accumulation rates, and increased SST's. It correlates to the Early Holocene wet period of terrestrial SW and SE Australia, as evidenced from high lake-level records and pollen data (Harrison and Dodson, 1993). The paleo-atmospheric circulation pattern corresponds to that of a long-term modern winter pattern with the sub-tropical high-pressure belt (STHB) shifted equatorward thus allowing for high precipitation low-pressure systems associated with the Westerlies to cross Southern Australia (Fig. 5.3). It also provides the mechanism for entraining dust to be transported into the area of the GAB. The South-Australian wet-period continued up to ~7,000 years BP, after which lake levels began to decrease, correlating with a decrease of Fe-abundances in the GAB record around that time. This correlation can be explained by a long-term southward shift of the STHB, displacing the Westerlies to a more southerly location, as best expressed by the modern Tasmania's year-round wet climate and growth of temperate rainforests. The absence of rain-bringing Westerlies and dust-scavenging precipitation would result in low Fe-abundances in the GAB record.

The mid-Holocene is characterized by a distinct decrease in $\delta^{18}O$ values, which can be attributed to an increase in SST and correlated to modern sea-level rise at ~6.8 ka BP (Belperio et al., 2002). Further, high SST estimates at ~7 ka BP correspond to maximum temperature estimates from pollen at this time. Since ~5 ka BP, pteridopythe spores (ferns and allies), originating from Indonesia or Papua New Guinea, are found in NW Australian marine sediment cores and interpreted as a change in the oceanic circulation of the region (DeDekker, 2001). Since ~5 ka BP, the GAB oxygen isotope record shows increased variability coinciding with the proposed increase in El Niño-Southern Ocean (ENSO) variability during the last 5 ka (McGlone et al., 1992). During El Niño events, the Leeuwin Current flow weakens due to a lower pressure gradient between the Pacific Warm Pool and the Southern Ocean. This results in coastal sea-level fall and an increased influence of cool Southern Ocean Waters on the shelf, affecting commercial fisheries, i.e. the rock lobster and larvae distribution of Western Australia (Pearce and Phillips, 1988). Increase in the influence of the ENSO could explain the variability observed in the SST record for the Late Holocene. Furthermore, intensified winds and storminess characterize continental Southern Australian since ~5 ka BP, which additionally indicates increased climate, most likely ENSO, variability. Southern Australia is especially affected the alterations in strength and direction of the Westerlies in association with ENSO events, i.e. strengthening and more southwesterly flow of the Westerlies during El Niño (McGlone et al., 1992). This phenomena, in turn, explains the observed decrease in Fe abundance in the GAB record and further supporting our dust hypothesis as the driving mechanism controlling dust input (Nicholls, 1992).

## 5.4   **Conclusions**

In summary, our combined oxygen-isotope and Fe-abundance stratigraphies provide the first high-resolution record of climate variability in the marine southern mid-latitudes extending back to the LGM. The data indicate a step-wise warming and sea-level rise during the deglaciation. The cold-reversal (CR2) towards the end of the deglaciation that is quasi-synchronous to the Younger Dryas Chronozone in the Northern Hemisphere, indicating the global nature of this event. The mid-Holocene climate change significantly affected the Australian southern mid-latitudes indicating fundamental change in atmospheric and oceanic circulation patterns in the region. The GAB record illustrates the potential of continental margin settings as sites of high sediment deposition forming the basis of high-resolution studies and providing climate records to link terrestrial, continental and open-ocean environments. The GAB setting records rapid climate and oceanographic changes adding a critical piece to the Southern Hemisphere mid-latitude puzzle of climate change.

## **Acknowledgements**

## **References**

Almond, D., McGowran, B., and Li, Q. (1993). Late Quaternary Foraminiferal record from the Great Australian Bight and its environmental significance. *Memoir Association Australasian Paleontologist* **15,** 417-428.

Bard, E., Hamelin, B., Arnold, M., Montaggioni, L. F., Cabioch, G., Faure, G., and Rougerie, F. (1996). Deglacial sea-level record from Tahiti corals and the timing of global meltwater discharge. *Nature* **382,** 241-244.

Bard, E., Rostek, F., and Sonzogni, C. (1997). Interhemispheric synchrony of the last deglaciation inferred from alkenone palaeothermometry. *Nature* **385**.

Barrows, T. T., Stone, J. O., Fifield, L. K., and Cresswell, R. G. (2001). Late Pleistocene Glaciation of the Kosciuszko Massif, Snowy Mountains, Australia. *Quaternary Research* **55,** 179-189.

Belperio, A. P., Harvey, N., and Bourman, R. P. (2002). Spatial and temporal variability in the Holocene sea-level record of the South Australian coastline. *Sedimentary Geology* **150,** 153-169.

Bye, J. A. T. (1972). Ocean Circulation South of Australia. *In* "Antarctic Oceanology II: The Australian-New Zealand Sector." (D. E. Hays, Ed.), pp. 95-100. A.G.U. Antarctic Research Series. A.G.U. Antarctic Research Series, Washington D.C.

Charles, C. D., Lynch-Stieglitz, J., Ninnemann, U. S., and Fairbanks, R. G. (1996). Climate connections between the hemisphere recealed by deep sea sediment core/ice core correlations. *Earth and Planetary Science Letters* **142,** 19-27.

DeDekker, P. (2001). Records fo Environmental Changes in the Australian Sector of Pep II Point to Broad Trends of Climate Change. *In* "PAGES News.", pp. 4-5. PAGES.

Feary, D. A., and James, N. P. (1998). Seismic Stratigraphy and Geological Evolution of the Cenzoic, Cool-Water Eucla Platform, Great Australian Bight. *AAPG Bulletin* **82,** 792-816.

Fleming, K., Johnston, P., Zwartz, D., Yokoyama, Y., Lambeck, K., and Chappell, J. (1998). Refining the eustatic sea-level curve since the Last Glacial Maximum using far- and intermediate-field sites. *Earth and Planetary Science Letters* **163,** 327-342.

Goldberg, E. D., and Griffin, J. J. (1970). The sediments of the northern Indian Ocean. *Deep-Sea Research* **17**.

Griffin, J. J., Windom, H., and Goldberg, E. D. (1968). The distribution of clay minerals in the worlds oceans. *Deep Sea Research Part II* **15,** 433-459.

Harrison, S. P., and Dodson, J. (1993). Climates of Australia and New Guinea since 18,000 yr B.P. *In* "Global Climates since the Last Glacial Maximum." (J. Wright, J.E., J. E. Kutzbach, T. Webb III, W. F. Ruddiman, F. A. Street-Perrott, and P. J. Bartlein, Eds.), pp. 265-293. University of Minnesota Press, Minneapolis.

Haug, G. H., Hughen, K. A., Sigman, D. M., Peterson, L. C., and Röhl, U. (2001). Southward Migration of the Intertropical Convergence Zone Through the Holocene. *Science* **293,** 1304-1308.

Hemleben, C., Spindler, M., and Anderson, O. R. (1989). "Modern Planktonic Foraminifera." Springer, New York, Berlin, Heidelberg.

Hufford, G. E., McCartney, M. S., and Donohue, K. A. (1997). Northern boundary current and adjacent recirculations off southwestern Australia. *Geophysical Research Letters* **24,** 2797-2800.

James, N. P., Bone, Y., Collins, L. B., and Kyser, T. K. (2001). Surficial Sediments of the Great Australian Bight: Facies Dynamics and Oceanography on a Vast Cool-Water Carbonate Shelf. *Journal of Sedimentary Research* **71,** 549-567.

James, N. P., and Clarke, J. A. D. (1997). Cool-Water Carbonates. *In* "SEPM Special Publication.", pp. 440. SEPM, Tulsa.

James, N. P., Feary, D. A., Surlyk, F., Simo, J. A. T., Betzler, C., Holburn, A. E., Qianyu, L., Matsuda, H., Machiyama, H., Brooks, G. R., Andres, M. S., Hine, A. C., Malone, M. J., and Party, O. D. P. L. S. (2000). Quaternary bryozoan reef mounds in cool-water, upper slope environments: Great Australian Bight. *Geololy* **28,** 647-650.

Kent, D. V. (1982). Apparent correlation of paleomagnetic intensity and climatic records in deep sea sediments. *Nature* **299,** 538-539.

Lamy, F., Hebbeln, D., Rohl, U., and Wefer, G. (2001). Holocene rainfall variabiliy in southern Chile: a marine record of latitudinal shifts of the Southern Westerlies. *Earth and Planetary Science Letters* **182,** 369-382.

Li, Q., James, N. P., Bone, Y., and McGowran, B. (1999). Paleoceanographic significance of recent foraminiferal biofacies on the southern shelf of Western Australia: a preliminary study. *Paleogeography, Paleoclimatology, Paleoecology* **147,** 101-120.

Markgraf, V. (2001). Interhemispheric Climate Linkage, pp. 454. Academic Press, San Diego.

McGlone, M. S., Kershaw, A. P., and Markgraf, V. (1992). El Niño/Southern Oscillation climatic variability in Australasian and South American paleoenvironmental records. *In* "El Niño: Historical and Paleoclimatic Aspects of the Southern Ocean Oscillation." (H. F. Diaz, and V. Markgraf, Eds.), pp. 435-462. Cambridge University Press, Cambridge.

McGlone, M. S., Salinger, M. J., and Moar, N. T. (1993). Paleovegetation Studies of New Zealand's Climate since the Last Glacial Maximum. *In* "Global Climates since the Last Glacial Maximum." (J. Wright, J.E., J. E. Kutzbach, T. Webb III, W. F. Ruddiman, F. A. Street-Perrott, and P. J. Bartlein, Eds.), pp. 294-317. University of Minnesota Press, Minneapolis.

McGowan, H. A., McTainsh, G. H., Zawar-Reza, P., and Sturman, A. P. (2000). Identifying regional dust transport pathways: application of kinematic trajectory modelling to a trans-Tasman case. *Earth Surface Processes and Landforms* **25,** 633-647.

McGowran, B., and al., e. (1997). Biogeographic impact of the Leeuwin Current in southern Australia since the late middle Eocene. *Paleogeography, Paleoclimatology, Paleoecology* **136,** 19-40.

McTainsh, G. H. (1989). Quaternary aeolian dust processes and sediments in the Australian region. *Quaternary Science Reviews* **8,** 235-253.

McTainsh, G. H., and Lynch, A. W. (1996). Quatitative estimates of the effect of climate change on dust storm activity in Australia during the Last Glacial Maximum. *Geomorphology* **17,** 263-271.

McTainsh, G. H., and Pitblado, J. R. (1987). Dust storms and related phenomena measured from meteorological records in Australia. *Earth Surface Processes and Landforms* **12,** 415-424.

Miller, G. H., Magee, J. W., and Jull, A. J. T. (1997). Low-latitude glacial cooling in the Southern Hemisphere from amino-acid racemization in emu eggshells. *Nature* **385,** 241-244.

Nicholls, N. (1992). Historical El Niño/Southern Oscillation variability in the Australasian region. *In* "El Niño: Historical and Paleoclimatic Aspects of the Southern Oscillation." (H. F. Diaz, and V. Markgraf, Eds.), pp. 151-173. Cambridge University Press, Cambridge.

Pearce, A. F., and Phillips, B. F. (1988). ENSO events, the Leeuwin Current and larval recruitment of the Western Rock Lobster. *Journal du Conseil* **45,** 13-21.

Petit, J. R., Jouzel, J., Raynaud, D., Barkov, N. I., Basile, I., Bender, M., Chappellaz, J., Davis, M., Delaygue, G., Delmotte, M., Kotlyakov, M., Legrand, M., Lipenkov, V. Y., Lorius, C., Pépin, L., Ritz, C., Saltzman, E., and Stievenard, M. (1999). Climate and atmospheric history of the past 420000 years from the Vostok ice core, Antarctica. *Nature* **399,** 429-436.

Röhl, U., and Abrams, L. J. (2000). High-resolution, downhole and non-destructive core measurements from Sites 999 and 1001 in the Caribbean Sea: Application to the late Paleocene thermal maximum. *Proceedings of the Ocean Drilling Program Scientific Results* **165,** 191-302.

Schrag, D. P., Adkins, J. F., McIntyre, K., Alexander, J. L., Hodell, D. A., Charles, C. D., and McManus, J. F. (2002). The oxygen isotopic composition of seawater during the Last Glacial Maximum. *Quaternary Science Reviews* **21,** 331-342.

Thiede, J. (1979). Wind regimes over the late Quaternary southwest Pacific ocean. *Geology* **7,** 259-262.

Wasson, R. J. (1984). Late Quaternary palaeoenvironments in the desert dunefields of Australia. *In* "Late Cainozoic Palaeoclimates of the Southern Hemisphere." (J. C. Vogel, Ed.), pp. 419-432. Balkema, Rotterdam.

Wasson, R. J. (1986). Geomorphology and Quaternary history of the Australian continental dunefields. *Geographical Review of Japan* **59,** 55-67.

Yokoyama, Y., Lambeck, K., DeDekker, P., Johnston, P., and Fifield, L. K. (2000). Timing of the Last Glacial Maximum from observed sea-level minima. *Nature* **406,** 713-716.

Yokoyama, Y., Purcell, A., Lambeck, K., and Johnston, P. (2001). Shore-line reconstruction around Australia during the Last Glacial Maximum and Late Glacial Stage. *Quaternary International* **83-85,** 9-18.

# 6   MULTI-PROXY PALEOCEANOGRAPHIC STUDY OF LGM TO HOLOCENE SEDIMENTS FROM THE GREAT AUSTRALIAN BIGHT, SITE 1127

## Abstract

Sediments from the upper 10 m of Site 1127 documents in unprecedented and continuous detail the last glacial-interglacial cycle. The combining of open-ocean and margin proxy records illustrates the effect of changing oceanographic conditions on the benthic shelf community and margin evolution. The last glacial maximum is characterized by cold, nutrient-rich oceanographic conditions promoting the growth of bryozoan mounds, but, since no sediment is produced on the exposed upper shelf, overall accumulation rates are low. During sea-level rise and transgression, the shelf is flooded and carbonate production and deposition resumes. The identification of a cold reversal at the end of the deglaciation is based on $\delta^{18}O$ data. Benthic data, however, indicate a significant lag of intermediate water masses relative to surface water changes. Unusually high sedimentation and accumulation rates are found in the Early Holocene, and the high productivity explained by a dominant Southern Ocean influence on the margin via the Flinders Current. Nitrogen isotope data, high $C_{org}$ content support the proposed hypothesis. Furthermore, increased iron input, from dust-entrainment fallout over the Bight, further enhanced primary productivity. In contrast, the Late Holocene sees the decline of carbonate production and accumulation to near-glacial levels, which is interpreted as the result of dominant oligotrophic Leeuwin Current flow and increasing ENSO variability.

## 6.1   Introduction

Continuous and high-resolution marine records spanning the last glacial cycle in temperate Southern Australia are absent. All southern Australian and Tasmanian palaeo-records over this time interval are of terrestrial nature. They are developed from an impressive variety of archives, settings and proxies ranging from pollen studies in lacustrine and peat settings, reconstruction of glacier advances (Barrows et al., 2001), vegetational changes inferred from stick-nest rat middens (McCarthy and Head, 2001) and temperature reconstruction from emu-shell amino-acid racemization (Miller et al., 1997). Although these records have greatly improved the understanding of southern Australian paleoclimatic change they all lack continuity and due to their terrestrial nature provide no information on the paleoceanographic change.

Marine studies from this area are either restricted to surface sediments (James et al., 2001) or cover the Late Pleistocene and, therefore, lack the temporal resolution across the here focussed interval of this study. The modern interplay of different oceanographic regimes on a well-documented seasonal cycle is complex and not fully understood (James et al., 2001; James et al., 2000) but produces a unique faunal and floral bioassemblage (Almond et al., 1993; McGowran and al., 1997), which, due to the

high-energy environment, is deposited on the shelf-edge and upper slope. Thus, the upper 10 m of sediment recovered at Site 1127 provided the unique opportunity to study paleoceanographic change and its effect on margin evolution in high-resolution detail over the last 20,000 years.

## 6.2   Methods and Materials

This study focuses on the uppermost 10 m of the 510-m long record of Site 1127, which is located just in front of the present-day shelf edge in 480.6 m of water depth. In the upper 6 m of the interval, the sediments are dominated by nannofossils and foraminiferal ooze (Feary et al., 2000). The lower interval (6-10 mbsf) consists of unlithified bioclastic packstone to wackestone. The terrestrial input is negligible due to widespread hinterland aridity and lack of rivers.

Carbon and oxygen isotopes were measured on planktonic and benthic foraminifera, and nitrogen isotopes analyzed on homogenized bulk sediment samples. Bulk sediment was also analyzed for carbonate and inorganic carbon content. Sand fraction percentages were calculated from the total dry and >63 μm fraction. Sediment treatment prior to analysis and a description of methods use are found in Chapter 3.

## 6.3   Results

### 6.3.1   $\delta^{18}O$ and $\delta^{13}C$ Results of Planktonic & Benthic Foraminifera

*Planktonic $\delta^{18}O$*

Stable oxygen isotope results for planktonic foraminiferal species *G. ruber* and *G. bulloides* are shown in a depth profile (Fig. 6.1a). Although the sample resolution for *G. ruber* is much higher (1 sample/5 cm) than for *G. bulloides*, both records approximately exhibit the same trends.

For *G. ruber,* isotopic values within the 10 m record range over 2‰, from 1.5 to –0.5‰. Values in the lowest part of the record (9.5-10 mbsf) plot around 1.35‰, before abruptly decreasing to 0.75‰ at 9.25 mbsf. Values continuously decrease to 0.0‰ at 8.41 mbsf before abruptly increasing by 0.5‰ to values ranging around 0.7‰ for the next 0.5 m before returning to values of around 0.0‰. The record between 7.7 and 6 mbsf is characterized initially by high-frequency low-amplitude variations, before values constantly, but gradually decrease over the next 3 m. At 3 mbsf, values decrease further to –0.25‰. The upper 2 m of the record fluctuate around –0.25‰. The last sample records another decrease to –0.5‰ at the core top.

For *G. bulloides*, most positive values (1.6-2‰) are found in the lowest part of the record before rapidly decreasing to 0‰ at 8.4 mbsf. The next 0.54 m (8.4-7.95 mbsf) are characterized by an abrupt 1‰ decrease followed by values ranging around 1-1.2‰, before values rapidly return to 0.1‰ at 7.95 mbsf. Between 7.9 and 5.3 mbsf values scatter over 1‰ range. For the remainder of the record, $\delta^{18}O$ values slowly decrease from 0.5 to 0‰.

## Benthic $\delta^{18}O$

Benthic $\delta^{18}O$ results are shown in Figure 6.1b. From 10 to 8.35 mbsf all three benthic species measured (*F. wullerstorfi, Cibicidoides spp* and *U. peregrina*) show a decrease (3.1 to 1‰ for *F.wullerstorfi*, 2.8 to 1.1‰ for *Cibicidoides spp.* and 3.3 to 1.9‰ for *U. peregrina*). A rapid increase, as observed in the planktonics, is recorded in a stepwise manner for *Cibicidoides spp* at 8.35 mbsf before returning to 1‰ at 8.65 mbsf. *F. wullerstorfi* increases over 1‰ at 8.1 mbsf as abruptly as it increases again at 7.9 mbsf, whereas *U. peregrina* over the same interval only decreases by 0.4‰ The upper part of the record (8 to 0 mbsf) is only documented in the $\delta^{18}O$ values of two species, *F. wullerstorfi* and *Cibicidoides spp.*, as *U. peregrina* is absent, except for one sample at 2 mbsf. Furthermore, there are no data from 6.3 to 5.3 mbsf as neither *F. wullerstorfi* nor *Cibicidoides spp.* were found in the sediment. The upper part of the record is characterized by benthic $\delta^{18}O$ values ranging from 1 to1.5‰, and no offset between *F. wullerstorfi* and *Cibicidoides spp.* was observed.
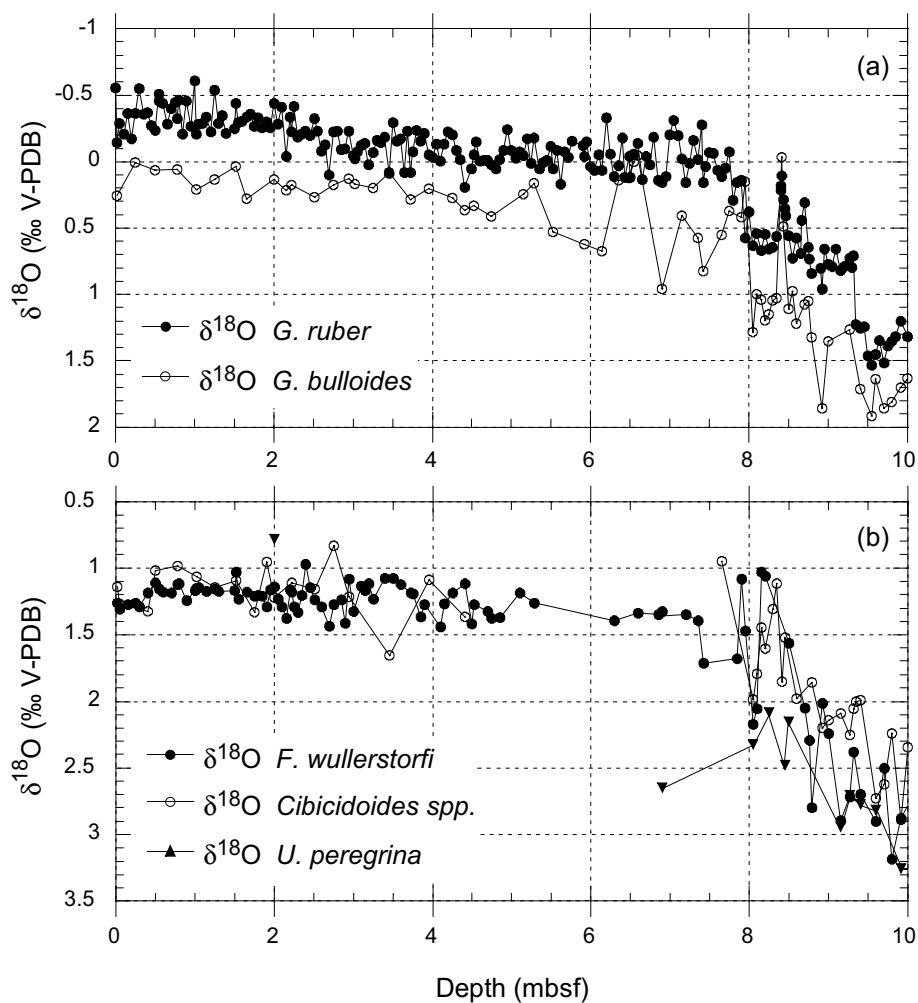


**Figure 6.1.** *Oxygen isotope results plotted against depth for (a) planktonic foraminifera G. ruber and G. bulloides and (b) for benthic foraminifera F. wullerstorfi, Cibicidoides spp. and U. peregrina.*

### Planktonic $\delta^{13}C$

The $\delta^{13}C$ results for *G. ruber* are marked by very little variation throughout the entire 10 m interval (Fig. 6.2a). Values slightly decrease in the lowest part of the record (10-8.5 mbsf) from 1.45 to 0.8‰. $\delta^{13}C$ values decrease slightly in the remainder of the record (8.55-0 mbsf). A generally decreasing trend from 10 to 6.75 mbsf is seen in the $\delta^{13}C$ values for *G. bulloides* (Fig. 6.2a). At 8.4 mbsf values increase rapidly before decreasing at 7.95 mbsf again. Up to 1.25 most of the record is characterized by values scattering from 0 to –1‰ before increasing to 1.4‰ at 0.78 mbsf returning to –0.7‰ at the top of the section.

### Benthic $\delta^{13}C$

In the benthic $\delta^{13}C$ results (Fig. 6.2b), the bottom part of the record (10-8 mbsf) is marked by a broad decreasing trend. *F.wullerstorfi* $\delta^{13}C$ values generally are the most positive values, followed by *Cibicidoides* spp. and *U. peregrina* with the most negative values. *U. peregrina* specimens are common in samples from below 8 mbsf and only rarely occur in the upper part of the record. As already discussed in the planktonic $\delta^{18}O$ results there is data-gap between 6.3 and 5.2 mbsf due to lack of benthics in the sediments. From 5 to 2 mbsf, the *F. wullerstorfi* $\delta^{13}C$ results increase from 1.25 to 2‰ before ranging roughly between 1.7 and 1.9‰ for the remainder of the record. The very low-resolution record for Cibicidoides spp. in the upper 4.5 mbsf shows scatter in the values of over 0.5‰, but the same increasing trend as for *F. wullerstorfi* is confirmed. Values in the upper 2 mbsf scatter between 1.1 and 1.6‰. *Cibicidoides* spp. values are in most cases more negative than the corresponding *F. wullerstorfi* values.

### Delta $\delta^{13}C$

Delta $\delta^{13}C$ results were calculated by subtracting the $\delta^{13}C$ results of *G. ruber* from *F. wullerstorfi* (Fig. 6.2c) in order to obtain information about the surface- to bottom-water gradient. The initially highly variable, but increasing trend (~-1.2 to 0.9‰) from 10 to 8 mbsf, is followed by a plateau of delta $\delta^{13}C$ values, ranging between 0 and –0.7‰ from 8 and 5 mbsf. Values then decrease up to 2 mbsf, after which they are constant (~-0.9‰) in the remainder of the record.
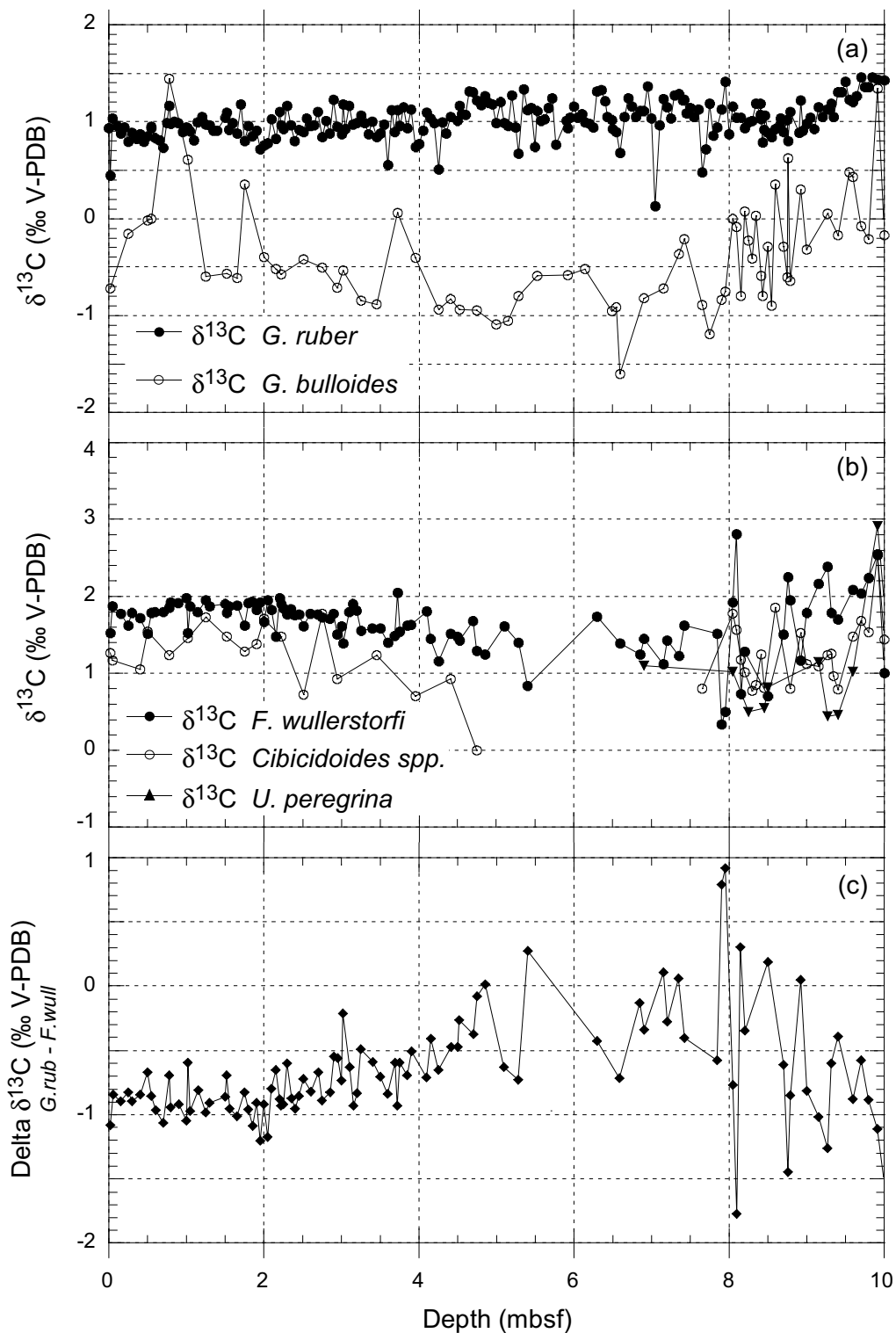
***Figure 6.2.*** *Carbon isotope results plotted against depth for (a) planktonic foraminifera G. ruber and G. bulloides and (b) for benthic foraminifera F. wullerstorfi, Cibicidoides spp. and U. peregrina. (c) Delta δ$^{13}$C results showing the surface- to bottom-water gradient calculated from G. ruber and F. wullerstofi data.*

### 6.3.2    Nitrogen Isotopes, %N and C/N Results

Bulk nitrogen isotope measurements over the 10 m, record $\delta^{15}N$ values ranging from 7.6 to 4.8‰ and are characterized into three intervals (Fig. 6.3a). The lower-most interval features the most positive values of 7 to 7.5‰ before continuously decreasing to ~5‰ at 7.9 mbsf. Following, in the middle interval from 7.9 to 5 mbsf, $\delta^{15}N$ results are marked by the lowest values ranging from 5 to 5.5‰. Above 5 mbsf, $\delta^{15}N$ values constantly decrease to 6.25‰ at 3.25 mbsf. In the upper 2.5 m of the record, values fluctuated around 6.5‰.

Nitrogen contents (weight percentages) range from 0.3 up to 0.12% and the curve generally reflects the opposite trends as seen in the $\delta^{15}N$ results (Fig. 6.3b). C/N ratios (Fig. 6.3c) in the lowest part of the record are characterized by rapid increase in ratios from 5 to 20, followed by a rapid decrease to 10 at 8 mbsf. From 7.5 to 3.5 mbsf C/N ratios continuously decrease from 15 to 9 before rising and fluctuating around 10-15. In the upper 1 m, ratios range from 7.5-9.5.

### 6.3.3    Coulometric Results

The total weight percent carbonate ($CaCO_3$) and organic carbon ($C_{org}$) contents vary quite significantly over the discussed 10 m interval (Fig. 6.4a,b). Total carbonate percentages show an overall decreasing trend from 98 to 90% (Fig. 6.4a). The $C_{org}$ percentages (Fig. 6.4b) are unusually high for a pure carbonate system. The lowest $C_{org}$ percentages are found in the bottom part of the record (0.17%) before rising rapidly to reach the highest $C_{org}$ values of 1.35% at 6.35 mbsf. From 6.35 to 0.65 mbsf, the $C_{org}$ content constantly decreases to 0.26% before rising again to 0.75% at 0.35 mbsf and then falling to 0.52 in the surface samples.

### 6.3.4    Sand Fraction Results

The most distinctive feature in the sand fraction record (Fig. 6.4c) is the high variability observed from 10 to 8 mbsf, ranging from over 50 to 15% and returning to 42% before falling to 20%. For the remainder of the record, sand fraction percentages range between 10 and 20% in the 8 to 6 m depth interval, whereas the upper part of the record contains percentages between 20 and 30%.

### 6.3.5    Bulk Sedimentary Iron Abundances

The lowest Fe abundances are recorded in the lowest 0.5 m of the record (Fig. 6.4d). Increasing Fe values from 10 to 7.5 mbsf are followed by a plateau of high values, on average 350 counts per seconds, before gradually decreasing towards the top of the record. The Fe record is discussed in detail in Chapter 5.
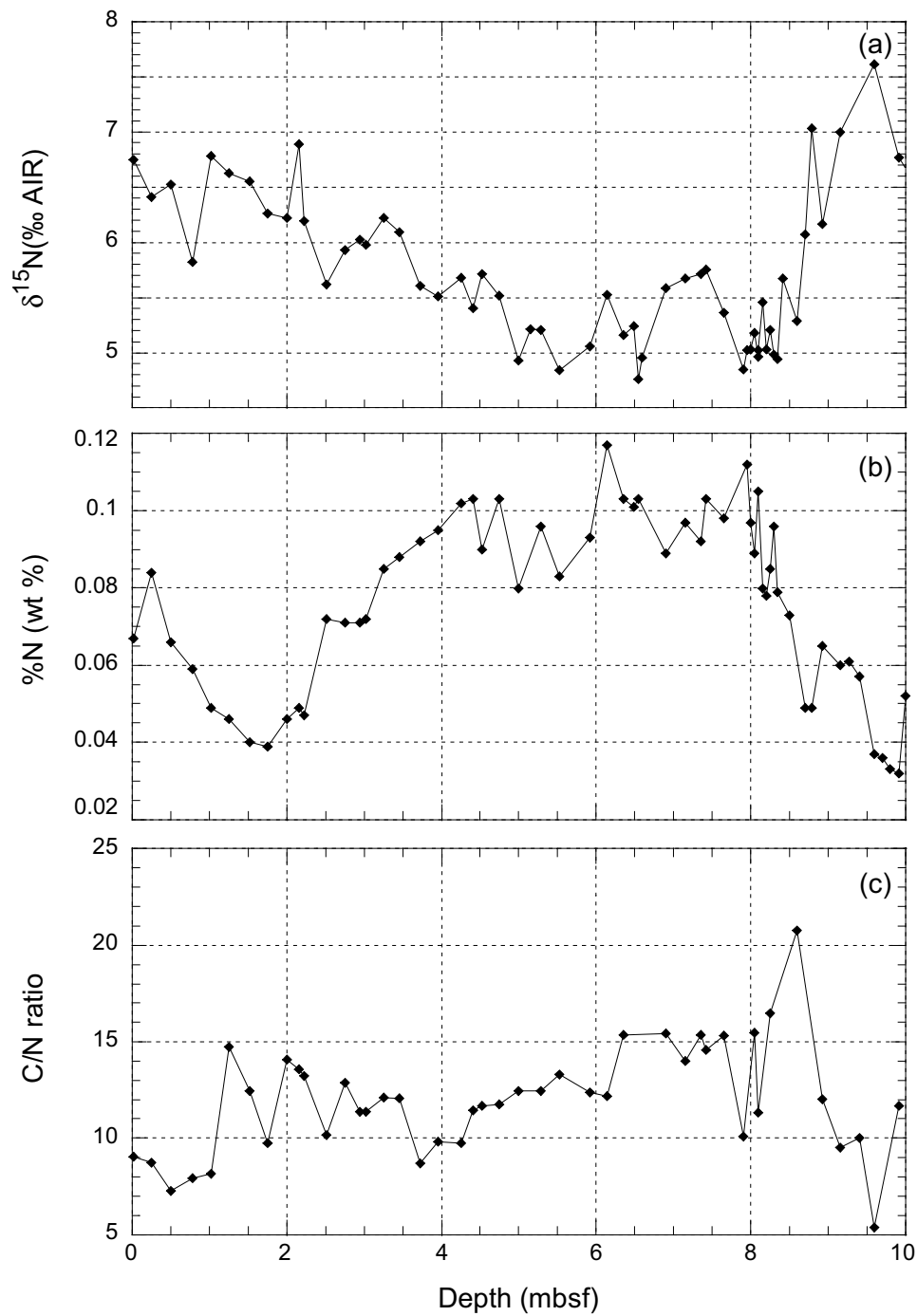
**Figure 6.3.** Results of (a) $\delta^{15}N$ measurements, (b) Nitrogen percentages, and (c) calculated C/N ratios plotted against depth.
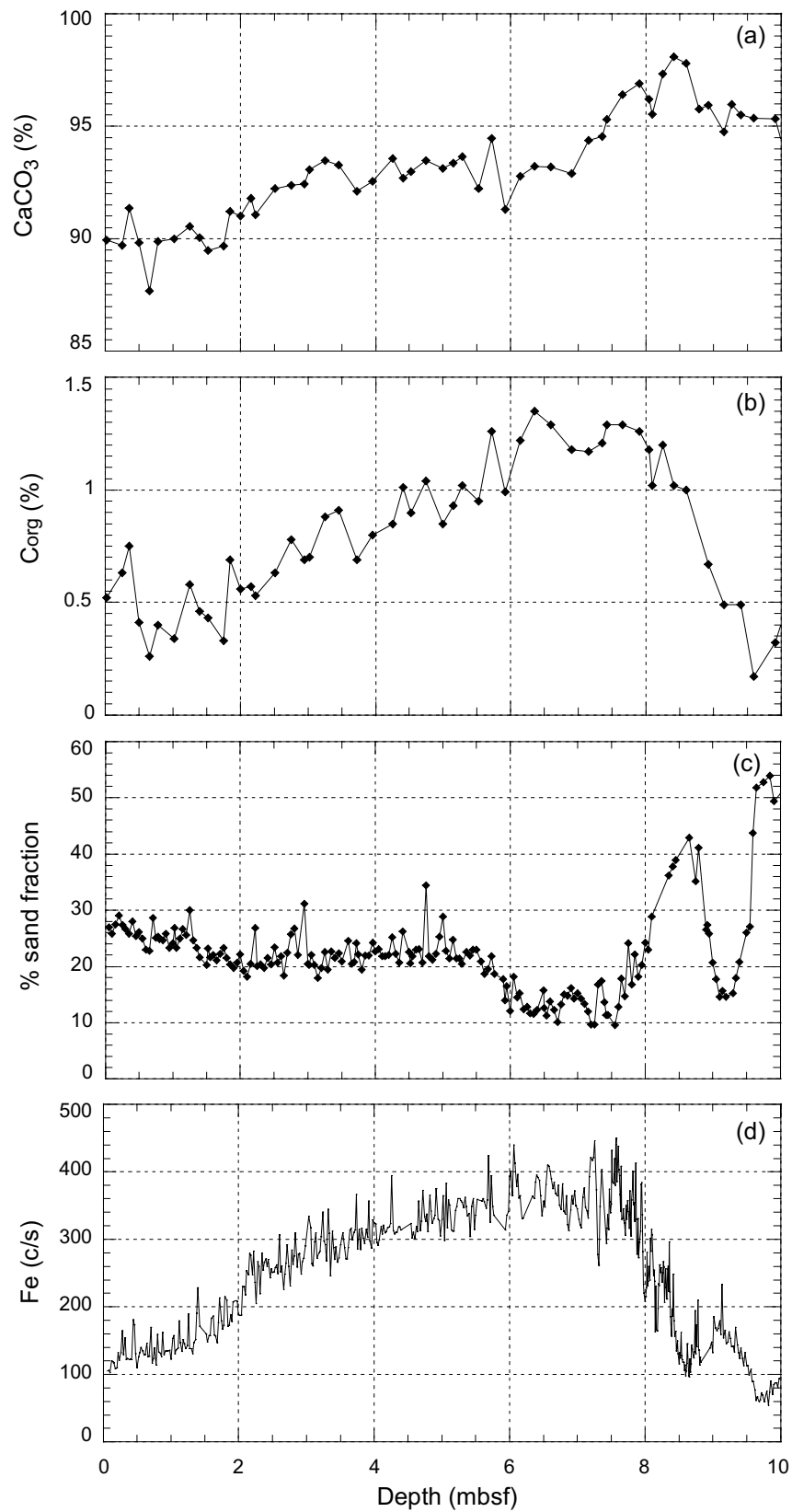
***Figure 6.4.*** *Results of (a) coulometric analysis of total carbon content, (b) organic carbon content, (c) sand fraction (>63 μm) percentages, and (d) bulk sedimentary iron abundances plotted against depth.*

## 6.4   Age Model

The age model for this study is based on 12 AMS radiocarbon dated horizons from monospecific planktonic foraminifera *G. inflata* samples (Fig. 6.5a). Radiocarbon dates were converted to calendar ages using the online CALIB HTML version 4.3 program (http://depts.washington.edu/qil/calib/), Method A and the marine calibration dataset MARINE98) (Stuiver et al., 1998a) (see Table 3.1 in Chapter 3). Besides the program-included 400-year correction for ocean surface reservoir effects, we added a local, GAB correction ($\Delta R = 61 \pm 29$ years). The weighted mean ages of the calibrated ranges (see Chapter 3, Table 3.1) are used in the age model that was then constructed by linear interpolation of age versus depth (Fig. 6.5a).

### 6.4.1   Sedimentation Rates

Sedimentation rates (SR) were calculated assuming constant sedimentation between dated horizons Ranging from 23 up to 183 cm/kyr, they vary significantly over the studied interval (Fig. 6.5b). The lowest sedimentation rates, on average 25 cm/kyr, are found from 10 to 8 mbsf, rapidly increasing from 8 to 7 mbsf. Highest sedimentation rates of ~180 cm/kyr are calculated for the interval from 7 to 3.75 mbsf, before step-wise decreasing to 100 cm/kyr at 3.75 mbsf and to 30 cm/kyr in the upper 2 m of the record.

### 6.4.2   MAR and Corg Accumulation Rates

Mass accumulation rates were calculated from the product of sedimentation rates and dry bulk density, which was taken from shipboard analysis (Feary et al., 2000) (see Chapter 3.9 for details). Mass accumulation rates (MAR), like the sedimentation rates, fluctuate significantly over the 10 m interval (Fig. 6.5c). Low MAR of 20-50 $g/cm^2/kyr$ are found in the lowest part of the record (10-8 mbsf), after which MAR increases rapidly from 8 to 7 mbsf. Constant high MAR of ~180 $g/cm^2/kyr$ are found from 7 to 3.75 mbsf, after which they decrease to 100 $g/cm^2/kyr$ from 3.75 to 2 mbsf. Low MAR (25 $g/cm^2/kyr$) are observed in the top part of the record, comparable to values found in the lowest part of the record (10-8 mbsf).

Organic carbon accumulation rates follow the overall trend observed in the MAR, ranging from 0.2 to 2.5 $gC_{org}/cm^2/kyr$. Note the difference in scales on Figure 6.5c.
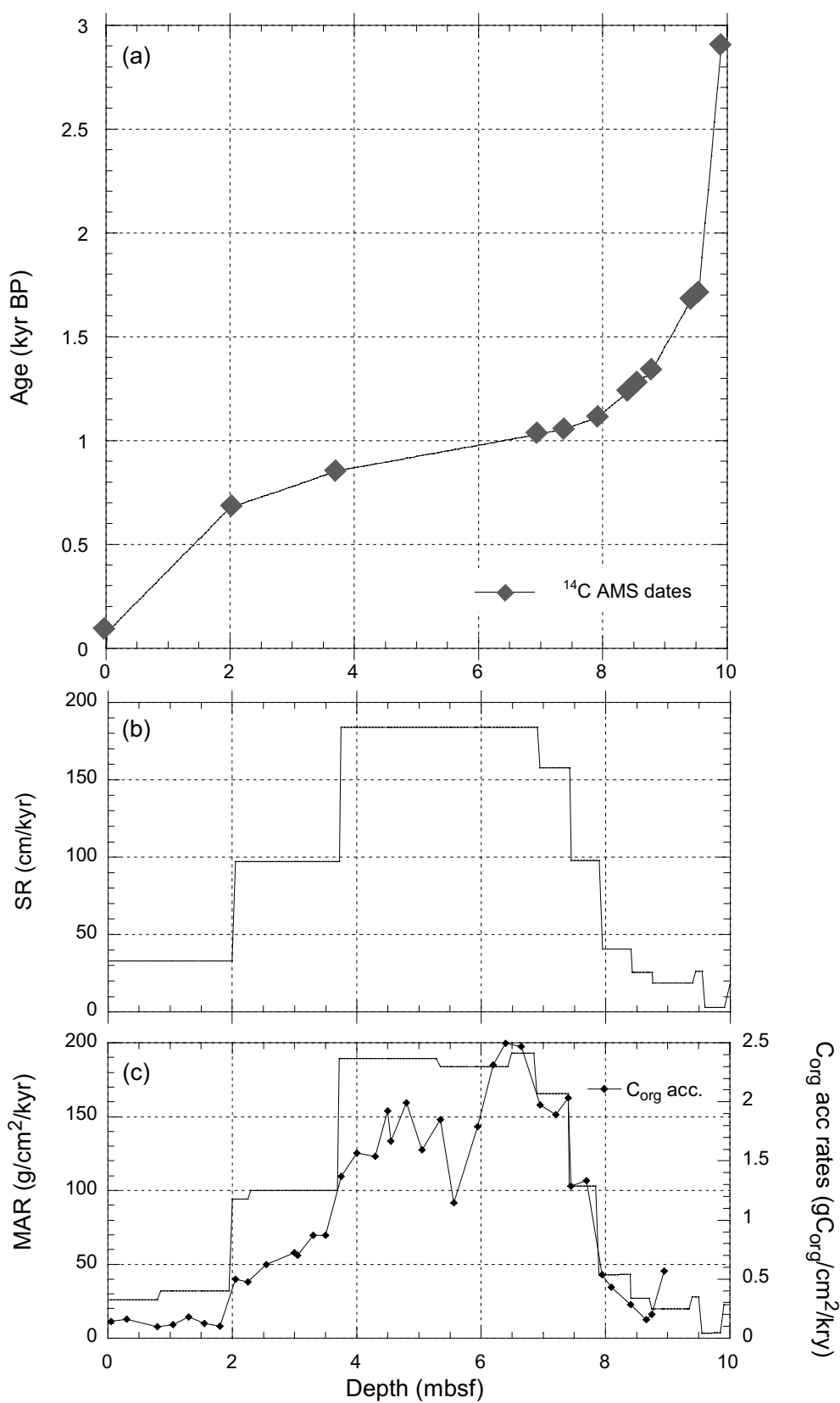
***Figure 6.5.*** *(a) age-depth relationship of $^{14}$C-chronology in comparison to (b) sedimentation rates and (c) mass accumulation and $C_{org}$ accumulation rates.*

### 6.4.3    Chronostratigraphy

The Site 1127 record is a product of massive off-shelf transport, which is the reason for the unusually high sedimentation and accumulation rates, as well as the variable sand-fraction percentages. Furthermore, the sediment is fully bioturbated and all aspects taken together raised questions about the stratigraphic integrity. However, detailed visual core-inspection shows no evidence of graded beds indicative of turbidites or erosional surfaces, indicative of a hiatus. Although, on the one side, off-shelf transport results in high-sedimentation rates, these, on the other side, also minimize the effect of bioturbation and disturbance. Furthermore, the absence of age reversals in the high-resolution radiocarbon chronology, with samples partially only 10 to 20 cm apart, argues for continues sedimentation, although highly variable, and, thus, a reliable chronology.

Uncertainties in the radiocarbon age and calibration to calendar years BP remain. The reservoir-age effect of Southern Ocean waters most likely varied over the LGM and early Holocene but, as this variation is unknown at the moment, it can, not be accounted for in the stratigraphy. Another uncertainty concerns the ages dated between 11,000 to 12,000 years B.P. that lie within the ^{14}C-plateau and significantly affect the error of dating. The core top, was dated at 763 calendar yrs B.P., indicating that the upper-most recent sediments are missing. Alternatively, this core-top age could reflect the current reservoir effect. However, it has to be kept in mind that core tops are only rarely preserved using ODP drilling techniques and the more plausible explanation of the 760-year-old core top represents missing youngest sediments.

Extremely low sedimentation and accumulation rates are calculated for the bottom of the record, between 9.55 and 9.91 mbsf. They indicate very condensed sedimentation, and although the core shows no clear sign of a break in sedimentation, a hiatus cannot be ruled out.

## 6.5    Discussion

Site 1127 results are first discussed in 4 time intervals: LGM, deglaciation phase, Early Holocene and Late Holocene. In a second step, we place the Site 1127 results into a regional southern Australian paleoceaonographic context. Planktonic and benthic $\delta^{18}O$ and $\delta^{13}C$ result are plotted against age in Figure 6.6. The $\delta^{18}O$ G. ruber results are added as the reference data set together with TC, Corg, and MAR plotted against age in Figure 6.7 and together with delta $\delta^{13}C$ results, $\delta^{15}N$, and Fe data in Figure 6.8.

### 6.5.1    LGM (22-18 ka BP)

The LGM in Site 1127 is constrained by the ^{14}C-dated horizon and maximum $\delta^{18}O$ values from planktonic and benthic foraminifera, which are interpreted to reflect colder oceanic conditions. $\delta^{13}C$ results of both planktonic and benthic foraminifera are the most positive of the entire record, and enriched carbon isotopes in plankton are classically interpreted to reflect increased paleoproductivity during the last glacial (Mulitza et al., 1999). This evidence is further supported by the presence of the benthic foraminifera *U. peregrina*, an indicator of elevated nutrient levels (Holbourn et al., 2002).

Enriched $\delta^{15}N$ values (7.6 ‰) suggest a more complete nitrate consumption, which could be either due to less nutrients or more production. Only small amounts of nitrogen are found in glacial sediments correlating to low organic but high total carbon content. High sand-fraction percentages are the result of prolific bryozoan mound growth (Holbourn et al., 2002; James et al., 2000) shedding coarse sediment down the slope. Low Fe abundances are hypothesized to be the result of strong westerly winds and the dust-entrained Fe is bypassing the GAB area (see Chapter 5 for detailed discussion).
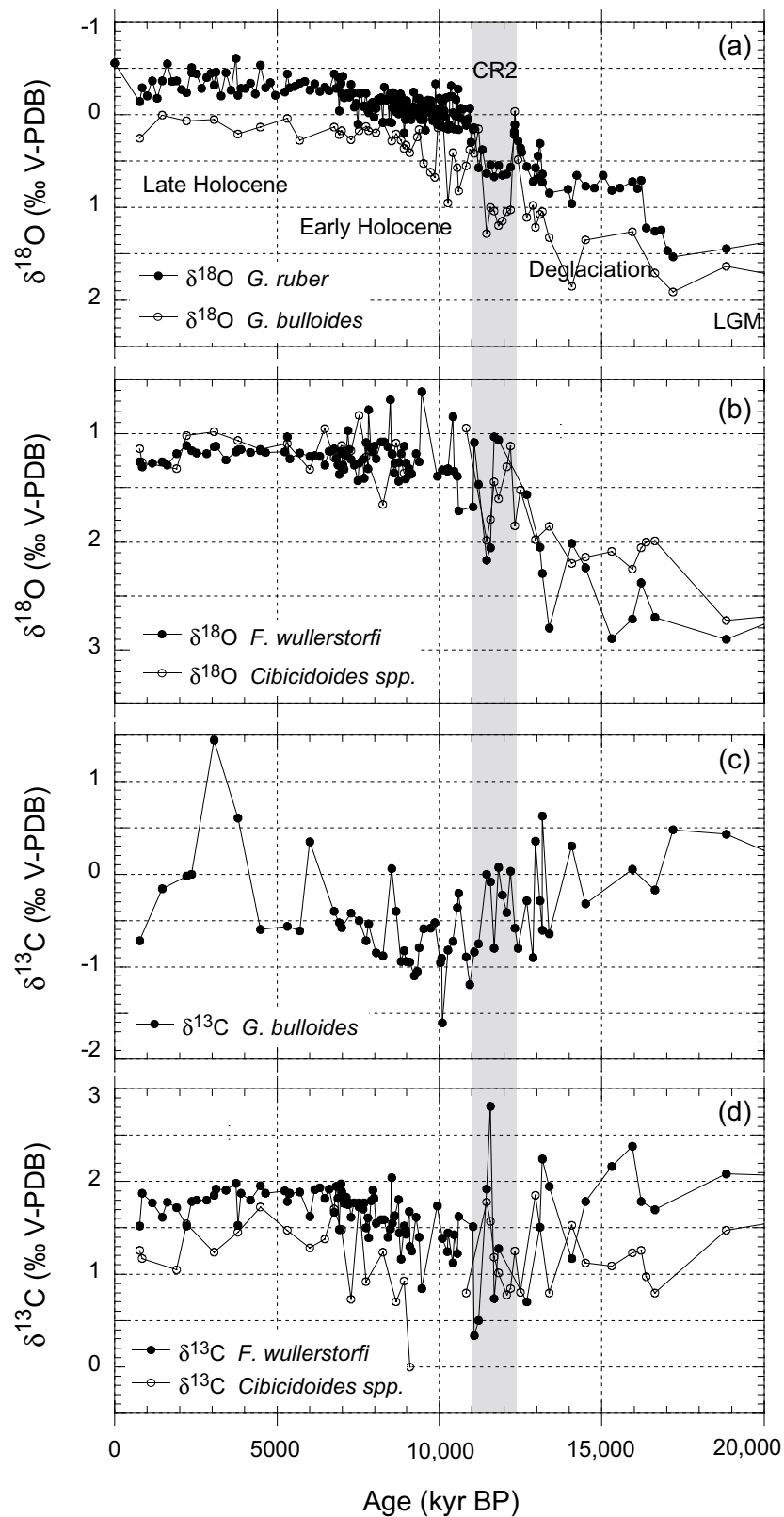
**Figure 6.6.** *Compilation of δ$^{18}$O and δ$^{13}$C results for benthic and planktonic foraminifera plotted against age. Cold reversal 2 (CR2) indicated by grey bar.*

### 6.5.2    The Deglaciation Phase (18-11 ka BP)

The transition from the LGM to Holocene is the most distinctive feature amongst all proxy-records presented. The planktonic $\delta^{18}O$ record is marked by rapid, stepwise warming at 17 and ~16.1 ka BP but the warming trend is interrupted by two significant cold reversals (see Chapter 4 and 5 for detailed discussion). Benthic $\delta^{18}O$ data from *Cibicidoides* spp. indicate similar initial step-wise warming at ~16.1 ka BP, whereas the *F. wullerstorfi* data is more variable. Cold reversals, as identified in the planktonic $\delta^{18}O$ record, are not as obvious in the benthic data, but an increase in the $\delta^{18}O$ seen in all three benthics correlates to the second part of the second cold reversal (CR2) as defined in the planktonic record (Fig 6.7a).

The magnitude of the $\delta^{18}O$ shift from maximum glacial to Holocene conditions inferred from the surface dweller *G. ruber* is ca 2‰. Assuming a $\delta^{18}O$ glacial-interglacial change of seawater by $1.0 \pm 0.1$‰ (Schrag et al., 2002) due to the storage of isotopically light water in the ice sheets, the remaining 1.0‰ change is attributed to a SST warming of ~4°C. For the benthic record (*F. wullerstorfi*) the 0.65‰ glacial-interglacial difference translates to ~2°C of temperature difference. This indicates that surface waters warmed only by 1-2°C more than bottom waters at Site 1127. These changes are slightly higher than the estimated 1-2°C bottom-water change for the eastern part of the southern Australian margin (Lynch-Stieglitz et al., 1994), indicating, that, during the last glaciation, the margin was located in the Subantarctic Zone. Decreasing $\delta^{13}C$ values in both planktonic and benthic foraminifera coincides with the demise of LGM bryozoan mounds growth, strong evidence for decreasing nutrient supply most likely related to changing oceanographic conditions. This is accompanied by rapidly decreasing $\delta^{15}N$ values (Fig. 6.8), which could be the result of the lower degree of nitrate utilization, but proves unlikely when considering the higher Corg accumulation rates. Alternatively, the decrease could be the result of increasing nitrogen fixation through cyanobacteria (Sachs and Repeta, 1999). In contrast, nitrogen percentages increase simultaneously with $C_{org}$ percentages. The significant drop in sand-sized sediment is the results of bryozon mound demise and halt in down-slope shedding. Increasingly, sediments consist of foraminiferal ooze. The high variability observed in the delta $\delta^{13}C$ record shows an overall increasing trend towards 0‰, which would suggest little to no surface-bottom water gradient.
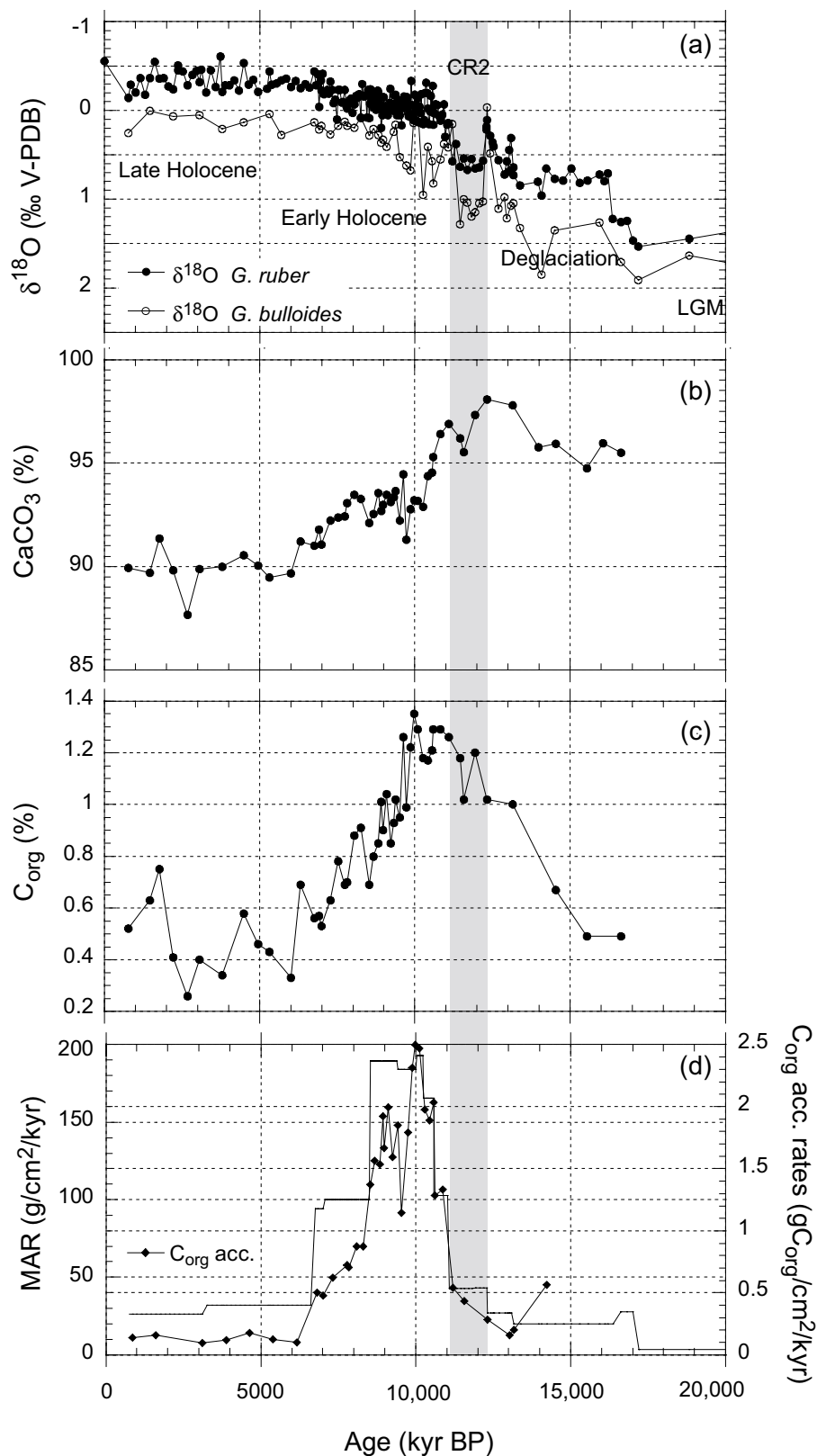
***Figure 6.7.*** *(a) $\delta^{18}O$ results of planktonic foraminifera plotted against age in comparison to (b) total carbon, (c) organic carbon content and, (d) mass accumulation and organic carbon accumulation rates. Cold reversal 2 (CR2) indicated by grey bar.*

The case for the cooling or hydrographic change synchronous with the Younger Dryas Chronozone (YDC) in the Northern Hemisphere was made based on the rapid $\delta^{18}O$ reversal (CR2) identified in the planktonic record (detailed discussion in Chapters 4 and 5). But is there further evidence for YDC change in the proxy-record of Site 1127? Within the benthic $\delta^{18}O$ record of *Cibicidoides* spp., an increase in $\delta^{18}O$ values at the beginning of CR2 occurs not only more gradually but also lags the planktonic record by ~150 years. Assuming no change in the isotopic composition of the seawater, the 1‰ change in *Cibicidoides* spp. $\delta^{18}O$ translates to a cooling of 4°C. The $\delta^{18}O$ decrease in the *F. wullerstorfi* record is abrupt and slightly larger but lags the planktonic record by ~ 600 years. With respect to water mass structure and ocean circulation, the obvious benthic lag suggests the different response of surface and bottom waters at Site 1127 during this interval. As the sea floor at Site 1127 is influenced by intermediate waters masses defined as the Subantarctic Mode Water. This could account for the difference between the timing of the CR2 onset in the planktonic and benthic records.

No change is seen within the $\delta^{13}C$ planktonic G. ruber record, whereas a nearly 1‰ increase is seen in the G. bulloides $\delta^{13}C$ record, possibly indicating a productivity increase during this time. Similar to the benthic $\delta^{18}O$ record, the *Cibicidoides* spp. $\delta^{13}C$ increase of ~0.55‰ lags CR2 by ~270 years. The 30-year difference between the 300 and 270-year lag between $\delta^{18}O$ and $\delta^{13}C$ records, respectively, lies within the resolution of one sample. Results from *F. wullerstorfi* are more variable and of lower resolution but support the *Cibicidoides* spp. evidence.

Nitrogen isotopes decrease to ~5‰ during this interval supporting the productivity argument made above. No significant change is seen in both total and organic carbon, and sand-fraction percentages. In addition, the bulk sedimentary iron abundances are highest in sediments deposited during the Early Holocene (see Chapter 5), and, irrespective of origin and transport, most likely contribute and help sustain the high paleoproductivity.

### 6.5.3   Early Holocene (10.5-6.25 ka BP)

In the early Holocene, $\delta^{18}O$ values decrease in both planktonic records, but, in contrast to *G. ruber*, *G. bulloides* data is much more variable in the earliest Early Holocene. The only benthic data from *F. wullerstorfi* shows a slight, overall decreasing trend with increasing 0.4‰ variability towards the end of the Early Holocene, suggesting that bottom water temperatures were fairly constant. Planktonic carbon results show increased variability in the *G. ruber* record, and slow, but large fluctuation in the *G. bulloides* data. Benthic carbon isotope data are variable too, but a clear trend is not obvious. $\Delta \delta^{13}C$ results show a clear decreasing trend towards –1‰ (Fig. 6.8c). The gradient in the Site 1127 water column is inversed from a typical surface water to bottom gradient, and suggests that surface- and bottom-water masses have two distinct different origins, i.e surface- and bottom-water are disconnected. At depth the continental slope has been influenced by Subantarctic Mode water during the LGM, whereas Flinders Current flow is proposed at the surface. Increasing Leeuwin Current flow towards the end of the Early Holocene and strong flow during the Late Holocene could explain the decreasing gradient in the late Early Holocene and constant negative gradient in the Late Holocene.

This not only supports the hypothesis of strong Leeuwin Current flow only in the later part of the Holocene, but also confirms that the Leeuwin Current is restricted to the upper water column. Nitrogen isotopes are generally depleted during the earliest Early Holocene, possibly implying that nitrogen was not the limiting element and more likely the biological pump was not efficient enough to use all available nutrients. This interpretation is also reflected in the very high nitrogen percentages, especially in a pure carbonate system and also can be noted in the impressively high $C_{org}$ content (1.2-0.8%). Together with the unusually high sedimentation and accumulation rates, the data suggest that the Early Holocene is characterized by prolific carbonate production on the newly flooded shelf and upper slope setting. Alternatively, this high accumulation phase could be interpreted as the result of sediment reworking and off-shelf transport due to sea-level rise. Visual inspection of the core indicates no distinct event and sediment of the >63 μm fraction did not contain unusually high percentages of abraded and reworked fragments.

Nutrient-rich waters are needed to sustain the high productivity of the biotic community. Modern oceanography in the GAB region is dominated by the Leeuwin and Flinders Current flow on a seasonal scale, i.e. the Flinders Current bringing cold and nutrient rich Southern Ocean waters into the Bight becomes an undercurrent to the Leeuwin Current during strong Leeuwin Current flow, but has been observed to move onto the continental shelf, when the Leeuwin Current weakens (Bye, 1971; Bye, 1972; James et al., 2001). Waters of the Leeuwin Current, tropical in origin, are one of the most oligotrophic waters in the Indian and Southern Ocean (Rochford, 1986). In this context, high productivity during the Early Holocene can be explained by prevailing nutrient-rich water masses brought by dominant Flinders Current flow. Or, alternatively, a weak Leeuwin Current flowed during only a part of the year and was restricted to the upper surface waters, since the $\delta^{18}O$ data of *G. ruber,* between the Early and Late Holocene changes by only 1-2°C, which is too small of a change to infer the total absence of the Leeuwin Current during the Early Holocene and a strong Leeuwin Current flow during the Late Holocene. Colder subsurface conditions during the Early Holocene could additionally explain the variable $\delta^{18}O$ values of *G. bulloides* and support the argument for a weak Leeuwin Current. SST, inferred from planktonic foraminiferal $\delta^{18}O$ data is often interpreted as an annual temperature signal, although in most cases, especially with pronounced seasonal difference it represents SST's during the season of growth. Therefore, these data also could reflect the seasonally different temperatures at time of growth.
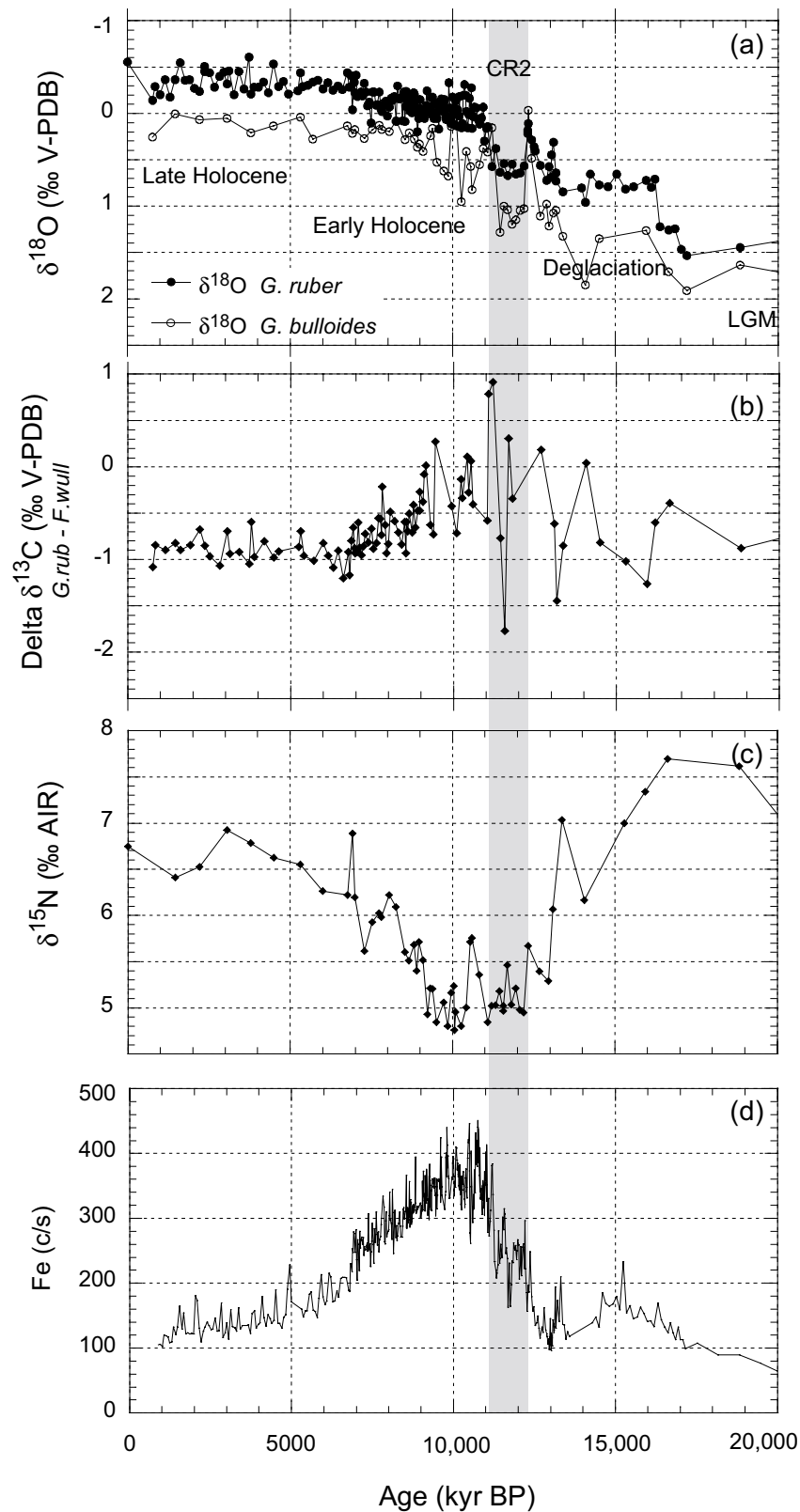
**Figure 6.8.** *(a) $\delta^{18}O$ results of planktonic foraminifera plotted against age in comparison to (b) delta $\delta^{13}C$ from (G. ruber-F.wullerstorfi), (c) $\delta^{15}N$ results and (d) bulk sedimentary iron abundances. Cold reversal 2 (CR2) indicated by grey bar.*

### 6.5.4   Late  Holocene (6.25-0 ka BP)

In the $\delta^{18}O$ values of *G. ruber*, the transition from the Early to the Late Holocene is marked by a decrease, coinciding with Holocene sea-level rise to modern heights. Furthermore, the *G. ruber* record is a bit more variable which has been attributed to increased ENSO variability (see Chapter 5 for detailed discussion). The *G. bulloides* record follows the trend, but the signal is less clear. Benthic $\delta^{18}O$ data record a slight mid-Holocene decrease, and remain uniform, except for an interesting increase of ~0.3‰ at approx. 1000 years B.P. Planktonic $\delta^{13}C$ data is fairly uniform for *G. ruber* and highly variable for *G. bulloides*, and could indicate differences in strength and depth of the Leeuwin Current flow and thus affecting the deeper-dwelling *G. bulloides*. Not much variability, however, is seen in the benthic $\delta^{13}C$ data for F. wullestorfi; a decrease can be inferred from the more variable *Cibicidoides* spp. data. Nitrogen isotopes of 6-7‰ suggest normal marine conditions. The Late Holocene increase of % nitrogen coinciding with a decrease in $C_{org}$ content results in a decrease of the C/N ratios in the Late Holocene and the reason for this pattern is not understood. Total carbonate content of ~90% is the lowest in the entire record. Sedimentation and MAR rates are as low as during the last glacial.

Overall, the Late Holocene is influenced by strong seasonal temperature fluctuations due to summer and winter insolation, but also due to the different temperatures of the Leeuwin and Flinders Current. On an interannual scale, the GAB region is influenced by ENSO variability, which strongly affects Leeuwin Current flow and has probably affected the area since ~5 ka (DeDekker, 2001). Strong Leeuwin Current flow during autumn and winter affects the upper 200 m of the water column, just enough to penetrate the entire water column at the shelf edge (Sites 1131 and 1129 are located in 202 and 218 m of water depth) and its low nutrient levels cannot sustain much growth on this vast shelf. In summer, the Leeuwin Current weakens, but high air temperatures and evaporation on the inner shelf produce saline shelf waters downwelling across the shelf and possibly prevent colder and nutrient rich waters reaching the shelf (James et al., 2001). During El Nino years, the Leeuwin current is absent and, thus, Flinders Current waters can reach the shelf in winter and autumn bringing nutrients to the overall nutrient depleted shelf.

## 6.6   Conclusion

The modern oceanographic setting of the GAB region is complex and not well understood, but the interplay of different currents and the seasonal cycle produces a unique faunal and floral bio-assemblage which, due to the high-energy environment, is deposited on the shelf-edge and upper slope. The upper 10 m of Site 1127 document in continuous and unprecedented detail the interplay of regional oceanography in response to the global transition from the LGM to Holocene. The record can be divided into 4 distinct intervals, characterized by a different paleoceanographic setting. Each set of conditions, in turn, produced a distinct margin response, as identified in the various proxy-records developed from Site 1127 sediments.

# References

Almond, D., McGowran, B., and Li, Q. (1993). Late Quaternary Foraminiferal record from the Great Australian Bight and its environmental significance. *Memoir Association Australasian Paleontologist* **15,** 417-428.

Barrows, T. T., Stone, J. O., Fifield, L. K., and Cresswell, R. G. (2001). Late Pleistocene Glaciation of the Kosciuszko Massif, Snowy Mountains, Australia. *Quaternary Research* **55,** 179-189.

Bye, J. A. T. (1971). Variability south of Australia. *In* "Proceedings of the International Science Symposium.", pp. 119-135, Sydney, Australia.

Bye, J. A. T. (1972). Ocean Circulation South of Australia. *In* "Antarctic Oceanology II: The Australian-New Zealand Sector." (D. E. Hays, Ed.), pp. 95-100. A.G.U. Antarctic Research Series. A.G.U. Antarctic Research Series, Washington D.C.

DeDekker, P. (2001). Records fo Environmental Changes in the Australian Sector of Pep II Point to Broad Trends of Climate Change. *In* "PAGES News.", pp. 4-5. PAGES.

Feary, D. A., Hine, A. C., Malone, M. J., and et al. (2000). Proceedings of the Ocean Drilling Program. *In* "Proceedings of the Ocean Drilling Program, Initial Reports, 182 [CD-ROM]:." (A. C. Hine, D. A. Feary, and M. J. Malone, Eds.), Available from: Ocean Drilling Program, Texas A&M University, College Station , TX 77845-9547, USA.

Holbourn, A. E., Kuhnt, W., and James, N. P. (2002). Late Pleistocene isotope stratigraphy and paleoceanography of the Great Australian Bight: The benthic foraminiferal record. *Plaeoceangoraphy***,** 14-23.

James, N. P., Bone, Y., Collins, L. B., and Kyser, T. K. (2001). Surficial Sediments of the Great Australian Bight: Facies Dynamics and Oceanography on a Vast Cool-Water Carbonate Shelf. *Journal of Sedimentary Research* **71,** 549-567.

James, N. P., Feary, D. A., Surlyk, F., Simo, J. A. T., Betzler, C., Holburn, A. E., Qianyu, L., Matsuda, H., Machiyama, H., Brooks, G. R., Andres, M. S., Hine, A. C., Malone, M. J., and Party, O. D. P. L. S. (2000). Quaternary bryozoan reef mounds in cool-water, upper slope environments: Great Australian Bight. *Geololy* **28,** 647-650.

Lynch-Stieglitz, J., Fairbanks, R. G., and Charles, C. D. (1994). Glacial interglacial history of Antarctic Intermediate Water: Relative strengths of Antarctic versus Indian Ocean sources. *Paleoceanography* **9,** 7-29.

McCarthy, L., and Head, L. (2001). Holocene variability in semi-arid vegetation: new evidence from Leporillus middens from the Flinders Ranges, South Australia. *The Holocene* **11,** 681-689.

McGowran, B., and al., e. (1997). Biogeographic impact of the Leeuwin Current in southern Australia since the late middle Eocene. *Paleogeography, Paleoclimatology, Paleoecology* **136,** 19-40.

Miller, G. H., Magee, J. W., and Jull, A. J. T. (1997). Low-latitude glacial cooling in the Southern Hemisphere from amino-acid racemization in emu eggshells. *Nature* **385,** 241-244.

Mulitza, S., Arz, H., Kemle-von Mücke, S., Moos, C., Niebler, H.-S., Pätzold, J., and Segl, M. (1999). The South Atlantic Carbon Isotope Record of Planktic Foraminifera. *In* "Use of Proxies in Paleoceanography." (G. Fischer, and G. Wefer, Eds.). Springer-Verlag, Berlin Heidelberg.

Rochford, D. J. (1986). Seasonal Changes in the Distribution of Leeuwin Current Waters off Southern Australia. *Australian Journal of Marine and Freshwater Research* **37,** 1-10.

Sachs, J. P., and Repeta, D. J. (1999). Oligotrophy and Nitrogen Fixation during Eastern Mediterranean Sapropel Events. *Science*, 2485-2488.

Schrag, D. P., Adkins, J. F., McIntyre, K., Alexander, J. L., Hodell, D. A., Charles, C. D., and McManus, J. F. (2002). The oxygen isotopic composition of seawater during the Last Glacial Maximum. *Quaternary Science Reviews* **21,** 331-342.

Stuiver, M., Reimer, P. J., Bard, E., Beck, J. W., Burr, G. S., Hughen, K. A., Kromer, B., McCormac, G., van der Plicht, H., and Spurk, M. (1998a). INTCAL98 Radiocarbon Age Calibration, 24,000-0 cal BP. *Radiocarbon* **40,** 1041-1083.

# 7 LATE PLEISTOCENE OXYGEN AND CARBON ISOTOPE STRATIGRAPHY IN BULK AND FINE-FRACTION CARBONATE FROM THE GREAT AUSTRALIAN BIGHT, ODP LEG 182, SITE 1127*

## Abstract

The aim of this study was to evaluate the potential of constructing an oxygen and carbon isotope stratigraphy for the late Pleistocene succession from Ocean Drilling Program Hole 1127B drilled on the Great Australian Bight. Stable isotope analyses were performed on bulk and fine-fraction (<38μm) sediment samples. The oxygen isotope variations are generally smaller in magnitude than expected from global pelagic records. This is most likely due to the neritic-dominated sediment composition. Correlation of the oxygen isotope data with carbonate mineralogy and downhole logging data shows simultaneous variations and trends, particularly evident in the mid-Pleistocene sediments. Correlation of the oxygen isotope data with the classic SPECMAP curve is used to evaluate the stratigraphic potential of the Site 1127 sediments. This study indicates that an isotope stratigraphy based on planktonic and benthic foraminifera is needed to fully evaluate the response of cool-water carbonates deposited in a margin setting to global ice-volume fluctuations, and hence, the associated sea level variations.

## 7.1 Introduction

Ocean Drilling Program (ODP) Leg 182, Site 1127 is the most seaward site of a three-site transect drilled through a set of prograding clinoforms immediately seaward of the present-day shelf edge on the Great Australian Bight (GAB) (James et al., 2000). The site is located in 480.6 m water depth and drilling recovered 510.7 m of sediment with an average of 95% recovery. The upper 467 m of this neritic sediment wedge represents an extraordinarily thick Pleistocene succession that unconformably overlies the Pliocene-upper Miocene sediments at a distinct sequence boundary. The entire sedimentary succession is characterized by fine-grained, bioturbated bioclastic carbonate wackestone to packstone. Based on shipboard magnetic data, the Bruhnes/Matuyama boundary (B/M boundary) was placed at 343.4 mbsf.

Herein, we evaluate the potential to develop an oxygen isotope stratigraphy for ODP Site 1127, based on δ^{18}O data compiled from bulk and fine-fraction analyses. The fine-fraction, defined as the smaller than 38μm fraction, was identified by scanning electron microscope (SEM) analysis as composed of

---

calcareous nannoplankton and bioclastic sediment. We undertook the analysis of bulk sediment, as it is far less labor-intensive and, therefore, a less time-consuming method (Shackleton et al., 1993), providing a rapid initial data set for evaluating the potential of conducting paleoceanographic research in cool-water open-marine carbonates.

## 7.2   Methods and procedures

### 7.2.1   Sample Preparation and Isotope Analysis

Splits of sediment samples from Hole 1127B were oven dried at 30°C and weighed. Approximately 1 cm$^3$ of material was ground for bulk stable isotope analyses. For fine-fraction analyses, a small split of the sample was sieved over a 38-μm stainless steel mesh sieve and the fine-fraction (<38 μm) collected beneath. The collected sediment was then sonicated, filtered over a 0.45-μm membrane filter and oven dried. Before isotopic analysis, ~0.5 mg of each sample was homogenized in a mortar and pestle. Stable isotope analysis of bulk and fine-fraction samples was carried out at the Geological Institute, ETH Zurich, using a PRISM dual inlet mass spectrometer. Results are expressed in the standard δ notation as permil relative to the Vienna Peedee Belemnite (V-PDB) carbonate standard. Instrument accuracy, referenced to an internal carbonate standard (Carrara Marble), is 0.08‰ ± 0.03‰ (1 σ) for δ$^{18}$O and 0.05‰ ± 0.03‰ (1 σ) for δ$^{13}$C. On average, 10 standards were measured during each run of 20 samples to determine precision for replicate analyses. The data are given in Table 7.1 and graphically displayed in Figures 7.1.

### 7.2.2   Mineralogical and Downhole Logging Data

All mineralogical X-ray diffraction data and downhole logging data presented in Figure 7.2 were acquired onboard the *JOIDES Resolution* (James et al., 2000). Analytical procedures are discussed in the "Explanatory Notes" chapter of the *Initial Reports* volume (James et al., 2000). For the downhole natural gamma ray (NGR) measurement, the data were smoothed using a five-point running average. The upper 80 m were logged through the pipe, and values were multiplied by a factor of five for comparable amplitudes.

## 7.3   Results and Discussion

### 7.3.1   Stable Isotope Results

The δ$^{18}$O values for bulk and fine fractions (<38 μm) are presented vs. depth (Figs. 7.1 and 7.2). The upper 340 m of the record is characterized by distinct cyclicity, whereas the record below 340 mbsf is marked by high-frequency, low-amplitude variations. Bulk and fine-fraction δ$^{18}$O data closely follow each other, with the bulk samples generally showing slightly more negative values. Bulk and fine-fraction δ$^{18}$O values show an overall range from 2.9‰ to 0.4‰. An upward trend toward more negative values is visible in both δ$^{18}$O records.

The $\delta^{13}$C isotope values from bulk and fine fractions (<38 μm) are presented vs. depth (Fig. 7.1). The upper 150 mbsf of the $\delta^{13}$C record are marked by high-frequency, high-amplitude fluctuations, followed by a 150-m interval with little variation. Below 300 mbsf, $\delta^{13}$C values shift 1‰ more negative and the remaining curve is again characterized by high-frequency, high-amplitude variations. As previously observed for $\delta^{18}$O values, bulk and fine-fraction $\delta^{13}$C values follow each other, with the bulk having a slightly more negative value. Overall, $\delta^{13}$C values range from 2.0‰-0.25‰. The carbon isotope record is presented but is not discussed further in this data report.
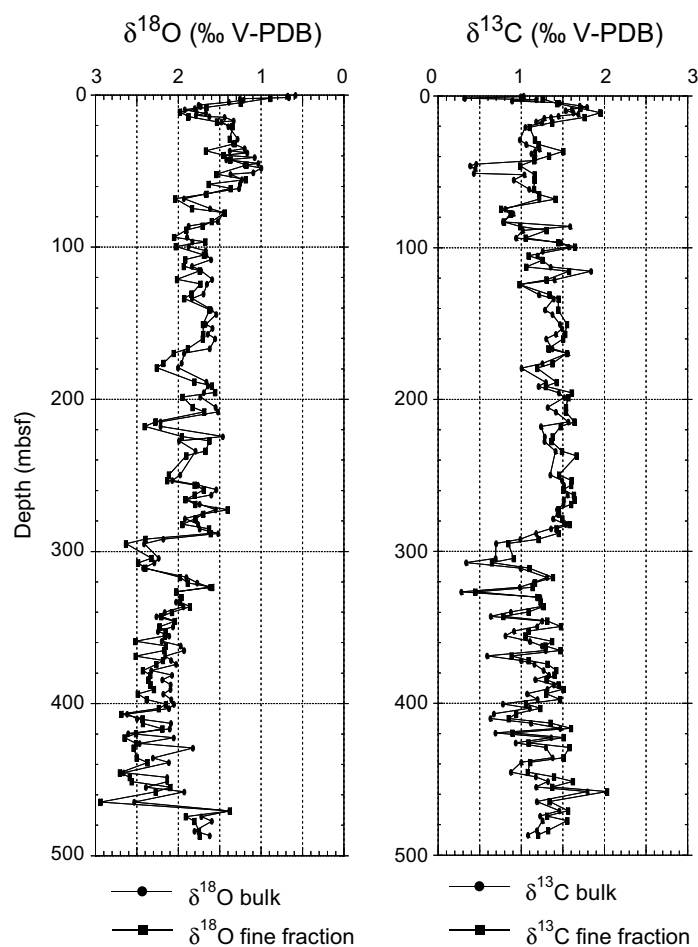


*Figure 7.1. Bulk and fine-fraction (<38 μm) $\delta^{18}$O and $\delta^{13}$C record, ODP Hole 1127B.*

### 7.3.2 Downhole Comparison

The transition between the Holocene and the last glacial maximum (LGM) is evident in the $\delta^{18}$O record with an amplitude-change of 1.4‰, comparable to global data sets. Except for Termination I, amplitudes, especially in the upper part of the record (20-170 mbsf), are small (less than ± 0.5‰) and variable, but they increase again between 170 and 320 mbsf. In summary, the bulk and fine-fraction isotopes do not record glacial-interglacial changes on a magnitude as seen in other global, mostly pelagic, records. The reason could lie within the continental shelf environment and the composition of

the bulk and fine-fraction samples from Site 1127. Although containing abundant planktonic and benthic foraminifera, as well as calcareous nannoplankton, the sediment is dominated by the bioclastic fragments of the benthic shelf-community.

A comparison with the lithostratigraphy of Site 1127 (James et al., 2000) provides a possible explanation as to why Termination I is better expressed compared with the underlying record. Lithostratigraphic Unit I (0-9.6 mbsf) consists of calcareous ooze with varying amounts of nannofossils and planktonic foraminifers, whereas Unit II (9.6-467.2 mbsf) is marked by alternating wackestone- and packstone sediments. The change in Unit II is, therefore, characterized by an increase in the grain size and bioclast abundance and a decrease in carbonate mud. The presented data illustrate the need for a stable isotope analysis based on planktonic and benthic foraminifera in order to validate the bulk and fine-fraction data and discuss the record in a stratigraphic and paleoceanographic context.

Initial shipboard comparison of mineralogic and seismic downhole logging data indicated cyclic packaging of the Pleistocene sediment wedge, probably in response to orbitally driven sea level fluctuations (James et al., 2000). By comparing isotopic data with other sea-level proxy data sets, this hypothesis can be tested. In Figure 7.2 we made a first order correlation of the three data sets, as indicated by gray and white bars. Based on shipboard bulk analysis, the carbonate mineralogy shows large variations within the high-Mg calcite (HMC) and low-Mg calcite (LMC) percentages (James et al., 2000). Variations are most obvious in the relative percentages of HMC and LMC that are characterized by an interfingering behavior, especially pronounced in the interval between 165 and 320 mbsf. Here, HMC-dominated intervals correspond to times of decreased isotopic values (sea level highstands) and LMC-dominated intervals to time of increased isotopic values (sea level lowstands). Although the mineralogical variations also fluctuate in the upper part of the record (0-165 mbsf), no consistent trend or interfingering behaviour is observed. Note that the LGM and Termination I are both HMC-dominated. Fluctuations within the NGR record in comparison to the isotope stratigraphy and mineralogical data are less pronounced; nevertheless, most abrupt decreases or increases in NGR counts can be correlated to mineralogic and isotopic changes. Below the B/M boundary, the decreased amplitude of the isotopic fluctuations and the abrupt increase of LMC are interpreted as due to diagenetic alteration and remineralization.

From a comparison of the $\delta^{18}O$ results, carbonate mineralogy and NGR records, we conclude: (1) for the middle part of the record (between the B/M boundary at 343.4 mbsf and 165 mbsf), the cyclic behavior of LMC and HMC, as well as NGR fluctuations, vary systematically with fluctuations observed in the oxygen isotope record; (2) the upper part of the record (165 to10 mbsf), where amplitudes within the isotopic record are small and variable, correlates to a HMC-dominated time as seen in the mineralogic record, (3) the LGM is well defined in all three data sets, and (4) below the B/M boundary, diagenetic overprinting has eliminated the original signal.
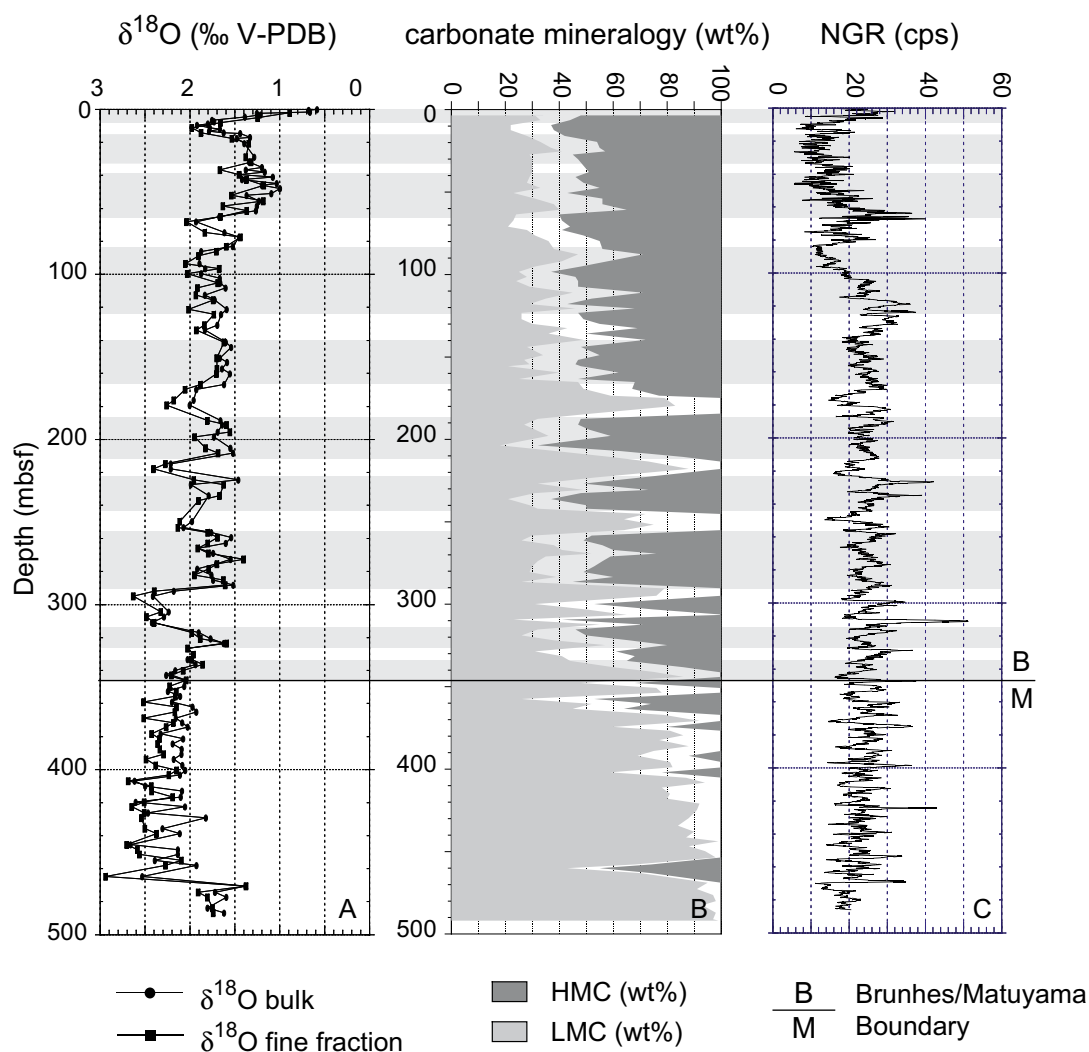
***Figure 7.2.*** *Comparison of ODP Hole 1127 data: (A) $\delta^{18}O$ stratigraphy, (B) mineralogical and (C) downhole logging NGR shipboard data.*

### 7.3.3   Comparison to SPECMAP

In order to test the potential usefulness of cool-water shelf-carbonates for paleoceanographic studies, we have correlated the Hole 1127B $\delta^{18}O$ record to the orbitally tuned SPECMAP $\delta^{18}O$ curve (Imbrie et al. 1984) (Fig. 7.3). Depths and ages of isotope boundaries that were used as tie-points are listed in Table 7.2. The correlation for the LGM is convincing, but it is poorer for MIS 3-11 where glacial-interglacial amplitudes are small. The mid-Pleistocene (MIS 12-17) correlation improves as glacial-interglacial amplitudes rise, and within MIS 15 even internal structures are visible. The reason for the poor correlation is most likely related to the strong neritic-influenced signal in the Site 1127 bulk and fine fractions opposed to the predominantly pelagic, planktonic foraminiferal values of the SPECMAP curve. We, nevertheless, tentatively identify 20 marine isotope stages (MIS) down to the level of the shipboard-observed B/M boundary (James et al., 2000).

Although this data set is preliminary, it represents a first attempt at developing a bulk and fine-fraction isotope stratigraphy for the cool-water carbonate realm of the Great Australian Bight. It illustrates the need for more precise stable isotope analysis of specific planktonic and benthic foraminifera in order to evaluate the true potential of these sediments as a sensitive recorder of global ice-volume fluctuations. Based on the promising results of this initial study, a stable isotope analysis of foraminifera is currently in progress to interpret paleoclimate fluctuations on the Great Australian Bight.
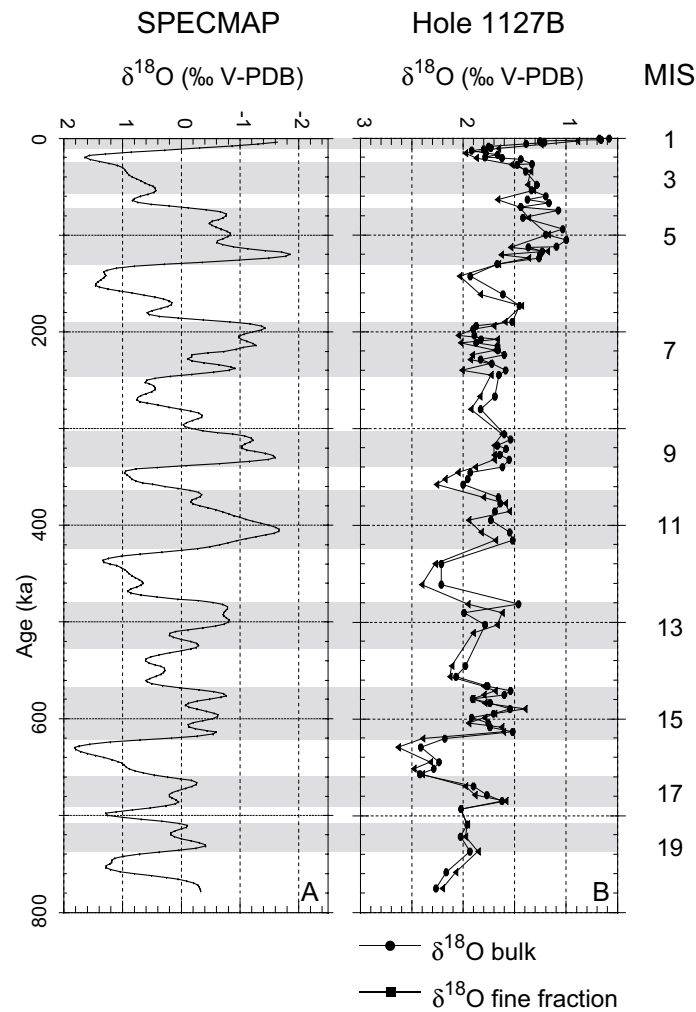


***Figure 7.3.*** *Comparison of the late Pleistocene $\delta^{18}O$ stratigraphies from (A) SPECMAP (Imbire et al., 1984) and (B) ODP Hole 1127B. The marine isotope stages (MIS) are indicated.*

| Core | Type | | Section | Top | | Bottom | Depth (mbsf) | $\delta^{13}$C bulk (‰ PDP) | $\delta^{18}$O bulk (‰ PDP) | $\delta^{13}$C ff (‰ PDP) | $\delta^{18}$O ff (‰ PDP) |
|---|---|---|---|---|---|---|---|---|---|---|---|
| 1 | H | - | 1 | 2 | - | 6 | 0.02 | 1.03 | 0.58 | | |
| 1 | H | - | 1 | 50 | - | 53 | 0.5 | 0.99 | 0.68 | | |
| 1 | H | - | 2 | 2 | - | 7 | 1.52 | 0.32 | 0.66 | | |
| 1 | H | - | 2 | 101 | - | 106 | 2.51 | 1.18 | 1.25 | | |
| 1 | H | - | 3 | 46 | - | 49 | 3.46 | 0.89 | 1.21 | | |
| 1 | H | - | 4 | 2 | - | 7 | 4.52 | 1.46 | 1.39 | | |
| 2 | H | - | 1 | 69 | - | 75 | 6.59 | 1.70 | 1.75 | | |
| 2 | H | - | 2 | 2 | - | 7 | 7.42 | 1.79 | 1.73 | | |
| 2 | H | - | 2 | 139 | - | 144 | 8.79 | 1.61 | 1.80 | | |
| 2 | H | - | 3 | 70 | - | 75 | 9.6 | 1.53 | 1.92 | | |
| 2 | H | - | 4 | 65 | - | 70 | 11.05 | 1.63 | 1.78 | 1.95 | 1.98 |
| 2 | H | - | 5 | 2 | - | 5 | 11.92 | 1.68 | 1.67 | | |
| 2 | H | - | 6 | 2 | - | 8 | 13.42 | 1.45 | 1.79 | | |
| 2 | H | - | 6 | 65 | - | 70 | 14.05 | 1.36 | 1.62 | 1.76 | 1.88 |
| 2 | H | - | 6 | 125 | - | 130 | 14.65 | 1.28 | 1.44 | | |
| 3 | H | - | 2 | 3 | - | 8 | 16.93 | 1.18 | 1.33 | | |
| 3 | H | - | 2 | 65 | - | 70 | 17.55 | 1.25 | 1.48 | 1.37 | 1.53 |
| 3 | H | - | 4 | 65 | - | 70 | 20.55 | 1.05 | 1.39 | 1.10 | 1.35 |
| 4 | H | - | 4 | 65 | - | 70 | 28.98 | 0.98 | 1.28 | 1.16 | 1.38 |
| 4 | H | - | 6 | 64 | - | 69 | 31.97 | 1.06 | 1.34 | 1.21 | 1.32 |
| 5 | H | - | 1 | 75 | - | 80 | 35.15 | 1.22 | 1.20 | | |
| 5 | H | - | 2 | 65 | - | 70 | 36.55 | 1.16 | 1.38 | 1.50 | 1.67 |
| 5 | H | - | 3 | 60 | - | 65 | 38 | 1.12 | 1.17 | | |
| 5 | H | - | 4 | 62 | - | 67 | 39.52 | 1.17 | 1.44 | 1.33 | 1.45 |
| 5 | H | - | 5 | 60 | - | 65 | 41 | 1.16 | 1.08 | | |
| 5 | H | - | 6 | 65 | - | 70 | 42.55 | 1.16 | 1.42 | 1.15 | 1.37 |
| 6 | H | - | 1 | 110 | - | 115 | 45 | 0.46 | 1.03 | | |
| 6 | H | - | 2 | 65 | - | 70 | 46.05 | 0.38 | 1.20 | 0.99 | 1.18 |
| 6 | H | - | 3 | 110 | - | 115 | 48 | 0.45 | 1.00 | | |
| 6 | H | - | 5 | 110 | - | 115 | 51 | 0.43 | 1.09 | | |
| 6 | H | - | 6 | 65 | - | 70 | 52.05 | 1.04 | 1.37 | 1.16 | 1.54 |
| 7 | H | - | 2 | 65 | - | 70 | 55.55 | 0.91 | 1.23 | 1.16 | 1.18 |
| 7 | H | - | 4 | 65 | - | 70 | 58.55 | 0.49 | 1.25 | 0.29 | 1.63 |
| 7 | H | - | 6 | 59 | - | 64 | 61.49 | 1.10 | 1.26 | 1.15 | 1.37 |
| 8 | H | - | 2 | 65 | - | 70 | 65.05 | 1.21 | 1.67 | 1.21 | 1.66 |
| 8 | H | - | 4 | 64 | - | 69 | 68.04 | 1.21 | 1.93 | 1.41 | 2.04 |
| 9 | H | - | 2 | 65 | - | 70 | 74.55 | 0.81 | 1.62 | 0.76 | 1.83 |
| 9 | H | - | 4 | 65 | - | 70 | 77.55 | 0.90 | 1.45 | 0.87 | 1.44 |
| 10 | H | - | 2 | 65 | - | 70 | 82.94 | 0.78 | 1.52 | 0.79 | 1.60 |
| 10 | H | - | 4 | 65 | - | 70 | 85.94 | 1.59 | 1.88 | 0.99 | 1.71 |
| 10 | H | - | 6 | 38 | - | 43 | 88.67 | 1.02 | 1.90 | 1.30 | 1.90 |
| 11 | H | - | 2 | 65 | - | 70 | 93.55 | 0.94 | 1.89 | 1.05 | 2.05 |
| 11 | H | - | 4 | 65 | - | 70 | 96.55 | 1.48 | 1.83 | 1.44 | 1.67 |
| 11 | H | - | 6 | 70 | - | 75 | 99.44 | 1.57 | 1.87 | 1.64 | 2.03 |
| 12 | H | - | 2 | 65 | - | 70 | 102.29 | 1.26 | 1.67 | | |
| 12 | H | - | 4 | 64 | - | 69 | 105.28 | 1.19 | 1.66 | 1.09 | 1.69 |
| 12 | H | - | 6 | 66 | - | 71 | 108.2 | 1.25 | 1.60 | 1.26 | 1.92 |
| 13 | H | - | 2 | 66 | - | 71 | 112.56 | 1.35 | 1.83 | 1.06 | 1.93 |
| 13 | H | - | 4 | 66 | - | 71 | 115.49 | 1.84 | 1.73 | 1.57 | 1.74 |
| 14 | H | - | 2 | 65 | - | 70 | 121.2 | 1.40 | 1.59 | 1.30 | 2.02 |
| 14 | H | - | 4 | 65 | - | 70 | 124.2 | 0.98 | 1.65 | 0.98 | 1.73 |
| 15 | H | - | 2 | 65 | - | 70 | 130.81 | 1.21 | 1.69 | 1.34 | 1.84 |
| 15 | H | - | 4 | 65 | - | 70 | 133.81 | 1.39 | 1.83 | 1.45 | 1.93 |
| 16 | H | - | 2 | 65 | - | 70 | 141.05 | 1.28 | 1.60 | 1.45 | 1.62 |

| Core | Type | | Section | Top | | Bottom | Depth (mbsf) | $\delta^{13}C$ bulk (‰ PDP) | $\delta^{18}O$ bulk (‰ PDP) | $\delta^{13}C$ ff (‰ PDP) | $\delta^{18}O$ ff (‰ PDP) |
|---|---|---|---|---|---|---|---|---|---|---|---|
| 17 | X | - | 2 | 65 | - | 70 | 150.55 | 1.47 | 1.67 | 1.55 | 1.70 |
| 17 | X | - | 4 | 61 | - | 66 | 153.34 | 1.49 | 1.59 | | |
| 18 | X | - | 2 | 65 | - | 70 | 157.05 | 1.42 | 1.64 | 1.53 | 1.70 |
| 18 | X | - | 4 | 65 | - | 70 | 160.05 | 1.30 | 1.55 | 1.50 | 1.70 |
| 19 | X | - | 2 | 65 | - | 70 | 166.65 | 1.37 | 1.62 | 1.33 | 1.88 |
| 19 | X | - | 4 | 65 | - | 70 | 169.65 | 1.56 | 1.93 | 1.55 | 2.05 |
| 20 | X | - | 2 | 65 | - | 70 | 176.25 | 1.25 | 1.96 | 1.37 | 2.18 |
| 20 | X | - | 4 | 68 | - | 73 | 179.28 | 1.00 | 2.00 | 1.19 | 2.26 |
| 21 | X | - | 4 | 66 | - | 71 | 188.57 | 1.29 | 1.66 | 1.43 | 1.81 |
| 21 | X | - | 6 | 68 | - | 73 | 191.17 | 1.21 | 1.64 | 1.29 | 1.59 |
| 22 | X | - | 2 | 65 | - | 70 | 195.55 | 1.45 | 1.69 | 1.61 | 1.55 |
| 22 | X | - | 4 | 65 | - | 70 | 198.55 | 1.52 | 1.73 | 1.56 | 1.95 |
| 23 | X | - | 2 | 65 | - | 70 | 205.15 | 1.32 | 1.55 | 1.54 | 1.83 |
| 23 | X | - | 4 | 65 | - | 70 | 208.15 | 1.42 | 1.52 | 1.54 | 1.69 |
| 24 | X | - | 2 | 65 | - | 70 | 214.75 | 1.56 | 2.21 | 1.64 | 2.27 |
| 24 | X | - | 4 | 65 | - | 70 | 217.75 | 1.24 | 2.21 | 1.47 | 2.40 |
| 25 | X | - | 2 | 65 | - | 70 | 224.45 | 1.28 | 1.46 | 1.38 | 1.96 |
| 25 | X | - | 4 | 65 | - | 70 | 227.45 | 1.28 | 1.99 | 1.36 | 1.62 |
| 26 | X | - | 2 | 65 | - | 70 | 234.05 | 1.41 | 1.79 | 1.49 | 1.67 |
| 26 | X | - | 4 | 65 | - | 70 | 237.05 | 1.20 | 1.08 | 1.67 | 1.90 |
| 27 | X | - | 2 | 65 | - | 70 | 243.65 | | | | |
| 27 | X | - | 4 | 63 | - | 67 | 246.63 | 0.67 | 0.21 | | |
| 27 | X | - | 6 | 64 | - | 69 | 249.64 | 1.35 | 1.98 | 1.45 | 2.11 |
| 28 | X | - | 2 | 65 | - | 70 | 253.25 | 1.49 | 2.07 | 1.61 | 2.13 |
| 28 | X | - | 4 | 65 | - | 70 | 256.25 | 1.51 | 1.76 | 1.60 | 1.80 |
| 28 | X | - | 6 | 66 | - | 70 | 259.26 | 1.51 | 1.54 | 1.51 | 1.69 |
| 29 | X | - | 2 | 65 | - | 70 | 262.95 | 1.56 | 1.60 | 1.63 | 1.80 |
| 29 | X | - | 4 | 65 | - | 70 | 265.95 | 1.51 | 1.91 | 1.64 | 1.91 |
| 29 | X | - | 6 | 65 | - | 70 | 268.95 | 1.51 | 1.74 | 1.60 | 1.79 |
| 30 | X | - | 2 | 65 | - | 70 | 272.55 | 1.43 | 1.55 | 1.45 | 1.40 |
| 30 | X | - | 4 | 64 | - | 69 | 275.54 | 1.44 | 1.71 | 1.45 | 1.70 |
| 30 | X | - | 6 | 65 | - | 70 | 278.55 | 1.38 | 1.92 | 1.49 | 1.79 |
| 31 | X | - | 2 | 65 | - | 70 | 282.15 | 1.53 | 1.76 | 1.58 | 1.95 |
| 31 | X | - | 4 | 64 | - | 69 | 285.14 | 1.36 | 1.74 | 1.42 | 1.63 |
| 31 | X | - | 6 | 65 | - | 70 | 288.15 | 1.18 | 1.52 | 1.45 | 1.61 |
| 32 | X | - | 2 | 66 | - | 68 | 291.86 | 0.99 | 2.18 | 1.21 | 2.40 |
| 32 | X | - | 4 | 64 | - | 66 | 294.84 | 0.70 | 2.41 | 0.84 | 2.63 |
| 33 | X | - | 2 | 63 | - | 68 | 301.43 | | | | |
| 33 | X | - | 4 | 62 | - | 67 | 304.42 | 0.69 | 2.24 | 0.91 | 2.32 |
| 33 | X | - | 6 | 62 | - | 67 | 307.42 | 0.33 | 2.29 | 0.65 | 2.48 |
| 34 | X | - | 2 | 65 | - | 70 | 311.05 | 0.99 | 2.42 | 1.10 | 2.40 |
| 34 | X | - | 4 | 65 | - | 70 | 314.05 | | | | |
| 34 | X | - | 6 | 66 | - | 71 | 317.06 | 1.31 | 1.90 | 1.38 | 1.98 |
| 35 | X | - | 2 | 65 | - | 70 | 320.65 | 1.15 | 1.77 | 1.16 | 1.89 |
| 35 | X | - | 4 | 65 | - | 70 | 323.65 | 0.98 | 1.62 | 1.14 | 1.59 |
| 35 | X | - | 6 | 66 | - | 71 | 326.66 | 0.28 | 2.02 | 0.45 | 2.03 |
| 36 | X | - | 2 | 67 | - | 69 | 330.27 | 1.23 | 1.96 | 1.19 | 1.96 |
| 36 | X | - | 4 | 65 | - | 70 | 333.25 | 1.23 | 2.02 | 1.23 | 1.98 |
| 36 | X | - | 6 | 65 | - | 70 | 336.25 | 1.25 | 1.94 | 1.27 | 1.86 |
| 37 | X | - | 2 | 65 | - | 70 | 339.85 | 0.87 | 2.16 | 1.09 | 2.08 |
| 37 | X | - | 4 | 65 | - | 70 | 342.85 | 0.63 | 2.26 | 0.78 | 2.21 |
| 37 | X | - | 6 | 66 | - | 71 | 345.86 | 1.25 | 2.05 | 1.31 | 2.04 |
| 38 | X | - | 2 | 66 | - | 71 | 349.46 | 1.19 | 2.06 | 1.48 | 2.23 |
| 38 | X | - | 4 | 66 | - | 71 | 352.46 | 0.91 | 2.24 | 1.09 | 2.15 |
| 38 | X | - | 6 | 67 | - | 72 | 355.47 | 0.81 | 2.11 | 1.05 | 2.16 |
| 39 | X | - | 2 | 65 | - | 70 | 359.15 | 1.10 | 2.20 | 1.37 | 2.52 |

| Core | Type | | Section | Top | | Bottom | Depth (mbsf) | δ¹³C bulk (‰ PDP) | δ¹⁸O bulk (‰ PDP) | δ¹³C ff (‰ PDP) | δ¹⁸O ff (‰ PDP) |
|------|------|---|---------|-----|---|--------|------|------|------|------|------|
| 39 | X | - | 4 | 65 | - | 70 | 362.15 | 1.25 | 1.97 | 1.29 | 2.15 |
| 39 | X | - | 6 | 67 | - | 69 | 365.17 | 1.29 | 1.93 | 1.47 | 2.17 |
| 40 | X | - | 2 | 65 | - | 70 | 368.75 | 0.59 | 2.16 | 0.88 | 2.51 |
| 40 | X | - | 4 | 65 | - | 70 | 371.75 | 1.00 | 2.09 | 1.09 | 2.18 |
| 40 | X | - | 6 | 61 | - | 64 | 374.21 | 1.16 | 2.03 | 1.32 | 2.27 |
| 41 | X | - | 2 | 65 | - | 70 | 378.35 | 1.27 | 2.33 | 1.42 | 2.43 |
| 41 | X | - | 4 | 65 | - | 70 | 381.35 | 1.33 | 2.07 | 1.40 | 2.34 |
| 41 | X | - | 6 | 65 | - | 70 | 384.35 | 1.17 | 2.19 | 1.30 | 2.36 |
| 42 | X | - | 2 | 65 | - | 70 | 387.75 | 1.39 | 2.09 | 1.45 | 2.33 |
| 42 | X | - | 4 | 65 | - | 70 | 390.75 | 1.31 | 2.09 | 1.51 | 2.29 |
| 42 | X | - | 6 | 67 | - | 72 | 393.77 | 1.07 | 2.18 | 1.30 | 2.49 |
| 43 | X | - | 2 | 65 | - | 70 | 397.35 | 1.19 | 2.08 | 1.46 | 2.38 |
| 43 | X | - | 4 | 65 | - | 70 | 400.35 | 0.78 | 2.05 | 1.06 | 2.15 |
| 43 | X | - | 6 | 65 | - | 69 | 403.35 | 1.10 | 2.11 | 1.23 | 2.24 |
| 44 | X | - | 2 | 65 | - | 71 | 406.95 | 0.67 | 2.62 | 0.94 | 2.69 |
| 44 | X | - | 4 | 64 | - | 69 | 409.94 | 0.63 | 2.50 | 0.85 | 2.43 |
| 44 | X | - | 6 | 66 | - | 71 | 412.96 | 1.12 | 2.09 | 1.35 | 2.43 |
| 45 | X | - | 2 | 66 | - | 71 | 416.56 | 1.47 | 2.10 | 1.60 | 2.19 |
| 45 | X | - | 4 | 66 | - | 71 | 419.56 | 0.69 | 2.60 | 0.89 | 2.51 |
| 45 | X | - | 6 | 66 | - | 71 | 422.56 | 1.36 | 2.05 | 1.51 | 2.65 |
| 46 | X | - | 2 | 64 | - | 68 | 426.14 | 0.93 | 2.47 | 1.09 | 2.51 |
| 46 | X | - | 4 | 65 | - | 69 | 429.15 | 1.29 | 1.82 | 1.58 | 2.54 |
| 47 | X | - | 2 | 65 | - | 70 | 435.85 | 1.38 | 2.31 | 1.51 | 2.50 |
| 47 | X | - | 4 | 65 | - | 70 | 438.85 | 1.00 | 2.11 | 1.11 | 2.37 |
| 48 | X | - | 2 | 65 | - | 70 | 445.45 | 0.87 | 2.66 | 1.08 | 2.70 |
| 48 | X | - | 4 | 65 | - | 70 | 448.45 | 1.17 | 2.13 | 1.39 | 2.58 |
| 48 | X | - | 6 | 66 | - | 71 | 451.46 | 1.32 | 2.13 | 1.62 | 2.56 |
| 49 | X | - | 2 | 65 | - | 70 | 455.05 | 1.18 | 2.39 | 1.37 | 2.10 |
| 49 | X | - | 4 | 65 | - | 70 | 458.05 | 1.79 | 1.93 | 2.03 | 2.27 |
| 50 | X | - | 2 | 65 | - | 68 | 464.65 | 1.19 | 2.53 | 1.34 | 2.94 |
| 50 | X | - | 6 | 66 | - | 69 | 470.66 | 1.46 | 1.38 | 1.56 | 1.38 |
| 51 | X | - | 2 | 65 | - | 70 | 474.25 | 1.23 | 1.72 | 1.31 | 1.91 |
| 51 | X | - | 4 | 65 | - | 70 | 477.25 | 1.25 | 1.59 | 1.55 | 1.81 |
| 52 | X | - | 2 | 65 | - | 70 | 483.85 | 1.19 | 1.80 | 1.32 | 1.75 |
| 52 | X | - | 4 | 64 | - | 69 | 486.84 | 1.08 | 1.62 | 1.20 | 1.74 |

**Table 7.1.** *Results of stable isotope analyses, ODP Hole 1127B.*

| Marine Isotopic Event | Age (ka) | Depth (mbsf) |
|:---:|:---:|:---:|
| 2 | 12 | 9.2 |
| 3 | 24 | 16 |
| 4 | 59 | 34.5 |
| 5 | 71 | 40.5 |
| 6 | 128 | 65.5 |
| 7 | 186 | 83 |
| 8 | 245 | 125 |
| 9 | 303 | 140 |
| 10 | 339 | 167 |
| 11 | 362 | 185 |
| 12 | 423 | 212 |
| 13 | 478 | 223 |
| 14 | 524 | 243 |
| 15 | 565 | 256 |
| 16 | 620 | 292 |
| 17 | 659 | 312 |
| 18 | 689 | 325 |
| 19 | 710 | 334 |
| 20 | 736 | 347 |

***Table* 7.2.** *Estimated depth of the marine isotope stages (MIS) in ODP Hole 1127B. Ages are in thousands of years (ka) and based on Imbrie et al. (1984).*

## Acknowledgements

## References

Imbrie, J., Hays, J. D., Martinson, D. G., McIntyre, A., Mix, A. C., Morley, J. J., Pisias, N. G., Prell, W. L., and Shackleton, N. J. (1984). The orbital theory of Pleistocene climate: support from a revised chronology of the marine d18O record. *In* "Milankovitch and Climate, Part 1." (A. J. Berger, J. Imbrie, J. D. Hays, G. Kukla, and B. Saltzman, Eds.), pp. 269-305. Dordrecht: Riedel Publishing Co.

James, N. P., Feary, D. A., Surlyk, F., Simo, J. A. T., Betzler, C., Holburn, A. E., Qianyu, L., Matsuda, H., Machiyama, H., Brooks, G. R., Andres, M. S., Hine, A. C., Malone, M. J., and Party, O. D. P. L. S. (2000). Quaternary bryozoan reef mounds in cool-water, upper slope environments: Great Australian Bight. *Geololy* **28,** 647-650.

Shackleton, N. J., Hall, M. A., and Pate, D. (1993). High-Resolution Stable Isotope Stratigraphy from Bulk Sediment. *Paleoceanography* **8,** 141-148.

# 8  PLEISTOCENE GLACIAL-INTERGLACIAL FLUCTUATIONS AND CONTINENTAL MARGIN RESPONSE: A PALEOCEANOGRAPHIC AND SEDIMENTOLOGIC RECORD FROM A COOL-WATER CARBONATE RAMP, GREAT AUSTRALIAN BIGHT

## Abstract

A continuous 450-m-thick core from a Pleistocene sediment wedge on the Great Australian Bight (GAB) was recovered at Site 1127 during ODP Leg 182. Glacial-interglacial variations were reconstructed using bulk, fine fraction and planktonic foraminiferal $\delta^{18}O$ for the past 850 kyrs from this cool-water carbonate sequence. High sedimentation rates and well-preserved foraminifera allow for stratigraphic analysis and the subsequent development of a reliable age model. Variations in carbonate mineralogy, sand-fraction percentage and Natural Gamma Ray measurements reflect the response of the neritic shelf community to sea-level rise and fall across the carbonate ramp. During the last 180 ka, glacial periods are characterized by cool nutrient-rich conditions resulting in prolific bryozoan mound growth along the continental shelf. Interglacial periods are dominantly influenced by the warm oligotrophic waters of the Leeuwin Current. The mid-Pleistocene glacial-interglacial fluctuations are less pronounced and the smaller glacial-interglacial variability is can be explained by a generally northerly position of the Subtropical Convergence Zone, which also occurs during interglacials, preventing Leeuwin Current flow into the GAB region. This paleoceanographic reconstruction explains bryozoan mound growth during the mid-Pleistocene interglacials as observed in the seismic profiles of the margin.

## 8.1   Introduction

Cool-water carbonates, in a manner similar to their warm-water counterparts in tropical settings, should record paleoceanographic and paleoclimatic changes in their depositional environment. In addition, these continental slope sediments should contain a mixed signal derived from both the shelf and open-ocean, environments, providing a link to evaluate processes occurring simultaneously in both settings. The cool-water carbonate slope of the Great Australian Bight (GAB) is an ideal location (Fig. 8.1) to test this working hypothesis. ODP Leg 182 dedicated an entire cruise to the GAB margin in order to recover long records and investigate their paleoceanographic and climatic potential. Herein, we report the development of an oxygen isotope stratigraphy for ODP Site 1127, based on $\delta^{18}O$ data compiled from bulk and fine fraction as well as planktonic foraminiferal analyses. Using the interpreted glacial/interglacial ice-volume fluctuations, we calculate an age model that allows us to evaluate the influence of sea-level fluctuations on the evolution of sedimentary deposition patterns in the cool-water carbonate environment.

## 8.2     Geologic and Oceanographic Setting

The GAB continental margin of southern Australia (124-134°E, 32-34°S) (Fig. 8.1) is a cool-water carbonate depositional realm, the largest of its kind on Earth today (Feary and James, 1998; James and Clarke, 1997). The shelf edge and upper slope setting and their associated sedimentary facies are poorly known, especially in the central GAB region (James, 1997; James et al., 2001). Comprising a 150 – 200 km wide ramp-type shelf, the GAB directly opens to the Southern Ocean. Although it is wind and wave-swept year-round, it is a site of abundant sediment production, but, due to the high-energy environment, most biogenic material is swept seaward where it accumulates at the shelf edge and slope setting (James, 1997; James et al., 2001). Geologically, this siliciclastic poor, divergent passive margin is the result of the separation between Australia and Antarctica in the Cretaceous and subsequent northward drift of Australia (Stagg et al., 1989; Veevers et al., 1990; Willcox and Stagg, 1990). Onset of faster spreading in the middle Eocene corresponds to the establishment of fully marine conditions and the initiation of carbonate sedimentation, which has continued throughout the Cenozoic until today (Bein and Taylor, 1981; Stagg et al., 1990).
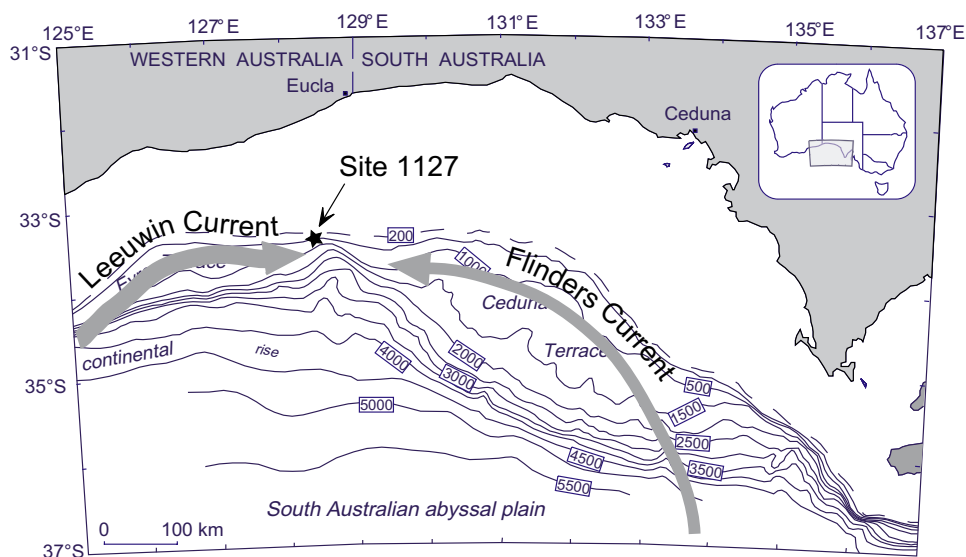


*Figure 8.1. Map of the Great Australian Bight (GAB) illustrating the general bathymetry, location of ODP Leg 182, Site 1127, and the schematic flow of the dominant water masses influencing the GAB area. Site 1127 is located on the upper slope of the present-day shelf edge in 480 m of water depth.*

The oceanography of the modern GAB is influenced by two distinct water masses: the Leeuwin Current and the Southern Ocean. The first is a warm, low-salinity flow, carrying low-latitude Indian Ocean Water waters around the tip of southwestern Australia and into the Bight. As a result, the west to east flowing shelf-water is relatively warm, with an average temperature of 17°C (Legeckis and Cresswell, 1981). Transport of warmer waters by the Leeuwin Current can also be verified by the lowered surface salinities (35.7 – 35.5‰), especially during the autumn and winter months when the

current is strongest (Cresswell and Golding, 1980). As for the influence of the Southern Ocean, the GAB lies to the north of the subtropical convergence zone (STC) centered south of 40°S (Almond et al., 1993). The Southern Ocean waters are cooler and nutrient richer than those of the Leeuwin Current. They reach the GAB via the westward flowing Flinders Current, the northern limb of a large anitgyral flow south of Australia. It is most influential during spring and summer, when the Leeuwin Current is weakest (Hufford et al., 1997).

Although the interchange of waters has been described in papers by (Rochford, 1984; Rochford, 1986), it is still poorly understood as to which degree the Leeuwin Current and the oceanic waters interact, and only a few studies have investigated their possible impact on the distribution on fauna and flora (Almond et al., 1993; Li et al., 1999) and sedimentation patterns (James et al., 2001; James and Clarke, 1997).

Thus, the aim of this study is to (1) identify glacial-interglacial variations and (2) link these onto the continental margin in order to evaluate (3) the response of a cool-water carbonate ramp to changing glacial-interglacial oceanographic conditions, such as sea-level rise and fall and changing trophic conditions.

## 8.3    Material and Methods

A core from Site 1127, located in 480 m of water depth on the upper slope, recovered 510 m of sediment of which the upper 343 m are the focus of this study. The lithology is dominated by fine-grained, bioturbated, unlithified bioclastic packstone to wackestone. Samples for the oxygen isotope stratigraphy were sampled at approximately 1 m interval, but the resolution was increased in several horizons.

### 8.3.1    Oxygen Isotope Analysis

Planktonic foraminifera species *Globigerinoides ruber* (white variety) and *Globigerina bulloides* were selected for stable isotope analyses. Both the surface-dwelling *G. ruber* and the slightly deeper-living *G. bulloides* are well preserved throughout the upper 400 m of the core. The mean sample size was 17 specimens, which were collected from the >250 μm fraction, with the exception of a few samples where the abundance was lower. Foraminiferal tests were inspected for diagenetic overprint, sonicated and crushed in alcohol prior to analysis. Isotope analysis was carried out at the Geological Institute, ETH-Zurich using a PRISM dual inlet mass spectrometer. Results are expressed in the standard $\delta$ notation in ‰ relative to the V-PDB standard. Instrument accuracy, as referred to an internal carbonate standard, is 0.06‰ ± 0.03‰ (1$\sigma$) for $\delta^{18}0$ values. 10 standards were measured during each run of 20 samples to determine precision for replicate analysis.

### 8.3.2    XRD, % Sand Fraction, NGR, and MAR Analyses

X-ray diffraction (XRD) measurements were performed to determine the relative percentages of high-Mg calcite, low-Mg calcite, aragonite, dolomite and quartz. Analytical procedures are discussed in the

Explanatory Notes Chapter of the Initial Reports Volume (Feary et al., 2000). All XRD data presented here are shipboard data taken from the Proceedings of the ODP: Initial Reports, Volume 182 (Feary et al., 2000).

The sand fraction is defined by the amount of sample larger than 63 μm. Sand fraction percentages were calculated by dividing the weighted, larger than 63μm sieved fraction by the weight of the total dried sediment and multiplied by 100 for percent (Bickert et al., 1997).

The Natural Gamma Radiation (NGR) tool detects the natural radioactivity of the formation. Most gamma radiation is emitted by the radioactive isotope $^{40}K$ and by radioactive elements in the U and Th series. Natural Gamma Radiation measurements were recorded with the Multisensor track tool (see Explanatory notes in (Feary et al., 2000) for more details). Shipboard data are taken from the Proceedings of the ODP: Initial Reports, Volume 182 (Feary et al., 2000). NGR was measured every 16 cm for a 26-second period and units are in counts per second (cps). Data were smoothed with a 5-point moving average.

Mass Accumulation Rates (MAR) of bulk sediment were calculated from sedimentation rates and dry bulk density data taken from shipboard analysis (Feary et al., 2000). Sedimentation rates are based on the age model developed for Site 1127.

## 8.4    Results

### 8.4.1    $\delta^{18}O$ Results

The stable oxygen isotope values from planktonic foraminiferal species *G. ruber* and *G. bulloides* are presented in profiles versus depth (Fig. 8.2a and b). Overall, isotopic values for *G. ruber* range from 2 to 0.6‰. The maximum fluctuation in amplitude is observed in the upper 10 m of the core and generally decreases downcore. A similar trend is seen in the oxygen isotope record for *G. ruber*, where overall isotope values range from 2.2 to 0‰. The isotopic offset between the two species of ~0.3 to 0.5‰ reflects their different depth-habitat in the water column (Hemleben et al., 1989). The 400-m long record is characterized by distinct cyclicity, which we identify as glacial-interglacial cyclicity as illustrated by the grey and white bars indicating marine oxygen isotope (MIS) stages during interglacial and glacials, respectively. It's notable that the width of the grey bars is, on average, greater than the white bars, reflecting higher sedimentation rates during interglacial periods.

***Figure 8.2. (next page)*** *Comparison of planktonic foraminiferal $\delta^{18}O$ results of (a) G. ruber and (b) G. bulloides with the (c) high-magnesium calcite (HMC) and low-magnesium calcite (LMC) mineralogy, (d) sand fraction weight % data, and (e) natural gamma ray (NGR) measurements in counts per second (cps). Data are plotted against metres below sea floor (mbsf). Depth of the shipboard identified Brunhes-Matuyama boundary (B/M) is marked. Interpreted interglacial marine isotope stages (MIS) are numbered and marked by grey bars.*
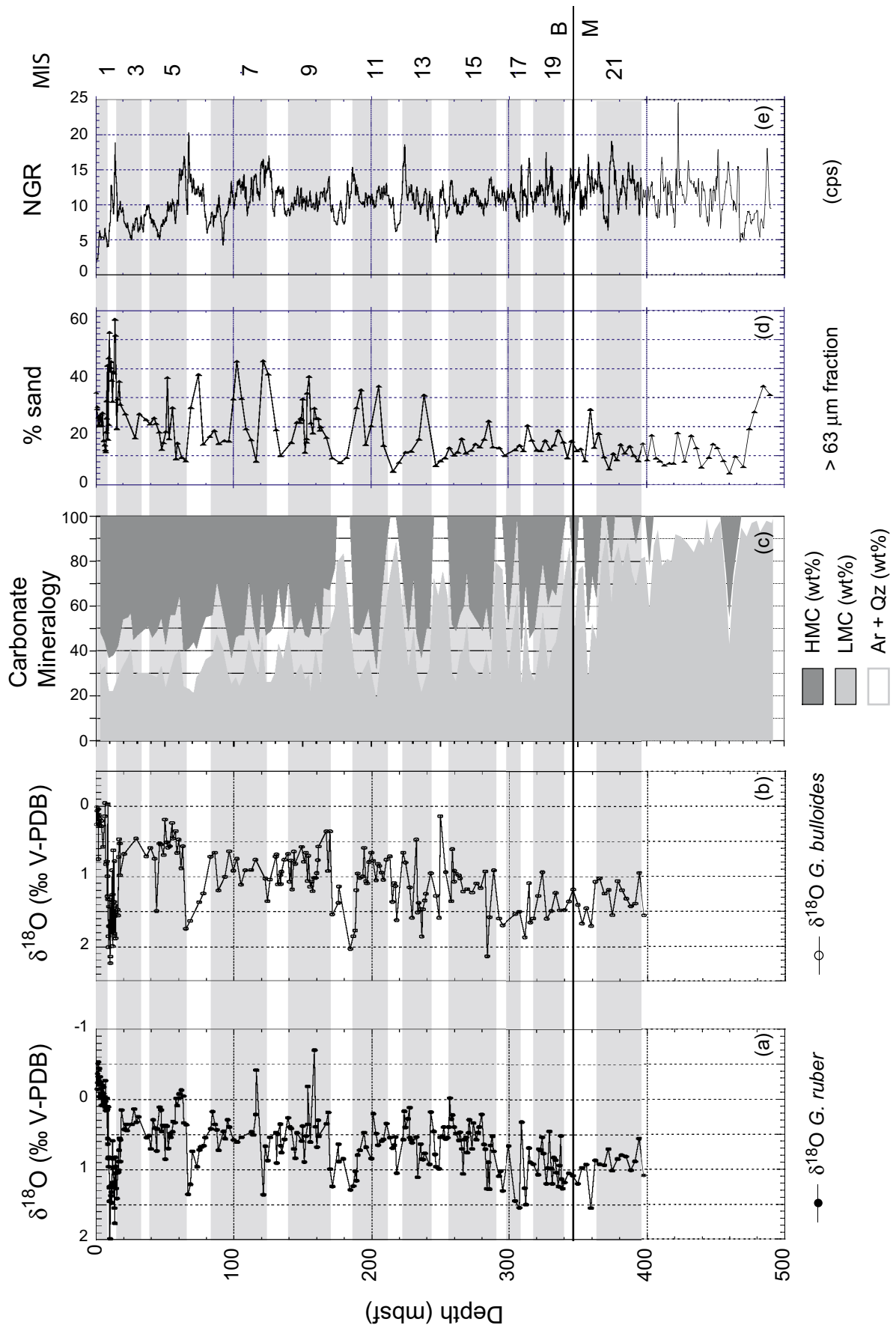
### 8.4.2    XRD, % Sand Fraction, and NGR Records

Based on shipboard bulk analysis (Feary et al., 2000), the carbonate mineralogy shows large variations (Fig. 8.2c) between the high-Mg calcite (HMC) and low-Mg calcite (LMC) percentages. Variations are most pronounced in the relative percentages of HMC and LMC that are characterized by an interfingering behavior, especially in the interval between 165-340 mbsf. When HMC is dominant (up to 55%), percentages of LMC are approximately 20%. During intervals of LMC-dominance (up to 80%), percentages of HMC are very low or even zero. The upper 165 m are dominated by HMC (varying around 40-60%) and the interfingering nature between HMC and LMC is not as obvious. In the lower part of the core, below 360 mbsf, HMC percentages gradually decline to zero with an exception at 460 mbsf, whereas LMC percentages increase.

The percent sand fraction is a measure of how much sand, defined as the larger than 63 μm sieved fraction, is present in the total sample (Fig. 8.2d). Values range between 5 and 58% and the curve can be divided into two differing phases. The first phase from 0 –250 mbsf is characterized by high-frequency, high-amplitude variations covering the entire range of 5-58%. Sand fraction percentages from 250 down to 373 mbsf are more or less stable, ranging between 5 and 20% (with one exception of 26% at 359 mbsf). At the very bottom of the core, the sand fraction increases to over 30% again.

Natural Gamma Ray variations indicate the presence of high-frequency cycles (Fig. 8.2e) with values ranging from 5 to 20 (cps). Similar to the sand fraction percentages (although not as dramatic) the curve differs above and below approximately 250 m. The upper part of the core (0-340 mbsf) shows low-frequency variations, compared to the rest of the core, but high amplitudes whereas the lowermost part (340-490 mbsf) is characterized by high-frequency and high-amplitude variations.

## 8.5    Stratigraphy and Age Model

### 8.5.1    Age Model

For the last 50 ka, the age model is based on the ^{14}C-dated chronology (Table 8.1). The remainder of the age model is based on the correlation of the oxygen isotope results of Site 1127 to the orbitally tuned and stacked record of Core MD900963 from the Indian Ocean (Bassinot et al., 1994). Oxygen isotopic results from bulk and fine fraction, discussed in Chapter 7 (Andres and McKenzie, 2002), are included. For the development of the age model, features identified in the Site 1127 and MD900963 $\delta^{18}$O records were aligned, and ages for Site 1127 record were obtained by linearly interpolating between tie-points. The age model generally assumes a lack of any significant hiatuses. Ages and depths of MIS boundaries and further tie-points are listed in Table 8.1.
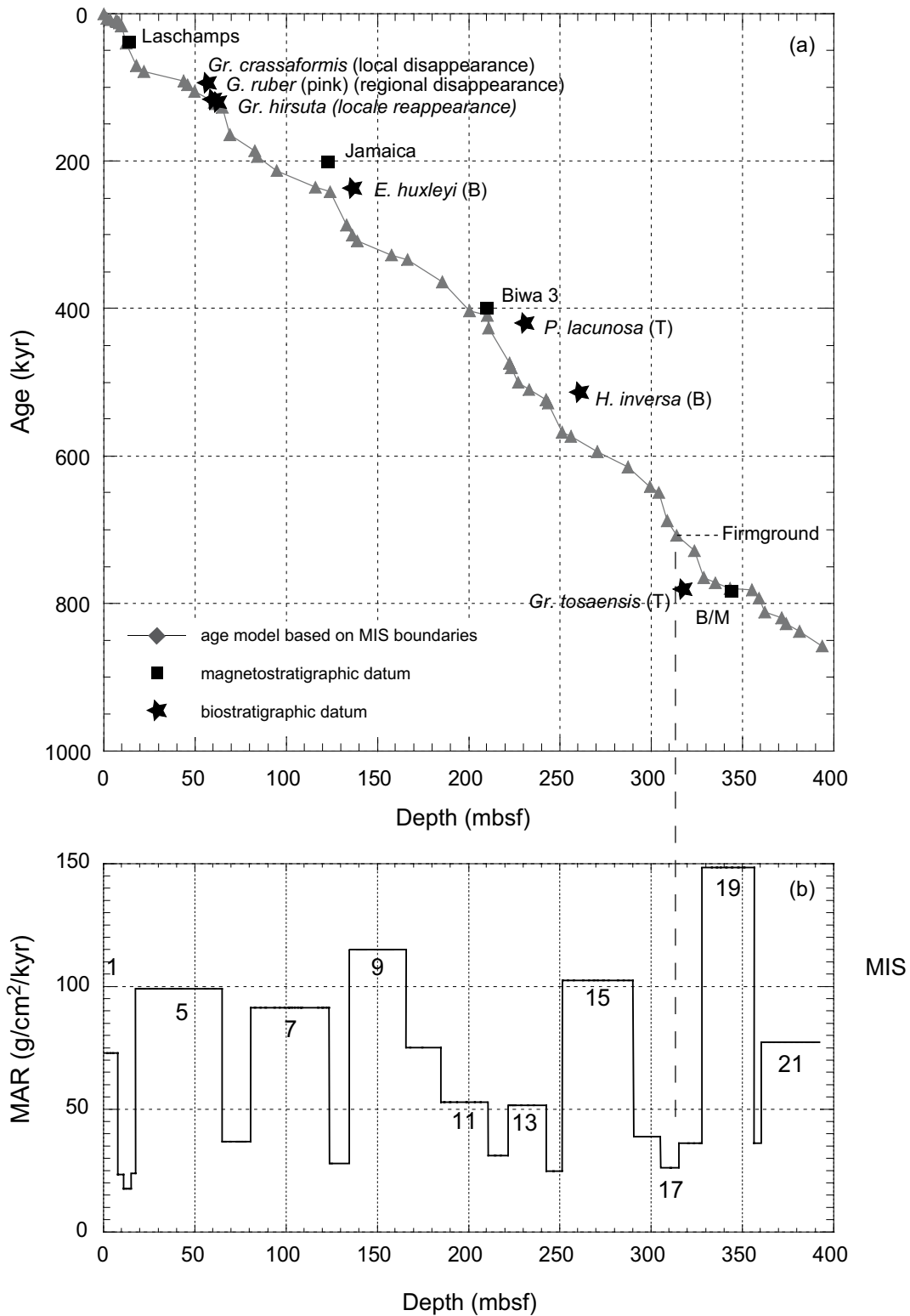
***Figure 8.3.*** *(a) Age versus depth plot based on [14]Cdated horizons and oxygen isotope stratigraphy developed from the correlation to Core MD900963 (Bassinot et al., 1994). Magnetostratigraphic and biostratigraphic datums (Brunner et al., 2002) are added. (b) Mass accumulation rates (MAR) are plotted against depth and illustrate the drastic fluctuations on a glacial-interglacial time scales.*

Figure 8.3a illustrates the age-depth relationship, suggesting fairly continuous sedimentation over the covered 850 ka time interval. Most importantly however, there is no indication of major hiatuses, except for a reported firmground at 314 mbsf, and no indication of sedimentary doubling as a result of sediment slumping or mass transport down shelf. For the last 200 ka, magneto- and biostratigraphic datums (Brunner et al., 2002) correlate well to the proposed age model. In the lower part of the record, however, the age model based on the $\delta^{18}O$ stratigraphy is systematically younger, with the exception of magnetostratigraphic datum Biwa 3 which fits the age model and the biostratigraphic datum of *Gr. Tosaensis* indicating an older age.

Average mass accumulation rates (MAR) vary quite drastically on a glacial-interglacial scale (Fig. 8.3b). MAR for interglacial periods are significantly higher than the preceding or following glacial, with the exception of MIS 17 and 11.

## 8.5.2   Pleistocene $\delta^{18}O$ Stratigraphy

The stratigraphic framework for Site 1127 is primarily based on the comparison of Marine Isotope Stage (MIS) boundaries of the orbitally tuned and stacked record of core MD900963 from the Indian Ocean (Bassinot et al., 1994) (Fig. 8.4). MIS 1 through 21 for the Late Pleistocene are recognized in the Site 1127 $\delta^{18}O$ record (Fig. 8.2 and 8.4). For most MIS stages, stage-internal characteristics could be correlated. Visual inspection of foraminiferal tests from below ~400 mbsf indicate significant secondary calcite overgrowth as a result of diagenetic alteration. Furthermore, this observation is supported by a change within the carbonate mineralogy, i.e. the abrupt increase of LMC (Fig. 8.2c) and good evidence for calcite recrystallisation. Results from below ~400 mbsf will, therefore, not be interpreted in a stratigraphic context.

Although the general glacial-interglacial fluctuations of the $\delta^{18}O$ record in Site 1127 are identified and comparable to global records, major differences exist. Most obvious are the significantly smaller amplitudes of Site 1127 record compared with that from MD900963, even though oxygen isotopes were measured on the same planktonic foraminifera. Also, the absolute $\delta^{18}O$ values of the *G. ruber* record reflect the cooler water temperatures of the GAB. Except for the last (MIS 2 to 1) and possibly penultimate (MIS 6 to 5) glacial cycles, glacial-interglacial $\delta^{18}O$ differences are small (0.5 to 1.0 ‰) and in part hardly visible, i.e. MIS 7 through 9. Furthermore, prominent warm interglacials, such as MIS 11, do not stand out in the Site 1127 record.

| Depth mbsf | Method 14C/MIS | cal age kyr BP |
|---|---|---|
| 0.02 | 14C | 0.76 |
| 2 | 14C | 6.76 |
| 3.72 | 14C | 8.53 |
| 6.9 | 14C | 10.26 |
| 7.42 | 14C | 10.59 |
| 7.9 | 14C | 11.08 |
| 8.41 | 14C | 12.33 |
| 9.4 | 14C | 16.63 |
| 9.91 | Mis 2.2 | 17.00 |
| 12.15 | 14C | 40.60 |
| 18 | peak | 70.60 |
| 21.95 | Mis 5.1 | 79.00 |
| 43.95 | peak low | 91.50 |
| 46.05 | Mis 5.3 | 97.00 |
| 49.93 | Mis 5.4 | 106.00 |
| 60.5 | G.ruber pink | 120.00 |
| 61.49 | Mis 5.5 | 122.00 |
| 65 | Mis 6.0 | 127.00 |
| 69.45 | peak inbetween | 164.30 |
| 82.94 | Mis 7.0 | 186.00 |
| 84.34 | Mis 7.1 | 194.00 |
| 94.95 | Mis 7.3 | 213.00 |
| 116.15 | Mis 7.5 | 236.00 |
| 124.15 | Mis 8.0 | 242.00 |
| 133.32 | Mis 8.5 | 287.00 |
| 136.43 | Mis 9.0 | 301.00 |
| 138.98 | Mis 9.1 | 309.00 |
| 157.93 | Mis 9.3 | 328.00 |
| 166.59 | Mis 10.0 | 334.00 |
| 185.56 | Mis 11 | 364.00 |
| 200.61 | Mis 11.x | 403.10 |
| 210.3 | Mis 11.y | 409.60 |
| 211.04 | Mis 12 | 427.00 |
| 222.45 | Mis 13 | 474.00 |
| 223.45 | Mis 13.11 | 481.00 |
| 227.12 | Mis 13.13 | 500.00 |
| 233.05 | Mis 13.2 | 510.00 |
| 242.65 | Mis 13.3 | 524.00 |
| 243.65 | Mis 14.0 | 528.00 |
| 251.33 | Mis 15 | 568.00 |
| 256.25 | Mis 15.1 | 573.00 |
| 270.51 | Mis 15.3 | 594.00 |
| 287.27 | Mis 15.5 | 615.00 |
| 299.44 | Mis 16.3 | 642.00 |
| 304.42 | low | 650.00 |
| 309.05 | Mis 17.3 | 688.00 |
| 314.05 | Mis 17.5 | 708.00 |
| 323.65 | Mis 18.3 | 729.00 |
| 328.87 | Mis 19.1 | 765.00 |
| 335.42 | Mis 19.2 | 772.00 |
| 343.4 | B/M boundary | 780.00 |
| 355.47 | Mid 19.3 | 782.00 |
| 359.15 | Mis 20.2 | 793.00 |
| 362.15 | low | 812.00 |
| 371.75 | Mis 21.1 | 820.00 |
| 374.21 | Mis 21.2 | 828.00 |
| 381.35 | Mis 21.3 | 838.00 |
| 393.77 | Mis 21.5 | 858.00 |

**Table 8.1.** *Depth and Age of tiepoints used to correlate Site 1127 $\delta^{18}O$ stratigraphy to the orbitally tuned and stacked record of Core MD 900963 (Bassinot et al., 1994). Tiepoints are based on $^{14}$C-dated horizons in the upper part of the core and marine isotope stages (MIS) in the lower part.*
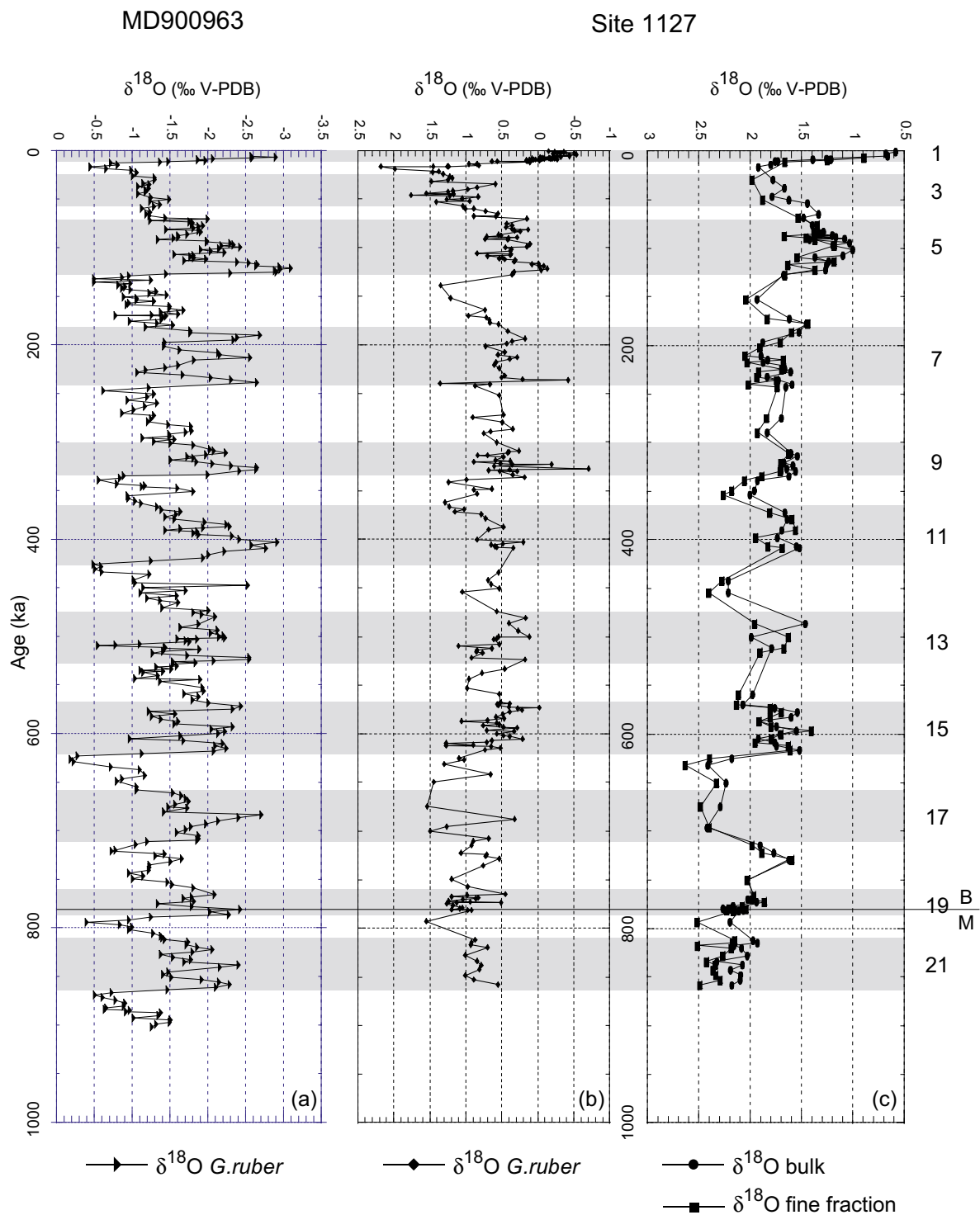
***Figure 8.4.*** *The $\delta^{18}O$ record of (a) core MD900963 from the Indian Ocean (Bassinot et al., 1994) in comparison with $\delta^{18}O$ records of Site 1127 based on (b) planktonic foraminifera species G. ruber and (c) bulk and fine fraction (<38 $\mu$m) analyses plotted against age. Interglacial marine isotope stages (MIS) are numbered and marked by grey bars. The Bruhnes-Matuyama boundary is indicated.*

In general, the Late Pleistocene $\delta^{18}O$ stratigraphy of Site 1127 can be discussed in three parts: the upper part 0-65 m (MIS 1-5), the middle part: 65-140 m (MIS 6-9) and the lower part: 140-340 m (MIS 10-21). The Holocene-LGM transition is well established within the bulk/ff and *G. ruber* $\delta^{18}O$ profile, showing 1.4‰/1.1‰ (bulk/ff) and 2.7‰ (*G. ruber*) decreases towards the Last Glacial Maximum. The stratigraphy is well constrained not only through MIS 2 stage boundary but also by several ^{14}C-dated horizons (Table 8.1). As for interglacial Stage 5, the planktonic $\delta^{18}O$ record readily identifies sub-Stages 5.1 through 5.5, but sub-Stages are difficult to identify in the bulk/ff $\delta^{18}O$ record. The penultimate termination, the MIS 5/6 transition, is well recorded in both bulk/ff curve and characterized by an abrupt, 2‰-shift in the planktonic foraminiferal record. The 120-kyr-dated disappearance of the pink-pigmented *G. ruber* from the Indian and Pacific Ocean (Thompson et al., 1979) has independently been recorded in this study and by (Brunner et al., 2002) to occur around 61 m at Site 1127, supporting evidence for the placement of the MIS 6 boundary at 65 m. The following glacial-interglacial stages, MIS 7 through 9, are characterized by very low amplitudes, with $\delta^{18}O$ values ranging between 0.5‰ or less for the bulk/ff record and 0.7‰ for *G. ruber*. In comparison to the record of core MD900963, the interglacials 11 to 21 never obtain Stage 5 or modern values. Glacial-interglacial amplitudes increase downcore (MIS 10/11 through 16/17) with a general trend towards more positive $\delta^{18}O$ values, especially pronounced in the bulk and ff record. Glacial $\delta^{18}O$ values become more and more positive (MIS 6, 8, 12, 18) whereas the interglacial values (MIS 7, 9, 11, 13, 15 and 19) remain fairly unchanged, resulting in increased glacial-interglacial amplitudes. This trend has also been observed in ff and planktonic foraminifera samples from cores of the western equatorial Pacific (Schiffelbein, 1984; Shackleton and Opdyke, 1976) and South Atlantic (Bollmann et al., 1998b). This mid-Brunhes phenomena has been addressed a number of times with (Bollmann et al., 1998a; Jansen et al., 1986; Raymo, 1997) these studies suggest long-term, global environmental change for which mechanisms and causes still remain unclear. MIS 11, proposed to have been as warm as today (Droxler and Farrell, 2000), fails to replicate the unusual warm SST conditions observed in other records. However when comparing these mid-Pleistocene interglacials from Site 1127 to core TN057-6 in the South-Atlantic Agulhas Ridge (Hodell et al., 2000), MIS 7, 9 and 11 also do not exceed MIS 5.5 or modern values. Hodell et al (2000) concluded that MIS 11 SST estimates were no warmer than today. For MIS 15, we note that the sub-Stages (MIS 15.1 through 15.5) are well defined in the bulk/ff record compared to the planktonic $\delta^{18}O$ record. Interglacial MIS 17 is not identified in the bulk/ff record and only defined in the planktonic record by one data point. Visual sediment description notes the existence of a firmground at ~313 mbsf corresponding to MIS 17. With the B/M boundary identified at 334.3 m, the MIS 19/20 boundary was placed at the midpoint of the measured increase towards more positive values. Although amplitudes are small, we are confident that the bottom 35 m of the analysed sediment correlates to MIS 21, supported by the 3-peaked structure most clearly identified in the *G. bulloides* $\delta^{18}O$ record.

## 8.6 Discussion

### 8.6.1 Site 1127 Sediments

ODP Leg 182, Site 1127 is the most seaward site of a three-site transect drilled through a set of late Neogene clinoforms just in front of the present-day shelf edge, as illustrated in the imaged seismic transect (Fig. 8.5). This upper-slope setting is located right at the boundary between the open ocean and shelf environment, as is expressed in the sediments by the mixture of neritic, shelf-derived benthic and planktonic carbonate. Thus, Site 1127 is ideally located to potentially link open-ocean changes onto the continental shelf, and furthermore to investigate the shelf-communities' environmental response to changes in the open ocean setting.
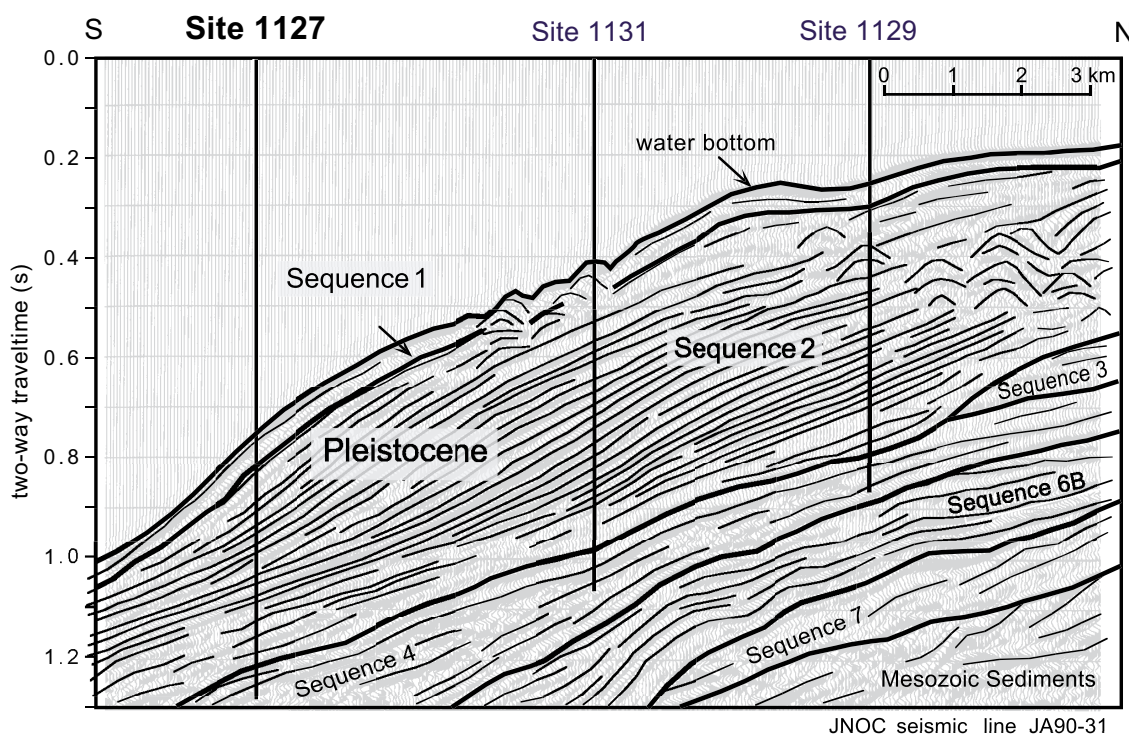


***Figure 8.5.*** *JNOC (Japan National Oil Company) seismic line for the eastern drilling transect, overlain by the three drill sites. Site 1127, located in 480 m of water depth penetrated through a set of Late Neogene clinoforms. Modified after (Feary et al., 1998).*

Images of the wet-sieved coarse fraction (>355 and 300 μm) from glacial-interglacial cycle MIS 11/12 are illustrated in Figure 8.6. The sedimentary changes observed from this glacial (MIS 12) to interglacial (MIS 11) period are representative of transitions throughout the core. Overall, the sand-sized (>63 μm) fraction of Site 1127 are characterized by a diverse and abundant benthic fauna (benthic foraminifera, bryozoa, bivalves, gastropods, echinoderms, ostracods, sponge spicules), with respect to the planktonic foraminiferal assemblage. In comparison to the interglacial times (Fig. 8.6a), the fauna in the sediments deposited during glacials are notably lower in diversity and abundance (Fig. 8.6c). This is especially seen in both benthic and planktonic foraminifera-assemblages and -

abundance. Furthermore, foraminifera are significantly smaller in size during interglacials. Sediments deposited during the glacial-interglacial transition (Fig. 8.6c) and during the early interglacial are characterized by the presence of fecal pellets, brown to yellow coloured organic (?algal) linings, and slightly cemented intraclasts consisting of small aggregated bioclastic fragments. Pteropods and pteropod fragments are present and aragonite is found throughout the core suggesting limited recrystallization during diagenesis.

a) MIS 11
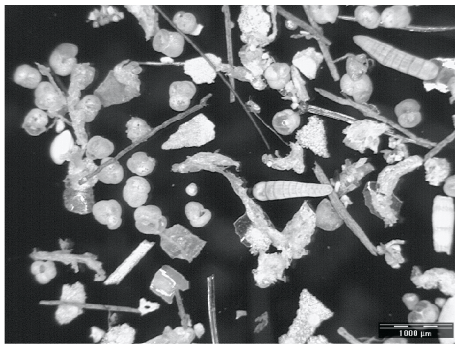


203.14 mbsf: 23X-1 14-19, >355 µm fraction
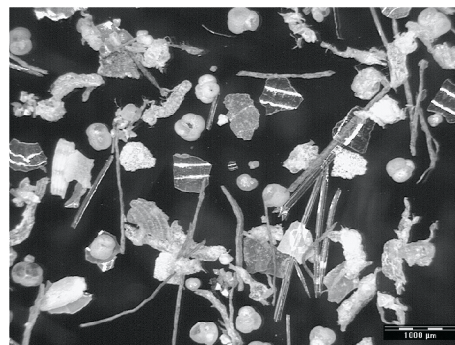
203.14 mbsf: 23X-1 14-19, >300 µm fraction

b) MIS 12/11 Transition



208.15 mbsf: 23X-4 65-70, >355 µm fraction
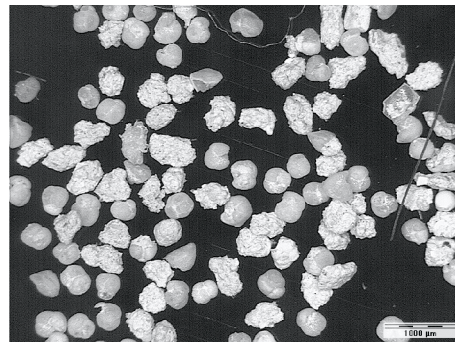
208.15 mbsf: 23X-4 65-70, >300 µm fraction

c) MIS 12
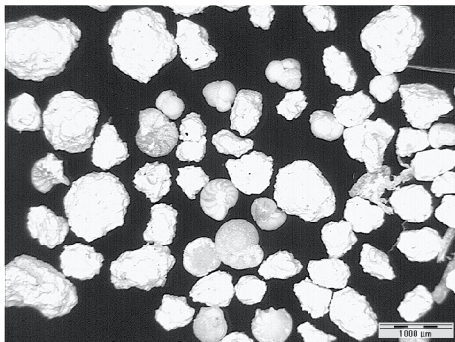


217.74 mbsf: 24X-4 65-70, >355 µm fraction
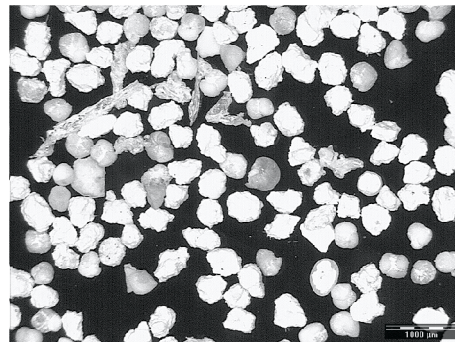
217.74 mbsf: 24X-4 65-70, >300 µm fraction

**Figure 8.6.** *(previous page) Light-microscope photographs of wet-sieved coarse-fraction sediment (> 355 and 300 μm) deposited during MIS 11/12 (a) interglacial, (c) glacial periods and (b) the transition inbetween. Note the change in diversity and nature of sediment.*

### 8.6.2 Margin Response to Eustatic Sea-Level Chages

Sea-level fluctuations during the last 860 ka impacted onto the continental margin significantly affecting the biota and, hence, carbonate production, which subsequently, in combination with the dominant hydrographic regime, controls the depositional geometry. The GAB margin is an almost pure carbonate setting with very little to no terrigenous input. Therefore, the signal obtained from environmental proxies, such as mineralogy, % sand fraction and NGR, represents the marine carbonate faunal and floral environment. We evaluate the stratigraphic record of sea-level fluctuations observed in the 'shelf proxies' with respect to the oxygen isotope stratigraphy developed from open marine planktonic foraminifera.

### *LGM-Holocene transition*

The Holocene sediment is composed of a nannofossil to foraminiferal ooze with sponge spicules. The wet-sieved coarse fraction illustrates the diversity of benthic fauna and flora (Fig. 8.6). Oxygen isotope composition of planktonic foraminifera reflect the influence of the warm Leeuwin Current and MAR documents the productive carbonate factory on the flooded shelf. Thus, the sediment contains a record of both open-ocean and margin environments.

During the last glacial (MIS 2) the shelf edge is characterized by prolific growth of bryozoan mounds, which were cored at upslope Sites 1131 and 1129 (Holbourn et al., 2002; James et al., 2000). These mounds are visible on seismic reflection as bumpy, mound-like structures (Fig. 8.5). They are interpreted as a lowstand-transgressive phenomena, growing during the last glacial lowstand (James et al., 2000). This time interval is also characterized by colder sea-surface temperatures (SST), as inferred from the planktonic foraminifera $\delta^{18}O$ record, by high (40-60%) sand fraction percentages and by elevated natural gamma radiation. Sand samples contain abundant bryozoan fragments and are most likely the result of downslope shedding of coarse, bryozoan-rich, mound-derived sediment. The NGR peak correlates well with the HMC-peak, but it is unclear exactly what produces the NGR fluctuations. Higher organic matter production by the glacial bryozoan mounds and associated benthic community could be the explanation. Increased upwelling and nutrient supply during the glacial period has been proposed as a possible mechanism to sustain the mound growth (Holbourn et al., 2002; James et al., 2000). MAR, however, are significantly lower than during the Holocene and preceding interglacial period (MIS 5; Fig. 8.3b), most likely reflecting the smaller area of possible biogenic carbonate production due to the lowered sea level. Alternatively, bryozoan mounds could act as natural barrier behind which sediment is trapped and prevented from reaching the upper slope location of Site 1127. Interestingly, the last glacial period (MIS2) is mineralogically dominated by HMC (Fig. 8.2c) and arguably the result of the bryozoan-dominated sediment composition. Yet, these benthic,

colonial animals typically calcify both high- or low-Mg calcite body walls (Nelson et al., 1988) and their mineralogy is highly species-dependent. The detailed identification and description of the bryozoan assemblage found on the GAB margin is part of ongoing work.

*Penultimate glacial-interglacial transition*

A similar pattern is repeated during interglacial MIS 5e, 122 ka ago, and corresponding glacial (MIS 6). The end of the glacial period, as indicated by increased $\delta^{18}O$ values in both *G. ruber* and *G. bulloides* records, coincides with a peak in HMC, high sand fraction percentages, elevated NGR values, and decreased MAR and correlates to bryozoan mound growth observed in Site 1129 during this time interval (Holbourn et al., 2002).

*Late Pleistocene record*

This pattern is not only observed during glacial-interglacial transitions as discussed above, but a detailed comparison suggests an impressively tight correlation between periods of abundant bryozoan mound growth at the shelf edge, Sites 1131 and 1129 (Holbourn et al., 2002), and the 'shelf-proxy' record from upper slope Site 1127. For most of the upper 200 m of the record (MIS 1 through 11), phases of prolific mound growth can be correlated to peaks in the HMC mineralogy, higher sand-fraction percentages, and elevated NGR values. Although mound growth has been attributed to glacial periods (MIS 2 and 6) (James et al., 2000), they are found within the interglacial periods of MIS 11, 9 and 7. This suggests that either mound growth is not restricted to glacial conditions but is limited by other physical factors, such as nutrient availability. Alternatively, interglacials 7 and 9 are locally not 'interglacial-like' in character and the more 'glacial-like' condition permits the growth of bryozoan mounds. Oxygen isotope results from bulk, fine fraction and planktonic foraminifera indicate very little glacial-interglacial variation and support the proposition that the oceanographic change observed for the LGM-Holocene transition may not be applicable to the older glacial cycles. Reduced glacial-interglacial variations for this interval have also been reported from benthic foraminifera $\delta^{18}O$ data from Sites 1131 and 1129 (Holbourn et al., 2002).

Site 1127 is ideally suited to monitor upper-shelf and shelf-edge changes due to its down-slope location in slightly deeper water. Both Site 1131 and 1129 located in 218 and 202 m of water depths, respectively, are profoundly influenced by sea-level fluctuations which are documented by several unconformities. The increase in HMC at Site 1127 in the middle of MIS 8 (Fig. 8.2c) can be directly correlated to the onset of prolific mound growth at the uppermost Site 1129. Afterwards, beginning with MIS 4, the core of bryozoan mound production moved downslope to Site 1131. This seaward shift, clearly visible in the seismic image (Fig. 8.5), is most likely the result of the outward progradation of the shelf edge as the sedimentary package thickens. Mounds developed around Site 1131 become the main source of HMC and coarse fraction sediment to Site 1127 during MIS 4 through 2. Thus, as mound proliferation during glacial periods moved closer to the location of Site 1127, the percentage of HMC in the Site 1127 sediments showed a corresponding glacial increase.

### *Mid-Pleistocene record*

The mid-Pleistocene (MIS 9 to 21) sedimentary record at Site 1127 is generally characterized by a different, interfingering pattern in the LMC and HMC mineralogy, during glacial and interglacial periods respectively. In contrast to the Late Pleistocene record, a complete disappearance of HMC was observed during glacial MIS 10, 12, 14, 16 and 20. This is especially striking since aragonite percentages remain constant between 15 to 20% and are virtually unaffected by this cyclicity. The source of the HMC, i.e. a specific organism or group of shallow-water organisms, partially or wholly precipitating their tests of HMC, remains unclear. One plausible explanation for the HMC appearance during interglacial periods is that the biogenic carbonate assemblage whose dominant carbonate mineralogy is HMC thrives under interglacial conditions. During times of sea-level highstands, the continental margin would be fully flooded, and the oligotrophic warmer waters of the Leeuwin current would dominate the surface water of the GAB. The cool-water carbonate production and downslope export would be at its maximum as evidenced by significantly higher MAR during MIS 9, 15, 19, 21, and to a lesser extent during MIS 11 and 13 (Fig. 8.3b). During glacials and sea-level lowstands, large portions of the upper shelf would be exposed and the more nutrient-rich, colder waters of the Flinders Current would dominate the surface water of the glacially reduced GAB. LMC enriched sediments would be produced by the remaining 'background' bioassemblage and open-ocean organisms, which are present during the interglacials (20%) but diluted by the HMC assemblage. Without the dominantly HMC producing organisms, the amount of sediment production is drastically reduced, or restricted to mound growth, as seen in the reduced MAR data for glacial periods (Fig. 8.3a).

In summary, during interglacial periods, the warmer oligotrophic waters of the Leeuwin Current is weak and the greater influence of the Flinders Current, promoting enhanced biological production areas on the GAB slope leading to increased MAR with high HMC content. During glacial periods, the cooler, nutrient-rich waters of the Flinders Current focus biological production predominantly in the bryozoan mounds, resulting in reduced MAR and less HMC transport to the slopes. As the loci of bryozoan mound growth moved closer to Site 1127 in more recent time, the HMC flux to the sediments increased.

The seismic image of Figure 8.5 not only illustrates mound growth during the late Pleistocene, which is well-documented in Site 1131 and 1129, but also confirms their presence throughout the entire Pleistocene section of Seismic Sequence 2. Currently, we are unable to define if these mounds are of glacial or interglacial origin, but, based on the measured proxies, we speculate that the Mid-Pleistocene mounds were present as early as MIS 20/19, becoming more extensive during MIS 13, 11 and 9. Interglacial mound growth, accompanied by wide-spread biological productivity on the slope, would shed more sand-fraction-sized material down slope as observed within the sand fraction record during MIS 13, 11 and 9 and again correlates with higher NGR counts. MAR during this interval, however, only show a partly consistent pattern with high MAR during interglacials 7, 9, 15, 19, and 21 and only intermediate rates for 11 and 13. MAR for glacial periods are generally lower compared to their immediately following interglacial. A possible mechanism for low MAR during interglacials

(MIS 13 and 11) is that locally grown bryozoan mound barriers trap sediment behind and prevent shedding onto the upper slope or that the Leeuwin Current influence on the slope was very weak, comparable to glacial times. During MIS 15, 9 and 7 however sediment was able to bypass the mounds and deposited on the upper slope setting. MIS 17 completely fails to reproduce any of the observed patterns and this is associated with firmground formation at the MIS 18/17 transition. The frimground within the MIS 17 inteval may represent a condensed horizon, or extended period of non-deposition. The $\delta^{18}O$ values for most of the MIS 17 section remain relatively similar to the surrounding glacial values of MIS 18 and 16 is consistent with a weak Leeuwin Current during this interglacial. Thus, biological productivity could remain low even during a high-stand, leading to reduced sedimentation and firmground formation.

*Paleoceanographic interpretation*

The modern oceanographic setting in GAB region is influenced by two significantly different water masses; i.e. the Leeuwin Current (LC), a warm, oligotrophic flow of tropical origin entering the GAB from the west and the cool Southern Ocean waters entering the GAB from the east as the anti-gyral Flinders Current. The interplay between these two water masses is complex and not fully understood, but, at least on a seasonal scale, hydrographic data indicate a strong austral-winter flow of the LC into the GAB which in turn forces the FC to become an undercurrent to the LC. As the LC weakens (i.e in Summer), the FC strengthens and moves onto the shelf edge. This seasonal variability has a great effect on the temperature distribution, apart from nutrient availability and thus productivity. The interplay of these water mases during glacial-interglacial cycles has been documented as the cessation and absence of the LC during glacials proposed from calcareous nannoplankton and foraminiferal studies (Almond et al., 1993; McGowran and al., 1997; Okada and Wells, 1997). In detail, however, these studies have only discussed records from the Late Quaternary, i.e. covering MIS 6 through 1. Site 1127 represents the first long record covering much of the Pleistocene history of the central GAB. For the MIS 6/5 and MIS 2/1 time intervals, the combined Site 1127 data support the hypothesis that LC flow was absent during these glacials and cool Southern Ocean conditions prevailed on the shelf. These nutrient rich waters sustained prolific bryozoan mound growth during MIS 6, 4, 3 and 2 (Holbourn et al., 2002; James et al., 2000). Interglacial stages MIS 5 and 1 are dominantly influenced by the oligotrophic warm LC, not only evidenced in the absence of bryozoan mounds but also in the large, and globally comparable $\delta^{18}O$ glacial-interglacial shift documented in the planktonic foraminifera of this study and benthic foraminifera (Holbourn et al., 2002).

In order to interpret the mid-Pleistocene record in a paleoceanographic context, for which no comparative study exists, large-scale oceanographic features, such as the Subtropical Convergence Zone are to be re-examined. The Subtropical Convergence Zone (STCZ) is an important component of the southeast Indian and Southern Ocean frontal structure. In the Australian sector, this includes the Polar Front and the Subantarctic Front. The STC is formed in response to high-latitude wind regimes and recognized by the very rapid change of water-temperature, salinity and productivity properties.

Changes in the position of the STC through the Pleistocene have been well documented in the southern and southeastern Indian Ocean (Hays et al., 1976; Howard and Prell, 1992; Prell et al., 1979; Prell et al., 1980) and shifts have profound changes in primary productivity but also significantly influence the flux to the seafloor (Francois et al., 1993; Mackensen et al., 1993). These studies propose a more equatorward position of the STC compared to its modern position for most of the Quaternary. Two significant poleward movements have been documented during the Holocene and oxygen isotope stage 5.5 (~122 ka) as for example, the dominantly subtropical faunal assemblage abundant during these two time intervals indicates poleward movement. A southward movement has also been proposed for MIS 9 and 11 (Howard and Prell, 1992), but a study on radiolarians (Morley, 1989) does not record a MIS 9 shift. (Jansen et al., 1986) compiled oceanic and continental records over this time and cores from the Southern Ocean indicate shifting polar fronts by ~5° latitude. Recently obtained data from meridional ocean transects south of Australia, as part of the Word Ocean Circulation Experiment (WOCE), found the STC 39°S in the west (120°E) and about 220 km further north in the east (132°E) (Schodlok et al., 1997). This implies that latitudinal changes in the position of the STC of only a few degrees could have a major effect on the GAB region

Taken together, the above discussed location and movement of the STC can explain much of the observed variations in Site 1127 sedimentary record. During interglacials, if the STC is markedly displaced to the south, it allows for the LC to enter the GAB as suggested for MIS 1 and 5 in numerous studies and indicated by oxygen isotope values of this study and the lack of bryozoan mound growth (Holbourn et al., 2002). An only slight southward displacement or unchanged position of the STC, however, results in very small or no glacial-interglacial variations as observed for most of the mid-Pleistocene interglacials at Site 1127. It further explains bryozoan mound growth during interglacial conditions, as reported for MIS 7 (Holbourn et al., 2002) and proposed from the interpretation of the seismic image, HMC cycles, sand-fraction percentages and NGR values.

Arguments for long-term environmental and circulation changes during the mid-Pleistocene have been proposed by several studies. Although interglacials during this time interval are reported to be have been warmer (Burckle, 1993), with MIS 11 as the warmest amongst the Pleistocene interglacial stages and often compared to today's interglacial (Howard, 1997), this seems not to have occured in records influenced by the Southern Ocean, as shown in this study but also by Hodell et al. (2000). Early studies across the Brunhes-Matuyama boundary in the Southern Ocean (Bandy et al., 1971) noted the disappearance of present-day radiolarians, which has been interpreted as evidence for the deterioration of climate conditions from warmer in the Matuyama to colder in the Brunhes chron, with the major change taking place around 900 ka. The onset of the Great Barrier Reef is proposed for the mid Pleistocene (Alexander et al., 2001) and studies on calcareous nannoplankton (Bollmann et al., 1998b) see a selective coccolith dominance interval. In summary, these studies demonstrate changing environmental conditions in the mid Pleistocene, but the underlying mechanism required to explain this paleoceanographic and paleoecologic change remains elusive.

## 8.7   Conclusions

The marine sedimentary record of the GAB identifies all 21 marine isotope stages to approximately the magnetostratigraphic Brunhes/Matuyama boundary, and, thus, continuously traces sea-level rise and fall on a continental margin for the last 850'000 years. Similar to their tropical counterparts, the cool-water carbonates of the Great Australian Bight have great potential to record paleoceanographic and intrinsically linked paleoclimatic changes. High sedimentation rates and well-preserved foraminifera allow for the development of a reliable oxygen isotope stratigraphy and age model. Fluctuations in the carbonate mineralogy, sand-fraction percentages and NGR counts express the response of the neritic shelf community to sea-level variations. The last 250 ka years, MIS 1 through 7, are dominated by significant bryzoan mound growth during nutrient-rich glacial conditions and warm Leeuwin influenced interglacials. The mid-Pleistocene glacial-interglacial fluctuations are less pronounced and explained by a generally northerly position of the Subtropical Convergence also during interglacials and therefore preventing Leeuwin Current flow into the GAB region. The Site 1127 record not only represents the longest continuous record of paleoceanographic change in the sparsely documented southern mid-latitude region but also links open-ocean changes onto the continental margin of cool-water carbonate deposition.

## Acknowledgments

## References

Alexander, I., Andres, M. S., Braithwaite, C., Braga, J.-C., Cooper, M. J., Davies, P. J., Elderfield, H., Gilmour, M. A., Kay, R. L. F., Kroon, D., McKenzie, J. A., Montaggioni, L., Skinner, A., Thomson, R., Vasconcelos, C., Webster, J., and Wilson, P. A. (2001). New Constraints on the origin of the Australian Great Barrier Reef: Results from an international project of deep coring. *Geology* **29,** 438-486.

Almond, D., McGowran, B., and Li, Q. (1993). Late Quaternary Foraminiferal record from the Great Australian Bight and its environmental significance. *Memoir Association Australasian Paleontologist* **15,** 417-428.

Andres, M. S., and McKenzie, J. A. (2002). Late Pleistocene Carbon and Oxygen Isotope Stratigraphy developed from ODP Leg 182 Site 1127 Bulk and Fine-Fraction Carbonate. *In* "Proceedings of the Ocean Drilling Program, Scientific Results, 182 [Online]. Available from World Wide Web: <http://www-odp.tamu.edu/publications/182_SR/011/011.htm>. [Cited YYYY-MM-DD]." (A. C. Hine, Feary, D.A., and Malone, M.J., Ed.).

Bandy, O. L., Casey, R. E., and Wright, R. C. (1971). Late Neogene planktonic zonation, magnetic reversals, and radiometric dates, Antarctic to tropics. *American geophysical Union Antarctic Research Service* **15,** 1-26.

Bassinot, F. C., Labeyrie, L. D., Vincent, E., Quidelleur, X., Shackleton, N. J., and Lancelot, Y. (1994). The astronomical theory of climate and the age of the Brunhes-Matuyama magnetic reversal. *Earth and Planetary Science Letters* **126,** 91-108.

Bein, J., and Taylor, M. L. (1981). The Eyre Sub-basin: recent exploration results. *The APEA Journal* **21,** 91-98.

Bickert, T., Cordes, R., and Wefer, G. (1997). Late Pliocene to Mid-Pleistocene (2.6-1.0 m.y.) carbonate dissolution in the western Equatorial Atlantic: Results from Leg 154, Ceara Rise.

Bollmann, J., Baumann, K.-H., and Thierstein, H. R. (1998a). Global dominace of Gephyrocapsa coccoliths in the late Pleistocene: Selective dissolution, evolution, or global environmental change? *Paleoceanography* **13,** 517-529.

Bollmann, J., Thierstein, H. R., and Mulitza, S. (1998b). The mid-Brunhes carbon isotope excursion of nannofossil fractions ? compositional changes, preservation effects or environmental change? *Volume Book of Abstracts: Lissabon, Aug. 24-28, p. 81.6th International Conference on Paleoceanography.*

Brunner, C. A., Andres, M. S., Holbourn, A. E., Siedlecki, S., Brooks, G. R., Molina Garza, R. S., Fuller, M. D., Ladner, B. C., Hine, A. C., and Li, Q. (2002). Quaternary Planktonic Foraminiferal Biostratigraphy, ODP Leg 182 Sites. *In* "Proceedings of the Ocean Drilling Program, Scientific Results, 182 [Online]. Available from World Wide Web: <http://www-odp.tamu.edu/publications/182_SR/011/011.htm>. [Cited YYYY-MM-DD]." (A. C. Hine, Feary, D.A., and Malone, M.J., Ed.).

Burckle, L. H. (1993). Late Quaternary interglacial stages warmer than present. *Quaternary Science Reviews* **12,** 825-831.

Cresswell, G. R., and Golding, T. J. (1980). Observations of a south flowing current in the south-eastern Indian Ocean. *Deep-Sea Research* **27A,** 449-466.

Droxler, A. W., and Farrell, J. W. (2000). Marine Isotope Stage 11 (MIS 11): new insights for a warm future. *Global and Planetary Change* **24,** 1-5.

Feary, D. A., Hine, A. C., and Malone, M. J. (1998). Leg 182 Scientific Prospectus: Great Australian Bight: Cenozoic Cool-Water Carbonates. ODP, Texas A&M University.

Feary, D. A., Hine, A. C., Malone, M. J., and et al. (2000). Proceedings of the Ocean Drilling Program. *In* "Proceedings of the Ocean Drilling Program, Initial Reports, 182 [CD-ROM]:." (A. C. Hine, D. A. Feary, and M. J. Malone, Eds.), Available from: Ocean Drilling Program, Texas A&M University, College Station , TX 77845-9547, USA.

Feary, D. A., and James, N. P. (1998). Seismic Stratigraphy and Geological Evolution of the Cenozoic, Cool-Water Eucla Platform, Great Australian Bight. *AAPG Bulletin* **82,** 792-816.

Francois, R., Bacon, M., Altabet, M. A., and Labeyrie, L. D. (1993). Glacial/interglacial changes in sediment rain rate in the SW Indian sector of Subantarctic waters as recorded by $^{230}$Th, $^{231}$Pa, and $\delta^{15}$N. *Paleoceanography* **8,** 611-629.

Hays, J. D., Imbrie, J., and Shackleton, N. J. (1976). Variations in the earth´s orbit: pacemaker of the ice ages. *Science* **194,** 1121-1132.

Hemleben, C., Spindler, M., and Anderson, O. R. (1989). "Modern Planktonic Foraminifera." Springer, New York, Berlin, Heidelberg.

Hodell, D. A., Charles, C. D., and Ninnemann, U. S. (2000). Comparison of interglacial stages in the South Atlantic sector of the southern ocean for the past 450 kyr: implication for Marine Isotope Stage (MIS) 11. *Global and Planetary Change* **24,** 7-26.

Holbourn, A. E., Kuhnt, W., and James, N. P. (2002). Late Pleistocene isotope stratigraphy and paleoceanography of the Great Australian Bight: The benthic foraminiferal record. *Plaeoceangoraphy***,** 14-23.

Howard, R. H., and Prell, W. L. (1992). Late Quaternary surface circulation of the southern Indian Ocean and its relationship to orbital variations. *Paleoceanography* **7,** 79-117.

Howard, W. R. (1997). A warm future in the past. *Nature* **388,** 418-419.

Hufford, G. E., McCartney, M. S., and Donohue, K. A. (1997). Northern boundary current and adjacent recirculations off southwestern Australia. *Geophysical Research Letters* **24,** 2797-2800.

James, N. P. (1997). The Cool-Water Carbonate Depositional Realm. *In* "Cool-Water Carbonates." (N. P. James, and J. D. A. Clarke, Eds.), pp. 1-20. S.E.P.M. Special Publication.

James, N. P., Bone, Y., Collins, L. B., and Kyser, T. K. (2001). Surficial Sediments of the Great Australian Bight: Facies Dynamics and Oceanography on a Vast Cool-Water Carbonate Shelf. *Journal of Sedimentary Research* **71,** 549-567.

James, N. P., and Clarke, J. A. D. (1997). Cool-Water Carbonates. *In* "SEPM Special Publication.", pp. 440. SEPM, Tulsa.

James, N. P., Feary, D. A., Surlyk, F., Simo, J. A. T., Betzler, C., Holburn, A. E., Qianyu, L., Matsuda, H., Machiyama, H., Brooks, G. R., Andres, M. S., Hine, A. C., Malone, M. J., and Party, O. D. P. L. S. (2000). Quaternary bryozoan reef mounds in cool-water, upper slope environments: Great Australian Bight. *Geololy* **28,** 647-650.

Jansen, J. H. F., Kuijpers, A., and Troelstra, S. R. (1986). A Mid-Brunhes Climatic Event: Long-Term Changes in Global Atmosphere and Ocean Circulation. *Science* **232,** 619-622.

Legeckis, R., and Cresswell, G. R. (1981). Satellite observations of sea-surface temperature fronts off the coast of western and southern Australia. *Deep-Sea Research* **28A,** 297-306.

Li, Q., James, N. P., Bone, Y., and McGowran, B. (1999). Paleoceanographic significance of recent foraminiferal biofacies on the southern shelf of Western Australia: a preliminary study. *Paleogeography, Paleoclimatology, Paleoecology* **147,** 101-120.

Mackensen, A., Hubberten, H.-W., Bickert, T., Fischer, G., and Fütterer, D. K. (1993). The $\delta^{13}C$ in benthic foraminiferal tests of *Fontbotia wuellerstorfi* (Schwager) relative to the δ13C of dissolved inorganic carbon in southern ocean deep water: implications for glacial ocean circulation models. *Paleoceanography* **8,** 587-610.

McGowran, B., and al., e. (1997). Biogeographic impact of the Leeuwin Current in southern Australia since the late middle Eocene. *Paleogeography, Paleoclimatology, Paleoecology* **136,** 19-40.

Morley, J. J. (1989). Variations in high-latitude oceanographic fronts in the southern Indian Ocean: An estimation based on faunal changes. *Paleoceanography* **4,** 547-554.

Nelson, C. S., Hyden, F. M., Keane, S. L., Leask, W. L., and Gordon, D. P. (1988). Application of bryozoan zoarial growth-form studies in facies analysis of non-tropical carbonate deposits in New Zealand. *Sedimentary Geology* **60,** 301-322.

Okada, H., and Wells, P. (1997). Late Quaternary nannofossil indicators of climate change in two deep-sea cores associated with the Leeuwin Current off Western Australia. *Palaeogeoraphy, Palaeoclimatology, Palaeoecology* **131,** 413-432.

Prell, W. L., Hutson, W. H., and Williams, D. F. (1979). The subtropical convergence and Late Quaternary circulation in the Southern Indian Ocean. *Marine Micropaleontology* **4,** 225-234.

Prell, W. L., Hutson, W. H., Williams, D. F., Be, A. W. H., Geitzenauer, K., and Molfino, B. (1980). Surface Circulation of the Indian Ocean during the Last Glacial Maximum, Approximately 18,000 yr B.P. *Quatenary Research* **14,** 309-336.

Raymo, M. E. (1997). The timing of major climate terminations. *Paleoceanography* **12,** 577-585.

Rochford, D. J. (1984). Effect of the Leeuwin Current upon Sea Surface Temperatures off South-western Australia. *Australian Journal of Marine and Freshwater Research* **35,** 487-489.

Rochford, D. J. (1986). Seasonal Changes in the Distribution of Leeuwin Current Waters off Southern Australia. *Australian Journal of Marine and Freshwater Research* **37,** 1-10.

Schiffelbein, P. (1984). "Stable isotope systematics in Pleistocene deep-see sediment records.", Universtiy of California.

Schodlok, M., Tomczak, M., and White, N. (1997). Deep sections through the South Australian Basin and across the Australian-Antarctic Discordance. *Geophysical Research Letters* **24,** 2785-2788.

Shackleton, N. J., and Opdyke, B. N. (1976). Oxygen-Isotope and Paleomagnetic Stratigraphy of Pacific Core V28-239 Late Pliocene to Latest Pleistocene. *In* " Investigation of the Late Quaternary Paleoceanography and Plaeoclimatology." (R. M. Cline, and J. D. Hays, Eds.), pp. 449-464. Geological Society of America.

Stagg, H. M. J., Cockshell, C. D., Willcox, J. B., Hill, A. J., Needham, D. J. L., Thomas, B., O'Brien, G. W., and Hough, L. P. (1990). Basins of the the Great Australian Bight region: Geology and petroleum potential:. *Australian Bureau of Mineral Resources Continental Margins Program* **Folio 5**.

Stagg, H. M. J., Willcox, J. B., and Needham, D. J. L. (1989). Werner deconvolution of magnetic data: Theorectical models and application to the Great Australian Bight. *Australian Journal of Earth Sciences* **36,** 109-122.

Thompson, P. R., Bé, A. W. H., Duplessy, J.-C., and Shackleton, N. J. (1979). Disappearance of pink-pigmented Globigerinoides ruber at 120,000 yr BOP in the Indian and Pacific Ocean. *Nature* **280,** 554-558.

Veevers, J. J., Stagg, H. M. J., Willcox, J. B., and Davies, H. L. (1990). Pattern of slow seafloor spreading (<4mm/year) from breakup (96 Ma) to  A20 (44.5 Ma) off the southern margin of Australia. *BMR Journal of Australian Geology & Geophysisics* **11,**  499-507.

Willcox, J. B., and Stagg, H. M. J. (1990). Australia's southern margin: a product of oblique extension. *Tectonophysics* **173,** 269-281.

# 9 GENERAL CONCLUSIONS AND OUTLOOK

## 9.1 Conclusions and Implications

This aim of this thesis was to define Late Quaternary paleoceanographic and paleoclimatic changes in the cool-water carbonate depositional realm of the Great Australian Bight. I used chemical, physical and biological signatures of paleo-change in order to assess the nature, amplitude, timing and significance of recorded events on a regional and global scale. Since this study presents the first high-resolution Late Quaternary record from a cool-water shelf carbonates, the initial research addressed the fundamental question of stratigraphic integrity and sedimentary expression of change. In conclusion, this study:

- **confirmed the Site 1127 stratigraphic integrity**
  High-resolution $^{14}$C chronology in the upper-most 30 m and $\delta^{18}$O stratigraphy in the upper 394 m of the core evidence the absence of major hiatuses but also ruled out sediment disturbance due shelf-edge slumping and mass transport.

- **demostrated that cool-water carbonates are ideal paleo-archives**
  Cool-water carbonates, similar to their warm-water counterparts in tropical settings, record paleoceanograhic and climatic information. For example, changes in isotopic and mineralogical composition, fluctuations in their sand-fraction percentages, and abundance and diversity variations of their planktonic and benthic faunal assemblages can be related to oceanographic change.

The focus of the thesis was divided into two time intervals, the Late Pleistocene and the LGM to Holocene. Both studies in both time intervals improved our understanding of the nature, amplitude and timing of glacial-interglacial fluctuations on a ramp-type setting, and it provided new data on paleoceanographic circulation patterns in this sparsely documented southern mid-latitude region. In particular, the data showed:

- **a cold reversal on the GAB during Termination I synchronous with the Younger Dryas Chronozone**
  High-resolution oxygen isotope data, representing a combination of temperature and hydrographic change, show initial step-wise warming from the LGM, which is interrupted by two significant cold reversals before the warming trend continues into the Holocene. The cold reversals, which are $^{14}$C-dated from 13.1 to 12.3 and 12.3 to 11.1 cal. ka BP are separated by a brief but significant warming. If interpreted as a pure temperature signal, the reversals

translate to an up to 3°C cooling in SST. Within the error of dating, the timing and nature of these two reversals correlates to the recently proposed Oceanic Cold Reversal observed in the mid-latitude Indian Ocean. The second, more intense abrupt reversal, although smaller in amplitude, resembles and is synchronous with the Younger Dryas Chronozone, as evidenced in the Northern Hemisphere. The oxygen isotope record of Site 1127, which most likely represents a combination of temperature and hydrographic change, indicates a direct link, probably ocean-driven, between Northern and Southern Hemisphere climate. The GAB sedimentary archive represents one of the few marine locations in the southern mid-latitudes with sufficiently high sedimentation rates to assess rapid oceanographic and climatic change on sub-centennial time scales.

- **a link between GAB and Southern Australian climate records for the last 20,000 years**
  High-resolution and unprecedented LGM-Holocene SST and dust proxy data developed in GAB sequence show a dramatic change from the cold, dry and windy LGM to the wet and warm Early Holocene and document the aridification and increased climate variability due to ENSO during the Late Holocene.

- **a 850,000-year record of sea-level fluctuation and margin evolution for the GAB**
  Late Quaternary glacial-interglacial cycles were reconstructed using $\delta^{18}O$ variations in planktonic foraminifera and supported by bulk and fine-fraction $\delta^{18}O$ variations. Correlation of the GAB data to the tuned record of core MD900963 identified the last 21 glacial-interglacial cycles.

- **the onset of Leeuwin Current interglacial influence on the GAB during MIS 5.5**
  Over the last 250 ka (MIS 1-6), bryozoan mound growth has been prolific during times when nutrient-rich glacial conditions prevailed, but absent during warm Leeuwin Current-influenced interglacials. The less pronounced mid-Pleistocene glacial-interglacial fluctuations (MIS 7 to 21) are explained by a generally northerly position of the Subtropical Convergence Zone, which also occurs during interglacials, preventing Leeuwin Current flow into the GAB region.

- **the impact of climate change and sea-level fluctuations on the cool-water carbonate sedimentation**
  Tropical carbonate platforms, e.g. Bahamas, are large carbonate producers during interglacials when the platform is flooded, but become exposed during glacial sea-level lowstands and are eroded. In contrast, cool-water carbonates deposited on the upper slope are continuous recorders of paleoceanographic and paleoclimatic change, since sea-level rise and fall simply shifts the centre of sediment production relative to the shoreline on the slightly inclined carbonate ramp. In particular, they are ideally suited to study sea-level rise and transgression as presented in the study of the last glacial cycle.

- **the applicability of continental margin sediments to study rapid climate change**

  High-sedimentation rates and a well-preserved carbonate assemblage, e.g. foraminifera, are the prerequisite for the development of a high-resolution chronology and proxy records needed to assess paleoclimatic changes occurring on the order of decadal to centennial time scales. Continental margins – regions of high primary production and accumulation rates are, thus, ideally suited for the study of paleo-change.


## 9.2 Outlook

The role of science is, in the end, to ask more questions than answers can be achieved. Below are my comments on questions that remain unanswered and suggestions for potential future work.

- **Temperature record of Termination I**

  Reversals shown in the $\delta^{18}O$ record across the last deglaciation most likely represent a combination of a temperature and hydrographic signal. The question remains, how much of the signal is due to a change in SST? Mg/Ca paleothermometry on planktonic foraminifera would be an ideal method to assess the temperature contribution to the overall signal.

  In Chapter 4, oceanic circulation is proposed to carry the YDC cooling signal across the globe. The feasibility of this hypothesis, i.e. changes in latent heat and current transport needed to propagate Northern Hemisphere cooling into the mid-latitudes of the Southern Ocean, could be assessed with the help of numerical ocean circulation models.

- **Origin and transport of bulk sedimentary iron**

  Relative bulk sedimentary iron abundances of Site 127 sediments are interpreted herein as dust originating from the Australian continental interior and entrained by winds and deposited into the GAB region with precipitation. Although this represents the current favourite working hypothesis, iron washed into the oceans by rivers, e.g. the Murray River, and further transported by currents cannot be ruled out. Alternatively, the observed iron distribution is merely effecting iron reworking due to sea-level rise with transgression over the formerly exposed shelf. To distinguish between these two mechanisms an identification of the Fe-phase carrying the signal would be important. Furthermore, grain-size analysis and distribution in the non-carbonate fraction offers a potential way of discriminating between current- or aeolian-transported iron.

- **Source of high-Mg-calcite**

  Mid-Pleistocene glacial-interglacial cycles are characterized by the distinct interfingering behaviour of high and low-Mg calcite with interglacials being dominated by high-Mg-calcite, which is absent during glacials. Aragonite, however, is present throughout glacial-interglacial cycles thus ruling out the disappearance of high-Mg-calcite due to dissolution. Bryozoan

mounds and the associated benthic shelf-assemblage are identified as the dominant high-Mg-calcite producer. This, however, has to be verified in detail, and sediment-fraction specific XRD analysis would be the appropriate method to determine the source of the high-Mg-calcite.

- **Detailed sedimentary analysis**

  Chapter 8 discusses the sensitive margin response to sea-level fluctuations based on variations in the carbonate mineralogy, grain size, and NGR measurements. Sediment micro-photographs illustrate the profound sedimentary change and effect of sea-level high- versus low-stand. Additional sedimentary studies, especially within the different size-fractions of sand, silt and clay, would provide data to answer the question if relative size-fraction changes are caused by sea-level rise and fall. It would further provide information on the hydrodynamics of the environment, e.g. are high sand-fraction percentages the result of current winnowing of the fine-fraction?

- **Site 1127 representative for GAB setting and southern mid-latitude?**

  This thesis focused on Site 1127, located on the upper slope, on the eastern transect. Site 1130, located in the same water depth on the western transect, although the sedimentary succession is not as expanded as Site 1127, would be an ideal site to validate results from Site 1127. A comparison would show if Site 1127 results are representative for the GAB region, and differences in the results would provide information on the spatial and temporal variability of the GAB margin.

  The Southern Ocean has been the focus of several expeditions in the last few years. In particular, results from cores recovered from the Australian-Antarctic Discordance (Leg 187), the Tasmanian Gateway (Leg 189) and the Southwest Pacific Gateway (Leg 181), are ideally suited for a comparison to the Site 1127 record, because of their proximity and temperate-water nature. In a comparison, the paleoceanography interpreted from Site 1127 results could be tested on a regional scale, and differences would improve the understanding of the regional paleoceanographic variability.

The southern mid-latitudes link the tropics and high-latitude Southern Ocean and, thus, are sensitive to changes triggered in either tropics or polar-regions. Records from the Cape Basin, continental margin off Argentine, and Tasman shelf, yield exiting new results with respect to southern mid-latitude change during the last glacial cycle. A future comparison, across these regions, and importantly including terrestrial data, would, for the first time, provide an integrated overview. Are the southern mid-latitudes mostly influenced by the Antarctic Circum Polar current connecting all of the Southern Ocean, or are they dominated by the Atlantic, Indian, and Pacific oceans to the north, and, further, has this influence changed over time?

## APPENDIX

**A1:** Carbon and oxygen stable isotope data from planktonic and benthic foraminfera

**A2:** Nitrogen isotopes, Nitrogen percentages, Corg percentages and C/N ratios of bulk sediment

**A3:** Coulometric analysis of bulk sediment

**A4:** XRF analysis on surface of core archive half

## A1: Carbon and oxygen stable isotope data from planktonic and benthic foraminfera

| Cor | T | Sct | Top | Bot | Depth | *G. ruber* | | *G. bulloides* | | *F. wullerstorfi* | | *Cibicidoides* spp | | *Uvigerina* | |
|---|---|---|---|---|---|---|---|---|---|---|---|---|---|---|---|
| | | | cm | cm | mbsf | $\delta^{13}$C ‰ | $\delta^{18}$O ‰ | $\delta^{13}$C ‰ | $\delta^{18}$O ‰ | $\delta^{13}$C ‰ | $\delta^{18}$O ‰ | $\delta^{13}$C ‰ | $\delta^{18}$O ‰ | $\delta^{13}$C ‰ | $\delta^{18}$O ‰ |
| 1 | H | 1 | 0 | 4 | 0 | 0.93 | -0.56 | | | | | | | | |
| 1 | H | 1 | 2 | 6 | 0.02 | 0.44 | -0.15 | -0.72 | 0.26 | 1.52 | 1.26 | 1.26 | 1.14 | | |
| 1 | H | 1 | 5 | 9 | 0.05 | 1.03 | -0.29 | | | 1.88 | 1.31 | 1.17 | 1.27 | | |
| 1 | H | 1 | 10 | 14 | 0.1 | 0.95 | -0.20 | | | | | | | | |
| 1 | H | 1 | 15 | 19 | 0.15 | 0.88 | -0.36 | | | 1.77 | 1.27 | | | | |
| 1 | H | 1 | 20 | 24 | 0.2 | 0.94 | -0.17 | | | | | | | | |
| 1 | H | 1 | 25 | 30 | 0.25 | 0.79 | -0.36 | -0.16 | 0.01 | 1.62 | 1.26 | | | | |
| 1 | H | 1 | 30 | 34 | 0.3 | 0.88 | -0.55 | | | 1.78 | 1.29 | | | | |
| 1 | H | 1 | 35 | 39 | 0.35 | 0.82 | -0.36 | | | | | | | | |
| 1 | H | 1 | 40 | 44 | 0.4 | 0.87 | -0.37 | | | 1.72 | 1.19 | 1.05 | 1.33 | | |
| 1 | H | 1 | 45 | 49 | 0.45 | 0.79 | -0.27 | | | | | | | | |
| 1 | H | 1 | 50 | 53 | 0.5 | 0.85 | -0.24 | -0.02 | 0.07 | 1.52 | 1.11 | 1.54 | 1.02 | | |
| 1 | H | 1 | 55 | 60 | 0.55 | 0.95 | -0.51 | | | | | | | | |
| 1 | H | 1 | 55 | 59 | 0.55 | 0.93 | -0.45 | | | 1.78 | 1.16 | | | | |
| 1 | H | 1 | 60 | 64 | 0.6 | 0.83 | -0.44 | | | 1.80 | 1.18 | | | | |
| 1 | H | 1 | 65 | 69 | 0.65 | 0.81 | -0.28 | | | | | | | | |
| 1 | H | 1 | 70 | 74 | 0.7 | 0.73 | -0.40 | | | 1.80 | 1.19 | | | | |
| 1 | H | 1 | 75 | 79 | 0.75 | 0.99 | -0.44 | | | | | | | | |
| 1 | H | 1 | 78 | 80 | 0.78 | 1.16 | -0.32 | 1.45 | 0.06 | 1.86 | 1.12 | 1.24 | 0.98 | | |
| 1 | H | 1 | 80 | 84 | 0.8 | 0.98 | -0.46 | | | 1.92 | 1.12 | | | | |
| 1 | H | 1 | 85 | 89 | 0.85 | 1.00 | -0.21 | | | | | | | | |
| 1 | H | 1 | 90 | 94 | 0.9 | 0.99 | -0.46 | | | 1.91 | 1.24 | | | | |
| 1 | H | 1 | 95 | 99 | 0.95 | 0.89 | -0.26 | | | | | | | | |
| 1 | H | 1 | 100 | 104 | 1 | 0.94 | -0.61 | | | 1.98 | 1.17 | | | | |
| 1 | H | 1 | 102 | 107 | 1.02 | 0.93 | -0.21 | 0.60 | 0.21 | 1.53 | 1.15 | 1.45 | 1.06 | | |
| 1 | H | 1 | 105 | 109 | 1.05 | 0.90 | -0.29 | | | 1.87 | 1.15 | | | | |
| 1 | H | 1 | 110 | 114 | 1.1 | 0.81 | -0.29 | | | | | | | | |
| 1 | H | 1 | 115 | 119 | 1.15 | 0.99 | -0.34 | | | 1.80 | 1.18 | | | | |
| 1 | H | 1 | 120 | 124 | 1.2 | 1.05 | -0.22 | | | | | | | | |
| 1 | H | 1 | 125 | 130 | 1.25 | 0.97 | -0.53 | -0.60 | 0.14 | 1.95 | 1.16 | 1.73 | 1.15 | | |
| 1 | H | 1 | 130 | 134 | 1.3 | 0.96 | -0.29 | | | 1.87 | 1.17 | | | | |
| 1 | H | 1 | 135 | 139 | 1.35 | 0.91 | -0.35 | | | | | | | | |
| 1 | H | 1 | 140 | 144 | 1.4 | 0.91 | -0.21 | | | | | | | | |
| 1 | H | 2 | 0 | 4 | 1.5 | 1.04 | -0.25 | | | 1.90 | 1.17 | | | | |
| 1 | H | 2 | 2 | 7 | 1.52 | 1.09 | -0.44 | -0.56 | 0.04 | 1.79 | 1.03 | 1.47 | 1.09 | | |
| 1 | H | 2 | 5 | 9 | 1.55 | 0.91 | -0.29 | | | 1.87 | 1.23 | | | | |
| 1 | H | 2 | 10 | 14 | 1.6 | 0.99 | -0.30 | | | | | | | | |
| 1 | H | 2 | 15 | 19 | 1.65 | 0.87 | -0.34 | -0.61 | 0.28 | 1.89 | 1.18 | | | | |
| 1 | H | 2 | 20 | 24 | 1.7 | 1.18 | -0.36 | | | | | | | | |
| 1 | H | 2 | 25 | 30 | 1.75 | 0.80 | -0.27 | 0.35 | | 1.63 | 1.21 | 1.28 | 1.33 | | |
| 1 | H | 2 | 30 | 34 | 1.8 | 0.95 | -0.33 | | | 1.91 | 1.21 | | | | |

| Cor | T | Sct | Top | Bot | Depth | G. ruber | | G. bulloides | | F. wullerstorfi | | Cibicidoides spp | | Uvigerina | |
|---|---|---|---|---|---|---|---|---|---|---|---|---|---|---|---|
| | | | cm | cm | mbsf | $\delta^{13}$C ‰ | $\delta^{18}$O ‰ | $\delta^{13}$C ‰ | $\delta^{18}$O ‰ | $\delta^{13}$C ‰ | $\delta^{18}$O ‰ | $\delta^{13}$C ‰ | $\delta^{18}$O ‰ | $\delta^{13}$C ‰ | $\delta^{18}$O ‰ |
| 1 | H | 2 | 35 | 39 | 1.85 | 0.84 | -0.25 | | | 1.93 | 1.21 | | | | |
| 1 | H | 2 | 40 | 44 | 1.9 | 0.91 | -0.30 | | | 1.82 | 1.29 | 1.38 | 0.96 | | |
| 1 | H | 2 | 45 | 49 | 1.95 | 0.72 | -0.26 | | | 1.92 | 1.17 | | | | |
| 1 | H | 2 | 50 | 55 | 2 | 0.75 | -0.44 | -0.40 | 0.14 | 1.67 | 1.14 | 1.71 | 1.22 | 1.19 | 0.78 |
| 1 | H | 2 | 55 | 59 | 2.05 | 0.78 | -0.28 | | | 1.95 | 1.23 | | | | |
| 1 | H | 2 | 60 | 64 | 2.1 | 1.02 | -0.41 | | | 1.82 | 1.29 | | | | |
| 1 | H | 2 | 65 | 70 | 2.15 | 0.83 | -0.04 | -0.52 | 0.22 | 1.48 | 1.38 | | | | |
| 1 | H | 2 | 70 | 74 | 2.2 | 1.10 | -0.34 | | | 1.98 | 1.17 | | | | |
| 1 | H | 2 | 72 | 75 | 2.22 | 0.97 | -0.22 | -0.57 | 0.17 | 1.90 | 1.18 | 1.48 | 1.11 | | |
| 1 | H | 2 | 75 | 79 | 2.25 | 0.92 | -0.42 | | | 1.84 | 1.29 | | | | |
| 1 | H | 2 | 80 | 84 | 2.3 | 1.17 | -0.19 | | | 1.77 | 1.33 | | | | |
| 1 | H | 2 | 85 | 89 | 2.35 | 0.96 | -0.21 | | | 1.84 | 1.21 | | | | |
| 1 | H | 2 | 90 | 94 | 2.4 | 0.80 | -0.23 | | | 1.75 | 0.97 | | | | |
| 1 | H | 2 | 95 | 99 | 2.45 | 0.91 | -0.19 | | | 1.77 | 1.14 | | | | |
| 1 | H | 2 | 101 | 106 | 2.51 | 0.89 | -0.32 | -0.42 | 0.27 | 1.61 | 1.24 | 0.73 | 1.16 | | |
| 1 | H | 2 | 105 | 109 | 2.55 | 1.03 | -0.23 | | | | | | | | |
| 1 | H | 2 | 110 | 114 | 2.6 | 0.95 | -0.08 | | | 1.77 | 1.29 | | | | |
| 1 | H | 2 | 115 | 119 | 2.65 | 0.96 | -0.12 | | | | | | | | |
| 1 | H | 2 | 120 | 124 | 2.7 | 1.10 | 0.10 | | | 1.77 | 1.43 | | | | |
| 1 | H | 2 | 125 | 130 | 2.75 | 0.84 | -0.23 | -0.50 | 0.18 | 1.73 | 1.28 | 1.77 | 0.83 | | |
| 1 | H | 2 | 130 | 134 | 2.8 | 1.01 | -0.23 | | | | | | | | |
| 1 | H | 2 | 135 | 139 | 2.85 | 0.88 | -0.09 | | | 1.70 | 1.24 | | | | |
| 1 | H | 2 | 140 | 144 | 2.9 | 1.22 | -0.10 | | | 1.77 | 1.41 | | | | |
| 1 | H | 2 | 145 | 150 | 2.95 | 0.95 | -0.23 | -0.72 | 0.13 | 1.50 | 1.08 | 0.92 | 1.22 | | |
| 1 | H | 3 | 0 | 4 | 3 | 0.87 | -0.04 | | | 1.61 | 1.33 | | | | |
| 1 | H | 3 | 2 | 7 | 3.02 | 1.18 | -0.02 | -0.54 | 0.17 | 1.39 | 0.78 | | | | |
| 1 | H | 3 | 5 | 9 | 3.05 | 0.92 | -0.07 | | | | | | | | |
| 1 | H | 3 | 10 | 14 | 3.1 | 1.17 | -0.12 | | | 1.79 | 1.14 | | | | |
| 1 | H | 3 | 15 | 19 | 3.15 | 0.97 | -0.14 | | | 1.90 | 1.17 | | | | |
| 1 | H | 3 | 20 | 24 | 3.2 | 0.99 | 0.02 | | | 1.82 | 1.12 | | | | |
| 1 | H | 3 | 25 | 30 | 3.25 | 1.06 | -0.07 | -0.85 | 0.20 | 1.55 | 1.23 | | | | |
| 1 | H | 3 | 30 | 34 | 3.3 | 0.98 | -0.16 | | | | | | | | |
| 1 | H | 3 | 35 | 39 | 3.35 | 0.87 | -0.14 | | | | | | | | |
| 1 | H | 3 | 40 | 44 | 3.4 | 1.00 | -0.18 | | | 1.59 | 1.08 | | | | |
| 1 | H | 3 | 46 | 49 | 3.46 | 0.84 | 0.09 | -0.88 | 0.08 | | | 1.24 | 1.66 | | |
| 1 | H | 3 | 50 | 54 | 3.5 | 0.88 | -0.30 | | | 1.59 | 1.08 | | | | |
| 1 | H | 3 | 55 | 60 | 3.55 | 0.97 | -0.16 | | | | | | | | |
| 1 | H | 3 | 60 | 64 | 3.6 | 0.56 | -0.17 | | | 1.40 | 1.12 | | | | |
| 1 | H | 3 | 65 | 69 | 3.65 | 1.12 | 0.08 | | | | | | | | |
| 1 | H | 3 | 69 | 73 | 3.69 | 0.89 | -0.23 | | | 1.49 | 0.69 | | | | |
| 1 | H | 3 | 72 | 75 | 3.72 | 1.11 | 0.09 | 0.06 | 0.28 | 2.04 | 1.19 | | | | |
| 1 | H | 3 | 75 | 79 | 3.75 | 0.95 | -0.07 | | | 1.55 | 1.19 | | | | |
| 1 | H | 3 | 80 | 84 | 3.8 | 1.15 | -0.24 | | | | | | | | |
| 1 | H | 3 | 85 | 89 | 3.85 | 0.93 | -0.15 | | | 1.63 | 1.37 | | | | |
| 1 | H | 3 | 90 | 94 | 3.9 | 1.12 | -0.22 | | | 1.63 | 1.28 | | | | |

| Cor | T | Sct | Top cm | Bot cm | Depth mbsf | *G. ruber* δ¹³C ‰ | *G. ruber* δ¹⁸O ‰ | *G. bulloides* δ¹³C ‰ | *G. bulloides* δ¹⁸O ‰ | *F. wullerstorfi* δ¹³C ‰ | *F. wullerstorfi* δ¹⁸O ‰ | *Cibicidoides* spp δ¹³C ‰ | *Cibicidoides* spp δ¹⁸O ‰ | *Uvigerina* δ¹³C ‰ | *Uvigerina* δ¹⁸O ‰ |
|---|---|---|---|---|---|---|---|---|---|---|---|---|---|---|---|
| 1 | H | 3 | 96 | 100 | 3.96 | 0.74 | -0.05 | -0.40 | 0.21 | | | 0.70 | 1.09 | | |
| 1 | H | 3 | 100 | 104 | 4 | 0.77 | -0.03 | | | | | | | | |
| 1 | H | 3 | 105 | 109 | 4.05 | 0.91 | -0.13 | | | | | | | | |
| 1 | H | 3 | 110 | 114 | 4.1 | 1.10 | -0.01 | | | 1.81 | 1.44 | | | | |
| 1 | H | 3 | 115 | 119 | 4.15 | 1.03 | -0.13 | | | 1.44 | 1.27 | | | | |
| 1 | H | 3 | 120 | 124 | 4.2 | 0.98 | -0.22 | | | | | | | | |
| 1 | H | 3 | 125 | 130 | 4.25 | 0.51 | -0.20 | -0.94 | 0.28 | 1.16 | 1.19 | | | | |
| 1 | H | 3 | 130 | 134 | 4.3 | 0.99 | -0.08 | | | | | | | | |
| 1 | H | 3 | 135 | 139 | 4.35 | 0.88 | -0.01 | | | | | | | | |
| 1 | H | 3 | 141 | 146 | 4.41 | 1.05 | 0.19 | -0.83 | 0.37 | 1.52 | 1.12 | 0.92 | 1.36 | | |
| 1 | H | 4 | 0 | 4 | 4.5 | 1.01 | 0.05 | | | 1.48 | 1.42 | | | | |
| 1 | H | 4 | 2 | 7 | 4.52 | 1.17 | -0.05 | -0.94 | 0.33 | 1.43 | 1.27 | | | | |
| 1 | H | 4 | 5 | 9 | 4.55 | 1.08 | -0.15 | | | | | | | | |
| 1 | H | 4 | 10 | 14 | 4.6 | 1.07 | 0.00 | | | | | | | | |
| 1 | H | 4 | 15 | 19 | 4.65 | 1.31 | -0.01 | | | | | | | | |
| 1 | H | 4 | 20 | 24 | 4.7 | 1.30 | -0.01 | | | 1.68 | 1.33 | | | | |
| 1 | H | 4 | 25 | 30 | 4.75 | 1.22 | 0.03 | -0.95 | 0.41 | 1.30 | 1.38 | | | | |
| 1 | H | 4 | 30 | 34 | 4.8 | 1.17 | 0.06 | | | | | | | | |
| 1 | H | 4 | 35 | 39 | 4.85 | 1.26 | -0.02 | | | 1.25 | 1.37 | | | | |
| 1 | H | 4 | 40 | 44 | 4.9 | 1.20 | -0.08 | | | | | | | | |
| 1 | H | 4 | 45 | 49 | 4.95 | 1.18 | -0.24 | | | | | | | | |
| 1 | H | 4 | 50 | 55 | 5 | 0.98 | -0.08 | | | | | | | | |
| 1 | H | 4 | 50 | 55 | 5 | 0.98 | -0.08 | -1.10 | | | | | | | |
| 1 | H | 4 | 55 | 59 | 5.05 | 1.20 | -0.02 | | | | | | | | |
| 1 | H | 4 | 60 | 64 | 5.1 | 0.99 | -0.07 | | | 1.62 | 1.19 | | | | |
| 1 | H | 4 | 65 | 70 | 5.15 | 0.95 | -0.04 | -0.45 | 0.58 | | | | | | |
| 1 | H | 4 | 65 | 70 | 5.15 | 0.95 | -0.04 | -1.05 | 0.24 | | | | | | |
| 1 | H | 4 | 70 | 74 | 5.2 | 1.27 | -0.17 | | | | | | | | |
| 1 | H | 4 | 75 | 79 | 5.25 | 0.94 | 0.01 | | | | | | | | |
| 1 | H | 4 | 78 | 83 | 5.28 | 0.67 | -0.18 | | | 1.40 | 1.26 | | | | |
| 1 | H | 4 | 78 | 83 | 5.28 | 0.67 | -0.18 | -0.80 | 0.16 | 1.40 | 1.26 | | | | |
| 1 | H | 4 | 85 | 89 | 5.35 | 1.34 | 0.05 | | | | | | | | |
| 1 | H | 4 | 90 | 94 | 5.4 | 1.12 | 0.01 | | | 0.84 | 0.61 | | | | |
| 1 | H | 4 | 95 | 99 | 5.45 | 1.14 | -0.01 | | | | | | | | |
| 1 | H | 4 | 100 | 104 | 5.5 | 0.74 | -0.11 | | | | | | | | |
| 1 | H | 4 | 102 | 107 | 5.52 | 1.11 | 0.06 | | | | | | | | |
| 1 | H | 4 | 102 | 107 | 5.52 | 1.11 | 0.06 | -0.59 | 0.53 | | | | | | |
| 1 | H | CC | 0 | 4 | 5.57 | 1.01 | -0.09 | | | | | | | | |
| 1 | H | CC | 5 | 9 | 5.62 | 1.02 | 0.17 | | | | | | | | |
| 1 | H | CC | 10 | 14 | 5.67 | 1.14 | -0.08 | | | | | | | | |
| 1 | H | CC | 15 | 19 | 5.72 | 1.24 | -0.03 | | | | | | | | |
| 1 | H | CC | 20 | 24 | 5.77 | 0.76 | -0.16 | | | | | | | | |
| 2 | H | 1 | 0 | 4 | 5.9 | 1.01 | -0.12 | | | | | | | | |
| 2 | H | 1 | 2 | 6 | 5.92 | 0.93 | -0.04 | | | | | | | | |
| 2 | H | 1 | 2 | 6 | 5.92 | 0.93 | -0.04 | -0.58 | 0.62 | | | | | | |

| Cor | T | Sct | Top cm | Bot cm | Depth mbsf | *G. ruber* $\delta^{13}$C ‰ | $\delta^{18}$O ‰ | *G. bulloides* $\delta^{13}$C ‰ | $\delta^{18}$O ‰ | *F. wullerstorfi* $\delta^{13}$C ‰ | $\delta^{18}$O ‰ | *Cibicidoides* spp $\delta^{13}$C ‰ | $\delta^{18}$O ‰ | *Uvigerina* $\delta^{13}$C ‰ | $\delta^{18}$O ‰ |
|---|---|---|---|---|---|---|---|---|---|---|---|---|---|---|---|
| 2 | H | 1 | 5 | 9 | 5.95 | 1.04 | -0.15 | | | | | | | | |
| 2 | H | 1 | 10 | 14 | 6 | 1.16 | 0.04 | | | | | | | | |
| 2 | H | 1 | 15 | 19 | 6.05 | 1.04 | 0.07 | | | | | | | | |
| 2 | H | 1 | 20 | 24 | 6.1 | 1.08 | -0.05 | | | | | | | | |
| 2 | H | 1 | 24 | 29 | 6.14 | 0.99 | 0.07 | | | | | | | | |
| 2 | H | 1 | 24 | 29 | 6.14 | 0.99 | 0.07 | -0.52 | 0.68 | | | | | | |
| 2 | H | 1 | 30 | 34 | 6.2 | 0.98 | -0.33 | | | | | | | | |
| 2 | H | 1 | 35 | 39 | 6.25 | 0.94 | -0.06 | | | | | | | | |
| 2 | H | 1 | 40 | 44 | 6.3 | 1.31 | 0.11 | | | 1.74 | 1.39 | | | | |
| 2 | H | 1 | 45 | 48 | 6.35 | 1.32 | 0.03 | -2.14 | 0.14 | | | | | | |
| 2 | H | 1 | 45 | 48 | 6.35 | 1.32 | 0.03 | -2.14 | 0.14 | | | | | | |
| 2 | H | 1 | 50 | 54 | 6.4 | 1.21 | -0.18 | | | | | | | | |
| 2 | H | 1 | 53 | 58 | 6.43 | 1.05 | 0.11 | | | | | | | | |
| 2 | H | 1 | 53 | 58 | 6.43 | 1.05 | 0.11 | | | | | | | | |
| 2 | H | 1 | 59 | 64 | 6.49 | 1.01 | -0.04 | -0.95 | 0.12 | | | | | | |
| 2 | H | 1 | 60 | 64 | 6.5 | 0.93 | 0.12 | | | | | | | | |
| 2 | H | 1 | 64 | 69 | 6.54 | 0.89 | -0.06 | -0.91 | | | | | | | |
| 2 | H | 1 | 69 | 75 | 6.59 | 1.35 | -0.27 | -1.60 | -0.05 | 1.39 | 1.34 | | | | |
| 2 | H | 1 | 69 | 75 | 6.59 | 0.67 | -0.14 | -1.60 | -0.05 | 1.39 | 1.34 | | | | |
| 2 | H | 1 | 75 | 79 | 6.65 | 1.05 | 0.13 | | | | | | | | |
| 2 | H | 1 | 80 | 84 | 6.7 | 1.24 | -0.04 | | | | | | | | |
| 2 | H | 1 | 85 | 89 | 6.75 | 1.16 | 0.02 | | | | | | | | |
| 2 | H | 1 | 90 | 94 | 6.8 | 1.05 | -0.18 | | | | | | | | |
| 2 | H | 1 | 95 | 99 | 6.85 | 1.11 | 0.14 | | | 1.24 | 1.35 | | | | |
| 2 | H | 1 | 100 | 103 | 6.9 | 1.11 | 0.16 | | | | | | | | |
| 2 | H | 1 | 100 | 102 | 6.9 | 1.11 | 0.16 | -0.82 | 0.96 | 1.45 | 1.32 | | | 1.11 | 2.65 |
| 2 | H | 1 | 105 | 109 | 6.95 | 1.37 | 0.11 | | | | | | | | |
| 2 | H | 1 | 110 | 114 | 7 | 1.03 | -0.20 | | | | | | | | |
| 2 | H | 1 | 115 | 119 | 7.05 | 0.13 | -0.31 | | | | | | | | |
| 2 | H | 1 | 120 | 124 | 7.1 | 0.96 | -0.20 | | | | | | | | |
| 2 | H | 1 | 125 | 130 | 7.15 | 1.23 | -0.02 | | | 1.12 | 0.85 | | | | |
| 2 | H | 1 | 125 | 130 | 7.15 | 1.23 | -0.02 | -0.72 | 0.41 | 1.12 | 0.85 | | | | |
| 2 | H | 1 | 130 | 134 | 7.2 | 1.15 | 0.16 | | | 1.43 | 1.35 | | | | |
| 2 | H | 1 | 135 | 139 | 7.25 | 1.03 | 0.01 | | | | | | | | |
| 2 | H | 1 | 140 | 144 | 7.3 | 1.27 | -0.16 | | | | | | | | |
| 2 | H | 1 | 145 | 150 | 7.35 | 1.28 | -0.02 | | | 1.22 | 1.39 | | | | |
| 2 | H | 1 | 145 | 150 | 7.35 | 1.28 | -0.02 | -0.36 | 0.57 | 1.22 | 1.39 | | | | |
| 2 | H | 2 | 0 | 2 | 7.4 | 1.22 | -0.28 | | | | | | | | |
| 2 | H | 2 | 2 | 7 | 7.42 | 1.22 | 0.16 | -0.21 | 0.82 | 1.63 | 1.71 | | | | |
| 2 | H | 2 | 2 | 4 | 7.42 | 1.22 | 0.16 | -0.21 | 0.82 | 1.63 | 1.71 | | | | |
| 2 | H | 2 | 5 | 9 | 7.45 | 1.08 | 0.04 | | | | | | | | |
| 2 | H | 2 | 10 | 14 | 7.5 | 1.14 | -0.07 | | | | | | | | |
| 2 | H | 2 | 15 | 19 | 7.55 | 1.05 | -0.06 | | | | | | | | |
| 2 | H | 2 | 20 | 24 | 7.6 | 1.13 | 0.07 | | | | | | | | |
| 2 | H | 2 | 25 | 30 | 7.65 | 0.48 | 0.11 | -0.90 | 0.55 | | | 0.80 | 0.95 | | |

| Cor | T | Sct | Top cm | Bot cm | Depth mbsf | *G. ruber* $\delta^{13}$C ‰ | $\delta^{18}$O ‰ | *G. bulloides* $\delta^{13}$C ‰ | $\delta^{18}$O ‰ | *F. wullerstorfi* $\delta^{13}$C ‰ | $\delta^{18}$O ‰ | *Cibicidoides* spp $\delta^{13}$C ‰ | $\delta^{18}$O ‰ | *Uvigerina* $\delta^{13}$C ‰ | $\delta^{18}$O ‰ |
|---|---|---|---|---|---|---|---|---|---|---|---|---|---|---|---|
| 2 | H | 2 | 30 | 34 | 7.7 | 0.71 | 0.05 | | | | | | | | |
| 2 | H | 2 | 35 | 39 | 7.75 | 1.18 | -0.07 | -1.19 | 0.37 | | | | | | |
| 2 | H | 2 | 40 | 44 | 7.8 | 0.85 | 0.29 | | | | | | | | |
| 2 | H | 2 | 45 | 49 | 7.85 | 0.94 | 0.16 | | | 1.52 | 1.68 | | | | |
| 2 | H | 2 | 50 | 55 | 7.9 | 1.13 | 0.14 | -0.14 | 0.78 | 0.34 | 1.08 | | | | |
| 2 | H | 2 | 50 | 55 | 7.9 | 1.13 | 0.14 | -0.84 | 0.42 | 0.34 | 1.08 | | | | |
| 2 | H | 2 | 55 | 59 | 7.95 | 1.41 | 0.57 | -0.75 | 0.15 | 0.50 | 1.47 | | | | |
| 2 | H | 2 | 60 | 64 | 8 | 0.87 | 0.38 | | | | | | | | |
| 2 | H | 2 | 65 | 70 | 8.05 | 1.16 | 0.64 | 0.00 | 1.28 | 1.92 | 2.17 | 1.78 | 1.99 | 1.02 | 2.32 |
| 2 | H | 2 | 65 | 70 | 8.05 | 1.16 | 0.64 | 0.00 | 1.28 | 1.92 | 2.17 | 1.78 | 1.99 | 1.02 | 2.32 |
| 2 | H | 2 | 70 | 75 | 8.1 | 0.53 | 0.56 | -0.09 | 1.00 | 2.81 | 2.05 | 1.57 | 1.79 | | |
| 2 | H | 2 | 70 | 74 | 8.1 | 1.04 | 0.54 | -0.09 | 1.00 | 2.81 | 2.05 | 1.57 | 1.79 | | |
| 2 | H | 2 | 75 | 79 | 8.15 | 1.04 | 0.67 | -0.80 | 1.04 | 0.73 | 1.03 | 1.18 | 1.45 | | |
| 2 | H | 2 | 80 | 84 | 8.2 | 0.93 | 0.55 | 0.07 | 1.20 | 1.28 | 1.06 | 1.01 | 1.60 | | |
| 2 | H | 2 | 85 | 89 | 8.25 | 0.99 | 0.66 | -0.23 | 1.15 | | | | | 0.50 | 2.09 |
| 2 | H | 2 | 90 | 94 | 8.3 | 1.01 | 0.64 | -0.41 | 1.05 | | | 0.77 | 1.31 | | |
| 2 | H | 2 | 95 | 99 | 8.35 | 1.18 | 0.57 | 0.03 | 1.03 | | | 0.85 | 1.12 | | |
| 2 | H | 2 | 100 | 104 | 8.4 | 1.07 | 0.21 | | | | | | | | |
| 2 | H | 2 | 100 | 104 | 8.4 | 1.19 | 0.18 | | | | | | | | |
| 2 | H | 2 | 101 | 107 | 8.41 | 1.03 | 0.11 | -0.59 | -0.04 | | | 1.25 | 1.85 | | |
| 2 | H | 2 | 101 | 107 | 8.41 | 1.03 | 0.11 | -0.59 | -0.04 | | | 1.25 | 1.85 | | |
| 2 | H | 2 | 103 | 106 | 8.43 | 0.79 | 0.29 | -0.80 | 0.49 | | | | | | |
| 2 | H | 2 | 105 | 109 | 8.45 | 0.92 | 0.36 | | | | | 0.81 | 1.52 | 0.55 | 2.48 |
| 2 | H | 2 | 106 | 108 | 8.46 | 1.07 | 0.41 | | | | | | | | |
| 2 | H | 2 | 110 | 114 | 8.5 | 0.89 | 0.56 | -0.29 | 1.11 | 0.70 | 1.56 | | | 0.82 | 2.16 |
| 2 | H | 2 | 115 | 119 | 8.55 | 0.84 | 0.73 | -0.90 | 0.98 | | | | | | |
| 2 | H | 2 | 120 | 124 | 8.6 | 0.93 | 0.58 | 0.36 | 1.22 | | | 1.86 | 1.98 | | |
| 2 | H | 2 | 125 | 129 | 8.65 | 0.96 | 0.69 | | | | | | | | |
| 2 | H | 2 | 126 | 128 | 8.66 | 1.03 | 0.44 | | | | | | | | |
| 2 | H | 2 | 130 | 134 | 8.7 | 0.90 | 0.31 | -0.29 | 1.07 | 1.51 | 2.05 | | | | |
| 2 | H | 2 | 135 | 139 | 8.75 | 1.02 | 0.64 | -0.60 | 1.05 | | | | | | |
| 2 | H | 2 | 136 | 138 | 8.76 | 0.80 | 0.73 | 0.62 | | 2.24 | 2.29 | | | | |
| 2 | H | 2 | 139 | 144 | 8.79 | 1.10 | 0.84 | -0.64 | 1.33 | 1.95 | 2.80 | 0.80 | 1.86 | | |
| 2 | H | 2 | 139 | 144 | 8.79 | 1.10 | 0.84 | -0.64 | 1.33 | 1.95 | 2.80 | 0.80 | 1.86 | | |
| 2 | H | 3 | 0 | 4 | 8.9 | 0.89 | 0.81 | | | | | | | | |
| 2 | H | 3 | 2 | 7 | 8.92 | 1.22 | 0.96 | 0.30 | 1.86 | 1.17 | 2.01 | 1.53 | 2.20 | | |
| 2 | H | 3 | 2 | 7 | 8.92 | 1.22 | 0.96 | 0.30 | 1.86 | 1.17 | 2.01 | 1.53 | 2.20 | | |
| 2 | H | 3 | 5 | 9 | 8.95 | 0.91 | 0.66 | | | | | | | | |
| 2 | H | 3 | 10 | 14 | 9 | 0.97 | 0.77 | -0.32 | 1.36 | 1.79 | 2.24 | 1.12 | 2.14 | | |
| 2 | H | 3 | 15 | 19 | 9.05 | 1.04 | 0.79 | | | | | | | | |
| 2 | H | 3 | 20 | 24 | 9.1 | 0.92 | 0.66 | | | | | | | | |
| 2 | H | 3 | 25 | 30 | 9.15 | 1.15 | 0.82 | -0.18 | 2.01 | 2.16 | 2.90 | 1.09 | 2.09 | 1.15 | 2.94 |
| 2 | H | 3 | 25 | 30 | 9.15 | 1.15 | 0.82 | -0.18 | 2.01 | 2.16 | 2.90 | 1.09 | 2.09 | 1.15 | 2.94 |
| 2 | H | 3 | 30 | 34 | 9.2 | 1.05 | 0.79 | | | | | | | | |
| 2 | H | 3 | 37 | 41 | 9.27 | 1.12 | 0.73 | 0.05 | 1.26 | 2.38 | 2.71 | 1.23 | 2.25 | 0.44 | 2.70 |

| Cor | T | Sct | Top cm | Bot cm | Depth mbsf | *G. ruber* δ¹³C ‰ | δ¹⁸O ‰ | *G. bulloides* δ¹³C ‰ | δ¹⁸O ‰ | *F. wullerstorfi* δ¹³C ‰ | δ¹⁸O ‰ | *Cibicidoides* spp δ¹³C ‰ | δ¹⁸O ‰ | *Uvigerina* δ¹³C ‰ | δ¹⁸O ‰ |
|---|---|---|---|---|---|---|---|---|---|---|---|---|---|---|---|
| 2 | H | 3 | 40 | 44 | 9.3 | 1.13 | 0.80 | | | | | | | | |
| 2 | H | 3 | 42 | 44 | 9.32 | 1.18 | 0.71 | | | 1.78 | 2.38 | 1.26 | 2.05 | | |
| 2 | H | 3 | 45 | 49 | 9.35 | 1.05 | 1.22 | | | | | 0.97 | 2.00 | | |
| 2 | H | 3 | 50 | 55 | 9.4 | 1.31 | 1.26 | -0.17 | 1.71 | 1.70 | 2.70 | 0.80 | 1.99 | 0.46 | 2.77 |
| 2 | H | 3 | 50 | 55 | 9.4 | 1.31 | 1.26 | -0.17 | 1.71 | 1.70 | 2.70 | 0.80 | 1.99 | 0.46 | 2.77 |
| 2 | H | 3 | 55 | 60 | 9.45 | 1.31 | 1.24 | | | | | | | | |
| 2 | H | 3 | 55 | 60 | 9.45 | 1.31 | 1.24 | | | | | | | | |
| 2 | H | 3 | 60 | 64 | 9.5 | 1.41 | 1.46 | | | | | | | | |
| 2 | H | 3 | 65 | 69 | 9.55 | 1.23 | 1.53 | 0.48 | 1.92 | | | | | | |
| 2 | H | 3 | 70 | 75 | 9.6 | 1.20 | 1.45 | -0.44 | 1.43 | 2.08 | 2.90 | 1.48 | 2.73 | 1.02 | 2.82 |
| 2 | H | 3 | 70 | 75 | 9.6 | 1.20 | 1.45 | 0.43 | 1.64 | 2.08 | 2.90 | 1.48 | 2.73 | 1.02 | 2.82 |
| 2 | H | 3 | 75 | 79 | 9.65 | 1.27 | 1.35 | | | | | | | | |
| 2 | H | 3 | 80 | 84 | 9.7 | 1.46 | 1.52 | -0.08 | 1.86 | 2.04 | 2.50 | 1.68 | 2.62 | | |
| 2 | H | 3 | 85 | 89 | 9.75 | 1.35 | 1.39 | | | | | | | | |
| 2 | H | 3 | 90 | 94 | 9.8 | 1.36 | 1.36 | -0.21 | 1.81 | 2.24 | 3.18 | 1.53 | 2.24 | | |
| 2 | H | 3 | 95 | 99 | 9.85 | 1.46 | 1.32 | | | | | | | | |
| 2 | H | 3 | 101 | 106 | 9.91 | 1.43 | 1.20 | 1.34 | 1.70 | 2.54 | 2.88 | 2.55 | 2.89 | 2.91 | 3.26 |
| 2 | H | 3 | 110 | 114 | 10 | 1.43 | 1.32 | -0.17 | 1.63 | | | 1.44 | 2.35 | | |
| 2 | H | 3 | 122 | 128 | 10.12 | -0.07 | 1.98 | 1.49 | 1.33 | 2.01 | 2.65 | 1.30 | 2.50 | 0.55 | 3.24 |
| 2 | H | 3 | 130 | 132 | 10.2 | 1.05 | 0.66 | | | | | | | | |
| 2 | H | 3 | 132 | 136 | 10.22 | 1.28 | 1.03 | -0.08 | 1.87 | 1.87 | 2.47 | 1.67 | 2.49 | 0.54 | 2.99 |
| 2 | H | 3 | 144 | 150 | 10.34 | 1.37 | 1.37 | 0.24 | 2.25 | 2.19 | 2.37 | 1.62 | 2.39 | 0.46 | 3.02 |
| 2 | H | 4 | 2 | 7 | 10.42 | 1.06 | 1.46 | 1.75 | 2.15 | 2.25 | 2.64 | 2.39 | 2.77 | 2.67 | 3.05 |
| 2 | H | 4 | 23 | 28 | 10.63 | 1.34 | 1.32 | -0.15 | 1.44 | 1.93 | 2.44 | 1.46 | 2.30 | 0.38 | 3.07 |
| 2 | H | 4 | 50 | 55 | 10.9 | 1.46 | 1.22 | -0.07 | 1.80 | 1.98 | 2.62 | 1.50 | 2.58 | 0.46 | 2.85 |
| 2 | H | 4 | 65 | 70 | 11.05 | 1.32 | 1.19 | -0.11 | 1.37 | 1.61 | 2.27 | 1.32 | 2.35 | 0.60 | 3.07 |
| 2 | H | 4 | 77 | 82 | 11.17 | 1.42 | 1.25 | -0.13 | 1.79 | 1.97 | 2.31 | 1.09 | 1.41 | 0.75 | 2.88 |
| 2 | H | 4 | 101 | 106 | 11.41 | 0.87 | 1.48 | -0.40 | 1.53 | 1.98 | 2.31 | 1.60 | 2.26 | -0.33 | 2.90 |
| 2 | H | 4 | 110 | 114 | 11.5 | 1.51 | 1.52 | 0.13 | 1.81 | 1.86 | 2.26 | 1.47 | 2.77 | 0.34 | 2.80 |
| 2 | H | 4 | 125 | 130 | 11.65 | 1.30 | 0.59 | -0.79 | 0.91 | 1.69 | 2.10 | 1.17 | 2.29 | -0.03 | 2.75 |
| 2 | H | 4 | 137 | 142 | 11.77 | 2.06 | 2.10 | -0.19 | 1.51 | 2.08 | 1.93 | 1.81 | 3.00 | 0.79 | 3.83 |
| 2 | H | 5 | 2 | 5 | 11.92 | 1.38 | 0.85 | 0.15 | 1.99 | 1.68 | 2.08 | 0.94 | 2.26 | -0.04 | 2.88 |
| 2 | H | 5 | 25 | 30 | 12.15 | 1.50 | 0.97 | -0.26 | 1.26 | 1.73 | 2.13 | | | 0.17 | 2.96 |
| 2 | H | 5 | 51 | 56 | 12.41 | 0.80 | 0.66 | -0.95 | 0.63 | 1.67 | 2.13 | 0.76 | 2.26 | 0.27 | 2.62 |
| 2 | H | 5 | 55 | 60 | 12.45 | 1.37 | 1.18 | | | | | | | | |
| 2 | H | 5 | 70 | 76 | 12.6 | 0.87 | 1.25 | 1.13 | 1.51 | 2.07 | 2.43 | 2.11 | 2.48 | 3.01 | 3.37 |
| 2 | H | 5 | 102 | 107 | 12.92 | 1.49 | 1.55 | -0.35 | 1.81 | 1.56 | 1.74 | 2.27 | 2.38 | 0.90 | 3.35 |
| 2 | H | 5 | 125 | 130 | 13.15 | 1.38 | 1.18 | -0.53 | 1.36 | 1.89 | 2.48 | 1.45 | 2.42 | 0.79 | 2.87 |
| 2 | H | 5 | 144 | 149 | 13.34 | 0.17 | 1.76 | 1.25 | 0.78 | 1.83 | 2.21 | 1.11 | 2.20 | | |
| 2 | H | 6 | 2 | 8 | 13.42 | 1.53 | 1.22 | -0.23 | 1.85 | 1.74 | 1.97 | 1.63 | 1.38 | 0.72 | 3.66 |
| 2 | H | 6 | 25 | 30 | 13.65 | 1.25 | 0.83 | -0.04 | 1.56 | 1.53 | 2.31 | | | 0.91 | 2.65 |
| 2 | H | 6 | 51 | 56 | 13.91 | 1.03 | 1.05 | -0.17 | 1.56 | 2.10 | 2.53 | 1.39 | 2.24 | 0.67 | 3.03 |
| 2 | H | 6 | 65 | 70 | 14.05 | 0.90 | 1.27 | -0.19 | 1.42 | 1.76 | 2.67 | 1.33 | 3.07 | 0.46 | 3.04 |
| 2 | H | 6 | 75 | 81 | 14.15 | 1.36 | 0.79 | -0.20 | 1.88 | 2.10 | 2.52 | 1.56 | 2.77 | 0.75 | 3.19 |
| 2 | H | 6 | 101 | 106 | 14.41 | 1.33 | 0.95 | 0.32 | 1.51 | 2.01 | 2.52 | | | 0.81 | 2.93 |

| Cor | T | Sct | Top cm | Bot cm | Depth mbsf | *G. ruber* δ¹³C ‰ | δ¹⁸O ‰ | *G. bulloides* δ¹³C ‰ | δ¹⁸O ‰ | *F. wullerstorfi* δ¹³C ‰ | δ¹⁸O ‰ | *Cibicidoides* spp δ¹³C ‰ | δ¹⁸O ‰ | *Uvigerina* δ¹³C ‰ | δ¹⁸O ‰ |
|---|---|---|---|---|---|---|---|---|---|---|---|---|---|---|---|
| 2 | H | 6 | 125 | 130 | 14.65 | 1.39 | 1.41 | | | 2.10 | 2.98 | 1.72 | 3.08 | 1.03 | 3.54 |
| 2 | H | 6 | 145 | 150 | 14.85 | | | | | 1.78 | 2.24 | | | 0.77 | 3.09 |
| 3 | H | 1 | 3 | 8 | 15.43 | 1.34 | 1.04 | 0.19 | 1.48 | 1.74 | 1.19 | | | 0.51 | 0.85 |
| 3 | H | 1 | 55 | 60 | 15.95 | 1.01 | 1.01 | | | | | | | | |
| 3 | H | 1 | 60 | 65 | 16 | 1.31 | 0.89 | 0.17 | 1.55 | 1.82 | 2.33 | | | 0.51 | 2.81 |
| 3 | H | 1 | 90 | 94 | 16.3 | 1.03 | 0.71 | -0.88 | 0.70 | | | 0.98 | 2.70 | -0.07 | 2.75 |
| 3 | H | 1 | 110 | 115 | 16.5 | 1.36 | 0.72 | -0.97 | 0.72 | | | 1.35 | 2.09 | 0.05 | 2.61 |
| 3 | H | 1 | 130 | 134 | 16.7 | 1.29 | 0.65 | -0.92 | 0.69 | 1.58 | 1.80 | | | 0.12 | 2.55 |
| 3 | H | 2 | 3 | 8 | 16.93 | 1.36 | 0.55 | -1.13 | 0.47 | | | | | 0.02 | 2.52 |
| 3 | H | 2 | 30 | 34 | 17.2 | 1.28 | 0.65 | -0.92 | 0.73 | 0.82 | 2.09 | 1.05 | 2.00 | -0.17 | 2.88 |
| 3 | H | 2 | 57 | 63 | 17.47 | | | | | | | | | -0.17 | 2.88 |
| 3 | H | 2 | 65 | 70 | 17.55 | 1.18 | 0.89 | -0.34 | 0.98 | | | | | -0.34 | 2.73 |
| 3 | H | 2 | 85 | 89 | 17.75 | 1.14 | 0.71 | -1.11 | 0.78 | | | 0.90 | 2.27 | 0.45 | 2.72 |
| 3 | H | 2 | 110 | 115 | 18 | 1.22 | 0.15 | -1.15 | 0.56 | 1.44 | 1.67 | 1.34 | 1.60 | -0.22 | 2.84 |
| 3 | H | 3 | 3 | 8 | 18.43 | 1.42 | 0.54 | -0.32 | 0.96 | | | 1.48 | 1.98 | 0.02 | 2.62 |
| 3 | H | 4 | 65 | 70 | 20.55 | 1.05 | 0.43 | -0.74 | 0.68 | 1.27 | 2.06 | 1.06 | 1.51 | -0.37 | 2.72 |
| 3 | H | 4 | 65 | 70 | 20.55 | 1.05 | 0.43 | -0.74 | 0.68 | 1.27 | 2.06 | 1.06 | 1.51 | -0.37 | 2.72 |
| 3 | H | 5 | 3 | 8 | 21.43 | 0.94 | 0.36 | | | 1.13 | 1.94 | | | | |
| 3 | H | 5 | 55 | 60 | 21.95 | 1.01 | 0.44 | | | | | | | | |
| 4 | H | 1 | 55 | 60 | 25.45 | 1.05 | 0.36 | | | | | | | | |
| 4 | H | 3 | 55 | 60 | 27.38 | 0.66 | 0.13 | | | | | | | | |
| 4 | H | 4 | 65 | 70 | 28.98 | 0.78 | 0.32 | -0.60 | 0.46 | 0.96 | 1.64 | | | | |
| 4 | H | 5 | 55 | 60 | 30.38 | 0.93 | 0.25 | | | | | | | | |
| 4 | H | 5 | 60 | 65 | 30.43 | 0.89 | 0.03 | -1.15 | 0.37 | | | | | | |
| 5 | H | 2 | 65 | 70 | 36.55 | 1.00 | 0.55 | -1.10 | 0.71 | 1.43 | 2.00 | 2.06 | 1.56 | | |
| 5 | H | 3 | 15 | 20 | 37.95 | 1.28 | 0.52 | | | | | | | | |
| 5 | H | 4 | 62 | 67 | 39.52 | 1.07 | 0.70 | -1.25 | 0.59 | 1.57 | 2.03 | 0.83 | 1.80 | | |
| 5 | H | 4 | 69 | 71 | 39.59 | | | | | | | | | | |
| 5 | H | 4 | 113 | 118 | 40.03 | | | | | | | | | | |
| 5 | H | 5 | 3 | 8 | 40.43 | | | | | | | | | | |
| 5 | H | 5 | 55 | 60 | 40.95 | 1.16 | 0.29 | | | | | | | | |
| 5 | H | 6 | 65 | 70 | 42.55 | 1.08 | 0.41 | -0.57 | 0.75 | | | 1.43 | 1.98 | | |
| 6 | H | 1 | 5 | 10 | 43.95 | 0.94 | 0.73 | 0.05 | 1.49 | 1.87 | 2.27 | 1.38 | 2.52 | 0.32 | 2.61 |
| 6 | H | 1 | 55 | 60 | 44.45 | 0.93 | 0.42 | | | | | | | | |
| 6 | H | 2 | 65 | 70 | 46.05 | 0.79 | 0.11 | -1.03 | 0.53 | 1.06 | 1.72 | 1.28 | 1.62 | -0.40 | 2.16 |
| 6 | H | 3 | 3 | 8 | 46.93 | 0.58 | 0.15 | -0.79 | 0.55 | 0.86 | 1.96 | 0.83 | 1.63 | -0.13 | 2.25 |
| 6 | H | 3 | 55 | 60 | 47.45 | 0.92 | 0.46 | | | | | | | | |
| 6 | H | 3 | 110 | 115 | 48 | 0.76 | 0.37 | | | 1.44 | 1.65 | | | | |
| 6 | H | 4 | 65 | 70 | 49.05 | 0.91 | 0.38 | -0.93 | 0.69 | | | | | | |
| 6 | H | 5 | 3 | 9 | 49.93 | 0.67 | 0.20 | -1.26 | 0.43 | | | | | | |
| 6 | H | 5 | 55 | 60 | 50.45 | 0.64 | 0.37 | | | | | | | | |
| 6 | H | 5 | 110 | 115 | 51 | 0.80 | 0.38 | -0.58 | 0.51 | | | 0.92 | 1.80 | 0.34 | 1.82 |
| 6 | H | 6 | 65 | 70 | 52.05 | 1.19 | 0.70 | -0.90 | 0.59 | | | 1.28 | 1.72 | -0.37 | 2.24 |
| 7 | H | 1 | 3 | 8 | 53.43 | 1.22 | 0.49 | -0.56 | 0.57 | 1.54 | 2.12 | 1.04 | 1.85 | -0.30 | 2.48 |
| 7 | H | 1 | 55 | 60 | 53.95 | 1.15 | 0.54 | | | | | | | | |

| Cor | T | Sct | Top cm | Bot cm | Depth mbsf | *G. ruber* $\delta^{13}$C ‰ | $\delta^{18}$O ‰ | *G. bulloides* $\delta^{13}$C ‰ | $\delta^{18}$O ‰ | *F. wullerstorfi* $\delta^{13}$C ‰ | $\delta^{18}$O ‰ | *Cibicidoides* spp $\delta^{13}$C ‰ | $\delta^{18}$O ‰ | *Uvigerina* $\delta^{13}$C ‰ | $\delta^{18}$O ‰ |
|---|---|---|---|---|---|---|---|---|---|---|---|---|---|---|---|
| 7 | H | 2 | 3 | 8 | 54.93 | 0.88 | 0.46 | -0.90 | 0.24 | 1.87 | 2.10 | 1.41 | 2.04 | -0.13 | 2.61 |
| 7 | H | 2 | 65 | 70 | 55.55 | 1.21 | 0.32 | -1.13 | 0.46 | 1.14 | 1.94 | 1.18 | 1.82 | 0.97 | 2.03 |
| 7 | H | 3 | 55 | 60 | 56.95 | 0.82 | 0.33 | | | | | | | | |
| 7 | H | 3 | 60 | 63 | 57 | | | | | 1.70 | 1.77 | 0.41 | 1.87 | -0.57 | 2.44 |
| 7 | H | 4 | 3 | 5 | 57.93 | 0.67 | -0.01 | -0.39 | 0.35 | 1.52 | 1.43 | 1.04 | 1.57 | 0.67 | 3.00 |
| 7 | H | 4 | 65 | 70 | 58.55 | 0.52 | 0.09 | -0.84 | 0.66 | 1.26 | 1.28 | 0.90 | 1.26 | 0.45 | 1.66 |
| 7 | H | 5 | 55 | 60 | 59.95 | 0.61 | -0.02 | | | | | | | | |
| 7 | H | 5 | 60 | 65 | 60 | 0.60 | -0.08 | 0.60 | 0.47 | | | 0.59 | 1.29 | | |
| 7 | H | 6 | 59 | 64 | 61.49 | 0.60 | -0.13 | -0.58 | 0.88 | | | 1.02 | 2.57 | 0.94 | 1.60 |
| 7 | H | CC | 10 | 15 | 61.64 | | | | | | | | | | |
| 8 | H | 1 | 3 | 8 | 62.93 | 1.25 | -0.05 | 1.17 | 0.57 | | | 1.29 | 2.70 | | |
| 8 | H | 1 | 55 | 60 | 63.45 | 1.06 | 0.33 | | | | | | | | |
| 8 | H | 2 | 65 | 70 | 65.05 | 0.80 | 0.36 | -0.23 | 1.74 | | | 1.22 | 1.51 | 0.13 | 2.08 |
| 8 | H | 3 | 55 | 60 | 66.45 | 0.94 | 1.35 | | | | | | | | |
| 8 | H | 4 | 64 | 69 | 68.04 | 0.79 | 1.21 | -0.39 | 1.63 | 1.83 | 2.47 | 1.36 | 2.23 | 0.21 | 2.71 |
| 8 | H | 5 | 55 | 60 | 69.45 | 0.83 | 0.74 | | | | | | | | |
| 9 | H | 1 | 55 | 60 | 72.95 | 0.52 | 0.96 | | | | | | | | |
| 9 | H | 2 | 65 | 70 | 74.55 | 0.71 | 0.72 | -0.93 | 1.37 | 0.83 | 2.47 | 0.98 | 2.02 | 0.07 | 2.59 |
| 9 | H | 3 | 55 | 60 | 75.95 | 0.70 | 0.67 | | | | | | | | |
| 9 | H | 4 | 65 | 70 | 77.55 | 0.87 | 0.66 | -0.46 | 1.24 | 0.85 | 2.07 | 1.12 | 2.03 | -0.48 | 3.12 |
| 9 | H | 5 | 55 | 60 | 78.88 | 0.34 | 0.55 | | | | | | | | |
| 10 | H | 2 | 65 | 70 | 82.94 | 0.58 | 0.42 | -0.73 | 0.72 | 1.44 | 1.49 | 0.90 | 1.42 | 0.15 | 1.93 |
| 10 | H | 3 | 55 | 60 | 84.34 | 0.58 | 0.17 | | | | | | | | |
| 10 | H | 4 | 65 | 70 | 85.94 | 0.72 | 0.36 | -0.72 | 0.66 | 1.73 | 1.56 | 1.16 | 1.70 | -0.16 | 1.99 |
| 10 | H | 5 | 55 | 60 | 87.34 | 0.08 | 0.44 | | | | | | | | |
| 10 | H | 6 | 38 | 43 | 88.67 | 1.06 | 0.72 | -0.31 | 1.20 | 1.13 | 1.54 | 1.40 | 1.86 | | |
| 11 | H | 1 | 55 | 60 | 91.95 | 0.98 | 0.46 | | | | | | | | |
| 11 | H | 2 | 65 | 70 | 93.55 | 0.51 | 0.56 | -0.43 | 1.01 | | | 1.10 | 1.60 | | |
| 11 | H | 3 | 55 | 60 | 94.95 | 0.80 | 0.29 | | | | | | | | |
| 11 | H | 4 | 65 | 70 | 96.55 | 0.65 | 0.39 | -0.96 | 0.64 | | | | | | |
| 11 | H | 6 | 70 | 75 | 99.44 | 0.60 | 0.58 | -0.83 | 0.91 | 1.59 | 1.70 | 1.19 | 1.86 | 0.12 | 1.86 |
| 12 | H | 2 | 65 | 70 | 102.29 | 0.92 | 0.61 | -0.78 | 0.74 | | | 1.62 | 1.51 | 0.18 | 2.77 |
| 12 | H | 4 | 64 | 69 | 105.28 | 0.85 | 0.54 | -0.60 | 1.12 | | | 0.91 | 2.38 | | |
| 12 | H | 6 | 66 | 71 | 108.2 | | | -0.58 | 0.91 | 1.24 | 2.30 | 1.21 | 2.37 | | |
| 13 | H | 2 | 66 | 71 | 112.56 | 0.87 | 0.46 | -0.70 | 0.90 | | | | | | |
| 13 | H | 3 | 55 | 59 | 113.95 | 1.02 | 0.50 | | | | | | | | |
| 13 | H | 4 | 66 | 71 | 115.49 | 0.91 | 0.21 | -0.36 | 0.76 | | | | | | |
| 13 | H | 5 | 3 | 8 | 116.15 | 0.67 | -0.42 | | | 1.45 | 2.29 | 1.02 | 1.71 | | |
| 14 | H | 2 | 65 | 70 | 121.2 | 0.83 | 1.36 | | | 1.40 | 2.45 | 1.29 | 2.69 | 0.42 | 2.59 |
| 14 | H | 3 | 62 | 67 | 122.67 | 0.98 | 0.67 | -0.38 | 1.02 | 0.89 | 2.65 | 1.03 | 2.19 | -0.07 | 3.04 |
| 14 | H | 4 | 65 | 70 | 124.2 | 1.02 | 0.87 | -0.51 | 1.35 | | | 1.43 | 2.02 | 0.53 | 2.41 |
| 14 | H | 5 | 110 | 115 | 126.15 | 0.62 | 0.54 | -0.66 | 1.05 | | | | | | |
| 15 | H | 2 | 8 | 10 | 130.24 | 0.72 | 0.47 | -0.84 | 0.72 | 1.29 | 1.82 | | | -0.48 | 2.42 |
| 15 | H | 2 | 65 | 70 | 130.81 | -0.50 | 0.91 | 0.58 | 0.68 | | | | | -0.20 | 2.68 |
| 15 | H | 3 | 15 | 20 | 131.81 | 0.94 | 0.49 | -0.29 | 1.11 | 1.69 | 1.94 | | | -0.49 | 2.77 |

| Cor | T | Sct | Top | Bot | Depth | *G. ruber* | | *G. bulloides* | | *F. wullerstorfi* | | *Cibicidoides* spp | | *Uvigerina* | |
|---|---|---|---|---|---|---|---|---|---|---|---|---|---|---|---|
| | | | cm | cm | mbsf | $\delta^{13}C$ ‰ | $\delta^{18}O$ ‰ | $\delta^{13}C$ ‰ | $\delta^{18}O$ ‰ | $\delta^{13}C$ ‰ | $\delta^{18}O$ ‰ | $\delta^{13}C$ ‰ | $\delta^{18}O$ ‰ | $\delta^{13}C$ ‰ | $\delta^{18}O$ ‰ |
| 15 | H | 4 | 16 | 20 | 133.32 | 1.05 | 0.35 | -0.52 | 0.98 | 1.36 | 2.10 | | | | |
| 15 | H | 4 | 65 | 70 | 133.81 | 0.80 | 0.66 | -0.50 | 1.11 | | | | | | |
| 15 | H | 4 | 110 | 115 | 134.26 | 1.29 | 0.75 | -0.69 | 0.94 | 1.62 | 2.24 | | | | |
| 15 | H | 6 | 27 | 32 | 136.43 | 0.71 | 0.57 | -0.59 | 0.76 | 1.77 | 2.31 | | | -0.25 | 2.81 |
| 16 | H | 1 | 8 | 10 | 138.98 | 0.72 | 0.26 | -0.58 | 0.68 | 0.69 | 1.76 | | | -0.62 | 2.41 |
| 16 | H | 2 | 8 | 10 | 140.48 | 0.87 | 0.40 | -0.47 | 1.07 | | | | | | |
| 16 | H | 2 | 65 | 70 | 141.05 | 0.62 | 0.42 | -0.24 | 0.77 | 0.90 | 1.91 | 1.88 | 1.51 | | |
| 16 | H | 3 | 25 | 27 | 142.15 | | | -0.04 | 1.18 | | | 1.42 | 1.96 | 0.27 | 2.48 |
| 16 | H | 4 | 15 | 20 | 143.55 | 1.15 | 0.70 | -0.69 | 0.64 | | | | | | |
| 16 | H | 4 | 65 | 70 | 144.05 | 1.27 | 0.84 | -0.62 | 0.82 | | | 1.54 | 1.48 | 0.08 | 2.30 |
| 16 | H | CC | 30 | 35 | 145.46 | 1.05 | 0.48 | | | | | | | -0.11 | 2.39 |
| 17 | X | 1 | 60 | 65 | 149 | 1.04 | 0.59 | -0.42 | 0.58 | 1.55 | 2.26 | 1.07 | 1.85 | | |
| 17 | X | 1 | 110 | 115 | 149.5 | 1.17 | 0.38 | | | | | | | | |
| 17 | X | 2 | 65 | 70 | 150.55 | 1.21 | 0.89 | -0.67 | 0.79 | | | 1.46 | 2.07 | | |
| 17 | X | 3 | 60 | 65 | 152 | 1.09 | 0.52 | -0.73 | 0.66 | 1.28 | 1.98 | 1.15 | 1.95 | | |
| 17 | X | 4 | 61 | 66 | 153.34 | 0.88 | 0.36 | -0.26 | 1.07 | | | 1.05 | 2.21 | | |
| 17 | X | 4 | 69 | 75 | 153.42 | 0.87 | -0.19 | | | 1.28 | 2.18 | | | | |
| 17 | X | 4 | 113 | 119 | 153.86 | -1.27 | | -1.00 | 0.70 | | | | | -0.29 | 2.68 |
| 18 | X | 1 | 6 | 10 | 154.96 | 1.39 | 0.61 | -0.06 | 1.15 | 1.18 | 2.71 | | | -0.08 | 2.97 |
| 18 | X | 1 | 113 | 119 | 156.03 | | | -0.39 | 1.07 | | | | | | |
| 18 | X | 2 | 65 | 70 | 157.05 | | | -0.38 | 1.21 | | | | | | |
| 18 | X | 3 | 3 | 8 | 157.93 | 0.61 | -0.70 | -0.39 | 1.02 | | | 0.85 | 2.51 | | |
| 18 | X | 3 | 113 | 118 | 159.03 | 1.16 | 0.39 | -0.27 | 1.02 | 1.21 | 2.08 | | | | |
| 18 | X | 4 | 65 | 70 | 160.05 | 1.10 | 0.68 | -0.36 | 0.95 | | | | | | |
| 18 | X | 5 | 4 | 9 | 160.94 | 1.08 | 0.29 | -0.25 | 0.77 | 1.63 | 2.21 | | | | |
| 18 | X | 5 | 46 | 52 | 161.36 | 1.47 | 0.53 | -0.74 | 0.57 | 1.83 | 2.13 | 0.96 | 2.23 | -0.26 | 2.73 |
| 19 | X | 2 | 65 | 70 | 166.65 | 0.66 | 0.35 | -0.38 | 0.36 | 1.37 | 2.25 | 1.45 | 2.16 | 0.76 | 2.28 |
| 19 | X | 3 | 60 | 65 | 168.1 | 0.89 | 0.18 | -0.46 | 0.92 | 1.54 | 1.94 | | | | |
| 19 | X | 4 | 65 | 70 | 169.65 | 1.05 | 0.99 | -0.86 | 0.36 | | | 1.30 | 1.70 | 0.15 | 2.75 |
| 19 | X | CC | 20 | 25 | 171.21 | 0.86 | 1.24 | 1.16 | 1.54 | 2.03 | 2.41 | | | | |
| 20 | X | 2 | 3 | 8 | 175.63 | 0.96 | 0.64 | -0.50 | 1.38 | 1.47 | 2.16 | | | | |
| 20 | X | 2 | 65 | 70 | 176.25 | 0.95 | 0.89 | -0.42 | 1.14 | 0.87 | 1.71 | 0.98 | 2.05 | | |
| 20 | X | 4 | 68 | 73 | 179.28 | 0.57 | 0.85 | | | | | | | 0.53 | 2.11 |
| 21 | X | 1 | 65 | 70 | 184.35 | 0.72 | 1.29 | -0.34 | 2.03 | 1.19 | 2.73 | | | 0.05 | 3.13 |
| 21 | X | 3 | 24 | 29 | 186.65 | 1.37 | 1.23 | 0.05 | 1.85 | 1.06 | 2.78 | | | 0.59 | 2.65 |
| 21 | X | 3 | 124 | 129 | 187.65 | 1.49 | 1.02 | -0.04 | 1.77 | 1.25 | 2.52 | 0.64 | 2.76 | 0.23 | 3.10 |
| 21 | X | 4 | 66 | 71 | 188.57 | 1.27 | 1.15 | -0.48 | 1.19 | | | 1.31 | 2.05 | 0.08 | 2.67 |
| 21 | X | 5 | 27 | 32 | 189.68 | 1.00 | 0.79 | -0.69 | 0.96 | 1.22 | 0.72 | | | | |
| 21 | X | 6 | 68 | 73 | 191.17 | 0.92 | 0.72 | -0.43 | 1.02 | | | 1.12 | 2.49 | -0.11 | 2.49 |
| 22 | X | 1 | 5 | 10 | 193.45 | | | -1.15 | 1.00 | 0.77 | 2.53 | | | | |
| 22 | X | 1 | 104 | 109 | 194.44 | 1.04 | 0.47 | -1.04 | 0.59 | | | 1.28 | 2.24 | | |
| 22 | X | 2 | 65 | 70 | 195.55 | 1.11 | 0.68 | -0.90 | 1.07 | | | 0.90 | 2.55 | -0.10 | 3.03 |
| 22 | X | 3 | 15 | 20 | 196.55 | | | -0.60 | 1.10 | 1.10 | 2.04 | | | | |
| 22 | X | 3 | 115 | 120 | 197.55 | | | -0.87 | 0.80 | | | 0.88 | 2.40 | | |
| 22 | X | 4 | 65 | 70 | 198.55 | | | | | | | 2.02 | 2.14 | | |

| Cor | T | Sct | Top cm | Bot cm | Depth mbsf | *G. ruber* δ¹³C ‰ | δ¹⁸O ‰ | *G. bulloides* δ¹³C ‰ | δ¹⁸O ‰ | *F. wullerstorfi* δ¹³C ‰ | δ¹⁸O ‰ | *Cibicidoides* spp δ¹³C ‰ | δ¹⁸O ‰ | *Uvigerina* δ¹³C ‰ | δ¹⁸O ‰ |
|---|---|---|---|---|---|---|---|---|---|---|---|---|---|---|---|
| 22 | X | 5 | 10 | 15 | 199.5 | 0.90 | 0.84 | -1.12 | 0.66 | | | 0.76 | 2.25 | | |
| 22 | X | CC | 18 | 23 | 200.61 | 0.86 | 0.20 | -1.15 | 0.77 | | | 0.41 | 1.24 | | |
| 23 | X | 1 | 14 | 19 | 203.14 | 0.96 | 0.49 | -0.77 | 1.05 | 1.09 | 2.06 | | | | |
| 23 | X | 1 | 115 | 120 | 204.15 | 1.04 | 0.65 | -1.14 | 0.82 | 1.68 | 2.40 | 0.60 | 2.30 | | |
| 23 | X | 2 | 65 | 70 | 205.15 | | | 1.40 | 0.85 | | | 1.22 | 2.47 | | |
| 23 | X | 3 | 102 | 107 | 207.02 | 1.41 | 0.59 | -0.40 | 0.94 | 1.54 | 2.40 | 0.87 | 2.37 | -0.50 | 3.10 |
| 23 | X | 4 | 65 | 70 | 208.15 | 1.14 | 0.57 | -0.56 | 1.05 | | | 1.51 | 2.27 | | |
| 23 | X | 5 | 130 | 135 | 210.3 | 0.71 | 0.34 | -0.71 | 0.76 | | | 0.69 | 2.15 | | |
| 24 | X | 1 | 25 | 30 | 212.85 | 1.20 | 0.55 | -0.71 | 0.71 | | | 1.04 | 1.93 | -0.02 | 2.45 |
| 24 | X | 2 | 65 | 70 | 214.75 | 1.04 | 0.69 | -0.07 | 1.36 | | | 0.74 | 2.45 | 0.04 | 2.62 |
| 24 | X | 3 | 14 | 19 | 215.74 | 1.43 | 0.65 | -0.04 | 1.09 | 1.58 | 2.24 | | | 0.07 | 2.70 |
| 24 | X | 3 | 122 | 128 | 216.82 | 1.27 | 0.53 | 0.74 | 1.13 | 1.68 | 2.07 | | | 2.34 | 2.73 |
| 24 | X | 4 | 65 | 70 | 217.75 | 1.20 | 1.05 | 0.47 | 1.62 | | | 1.58 | 1.58 | 0.58 | 2.11 |
| 25 | X | 1 | 15 | 19 | 222.45 | 0.79 | 0.57 | -0.59 | 0.66 | 1.32 | 1.65 | | | -0.59 | 2.05 |
| 25 | X | 1 | 115 | 120 | 223.45 | 0.79 | 0.17 | | | | | | | | |
| 25 | X | 2 | 65 | 70 | 224.45 | 0.85 | 0.40 | -0.61 | 0.80 | | | | | | |
| 25 | X | 3 | 78 | 82 | 226.08 | 0.93 | 0.28 | | | | | | | | |
| 25 | X | 4 | 32 | 37 | 227.12 | 0.85 | 0.12 | | | | | | | | |
| 25 | X | 4 | 65 | 70 | 227.45 | 0.42 | 0.54 | -0.20 | 1.15 | | | 0.58 | 1.91 | 0.94 | 1.49 |
| 25 | X | 4 | 135 | 140 | 228.15 | 0.97 | 0.57 | | | | | | | | |
| 25 | X | 5 | 84 | 89 | 229.14 | 0.87 | 0.62 | 0.13 | 1.59 | 0.95 | 2.39 | | | -0.39 | 2.69 |
| 26 | X | 1 | 14 | 19 | 232.04 | 0.89 | 0.53 | -1.31 | 0.47 | 1.12 | 2.88 | | | -0.18 | 3.19 |
| 26 | X | 1 | 115 | 120 | 233.05 | 0.78 | 1.11 | -0.66 | 1.51 | 0.59 | 2.77 | | | | |
| 26 | X | 2 | 65 | 70 | 234.05 | | | -0.63 | 1.38 | | | 0.68 | 2.86 | | |
| 26 | X | 3 | 12 | 17 | 235.02 | 0.24 | 0.64 | -0.39 | 1.46 | 0.76 | 2.51 | | | | |
| 26 | X | 3 | 114 | 119 | 236.04 | 1.38 | 0.85 | 0.41 | 1.86 | 1.20 | 2.67 | | | | |
| 26 | X | 4 | 65 | 70 | 237.05 | 1.12 | 0.86 | -0.20 | 1.47 | | | 1.81 | 2.11 | | |
| 26 | X | 5 | 15 | 20 | 238.05 | 1.21 | 0.77 | -0.38 | 1.34 | | | | | | |
| 26 | X | CC | 16 | 21 | 239.19 | | | -0.47 | 1.25 | | | | | | |
| 27 | X | 1 | 3 | 18 | 241.53 | -0.51 | 0.93 | | | | | | | | |
| 27 | X | 1 | 115 | 120 | 242.65 | 0.66 | 0.18 | -0.31 | 0.95 | 0.86 | 2.11 | 0.77 | 2.31 | -0.53 | 2.90 |
| 27 | X | 3 | 11 | 15 | 244.61 | 1.20 | 0.46 | | | | | | | | |
| 27 | X | 3 | 108 | 112 | 245.58 | 1.41 | 0.78 | | | | | | | | |
| 27 | X | 4 | 63 | 67 | 246.63 | 0.88 | 0.96 | 0.27 | 1.28 | | | 1.00 | 2.19 | 0.45 | 2.65 |
| 27 | X | 5 | 105 | 110 | 248.55 | 1.26 | 0.99 | 0.32 | 1.59 | | | 1.08 | 2.08 | 0.57 | 2.59 |
| 27 | X | 6 | 64 | 69 | 249.64 | 0.58 | 0.54 | -0.54 | 0.14 | | | 1.51 | 1.91 | | |
| 28 | X | 1 | 23 | 28 | 251.33 | 1.06 | 0.52 | | | | | | | | |
| 28 | X | 1 | 121 | 126 | 252.31 | 1.01 | 0.39 | | | | | | | | |
| 28 | X | 2 | 65 | 70 | 253.25 | 0.99 | 0.56 | -0.28 | 0.94 | | | 1.32 | 2.15 | | |
| 28 | X | 3 | 34 | 39 | 254.44 | 1.01 | 0.55 | | | | | | | | |
| 28 | X | 4 | 9 | 14 | 255.69 | 1.02 | 0.40 | | | | | | | | |
| 28 | X | 4 | 65 | 70 | 256.25 | 0.48 | -0.02 | | | | | 1.55 | 1.94 | 0.11 | 2.37 |
| 28 | X | 5 | 22 | 28 | 257.32 | 1.01 | 0.28 | 0.24 | 1.35 | 1.22 | 1.97 | | | 0.02 | 2.53 |
| 28 | X | 5 | 122 | 127 | 258.32 | 0.65 | 0.22 | -1.05 | 0.61 | 0.49 | 1.94 | | | 0.18 | 2.77 |
| 28 | X | 6 | 66 | 70 | 259.26 | | | -0.10 | 1.07 | | | | | 0.24 | 2.44 |

| Cor | T | Sct | Top cm | Bot cm | Depth mbsf | *G. ruber* δ¹³C ‰ | δ¹⁸O ‰ | *G. bulloides* δ¹³C ‰ | δ¹⁸O ‰ | *F. wullerstorfi* δ¹³C ‰ | δ¹⁸O ‰ | *Cibicidoides* spp δ¹³C ‰ | δ¹⁸O ‰ | *Uvigerina* δ¹³C ‰ | δ¹⁸O ‰ |
|---|---|---|---|---|---|---|---|---|---|---|---|---|---|---|---|
| 28 | X | 6 | 69 | 74 | 259.29 | 0.90 | 0.40 | -0.34 | 0.92 | 1.32 | 2.11 | 1.37 | 2.17 | 0.82 | 2.41 |
| 29 | X | 1 | 15 | 20 | 260.95 | 0.95 | 0.49 | -0.79 | 0.96 | 1.43 | 2.34 | | | | |
| 29 | X | 2 | 65 | 70 | 262.95 | 1.08 | 0.58 | -0.16 | 0.99 | | | 1.51 | 1.41 | | |
| 29 | X | 3 | 14 | 19 | 263.94 | 1.01 | 0.47 | -0.82 | 1.02 | 1.03 | 1.10 | 1.01 | 2.21 | 0.00 | 2.73 |
| 29 | X | 3 | 128 | 135 | 265.08 | 1.39 | 0.70 | | | | | | | | |
| 29 | X | 4 | 65 | 70 | 265.95 | 1.36 | 1.06 | 0.25 | 1.21 | 2.75 | 2.07 | 1.88 | 2.49 | | |
| 29 | X | 5 | 16 | 21 | 266.96 | 1.35 | 0.57 | | | | | | | | |
| 29 | X | 5 | 123 | 128 | 268.03 | 1.34 | 0.54 | | | | | | | | |
| 29 | X | 6 | 65 | 70 | 268.95 | 1.28 | 0.76 | -0.18 | 1.18 | | | 1.72 | 2.27 | 0.05 | 2.84 |
| 29 | X | 7 | 80 | 85 | 269.95 | 1.12 | 0.48 | | | | | | | | |
| 29 | X | CC | 50 | 55 | 270.75 | 1.20 | 0.29 | | | | | | | | |
| 30 | X | 2 | 65 | 70 | 272.55 | 1.19 | 0.70 | 0.55 | 1.23 | 1.50 | 2.14 | 1.69 | 1.44 | -0.34 | 2.60 |
| 30 | X | 3 | 13 | 18 | 273.53 | 0.96 | 0.33 | | | | | | | | |
| 30 | X | 4 | 64 | 69 | 275.54 | 0.78 | 0.58 | -0.33 | 1.10 | | | 1.49 | 2.27 | -0.30 | 2.51 |
| 30 | X | 5 | 30 | 35 | 276.7 | 0.55 | 0.47 | | | | | | | | |
| 30 | X | 5 | 134 | 139 | 277.74 | 0.67 | 0.39 | | | | | | | | |
| 30 | X | 6 | 65 | 70 | 278.55 | | | -0.50 | 1.17 | | | 1.52 | 2.57 | 0.20 | 2.28 |
| 30 | X | 7 | 21 | 26 | 279.61 | 0.54 | 0.21 | | | | | | | | |
| 31 | X | 1 | 114 | 119 | 281.14 | 0.63 | 0.64 | | | | | | | | |
| 31 | X | 2 | 65 | 70 | 282.15 | 0.63 | 0.71 | -0.83 | 0.93 | | | 1.22 | 2.44 | | |
| 31 | X | 3 | 23 | 28 | 283.23 | 0.88 | 1.27 | 1.75 | 2.15 | 0.92 | 2.66 | | | | |
| 31 | X | 3 | 129 | 134 | 284.29 | 0.88 | 0.90 | | | | | | | | |
| 31 | X | 4 | 64 | 69 | 285.14 | 0.25 | 1.28 | -0.87 | 1.58 | | | 1.06 | 2.72 | -0.25 | 3.18 |
| 31 | X | 5 | 24 | 29 | 286.24 | 0.52 | 0.65 | | | | | | | | |
| 31 | X | 5 | 127 | 132 | 287.27 | 0.72 | 0.52 | | | | | | | | |
| 31 | X | 6 | 65 | 70 | 288.15 | 0.90 | 0.74 | -1.00 | 0.91 | 1.10 | 2.06 | 0.64 | 2.51 | -0.79 | 2.85 |
| 32 | X | 2 | 66 | 68 | 291.86 | 0.38 | 1.09 | -0.39 | 1.60 | | | 0.60 | 2.13 | -0.56 | 2.59 |
| 32 | X | 3 | 15 | 18 | 292.85 | 0.40 | 1.02 | | | | | | | | |
| 32 | X | 4 | 64 | 66 | 294.84 | 0.71 | 1.30 | -0.35 | 1.69 | 1.31 | 2.30 | 0.96 | 2.22 | 0.03 | 2.74 |
| 33 | X | 1 | 14 | 18 | 299.44 | 0.96 | 0.66 | | | | | | | | |
| 33 | X | 4 | 62 | 67 | 304.42 | 0.58 | 1.44 | -0.44 | 1.53 | | | 0.77 | 2.13 | | |
| 33 | X | 6 | 62 | 67 | 307.42 | 0.75 | 1.54 | -0.82 | 1.50 | | | 0.90 | 2.53 | | |
| 34 | X | 1 | 15 | 19 | 309.05 | 0.46 | 0.32 | | | | | | | | |
| 34 | X | 2 | 65 | 70 | 311.05 | 0.31 | 1.26 | -0.44 | 1.87 | | | 0.73 | 2.20 | 0.10 | 3.04 |
| 34 | X | 3 | 16 | 20 | 312.06 | 0.53 | 1.50 | | | | | | | | |
| 34 | X | 4 | 65 | 70 | 314.05 | 0.50 | 0.69 | -0.55 | 1.09 | | | 1.05 | 2.61 | 0.14 | 2.80 |
| 34 | X | 5 | 23 | 27 | 315.13 | 0.70 | 0.90 | -1.03 | 1.66 | 0.40 | 2.85 | | | | |
| 34 | X | 6 | 66 | 71 | 317.06 | 0.78 | 0.92 | -0.61 | 1.60 | | | 0.86 | 2.90 | | |
| 35 | X | 2 | 65 | 70 | 320.65 | 0.61 | 1.07 | -0.90 | 1.28 | | | 0.97 | 2.66 | -0.07 | 3.04 |
| 35 | X | 3 | 15 | 19 | 321.65 | 0.32 | 0.71 | | | | | | | | |
| 35 | X | 3 | 110 | 115 | 322.6 | 0.56 | 0.72 | | | | | | | | |
| 35 | X | 4 | 65 | 70 | 323.65 | 0.48 | 0.54 | -1.25 | 0.94 | | | 0.62 | 2.27 | -0.25 | 2.78 |
| 35 | X | 5 | 16 | 20 | 324.66 | 0.49 | 0.76 | | | | | | | | |
| 35 | X | 6 | 66 | 71 | 326.66 | 0.00 | 1.20 | 0.00 | 1.60 | | | 0.78 | 2.09 | | |
| 35 | X | 7 | 30 | 34 | 327.8 | 0.56 | 0.98 | | | | | | | | |

| Cor | T | Sct | Top cm | Bot cm | Depth mbsf | *G. ruber* δ¹³C ‰ | δ¹⁸O ‰ | *G. bulloides* δ¹³C ‰ | δ¹⁸O ‰ | *F. wullerstorfi* δ¹³C ‰ | δ¹⁸O ‰ | *Cibicidoides* spp δ¹³C ‰ | δ¹⁸O ‰ | *Uvigerina* δ¹³C ‰ | δ¹⁸O ‰ |
|---|---|---|---|---|---|---|---|---|---|---|---|---|---|---|---|
| 36 | X | 1 | 77 | 79 | 328.87 | 0.14 | 0.45 | | | | | | | | |
| 36 | X | 2 | 67 | 69 | 330.27 | 0.18 | 0.98 | -0.69 | 1.49 | | | 0.49 | 2.23 | 0.14 | 2.99 |
| 36 | X | 3 | 5 | 8 | 331.15 | 0.41 | 1.20 | | | | | | | | |
| 36 | X | 3 | 107 | 111 | 332.17 | 0.18 | 0.82 | | | | | | | | |
| 36 | X | 4 | 65 | 70 | 333.25 | 0.05 | 0.86 | -0.85 | 1.23 | 1.13 | 2.46 | 0.42 | 2.49 | | |
| 36 | X | 5 | 24 | 27 | 334.34 | 0.12 | 1.04 | | | | | | | | |
| 36 | X | 5 | 132 | 137 | 335.42 | 0.23 | 1.24 | | | | | | | | |
| 36 | X | 6 | 65 | 70 | 336.25 | 0.42 | 0.94 | -0.58 | 1.48 | | | 1.00 | 2.72 | 0.04 | 2.41 |
| 36 | X | 7 | 28 | 33 | 337.38 | 0.37 | 0.52 | | | | | | | | |
| 37 | X | 1 | 3 | 6 | 337.73 | 0.44 | 1.13 | | | | | | | | |
| 37 | X | 1 | 95 | 99 | 338.65 | 0.39 | 1.27 | | | | | | | | |
| 37 | X | 2 | 65 | 70 | 339.85 | 0.30 | 1.18 | -0.75 | 1.48 | | | 0.68 | 2.39 | | |
| 37 | X | 4 | 65 | 70 | 342.85 | 0.63 | 1.05 | -0.33 | 1.36 | | | 1.06 | 2.05 | | |
| 37 | X | 6 | 66 | 71 | 345.86 | 0.46 | 1.08 | -0.92 | 1.19 | 0.92 | 2.13 | 0.80 | 1.81 | 0.26 | 1.41 |
| 38 | X | 2 | 66 | 71 | 349.46 | 0.60 | 1.20 | -0.64 | 1.40 | | | 0.90 | 2.54 | | |
| 38 | X | 4 | 66 | 71 | 352.46 | 0.52 | 0.97 | -0.30 | 1.67 | | | 0.93 | 2.14 | 0.11 | 2.46 |
| 38 | X | 6 | 67 | 72 | 355.47 | 0.41 | 0.92 | -0.42 | 1.45 | 0.80 | 2.17 | 1.00 | 2.22 | 0.08 | 2.55 |
| 39 | X | 2 | 65 | 70 | 359.15 | 0.59 | 1.55 | -0.52 | 1.70 | 1.27 | 2.80 | | | 0.52 | 2.58 |
| 39 | X | 4 | 65 | 70 | 362.15 | 0.39 | 0.87 | -1.13 | 1.08 | 1.08 | 2.18 | 0.86 | 2.38 | | |
| 39 | X | 6 | 67 | 69 | 365.17 | 0.77 | 0.92 | -0.45 | 1.03 | | | 1.19 | 2.37 | | |
| 40 | X | 2 | 65 | 70 | 368.75 | 0.61 | 0.93 | -0.83 | 1.24 | 0.97 | 1.74 | 0.73 | 2.20 | | |
| 40 | X | 4 | 65 | 70 | 371.75 | 0.57 | 0.70 | 0.23 | 1.19 | | | 0.65 | 1.68 | -0.14 | 2.07 |
| 40 | X | 6 | 61 | 64 | 374.21 | 0.29 | 1.01 | -0.86 | 1.55 | 0.63 | 2.48 | 0.45 | 2.57 | | |
| 41 | X | 2 | 65 | 70 | 378.35 | 0.63 | 0.85 | -0.13 | 1.07 | 1.37 | 2.49 | 0.89 | 2.60 | | |
| 41 | X | 4 | 65 | 70 | 381.35 | 0.56 | 0.79 | -0.60 | 1.19 | | | 0.92 | 2.31 | 0.13 | 2.71 |
| 41 | X | 6 | 65 | 70 | 384.35 | 0.51 | 0.81 | -0.29 | 1.31 | | | 0.82 | 2.58 | | |
| 42 | X | 2 | 65 | 70 | 387.75 | 0.60 | 1.01 | -0.15 | 1.42 | | | 0.68 | 2.35 | | |
| 42 | X | 4 | 65 | 70 | 390.75 | 0.71 | 0.88 | -0.39 | 1.39 | | | 0.97 | 2.59 | | |
| 42 | X | 6 | 67 | 72 | 393.77 | 0.64 | 0.55 | -0.52 | 0.95 | 1.21 | 2.41 | 0.92 | 2.51 | | |
| 43 | X | 2 | 65 | 70 | 397.35 | 0.67 | 1.09 | -0.12 | 1.56 | 1.26 | 2.32 | 0.85 | 2.37 | | |
| 43 | X | 4 | 65 | 70 | 400.35 | | | | | | | 0.87 | 2.09 | 0.37 | 2.62 |

## A2: Nitrogen isotopes, Nitrogen percentages, C$_{org}$ percentages and C/N ratios of bulk sediment

| Cor | T | Sct | Top cm | Bot cm | Depth mbsf | δ$^{15}$N ‰ Air | N wt % | Corg wt % | C/N |
|---|---|---|---|---|---|---|---|---|---|
| 1 | H | 1 | 2 | 6 | 0.02 | 6.75 | 0.07 | 0.52 | 9.03 |
| 1 | H | 1 | 25 | 30 | 0.25 | 6.41 | 0.08 | 0.63 | 8.76 |
| 1 | H | 1 | 50 | 53 | 0.50 | 6.52 | 0.07 | 0.41 | 7.27 |
| 1 | H | 1 | 78 | 80 | 0.78 | 6.92 | 0.06 | 0.40 | 7.92 |
| 1 | H | 1 | 102 | 107 | 1.02 | 6.78 | 0.05 | 0.34 | 8.16 |
| 1 | H | 1 | 125 | 130 | 1.25 | 6.62 | 0.05 | 0.58 | 14.74 |
| 1 | H | 2 | 2 | 7 | 1.52 | 6.55 | 0.04 | 0.43 | 12.44 |
| 1 | H | 2 | 25 | 30 | 1.75 | 6.26 | 0.04 | 0.33 | 9.75 |
| 1 | H | 2 | 50 | 55 | 2.00 | 6.22 | 0.05 | 0.56 | 14.08 |
| 1 | H | 2 | 65 | 70 | 2.15 | 6.89 | 0.05 | 0.57 | 13.57 |
| 1 | H | 2 | 72 | 75 | 2.22 | 6.20 | 0.05 | 0.53 | 13.23 |
| 1 | H | 2 | 101 | 106 | 2.51 | 5.62 | 0.07 | 0.63 | 10.18 |
| 1 | H | 2 | 125 | 130 | 2.75 | 5.93 | 0.07 | 0.78 | 12.88 |
| 1 | H | 2 | 145 | 150 | 2.95 | 6.02 | 0.07 | 0.69 | 11.35 |
| 1 | H | 3 | 2 | 7 | 3.02 | 5.98 | 0.07 | 0.70 | 11.36 |
| 1 | H | 3 | 25 | 30 | 3.25 | 6.22 | 0.09 | 0.88 | 12.10 |
| 1 | H | 3 | 46 | 49 | 3.46 | 6.09 | 0.09 | 0.91 | 12.06 |
| 1 | H | 3 | 72 | 75 | 3.72 | 5.60 | 0.09 | 0.69 | 8.72 |
| 1 | H | 3 | 96 | 100 | 3.96 | 5.51 | 0.10 | 0.80 | 9.82 |
| 1 | H | 3 | 125 | 130 | 4.25 | 5.68 | 0.10 | 0.85 | 9.74 |
| 1 | H | 3 | 141 | 146 | 4.41 | 5.40 | 0.10 | 1.01 | 11.46 |
| 1 | H | 4 | 2 | 7 | 4.52 | 5.71 | 0.09 | 0.90 | 11.68 |
| 1 | H | 4 | 25 | 30 | 4.75 | 5.52 | 0.10 | 1.04 | 11.77 |
| 1 | H | 4 | 50 | 55 | 5.00 | 4.93 | 0.08 | 0.85 | 12.45 |
| 1 | H | 4 | 78 | 83 | 5.28 | 5.20 | 0.10 | 1.02 | 12.44 |
| 1 | H | 4 | 102 | 107 | 5.52 | 4.84 | 0.08 | 0.95 | 13.31 |
| 2 | H | 1 | 2 | 6 | 5.92 | 5.06 | 0.09 | 0.99 | 12.38 |
| 2 | H | 1 | 24 | 29 | 6.14 | 4.80 | 0.12 | 1.22 | 12.16 |
| 2 | H | 1 | 45 | 48 | 6.35 | 5.16 | 0.10 | 1.35 | 15.34 |
| 2 | H | 1 | 59 | 64 | 6.49 | 5.24 | 0.10 | | |
| 2 | H | 1 | 64 | 69 | 6.54 | 4.76 | 0.10 | | |
| 2 | H | 1 | 69 | 75 | 6.59 | 4.96 | 0.06 | 1.29 | 23.56 |
| 2 | H | 1 | 100 | 103 | 6.90 | 4.80 | 0.09 | 1.18 | 15.43 |
| 2 | H | 1 | 125 | 130 | 7.15 | 5.00 | 0.10 | 1.17 | 14.01 |
| 2 | H | 1 | 145 | 150 | 7.35 | 5.72 | 0.09 | 1.21 | 15.35 |
| 2 | H | 2 | 2 | 7 | 7.42 | 5.75 | 0.10 | 1.29 | 14.60 |
| 2 | H | 2 | 25 | 30 | 7.65 | 5.36 | 0.10 | 1.29 | 15.30 |
| 2 | H | 2 | 50 | 55 | 7.90 | 4.85 | 0.15 | 1.26 | 10.09 |
| 2 | H | 2 | 55 | 59 | 7.95 | 5.02 | 0.11 | | |
| 2 | H | 2 | 60 | 64 | 8.00 | 5.03 | 0.10 | | |
| 2 | H | 2 | 65 | 70 | 8.05 | 5.18 | 0.09 | 1.18 | 15.46 |

| Cor | T | Sct | Top cm | Bot cm | Depth mbsf | $\delta^{15}$N ‰ Air | N wt % | Corg wt % | C/N |
|---|---|---|---|---|---|---|---|---|---|
| 2 | H | 2 | 70 | 75 | 8.10 | 5.02 | 0.11 | 1.02 | 11.33 |
| 2 | H | 2 | 75 | 79 | 8.15 | 5.46 | 0.08 | | |
| 2 | H | 2 | 80 | 84 | 8.20 | 5.03 | 0.08 | | |
| 2 | H | 2 | 85 | 89 | 8.25 | 5.21 | 0.09 | 1.20 | 16.47 |
| 2 | H | 2 | 90 | 94 | 8.30 | 4.98 | 0.10 | | |
| 2 | H | 2 | 95 | 99 | 8.35 | 4.95 | 0.08 | | |
| 2 | H | 2 | 101 | 107 | 8.41 | 5.67 | 0.04 | 1.02 | 34.00 |
| 2 | H | 2 | 110 | 114 | 8.50 | 5.40 | 0.07 | | |
| 2 | H | 2 | 120 | 124 | 8.60 | 5.29 | 0.06 | 1.00 | 20.77 |
| 2 | H | 2 | 130 | 134 | 8.70 | 6.07 | 0.05 | | |
| 2 | H | 2 | 139 | 144 | 8.79 | 7.04 | 0.05 | | |
| 2 | H | 3 | 2 | 7 | 8.92 | 6.17 | 0.07 | 0.67 | 12.03 |
| 2 | H | 3 | 25 | 30 | 9.15 | 7.00 | 0.06 | 0.49 | 9.53 |
| 2 | H | 3 | 37 | 41 | 9.27 | 7.34 | 0.06 | | |
| 2 | H | 3 | 50 | 55 | 9.40 | 7.70 | 0.06 | 0.49 | 10.03 |
| 2 | H | 3 | 70 | 75 | 9.60 | 7.62 | 0.04 | 0.17 | 5.36 |
| 2 | H | 3 | 80 | 84 | 9.70 | 6.17 | 0.04 | | |
| 2 | H | 3 | 90 | 94 | 9.80 | 6.94 | 0.03 | | |
| 2 | H | 3 | 101 | 106 | 9.91 | 6.77 | 0.03 | 0.32 | 11.67 |
| 2 | H | 3 | 110 | 114 | 10.00 | 7.02 | 0.05 | | |
| 2 | H | 3 | 122 | 128 | 10.12 | 5.40 | 0.03 | 0.52 | 17.84 |
| 2 | H | 3 | 132 | 136 | 10.22 | | 0.04 | | |
| 2 | H | 3 | 144 | 150 | 10.34 | 6.33 | 0.04 | 0.55 | 14.92 |
| 2 | H | 4 | 2 | 7 | 10.42 | 5.76 | 0.04 | 0.52 | 14.11 |
| 2 | H | 4 | 23 | 28 | 10.63 | 5.74 | 0.05 | 0.54 | 13.12 |
| 2 | H | 4 | 50 | 55 | 10.90 | 5.73 | 0.05 | 0.62 | 13.39 |
| 2 | H | 4 | 65 | 70 | 11.05 | 6.27 | 0.05 | 0.55 | 14.26 |
| 2 | H | 4 | 77 | 82 | 11.17 | 6.34 | 0.06 | 0.63 | 13.36 |
| 2 | H | 4 | 101 | 106 | 11.41 | 6.25 | 0.05 | 0.51 | 11.67 |
| 2 | H | 4 | 110 | 114 | 11.50 | 6.42 | 0.06 | | |
| 2 | H | 4 | 125 | 130 | 11.65 | 6.55 | 0.05 | 0.62 | 14.18 |
| 2 | H | 4 | 137 | 142 | 11.77 | 6.30 | 0.05 | 0.67 | 15.03 |
| 2 | H | 5 | 2 | 5 | 11.92 | 6.58 | 0.05 | 0.52 | 13.22 |
| 2 | H | 5 | 25 | 30 | 12.15 | 5.94 | 0.05 | 0.75 | 17.57 |
| 2 | H | 5 | 51 | 56 | 12.41 | 6.38 | 0.06 | 0.60 | 12.73 |
| 2 | H | 5 | 70 | 76 | 12.60 | 5.32 | 0.06 | 0.58 | 12.33 |
| 2 | H | 5 | 102 | 107 | 12.92 | 6.03 | 0.04 | | |
| 2 | H | 5 | 125 | 130 | 13.15 | 6.39 | 0.04 | 0.52 | 13.74 |
| 2 | H | 5 | 144 | 149 | 13.34 | 6.67 | 0.05 | 0.66 | 15.37 |
| 2 | H | 6 | 2 | 8 | 13.42 | 5.99 | 0.04 | 0.51 | 14.38 |
| 2 | H | 6 | 25 | 30 | 13.65 | 6.28 | 0.05 | 0.65 | 15.51 |
| 2 | H | 6 | 51 | 56 | 13.91 | 6.02 | 0.03 | 0.45 | 19.42 |
| 2 | H | 6 | 65 | 70 | 14.05 | 6.72 | 0.03 | 0.33 | 12.18 |
| 2 | H | 6 | 75 | 81 | 14.15 | 5.88 | 0.03 | 0.34 | 11.70 |
| 2 | H | 6 | 101 | 106 | 14.41 | 5.97 | 0.04 | 1.33 | 40.87 |
| 2 | H | 6 | 125 | 130 | 14.65 | 5.85 | 0.04 | 0.36 | 10.95 |
| 2 | H | 6 | 145 | 150 | 14.85 | 5.29 | 0.11 | 0.61 | 6.81 |

| Cor | T | Sct | Top cm | Bot cm | Depth mbsf | $\delta^{15}N$ ‰ Air | N wt % | Corg wt % | C/N |
|---|---|---|---|---|---|---|---|---|---|
| 2 | H | 7 | 3 | 9 | 14.93 | 5.91 | 0.05 | 0.74 | 17.02 |
| 3 | H | 1 | 3 | 8 | 15.43 | 5.57 | 0.09 | 1.11 | 14.03 |
| 3 | H | 1 | 60 | 65 | 16.00 | 5.61 | 0.08 | 1.29 | 18.99 |
| 3 | H | 1 | 110 | 115 | 16.50 | 5.12 | 0.05 | 0.65 | 15.28 |
| 3 | H | 2 | 3 | 8 | 16.93 | 5.03 | 0.05 | 0.52 | 12.71 |
| 3 | H | 2 | 57 | 63 | 17.47 | 5.16 | 0.05 | 0.52 | 11.61 |
| 3 | H | 2 | 65 | 70 | 17.55 | 4.57 | 0.05 | 0.52 | 12.74 |
| 3 | H | 2 | 110 | 115 | 18.00 | 5.70 | 0.05 | 0.52 | 12.48 |

## A3: Coulometric analysis of bulk sediment

| Core | Type | Section | Top cm | Bottom cm | Depth mbsf | TC (%C) wt % | TC (%CaCO$_3$) wt % | IC %c wt % | IC (%CaCO$_3$) wt % | % C$_{org}$ wt % |
|------|------|---------|--------|-----------|------------|--------------|---------------------|------------|---------------------|------------------|
| 1 | H | 1 | 2 | 6 | 0.02 | 10.80 | 89.95 | 10.28 | 85.63 | 0.52 |
| 1 | H | 1 | 25 | 30 | 0.25 | 10.77 | 89.71 | 10.14 | 84.46 | 0.63 |
| 1 | H | 1 | 35 | 39 | 0.35 | 10.97 | 91.35 | 10.21 | 85.07 | 0.75 |
| 1 | H | 1 | 50 | 53 | 0.5 | 10.78 | 89.82 | 10.37 | 86.39 | 0.41 |
| 1 | H | 1 | 65 | 69 | 0.65 | 10.53 | 87.67 | 10.26 | 85.48 | 0.26 |
| 1 | H | 1 | 78 | 80 | 0.78 | 10.79 | 89.89 | 10.39 | 86.55 | 0.40 |
| 1 | H | 1 | 102 | 107 | 1.02 | 10.80 | 89.99 | 10.46 | 87.13 | 0.34 |
| 1 | H | 1 | 125 | 130 | 1.25 | 10.87 | 90.56 | 10.29 | 85.72 | 0.58 |
| 1 | H | 1 | 140 | 144 | 1.4 | 10.81 | 90.05 | 10.35 | 86.25 | 0.46 |
| 1 | H | 2 | 2 | 7 | 1.52 | 10.74 | 89.48 | 10.32 | 85.92 | 0.43 |
| 1 | H | 2 | 25 | 30 | 1.75 | 10.77 | 89.68 | 10.44 | 86.97 | 0.33 |
| 1 | H | 2 | 35 | 39 | 1.85 | 10.95 | 91.20 | 10.26 | 85.47 | 0.69 |
| 1 | H | 2 | 50 | 55 | 2 | 10.93 | 91.01 | 10.37 | 86.38 | 0.56 |
| 1 | H | 2 | 65 | 70 | 2.15 | 11.02 | 91.79 | 10.45 | 87.04 | 0.57 |
| 1 | H | 2 | 72 | 75 | 2.22 | 10.93 | 91.07 | 10.40 | 86.63 | 0.53 |
| 1 | H | 2 | 101 | 106 | 2.51 | 11.07 | 92.23 | 10.44 | 87.00 | 0.63 |
| 1 | H | 2 | 125 | 130 | 2.75 | 11.09 | 92.36 | 10.30 | 85.83 | 0.78 |
| 1 | H | 2 | 145 | 150 | 2.95 | 11.10 | 92.43 | 10.41 | 86.67 | 0.69 |
| 1 | H | 3 | 2 | 7 | 3.02 | 11.17 | 93.06 | 10.47 | 87.22 | 0.70 |
| 1 | H | 3 | 25 | 30 | 3.25 | 11.22 | 93.46 | 10.34 | 86.12 | 0.88 |
| 1 | H | 3 | 46 | 49 | 3.46 | 11.20 | 93.27 | 10.29 | 85.70 | 0.91 |
| 1 | H | 3 | 72 | 75 | 3.72 | 11.06 | 92.11 | 10.37 | 86.38 | 0.69 |
| 1 | H | 3 | 96 | 100 | 3.96 | 11.11 | 92.54 | 10.31 | 85.88 | 0.80 |
| 1 | H | 3 | 125 | 130 | 4.25 | 11.23 | 93.56 | 10.38 | 86.47 | 0.85 |
| 1 | H | 3 | 141 | 146 | 4.41 | 11.13 | 92.69 | 10.12 | 84.27 | 1.01 |
| 1 | H | 4 | 2 | 7 | 4.52 | 11.16 | 92.99 | 10.26 | 85.48 | 0.90 |
| 1 | H | 4 | 25 | 30 | 4.75 | 11.22 | 93.46 | 10.18 | 84.80 | 1.04 |
| 1 | H | 4 | 50 | 55 | 5 | 11.18 | 93.13 | 10.33 | 86.02 | 0.85 |
| 1 | H | 4 | 65 | 70 | 5.15 | 11.21 | 93.37 | 10.28 | 85.60 | 0.93 |
| 1 | H | 4 | 78 | 83 | 5.28 | 11.24 | 93.66 | 10.22 | 85.13 | 1.02 |
| 1 | H | 4 | 102 | 107 | 5.52 | 11.07 | 92.22 | 10.12 | 84.33 | 0.95 |
| 1 | H | CC | 15 | 19 | 5.72 | 11.34 | 94.45 | 10.08 | 83.92 | 1.26 |
| 2 | H | 1 | 2 | 6 | 5.92 | 10.96 | 91.30 | 9.97 | 83.08 | 0.99 |
| 2 | H | 1 | 24 | 29 | 6.14 | 11.14 | 92.79 | 9.92 | 82.63 | 1.22 |
| 2 | H | 1 | 45 | 48 | 6.35 | 11.19 | 93.21 | 9.84 | 81.93 | 1.35 |
| 2 | H | 1 | 69 | 75 | 6.59 | 11.19 | 93.19 | 9.90 | 82.43 | 1.29 |
| 2 | H | 1 | 100 | 103 | 6.9 | 11.15 | 92.89 | 9.97 | 83.08 | 1.18 |
| 2 | H | 1 | 125 | 130 | 7.15 | 11.33 | 94.36 | 10.16 | 84.66 | 1.17 |
| 2 | H | 1 | 145 | 150 | 7.35 | 11.35 | 94.55 | 10.14 | 84.47 | 1.21 |
| 2 | H | 2 | 2 | 7 | 7.42 | 11.44 | 95.29 | 10.15 | 84.55 | 1.29 |
| 2 | H | 2 | 25 | 30 | 7.65 | 11.57 | 96.39 | 10.29 | 85.68 | 1.29 |
| 2 | H | 2 | 50 | 55 | 7.9 | 11.63 | 96.90 | 10.37 | 86.38 | 1.26 |

| Core | Type | Section | Top cm | Bottom cm | Depth mbsf | TC (%C) wt % | TC (%CaCO$_3$) wt % | IC %c wt % | IC (%CaCO$_3$) wt % | % C$_{org}$ wt % |
|------|------|---------|--------|-----------|------------|--------------|---------------------|------------|---------------------|------------------|
| 2 | H | 2 | 65 | 70 | 8.05 | 11.55 | 96.21 | 10.37 | 86.38 | 1.18 |
| 2 | H | 2 | 70 | 75 | 8.1 | 11.47 | 95.54 | 10.45 | 87.04 | 1.02 |
| 2 | H | 2 | 85 | 89 | 8.25 | 11.68 | 97.33 | 10.49 | 87.37 | 1.20 |
| 2 | H | 2 | 101 | 107 | 8.41 | 11.77 | 98.07 | 10.75 | 89.53 | 1.02 |
| 2 | H | 2 | 120 | 124 | 8.6 | 11.74 | 97.80 | 10.74 | 89.50 | 1.00 |
| 2 | H | 2 | 139 | 144 | 8.79 | 11.50 | 95.76 | | | |
| 2 | H | 3 | 2 | 7 | 8.92 | 11.52 | 95.93 | 10.85 | 90.36 | 0.67 |
| 2 | H | 3 | 25 | 30 | 9.15 | 11.37 | 94.74 | 10.88 | 90.66 | 0.49 |
| 2 | H | 3 | 37 | 41 | 9.27 | 11.52 | 95.98 | 10.62 | 88.50 | |
| 2 | H | 3 | 50 | 55 | 9.4 | 11.47 | 95.51 | 10.97 | 91.40 | 0.49 |
| 2 | H | 3 | 70 | 75 | 9.6 | 11.45 | 95.35 | 11.28 | 93.96 | 0.17 |
| 2 | H | 3 | 101 | 106 | 9.91 | 11.44 | 95.32 | 11.12 | 92.63 | 0.32 |
| 2 | H | 3 | 122 | 128 | 10.12 | 11.17 | 93.02 | 10.65 | 88.71 | 0.52 |
| 2 | H | 3 | 144 | 150 | 10.34 | 11.61 | 96.69 | 11.06 | 92.13 | 0.55 |
| 2 | H | 4 | 2 | 7 | 10.42 | 11.50 | 95.77 | 10.97 | 91.41 | 0.52 |
| 2 | H | 4 | 23 | 28 | 10.63 | 11.52 | 95.97 | 10.99 | 91.51 | 0.54 |
| 2 | H | 4 | 50 | 55 | 10.9 | 11.57 | 96.39 | 10.95 | 91.21 | 0.62 |
| 2 | H | 4 | 65 | 70 | 11.05 | 11.53 | 96.05 | 10.98 | 91.50 | 0.55 |
| 2 | H | 4 | 77 | 82 | 11.17 | 11.65 | 97.07 | 11.02 | 91.80 | 0.63 |
| 2 | H | 4 | 101 | 106 | 11.41 | 11.48 | 95.66 | 10.97 | 91.38 | 0.51 |
| 2 | H | 4 | 125 | 130 | 11.65 | 11.61 | 96.73 | 11.00 | 91.59 | 0.62 |
| 2 | H | 4 | 137 | 142 | 11.77 | 11.63 | 96.85 | 10.96 | 91.30 | 0.67 |
| 2 | H | 5 | 2 | 5 | 11.92 | 11.57 | 96.39 | 11.05 | 92.05 | 0.52 |
| 2 | H | 5 | 25 | 30 | 12.15 | 11.62 | 96.82 | 10.87 | 90.55 | 0.75 |
| 2 | H | 5 | 51 | 56 | 12.41 | 11.64 | 96.98 | 11.05 | 92.00 | 0.60 |
| 2 | H | 5 | 70 | 76 | 12.6 | 11.62 | 96.81 | 11.04 | 91.97 | 0.58 |
| 2 | H | 5 | 102 | 107 | 12.92 | 11.56 | 96.32 | | | |
| 2 | H | 5 | 125 | 130 | 13.15 | 11.54 | 96.16 | 11.03 | 91.84 | 0.52 |
| 2 | H | 5 | 144 | 149 | 13.34 | 11.62 | 96.78 | 10.96 | 91.30 | 0.66 |
| 2 | H | 6 | 2 | 8 | 13.42 | 11.51 | 95.85 | 11.00 | 91.64 | 0.51 |
| 2 | H | 6 | 25 | 30 | 13.65 | 11.57 | 96.37 | 10.92 | 90.94 | 0.65 |
| 2 | H | 6 | 51 | 56 | 13.91 | 11.46 | 95.44 | 11.01 | 91.70 | 0.45 |
| 2 | H | 6 | 65 | 70 | 14.05 | 11.37 | 94.69 | 11.03 | 91.90 | 0.33 |
| 2 | H | 6 | 75 | 81 | 14.15 | 11.32 | 94.33 | 10.98 | 91.49 | 0.34 |
| 2 | H | 6 | 101 | 106 | 14.41 | 11.49 | 95.71 | 10.16 | 84.62 | 1.33 |
| 2 | H | 6 | 125 | 130 | 14.65 | 11.41 | 95.03 | 11.05 | 92.05 | 0.36 |
| 2 | H | 6 | 145 | 150 | 14.85 | 11.45 | 95.35 | 10.83 | 90.24 | 0.61 |
| 2 | H | 7 | 3 | 9 | 14.93 | 11.50 | 95.80 | 10.76 | 89.60 | 0.74 |
| 3 | H | 1 | 3 | 8 | 15.43 | 11.39 | 94.90 | 10.29 | 85.69 | 1.11 |
| 3 | H | 1 | 60 | 65 | 16 | 11.50 | 95.81 | 10.22 | 85.10 | 1.29 |
| 3 | H | 1 | 110 | 115 | 16.5 | 11.58 | 96.48 | 10.93 | 91.03 | 0.65 |
| 3 | H | 2 | 3 | 8 | 16.93 | 11.49 | 95.69 | 10.96 | 91.33 | 0.52 |
| 3 | H | 2 | 57 | 63 | 17.47 | 11.45 | 95.42 | 10.94 | 91.11 | 0.52 |
| 3 | H | 2 | 65 | 70 | 17.55 | 11.35 | 94.53 | 10.82 | 90.16 | 0.52 |
| 3 | H | 2 | 110 | 115 | 18 | 11.47 | 95.51 | 10.94 | 91.15 | 0.52 |

## A4: XRF analysis on surface of core archive half

| Depth mbsf | K cps | Ca cps | Ti cps | Mn cps | Fe cps | Cu cps | Sr cps |
|---|---|---|---|---|---|---|---|
| 0.06 | 119.6 | 8515.4 | 1.8 | 6.9 | 104.9 | 11.8 | 234.2 |
| 0.08 | 139.6 | 9365.4 | 0 | 5.1 | 105.6 | 12.7 | 238 |
| 0.1 | 127.3 | 8871.1 | 2.1 | 5.9 | 102.7 | 19.9 | 232.6 |
| 0.12 | 142.4 | 9759.8 | 1.6 | 6 | 120.1 | 26.5 | 235.4 |
| 0.14 | 138.7 | 9746.6 | 0 | 13.7 | 119.2 | 12 | 245.9 |
| 0.16 | 132.5 | 9464.6 | 3.7 | 11.9 | 117.5 | 14.7 | 230.3 |
| 0.18 | 112.6 | 7822.2 | 2.1 | 7.4 | 108.3 | 15.3 | 232.5 |
| 0.2 | 122.7 | 9056.3 | 2.9 | 0 | 109.4 | 22.7 | 226.7 |
| 0.22 | 141.1 | 9869.3 | 2.1 | 2.3 | 132.2 | 17.5 | 246.4 |
| 0.24 | 125.3 | 9317.7 | 6 | 8.2 | 121.1 | 15.3 | 254.2 |
| 0.26 | 136.3 | 9914.7 | 1.8 | 6.4 | 131.7 | 16.2 | 232.8 |
| 0.28 | 143.5 | 10187.5 | 2.9 | 12.1 | 164.6 | 30 | 241.5 |
| 0.3 | 148.6 | 9983.3 | 3 | 5.8 | 129.4 | 24.4 | 234.8 |
| 0.32 | 136.1 | 9644.6 | 1.4 | 8.9 | 153.8 | 17.5 | 236 |
| 0.34 | 127.1 | 9836 | 3.5 | 6.7 | 121.8 | 22.1 | 240.6 |
| 0.36 | 125.6 | 9642.8 | 3.6 | 3.7 | 123.7 | 20.9 | 244.1 |
| 0.38 | 124.8 | 9174.7 | 3.2 | 6.7 | 121.9 | 14.9 | 222.7 |
| 0.4 | 111.8 | 8701 | 1.8 | 9.8 | 122.4 | 10.6 | 223.3 |
| 0.42 | 117 | 7760.9 | 2.6 | 7.1 | 121.5 | 36.1 | 230.5 |
| 0.44 | 153.7 | 10148.5 | 1.4 | 15.8 | 180.8 | 32.6 | 236.9 |
| 0.46 | 141.2 | 9813.8 | 4.2 | 6.5 | 173.4 | 25.7 | 243.7 |
| 0.48 | 126.8 | 8751.4 | 2.2 | 8.2 | 130.3 | 18.3 | 248.3 |
| 0.5 | 95.5 | 7565.1 | 1.5 | 3.4 | 109.5 | 22.8 | 214.7 |
| 0.52 | 114.9 | 9262 | 2.7 | 6.6 | 125.7 | 15.9 | 243.7 |
| 0.54 | 114.4 | 8281.3 | 3.2 | 3.7 | 132.4 | 10.3 | 226.1 |
| 0.56 | 133 | 9470.6 | 0 | 9.3 | 139.9 | 13.7 | 237.3 |
| 0.58 | 119.3 | 8865.1 | 4.1 | 3.4 | 134.7 | 26.1 | 236.1 |
| 0.6 | 125.6 | 8540.6 | 2.6 | 7.5 | 128.4 | 22.5 | 242.2 |
| 0.62 | 129.7 | 9658.8 | 1.8 | 6.5 | 129.7 | 19.9 | 224.8 |
| 0.64 | 143.6 | 10322.3 | 2.4 | 9.8 | 145.9 | 22.5 | 255.8 |
| 0.66 | 120.9 | 9117.9 | 1.9 | 7.8 | 125.6 | 23.3 | 231.4 |
| 0.68 | 142.5 | 9827.8 | 2.3 | 0 | 127.2 | 46 | 238.8 |
| 0.7 | 134.8 | 10018.1 | 2 | 14.4 | 170 | 24.4 | 248.3 |
| 0.72 | 120.2 | 9480.9 | 0 | 4.2 | 116.5 | 13.7 | 227.3 |
| 0.74 | 121.7 | 9466.4 | 5 | 7.2 | 123.2 | 17 | 230.6 |
| 0.76 | 137.2 | 9816.3 | 1.9 | 11.2 | 139.3 | 11.8 | 236.3 |
| 0.78 | 122.4 | 8899.9 | 3.3 | 5.7 | 114 | 30.8 | 234.1 |
| 0.8 | 134.9 | 9761.1 | 3.7 | 13 | 158.9 | 9.4 | 241 |
| 0.82 | 133.3 | 9788.4 | 0 | 6 | 132.8 | 19.9 | 244.3 |
| 0.84 | 133.3 | 9677.1 | 2.6 | 7.2 | 130.8 | 18.7 | 243.7 |
| 0.86 | 129.9 | 9452.4 | 2.7 | 2.9 | 126.1 | 14.7 | 232.7 |
| 0.88 | 121 | 9437.6 | 2.6 | 15.7 | 161.9 | 12.3 | 235.9 |

| Depth | K | Ca | Ti | Mn | Fe | Cu | Sr |
|-------|------|--------|------|------|-------|------|-------|
| mbsf | cps | cps | cps | cps | cps | cps | cps |
| 0.9 | 121.6 | 8831.2 | 5 | 9.7 | 129.5 | 15.7 | 228.6 |
| 0.92 | 127.9 | 9577.1 | 2.8 | 8.6 | 134.5 | 18.1 | 241.3 |
| 0.94 | 122.8 | 9237.2 | 2.7 | 3.2 | 135.1 | 18.2 | 248.4 |
| 0.96 | 130 | 9639.6 | 1.8 | 8.7 | 134.8 | 16.4 | 227 |
| 0.98 | 126.9 | 9618.1 | 3.9 | 5.5 | 136.1 | 15.4 | 243 |
| 1 | 134 | 9377.8 | 1.8 | 6.8 | 122.8 | 11.4 | 234.6 |
| 1.02 | 118.7 | 9536.1 | 3.7 | 10.1 | 153.1 | 23.3 | 231.6 |
| 1.04 | 134.3 | 9988.7 | 6.1 | 7.4 | 157.4 | 18.3 | 252.7 |
| 1.06 | 134.5 | 9689.1 | 4.5 | 2.8 | 130.2 | 10.9 | 223.4 |
| 1.08 | 127.5 | 9197.1 | 3.5 | 8.5 | 136.5 | 22.1 | 240.4 |
| 1.1 | 131.3 | 9510.4 | 4.5 | 9.4 | 138.9 | 19.7 | 223.7 |
| 1.12 | 143.5 | 10327.4 | 5.1 | 16.6 | 179.7 | 25.1 | 246.8 |
| 1.14 | 132.8 | 10196.8 | 3.3 | 3.7 | 147.2 | 18.7 | 239.9 |
| 1.16 | 138.5 | 9931.7 | 0 | 5.6 | 133.7 | 20.3 | 241.3 |
| 1.18 | 140 | 9962.1 | 6 | 9.7 | 151.6 | 21 | 231.6 |
| 1.2 | 127.7 | 9988.5 | 0 | 10.4 | 145.5 | 19.1 | 249.4 |
| 1.22 | 122.7 | 10320.9 | 3.9 | 8.8 | 138.4 | 17.9 | 238.1 |
| 1.24 | 148.5 | 10527.4 | 4.5 | 7.6 | 142.7 | 19.1 | 250.9 |
| 1.26 | 133.1 | 10651.6 | 5.4 | 13.9 | 189.7 | 24.9 | 248.4 |
| 1.28 | 137.2 | 10272.2 | 0 | 9.5 | 138 | 24.1 | 232.8 |
| 1.3 | 119.2 | 8623.4 | 0 | 5.1 | 138.2 | 16 | 246.5 |
| 1.32 | 120.3 | 8582.2 | 5.3 | 5.4 | 130 | 6.3 | 216.1 |
| 1.34 | 134 | 10100.8 | 4.2 | 5.6 | 146.9 | 13.1 | 241.4 |
| 1.36 | 142.4 | 10597.3 | 1.9 | 6.2 | 151.1 | 17.6 | 239.8 |
| 1.38 | 138.5 | 10216.9 | 2 | 12.4 | 191.1 | 22.6 | 223.8 |
| 1.4 | 162.7 | 11719.8 | 3.7 | 17.5 | 228.2 | 26.8 | 267.9 |
| 1.42 | 161.2 | 11502.4 | 5.9 | 8 | 171.1 | 30.9 | 263 |
| 1.52 | 133.3 | 9910.6 | 2.9 | 9.5 | 160.1 | 26.3 | 243.9 |
| 1.54 | 130.5 | 9223.4 | 0 | 6.2 | 147.8 | 17.5 | 238.5 |
| 1.56 | 129.2 | 8467.5 | 2.3 | 6.4 | 157.8 | 26.8 | 239.1 |
| 1.58 | 122.9 | 9294.5 | 3.1 | 7.7 | 157.3 | 10.8 | 250.8 |
| 1.6 | 139.6 | 10315.8 | 5 | 11.3 | 182.8 | 15.3 | 240.9 |
| 1.62 | 121.6 | 10213.5 | 2.9 | 17.2 | 186.4 | 17.2 | 240.4 |
| 1.64 | 131.3 | 10271.2 | 0 | 4.6 | 158.2 | 18.4 | 239.9 |
| 1.66 | 132.6 | 10079 | 4.7 | 9.9 | 156.2 | 14.3 | 229.5 |
| 1.68 | 100 | 7470 | 2.6 | 20.9 | 146.9 | 12.6 | 226.4 |
| 1.7 | 136.7 | 10217.2 | 3.1 | 7.3 | 176.8 | 23.4 | 250.1 |
| 1.72 | 142.5 | 10170.9 | 1.7 | 13.7 | 213.7 | 27.3 | 224.6 |
| 1.74 | 147.2 | 10322 | 1.6 | 5.6 | 179.2 | 14.8 | 242.7 |
| 1.76 | 136 | 10307.8 | 4.1 | 9.7 | 167.3 | 24.3 | 234.7 |
| 1.78 | 133 | 9692.1 | 4.5 | 9 | 172.3 | 14.9 | 223 |
| 1.8 | 124.5 | 10302.4 | 2.2 | 16 | 215.2 | 21.1 | 250 |
| 1.82 | 131.2 | 10162.2 | 2.9 | 11.8 | 209.6 | 21.6 | 234.8 |
| 1.84 | 132.6 | 9841.2 | 2.7 | 10.4 | 171.9 | 19.8 | 245.6 |
| 1.86 | 131.6 | 9248.6 | 5 | 6.3 | 172.4 | 22.2 | 230.1 |
| 1.88 | 139.1 | 10052 | 2.7 | 6.8 | 187.7 | 23.4 | 243.6 |
| 1.9 | 118.5 | 8758.4 | 6 | 7.1 | 178.9 | 27 | 228.3 |

| Depth | K | Ca | Ti | Mn | Fe | Cu | Sr |
|-------|-----|-----|-----|-----|-----|-----|-----|
| mbsf | cps | cps | cps | cps | cps | cps | cps |
| 1.92 | 131.7 | 9068.8 | 2.7 | 7.8 | 207.4 | 27.9 | 227.4 |
| 1.94 | 129.8 | 9143.5 | 1.8 | 15.9 | 209.2 | 31.2 | 232.5 |
| 1.96 | 134.9 | 9956.8 | 6.4 | 9.3 | 209.5 | 33.7 | 234.9 |
| 1.98 | 141.3 | 9680.1 | 2.9 | 7.7 | 207.8 | 34.7 | 234.6 |
| 2 | 108.8 | 8533.2 | 2.6 | 8.7 | 189.3 | 13.1 | 233.2 |
| 2.02 | 131.6 | 9852.8 | 1.5 | 6.6 | 187.2 | 16.1 | 230.4 |
| 2.04 | 120.7 | 9432.7 | 1.7 | 8.5 | 188 | 24.3 | 225.7 |
| 2.06 | 130.8 | 9908.4 | 3.2 | 7.6 | 230.1 | 26.1 | 238.8 |
| 2.08 | 134.7 | 10167.8 | 0 | 9.5 | 230.1 | 29.1 | 242.5 |
| 2.1 | 130.8 | 9307.4 | 0 | 3.2 | 217.7 | 25.2 | 237 |
| 2.12 | 141.1 | 10804.7 | 2.9 | 12.2 | 253.7 | 28.3 | 238.6 |
| 2.14 | 151.9 | 11203.1 | 1.8 | 4.2 | 247.5 | 41.8 | 244.2 |
| 2.16 | 152.7 | 10628.4 | 3.1 | 14.7 | 278.8 | 23.3 | 225.7 |
| 2.18 | 150.2 | 10757.2 | 7.5 | 6.2 | 276.1 | 19.6 | 229.5 |
| 2.2 | 142.9 | 10817.8 | 2.2 | 5.6 | 247.1 | 19.3 | 232.2 |
| 2.22 | 152.5 | 10842.2 | 0 | 10.2 | 282.7 | 28.6 | 238.6 |
| 2.24 | 151.1 | 11472.9 | 5.3 | 17.1 | 236.3 | 20.3 | 261.8 |
| 2.26 | 132.8 | 10677 | 4.8 | 0 | 204.6 | 23.8 | 241.6 |
| 2.28 | 152.5 | 11192.9 | 0 | 11.3 | 266.8 | 22.2 | 242.2 |
| 2.3 | 144.7 | 10441.3 | 4.5 | 5.7 | 259.7 | 23.9 | 226.8 |
| 2.32 | 132.4 | 9747.9 | 4.5 | 5.4 | 219.1 | 39 | 229.3 |
| 2.34 | 149 | 11144.3 | 5.7 | 18.9 | 280.1 | 17.8 | 235.2 |
| 2.36 | 128.9 | 9300.4 | 5.7 | 8 | 254.3 | 17.5 | 203.4 |
| 2.38 | 141.4 | 9972.7 | 4.4 | 9 | 266.2 | 16.4 | 230.3 |
| 2.4 | 128.1 | 9429.4 | 2.3 | 13.8 | 271.4 | 17.5 | 229.6 |
| 2.42 | 133.8 | 9090.2 | 0 | 8.7 | 259.5 | 23.4 | 223.3 |
| 2.44 | 146.9 | 9620.2 | 0 | 8.4 | 270.5 | 29.8 | 223.2 |
| 2.46 | 118.8 | 8543.8 | 5.8 | 7.7 | 243.1 | 37.9 | 212.1 |
| 2.48 | 135.1 | 10100.1 | 2.9 | 3.6 | 255.9 | 23.6 | 233.1 |
| 2.5 | 143.9 | 9533.4 | 2.4 | 13.2 | 251 | 11.5 | 223.8 |
| 2.52 | 124.1 | 8883.2 | 1.9 | 8.9 | 251.7 | 4.5 | 229.3 |
| 2.54 | 141.7 | 9842.5 | 3 | 6.8 | 257.8 | 25.9 | 210.5 |
| 2.56 | 137.4 | 9917.3 | 0 | 6.6 | 262.5 | 20.5 | 224.1 |
| 2.58 | 150.7 | 10021.4 | 5.1 | 10.5 | 249.2 | 22.7 | 230.9 |
| 2.6 | 144 | 10076.9 | 1.9 | 11.4 | 307.1 | 28.5 | 229.6 |
| 2.62 | 147.7 | 10478 | 3.1 | 4.7 | 251.5 | 24 | 240.2 |
| 2.64 | 152.2 | 10666.6 | 3.5 | 9.9 | 260.6 | 31 | 227.9 |
| 2.66 | 149.8 | 10697.9 | 5.8 | 6.5 | 225.9 | 23.4 | 221.1 |
| 2.68 | 142.8 | 10004.3 | 2.4 | 9.4 | 248.2 | 19.9 | 223.4 |
| 2.7 | 139.7 | 10009.2 | 2 | 4.9 | 265.1 | 20.6 | 221.4 |
| 2.72 | 156.4 | 10878.7 | 4.3 | 8.1 | 292.3 | 20.5 | 241.7 |
| 2.74 | 142.5 | 10797.8 | 0 | 8.4 | 259.9 | 19.7 | 223.2 |
| 2.76 | 128.7 | 10057.7 | 5.7 | 8.3 | 231.1 | 22.9 | 218.3 |
| 2.78 | 136.2 | 10196.7 | 0 | 10.4 | 284.5 | 18.7 | 214.5 |
| 2.8 | 149.3 | 10517.6 | 1.7 | 4.3 | 262.8 | 33.7 | 219.7 |
| 2.82 | 139.7 | 10233.7 | 4.2 | 6.7 | 275.7 | 17 | 224.7 |
| 2.84 | 151.7 | 10777.7 | 4.9 | 18.6 | 309.6 | 15 | 224.9 |

| Depth | K | Ca | Ti | Mn | Fe | Cu | Sr |
| mbsf | cps | cps | cps | cps | cps | cps | cps |
|---|---|---|---|---|---|---|---|
| 2.86 | 150.8 | 10334.2 | 3.8 | 7.1 | 258.4 | 5.3 | 222.8 |
| 2.88 | 149.7 | 10473.9 | 4.4 | 3.2 | 277.7 | 30.8 | 228 |
| 2.9 | 151 | 10478.1 | 5.6 | 6.2 | 279.1 | 18.8 | 228.4 |
| 2.92 | 140.3 | 10304.3 | 5.1 | 5.5 | 248.6 | 16.4 | 220.3 |
| 2.94 | 144.6 | 10508.1 | 6.8 | 6.3 | 266.8 | 34.5 | 230.9 |
| 2.96 | 152.6 | 10815.7 | 3.8 | 9.3 | 272.2 | 18.7 | 229.9 |
| 2.98 | 141.6 | 9827.2 | 5.9 | 13.5 | 289.9 | 15.7 | 228.6 |
| 3.04 | 157.5 | 9888.4 | 6 | 7.8 | 333.8 | 26.3 | 216.5 |
| 3.06 | 127.5 | 10065.4 | 3.1 | 31 | 317 | 43.6 | 221.3 |
| 3.08 | 144.4 | 10345 | 5.5 | 12.4 | 264.3 | 15 | 228.8 |
| 3.1 | 157.5 | 10373.6 | 2.7 | 11.8 | 260.4 | 19.5 | 211.5 |
| 3.12 | 146.9 | 10499.1 | 1.9 | 12.2 | 296.1 | 18.3 | 219.5 |
| 3.14 | 148 | 10794.4 | 0 | 17.5 | 309.9 | 49.5 | 223.1 |
| 3.16 | 161.8 | 10966.1 | 1.8 | 8.1 | 271.6 | 15.8 | 241.4 |
| 3.18 | 145.4 | 10331.7 | 5 | 2.9 | 280 | 23.5 | 218.4 |
| 3.2 | 145.9 | 10570.6 | 0 | 7 | 282.1 | 16.1 | 226.5 |
| 3.22 | 151.4 | 10371.3 | 3.2 | 7.1 | 303.9 | 28.7 | 222.6 |
| 3.24 | 160.7 | 10912.6 | 2.9 | 12.9 | 339.9 | 17.6 | 231 |
| 3.26 | 156.2 | 10333.2 | 6.9 | 16.4 | 297.5 | 10.9 | 211.5 |
| 3.28 | 158.2 | 10968.9 | 6.8 | 8.3 | 292 | 30.9 | 217.5 |
| 3.3 | 155.8 | 10212 | 4.5 | 6.6 | 267.6 | 17.7 | 222 |
| 3.32 | 144.5 | 10358.3 | 4.3 | 14.2 | 344.9 | 29 | 215.6 |
| 3.34 | 155.7 | 10455.6 | 0 | 9.4 | 308.2 | 16.3 | 216.2 |
| 3.36 | 138.7 | 9902.9 | 3.7 | 13.2 | 245.9 | 22.9 | 210 |
| 3.38 | 164.9 | 10095.2 | 2.6 | 10.7 | 311.9 | 21 | 222.5 |
| 3.4 | 135.8 | 9940 | 0 | 4.7 | 287.8 | 25.5 | 220.9 |
| 3.42 | 140 | 9727.9 | 0 | 6.2 | 269.7 | 21.3 | 227.2 |
| 3.44 | 143.1 | 10246.3 | 2.5 | 8.2 | 288.2 | 26.7 | 220.6 |
| 3.46 | 140.4 | 9760.6 | 3.2 | 15.5 | 265.8 | 22.2 | 221.3 |
| 3.48 | 142.9 | 10388.9 | 6.9 | 5.4 | 273 | 22.7 | 223.3 |
| 3.5 | 151.5 | 10256.9 | 0 | 4.5 | 292.5 | 21.2 | 222.3 |
| 3.52 | 139 | 9793.7 | 0 | 10.1 | 302 | 27.2 | 207.8 |
| 3.54 | 159.5 | 10668.5 | 2.3 | 6.3 | 309.5 | 21.8 | 225.9 |
| 3.56 | 147.3 | 10362.5 | 3.3 | 12.5 | 287.8 | 25.7 | 217.8 |
| 3.58 | 149.3 | 10483.3 | 0 | 7.5 | 271.2 | 12.8 | 238.3 |
| 3.6 | 145 | 10141.8 | 6.6 | 7.6 | 270.7 | 18.8 | 220.7 |
| 3.62 | 149.3 | 10553 | 2.9 | 6 | 287.8 | 18 | 222.7 |
| 3.64 | 154.2 | 9867.5 | 4.8 | 5.5 | 313.7 | 19.1 | 212.7 |
| 3.66 | 163.9 | 10804.7 | 0 | 8.7 | 316.4 | 22.5 | 228.8 |
| 3.68 | 147.1 | 10441.3 | 5.1 | 13.4 | 298.7 | 19.7 | 214.9 |
| 3.7 | 154.7 | 9943.5 | 6.4 | 15 | 310 | 19 | 205.3 |
| 3.72 | 151.3 | 10238.1 | 6.5 | 7 | 313.7 | 15.7 | 226.9 |
| 3.74 | 154 | 10372.3 | 3.3 | 16.8 | 366.5 | 15.7 | 216.3 |
| 3.76 | 146.3 | 10378.8 | 1.9 | 8.5 | 286.4 | 33.6 | 215.5 |
| 3.78 | 147.4 | 10299.5 | 3.4 | 12 | 314.4 | 17 | 210.1 |
| 3.8 | 151.4 | 9810.2 | 4.4 | 8.7 | 285.5 | 25 | 208.5 |
| 3.82 | 153.7 | 10412.5 | 4.5 | 14 | 316.9 | 19.7 | 224.6 |

| Depth | K | Ca | Ti | Mn | Fe | Cu | Sr |
| mbsf | cps | cps | cps | cps | cps | cps | cps |
| --- | --- | --- | --- | --- | --- | --- | --- |
| 3.84 | 153.3 | 9461.5 | 0 | 9 | 301.7 | 17.2 | 214.2 |
| 3.86 | 152.8 | 10403.7 | 2.6 | 8.2 | 294 | 19.6 | 218 |
| 3.88 | 158.3 | 10626.9 | 4.6 | 4.9 | 314.5 | 17.4 | 217.9 |
| 3.9 | 137.5 | 9415.2 | 3.7 | 7.1 | 303.8 | 18.8 | 210.1 |
| 3.92 | 152.9 | 10204.9 | 3.4 | 17 | 356.7 | 18.4 | 207 |
| 3.94 | 152.2 | 10299.5 | 2 | 8.2 | 297.5 | 13.9 | 219.8 |
| 3.96 | 148.2 | 10055.8 | 3.2 | 8.1 | 286.5 | 19.2 | 203.6 |
| 3.98 | 155.5 | 10296.2 | 4 | 8.4 | 328.4 | 26 | 213.8 |
| 4 | 145.1 | 9283.3 | 0 | 8.2 | 324.8 | 28.1 | 208.5 |
| 4.02 | 134.3 | 9736.2 | 3.9 | 11.5 | 322.2 | 16.2 | 217.3 |
| 4.04 | 143.6 | 9244.5 | 6.1 | 10.1 | 295.9 | 12.1 | 204.5 |
| 4.06 | 130.7 | 9726.7 | 3 | 2.9 | 290.8 | 24.4 | 214.3 |
| 4.08 | 173.8 | 10041.9 | 6.2 | 9.2 | 299.3 | 17.2 | 224.5 |
| 4.1 | 142.3 | 9907.5 | 0 | 9.4 | 318.9 | 38.9 | 212.3 |
| 4.12 | 142.6 | 9644.3 | 5 | 7.9 | 307.7 | 16.4 | 214.1 |
| 4.14 | 152.6 | 10366.5 | 7.3 | 8 | 320.7 | 15.4 | 210.6 |
| 4.16 | 150.9 | 10734.9 | 2.1 | 9.3 | 309.6 | 14.2 | 222.6 |
| 4.18 | 145.4 | 9455.7 | 0 | 5.2 | 311.1 | 17.3 | 207.3 |
| 4.2 | 146.4 | 10064.3 | 2.3 | 5.4 | 317.8 | 13.9 | 208.5 |
| 4.22 | 137.9 | 10062.7 | 5.3 | 9.4 | 318.3 | 20.9 | 210.2 |
| 4.24 | 158.8 | 10317.9 | 0 | 12.9 | 323.9 | 31.8 | 214.8 |
| 4.26 | 161.5 | 10744.1 | 5.1 | 45.8 | 394.7 | 21 | 218.4 |
| 4.28 | 143.4 | 10164 | 6.4 | 6.1 | 312.8 | 21 | 227.5 |
| 4.3 | 141.5 | 9777.1 | 4.9 | 8.6 | 307.6 | 20 | 197.6 |
| 4.32 | 145.2 | 9275.6 | 5.4 | 7.4 | 310.8 | 13.3 | 202.1 |
| 4.34 | 147.9 | 10240.9 | 3.4 | 10.7 | 310.6 | 27.7 | 206.9 |
| 4.36 | 145.2 | 9750.9 | 0 | 7.5 | 318.3 | 12.6 | 204.7 |
| 4.38 | 147 | 10384.2 | 5.4 | 8.5 | 317.9 | 14.8 | 219.1 |
| 4.4 | 142.6 | 10526.9 | 4.5 | 4.7 | 313.9 | 16.4 | 218.4 |
| 4.54 | 160.8 | 10064.1 | 3.1 | 8.9 | 323.5 | 10.7 | 215.6 |
| 4.56 | 152.9 | 9960.4 | 3.5 | 9 | 301.8 | 14.6 | 209.3 |
| 4.58 | 149.9 | 9338.6 | 1.5 | 10.9 | 310.7 | 19.7 | 220.2 |
| 4.6 | 148.9 | 9500.1 | 6.7 | 7 | 300.6 | 17.9 | 223.2 |
| 4.62 | 152.3 | 9321.3 | 2.5 | 8.1 | 319.2 | 14.2 | 210.6 |
| 4.64 | 151.2 | 9453.7 | 5.7 | 8.4 | 311.3 | 18.9 | 213.5 |
| 4.66 | 161.3 | 10189.1 | 3.7 | 4.4 | 357.1 | 14 | 215 |
| 4.68 | 146.7 | 9265.3 | 3.5 | 8.8 | 313.1 | 15.1 | 197.4 |
| 4.7 | 147.6 | 10028.5 | 5.4 | 6.7 | 327.2 | 10.5 | 207.6 |
| 4.72 | 156.4 | 10245.2 | 4.5 | 18.6 | 372.2 | 17.8 | 201.2 |
| 4.74 | 150.8 | 10115 | 6.1 | 4.7 | 333.5 | 23.9 | 211.7 |
| 4.76 | 153.1 | 9828.5 | 6.4 | 5.8 | 327 | 39.1 | 210.2 |
| 4.78 | 154 | 10275.6 | 6.3 | 5.2 | 337.7 | 20.1 | 216.2 |
| 4.8 | 157.6 | 10352.7 | 8.8 | 5.3 | 311.7 | 15.1 | 219.1 |
| 4.82 | 152.6 | 10255.5 | 4.3 | 15.1 | 365.5 | 32.6 | 219.2 |
| 4.84 | 151.2 | 10219.3 | 7.6 | 7.2 | 342.2 | 37.7 | 196.8 |
| 4.86 | 142.3 | 9430.1 | 7.9 | 5.8 | 323.7 | 11.3 | 205.9 |
| 4.88 | 144.4 | 9429.2 | 3.4 | 14.5 | 330.9 | 13.6 | 198 |

| Depth | K | Ca | Ti | Mn | Fe | Cu | Sr |
|---|---|---|---|---|---|---|---|
| mbsf | cps | cps | cps | cps | cps | cps | cps |
| 4.9 | 150.4 | 10228.7 | 5.1 | 12.2 | 335.6 | 15.1 | 207.9 |
| 4.92 | 152.6 | 10469.5 | 1.9 | 21.2 | 374.9 | 15.6 | 200 |
| 4.94 | 149.7 | 10511.3 | 2.3 | 8.5 | 329.8 | 35.1 | 209.3 |
| 4.96 | 165 | 10842.5 | 3.5 | 13.5 | 328.1 | 21.7 | 219.5 |
| 4.98 | 152.4 | 10572 | 5.8 | 9.5 | 305.3 | 18.1 | 211.1 |
| 5 | 162.3 | 10677.1 | 5.6 | 10.9 | 329.9 | 19.9 | 212.7 |
| 5.02 | 148.7 | 10491.3 | 0 | 13.7 | 364.3 | 15.5 | 208.6 |
| 5.04 | 151.9 | 10099.6 | 2 | 7.9 | 298 | 17.6 | 204.9 |
| 5.06 | 151.9 | 10426.5 | 4.4 | 15.9 | 383 | 23.8 | 211.6 |
| 5.08 | 148.3 | 10583.5 | 4 | 9.7 | 317.3 | 27.3 | 197.8 |
| 5.1 | 149.5 | 10242.1 | 2.7 | 9.6 | 358.1 | 24.3 | 198.8 |
| 5.12 | 157.9 | 10387.2 | 3.2 | 8.8 | 350.9 | 23.7 | 214.9 |
| 5.14 | 155.2 | 9747.2 | 3.4 | 10 | 314.2 | 24.9 | 192.1 |
| 5.16 | 156.6 | 10681.4 | 5.3 | 10.1 | 311.9 | 13.3 | 205.6 |
| 5.18 | 159.6 | 10605.2 | 7.1 | 9.4 | 312.4 | 13.6 | 201.1 |
| 5.2 | 162 | 10658.3 | 2.5 | 7 | 342.4 | 22.1 | 206.4 |
| 5.22 | 158.2 | 10657.7 | 4.6 | 8.1 | 348.6 | 44.3 | 199.9 |
| 5.24 | 149 | 9770.7 | 3.4 | 15.3 | 360.6 | 7 | 194.8 |
| 5.26 | 156.2 | 10499.1 | 6 | 6.4 | 360.5 | 22.4 | 198.9 |
| 5.28 | 161.4 | 10396.5 | 5 | 12.1 | 357.4 | 29.2 | 209.9 |
| 5.3 | 155.9 | 10050.6 | 8.4 | 8.2 | 355.2 | 22.3 | 194.2 |
| 5.32 | 156.4 | 9743.8 | 2.6 | 9.7 | 347.4 | 17.7 | 205.2 |
| 5.34 | 161.8 | 10101.5 | 3.2 | 13 | 361.6 | 24.1 | 205.3 |
| 5.36 | 161.3 | 10499.5 | 5.6 | 8.7 | 348.9 | 21 | 204.9 |
| 5.38 | 161.8 | 10455.6 | 8 | 14.1 | 335.2 | 18.5 | 200.8 |
| 5.4 | 163.6 | 10507 | 4 | 6.3 | 338.1 | 23.4 | 201.4 |
| 5.42 | 171.8 | 10695.8 | 3.7 | 8 | 304.1 | 13.2 | 210.3 |
| 5.44 | 148.2 | 10045 | 6.9 | 6.5 | 348.7 | 23.6 | 205.2 |
| 5.46 | 156.6 | 10416.1 | 1.9 | 7.8 | 360.4 | 23.1 | 200.6 |
| 5.48 | 154.3 | 10473.4 | 6.7 | 11.6 | 315 | 16.6 | 197.1 |
| 5.5 | 159.2 | 10168.5 | 4.9 | 7.4 | 335.4 | 20.8 | 185.8 |
| 5.52 | 159.3 | 10467.5 | 2.4 | 12.8 | 359.7 | 17 | 180.5 |
| 5.59 | 161.6 | 10259.3 | 3.5 | 17.4 | 356.9 | 22.6 | 199.2 |
| 5.61 | 181.2 | 11232.5 | 3.3 | 9.2 | 359.9 | 27.1 | 228.7 |
| 5.63 | 165.2 | 10471.7 | 4.1 | 11.4 | 356.3 | 10.9 | 200.6 |
| 5.65 | 155.1 | 9606 | 2.5 | 11 | 346.2 | 12.7 | 187 |
| 5.67 | 165.6 | 9903.3 | 6.6 | 12.4 | 358.5 | 19.9 | 196 |
| 5.69 | 164.8 | 10665.3 | 5.9 | 19.2 | 424.3 | 10.7 | 212.7 |
| 5.71 | 135.2 | 9380.6 | 0 | 11.2 | 325.7 | 11.5 | 199.8 |
| 5.73 | 169.8 | 10611.9 | 2.2 | 17.1 | 394.6 | 20.9 | 193.6 |
| 5.75 | 165.5 | 10214.1 | 3.5 | 8.2 | 349.1 | 15.3 | 196.7 |
| 5.77 | 139.9 | 10103.4 | 13.7 | 8.1 | 336.1 | 19.5 | 206.6 |
| 5.94 | 124.8 | 8893 | 9.6 | 22.6 | 314 | 8.6 | 201.8 |
| 5.96 | 124.9 | 8492 | 8.7 | 2.9 | 336 | 15 | 182.7 |
| 5.98 | 122.3 | 8029.7 | 9.9 | 8.9 | 340.9 | 17.5 | 176.8 |
| 6 | 142.6 | 9214.6 | 4.2 | 9.5 | 393.1 | 21.1 | 201.4 |
| 6.02 | 154 | 9906.1 | 4.7 | 9.1 | 401.8 | 22.5 | 201.3 |

| Depth | K | Ca | Ti | Mn | Fe | Cu | Sr |
| mbsf | cps | cps | cps | cps | cps | cps | cps |
|---|---|---|---|---|---|---|---|
| 6.04 | 160.8 | 10519 | 0 | 6.6 | 364.7 | 22.5 | 214.2 |
| 6.06 | 161.2 | 10264.3 | 9.4 | 18.4 | 439.6 | 21.8 | 191.8 |
| 6.08 | 146.7 | 9712.2 | 7.5 | 6.5 | 412.4 | 19.4 | 201.7 |
| 6.1 | 162.9 | 9986.9 | 6.9 | 6.3 | 378.1 | 19.9 | 198.9 |
| 6.12 | 150.3 | 9387 | 6.5 | 6.1 | 396.3 | 7.4 | 189.8 |
| 6.14 | 167.3 | 10116.5 | 6.9 | 7.2 | 361.1 | 19.2 | 200.5 |
| 6.16 | 134 | 9939.2 | 4.9 | 3.3 | 364.8 | 14.6 | 195.6 |
| 6.18 | 102 | 8184.2 | 4.6 | 17.9 | 330.3 | 42.9 | 172.8 |
| 6.2 | 127.8 | 8299.9 | 8.8 | 8.1 | 331.8 | 15.6 | 174.5 |
| 6.34 | 113.9 | 8340.4 | 10.4 | 17 | 363.9 | 31.7 | 178.6 |
| 6.36 | 128.2 | 8937.3 | 10.6 | 10.6 | 359.8 | 18.4 | 178.7 |
| 6.38 | 167.4 | 9349.9 | 4.4 | 8.2 | 384.2 | 10.1 | 196 |
| 6.4 | 158.6 | 9949.8 | 3.1 | 11.9 | 395.2 | 10.5 | 199.4 |
| 6.42 | 155.2 | 10028.5 | 7.2 | 6.3 | 391.9 | 14.6 | 201.1 |
| 6.44 | 162.1 | 9824.5 | 2.6 | 12.4 | 386.9 | 16.1 | 202.1 |
| 6.46 | 148.3 | 9467.2 | 7 | 13.2 | 364.3 | 23.3 | 205.3 |
| 6.48 | 145 | 9014.5 | 7.1 | 12.5 | 335.1 | 14.7 | 195.3 |
| 6.5 | 144.8 | 9821.9 | 3.9 | 14.6 | 356.7 | 10.3 | 208.2 |
| 6.52 | 157 | 9755.3 | 2.8 | 6.5 | 347.7 | 18.8 | 185.9 |
| 6.54 | 149.7 | 9752.8 | 2.5 | 9.3 | 381.5 | 16.6 | 200.5 |
| 6.56 | 151.3 | 9511.1 | 6.1 | 11.8 | 409.9 | 24.3 | 197.9 |
| 6.58 | 149.7 | 9217 | 6.4 | 18.9 | 408 | 16.8 | 199.1 |
| 6.6 | 185.1 | 9749.7 | 0 | 10.2 | 401.4 | 28.9 | 203.6 |
| 6.62 | 175.8 | 10623.6 | 6.8 | 15.7 | 389.6 | 22 | 202.1 |
| 6.64 | 162.6 | 9949.9 | 6 | 14.8 | 375.3 | 13.5 | 199.9 |
| 6.66 | 160.6 | 9981.8 | 6.8 | 7.3 | 385 | 16 | 193.6 |
| 6.68 | 167.5 | 10014.9 | 6.1 | 4.3 | 368.3 | 13.2 | 195.5 |
| 6.7 | 148 | 9675.4 | 4.8 | 6 | 364.8 | 22 | 201.6 |
| 6.72 | 148.3 | 9657.1 | 4.3 | 26.3 | 380.6 | 22.5 | 191.9 |
| 6.74 | 157 | 9725 | 5.1 | 10.2 | 350.6 | 22.4 | 207.3 |
| 6.76 | 156.5 | 10508.3 | 3.1 | 5.8 | 344.3 | 26.6 | 203.6 |
| 6.78 | 147.7 | 10216.6 | 3.3 | 37.6 | 382 | 11.5 | 204.6 |
| 6.8 | 153.6 | 9850.8 | 2.5 | 5.1 | 341.8 | 15.7 | 207.6 |
| 6.82 | 153.8 | 10036.3 | 3.7 | 8.5 | 337.5 | 22 | 205.8 |
| 6.84 | 157.6 | 10500.6 | 4.8 | 11.9 | 364.4 | 23.5 | 209.2 |
| 6.86 | 162.4 | 10898.5 | 8.3 | 7.9 | 321.5 | 27.1 | 203.6 |
| 6.88 | 152.9 | 9966.1 | 5.4 | 10.9 | 313 | 18.9 | 202.8 |
| 6.9 | 163.8 | 10908.9 | 6.9 | 14.7 | 343.7 | 27.2 | 198.1 |
| 6.92 | 157.6 | 9977.5 | 8.4 | 23 | 364.9 | 15.4 | 195 |
| 6.94 | 159.5 | 10253.6 | 5 | 10.3 | 352.5 | 11.5 | 202.8 |
| 6.96 | 165.6 | 10941.1 | 5.1 | 18.4 | 371.9 | 18.8 | 209.5 |
| 6.98 | 165 | 11040 | 8.6 | 10.3 | 349.7 | 27.6 | 214.5 |
| 7 | 171.4 | 10321.2 | 3.4 | 11.8 | 345.3 | 14.4 | 191.2 |
| 7.02 | 178.2 | 11435.4 | 4.6 | 10 | 330 | 18.3 | 213.7 |
| 7.04 | 152 | 10993.7 | 6.8 | 9.5 | 321.9 | 13.4 | 201.6 |
| 7.06 | 156.9 | 11080.3 | 5.4 | 11.6 | 317.4 | 14.4 | 211.5 |
| 7.08 | 160.8 | 10782.2 | 6.7 | 13.8 | 362.1 | 10 | 209.1 |

| Depth | K | Ca | Ti | Mn | Fe | Cu | Sr |
| mbsf | cps | cps | cps | cps | cps | cps | cps |
|---|---|---|---|---|---|---|---|
| 7.1 | 157.1 | 10767.9 | 7.8 | 18.5 | 376.2 | 14.8 | 207.2 |
| 7.12 | 151.9 | 10580.6 | 4 | 10.6 | 348 | 15.6 | 201 |
| 7.14 | 163.7 | 10658.9 | 6.4 | 13.7 | 341.9 | 15.7 | 195.3 |
| 7.16 | 152.4 | 10770.7 | 7.1 | 8.9 | 331.9 | 14.5 | 202.1 |
| 7.18 | 160.2 | 10451 | 4.9 | 22.3 | 392.5 | 14.8 | 188.4 |
| 7.2 | 152.9 | 10577.7 | 4.1 | 15.6 | 421.3 | 12.7 | 203.8 |
| 7.22 | 172.5 | 10718.9 | 1.8 | 16.3 | 416.9 | 12.2 | 198.4 |
| 7.24 | 166.7 | 10566.7 | 5.5 | 13.1 | 421.1 | 14.5 | 198.6 |
| 7.26 | 160.1 | 10360.9 | 6.8 | 54.5 | 445.5 | 17.5 | 187.3 |
| 7.28 | 148.5 | 10781.9 | 1.6 | 13.1 | 372.9 | 15.5 | 211.9 |
| 7.3 | 140.9 | 9866.6 | 5.8 | 4.5 | 276.7 | 19.5 | 195.3 |
| 7.32 | 148.1 | 10196.8 | 1.6 | 8.8 | 261.9 | 14.4 | 205.5 |
| 7.34 | 161.9 | 10469.7 | 5.6 | 15.1 | 349.1 | 14.8 | 200.7 |
| 7.36 | 161 | 10781.2 | 3.5 | 21.3 | 402.7 | 10.4 | 206.3 |
| 7.43 | 140.1 | 9696.9 | 2.6 | 8.1 | 293.6 | 29.7 | 210.3 |
| 7.44 | 149.9 | 10151 | 0 | 15.9 | 316.3 | 33.6 | 215.2 |
| 7.45 | 152.8 | 9850.8 | 2.1 | 7.5 | 336.2 | 22.1 | 213.7 |
| 7.46 | 161.6 | 9851 | 7.2 | 11 | 314.3 | 17.1 | 216.9 |
| 7.47 | 157.2 | 10448.5 | 3.1 | 5.7 | 373.9 | 18 | 205.1 |
| 7.48 | 155.2 | 10814.6 | 5.5 | 10.4 | 355.8 | 23.4 | 209.1 |
| 7.49 | 149.4 | 10043.1 | 5.4 | 7.6 | 339.2 | 16.9 | 207.8 |
| 7.5 | 154.9 | 9995.1 | 7.2 | 12 | 352.6 | 16.4 | 210.5 |
| 7.51 | 172.1 | 10356.9 | 5.4 | 19.5 | 431.6 | 17.5 | 197 |
| 7.52 | 158.7 | 10400.2 | 4.1 | 9.7 | 384.5 | 23.1 | 200.5 |
| 7.53 | 146.3 | 10347.3 | 2.4 | 11.9 | 383 | 22.7 | 203.4 |
| 7.54 | 171.6 | 10379.6 | 4.1 | 11.1 | 396.2 | 21.6 | 207.3 |
| 7.55 | 166.8 | 11376.1 | 4.1 | 16.7 | 420 | 20.2 | 220 |
| 7.56 | 170.9 | 11060.6 | 4.7 | 8.7 | 380.5 | 24.3 | 218.3 |
| 7.57 | 168.8 | 10327.3 | 5.9 | 11.6 | 440.3 | 15.6 | 203.4 |
| 7.58 | 170.1 | 10394.8 | 4.7 | 7.8 | 450.3 | 8.2 | 186.8 |
| 7.59 | 176.1 | 10332.2 | 3.3 | 9.5 | 385.5 | 16.4 | 194.8 |
| 7.6 | 153.7 | 10211.6 | 0 | 10 | 438 | 21.9 | 212.3 |
| 7.61 | 156.8 | 10279.4 | 6.6 | 12.1 | 402.8 | 23 | 201.7 |
| 7.62 | 152.3 | 10494.7 | 2.9 | 12.5 | 393.9 | 27.5 | 201.1 |
| 7.63 | 157.7 | 10646.7 | 3.2 | 10 | 366.2 | 23.9 | 209.3 |
| 7.64 | 156.7 | 10379.8 | 5.8 | 11.1 | 341.4 | 20 | 204.4 |
| 7.65 | 149.6 | 10265.4 | 2.9 | 17.1 | 408.1 | 22.1 | 200.9 |
| 7.66 | 143.2 | 10145.6 | 0 | 24.8 | 329.9 | 46.5 | 217.8 |
| 7.67 | 152.2 | 9935.4 | 2.4 | 8.8 | 330.3 | 18 | 207.3 |
| 7.68 | 154.9 | 10528.6 | 1.5 | 7.7 | 345.6 | 23.5 | 212 |
| 7.69 | 153.4 | 10330.2 | 5 | 7.5 | 327.6 | 18.1 | 214.4 |
| 7.7 | 139.1 | 10200 | 3.1 | 11.4 | 324.7 | 21.5 | 215.9 |
| 7.71 | 135.4 | 10276.8 | 4.5 | 7.6 | 306.4 | 16.8 | 211.7 |
| 7.72 | 149 | 9999.7 | 2 | 11.5 | 349.4 | 22.1 | 199.3 |
| 7.73 | 136 | 10090.5 | 1.8 | 13.6 | 329.4 | 19.7 | 202.5 |
| 7.74 | 149.1 | 10436.6 | 2.9 | 9.8 | 357.4 | 30 | 206.4 |
| 7.75 | 152.5 | 10134.3 | 6.2 | 6.3 | 340.6 | 23.9 | 221.1 |

| Depth | K | Ca | Ti | Mn | Fe | Cu | Sr |
| mbsf | cps | cps | cps | cps | cps | cps | cps |
|---|---|---|---|---|---|---|---|
| 7.76 | 145.4 | 10240.9 | 4.5 | 10.2 | 336.8 | 18.7 | 206.4 |
| 7.77 | 141.1 | 10569.5 | 6.3 | 7.9 | 316.8 | 20.4 | 228.1 |
| 7.78 | 149.1 | 10791.5 | 0 | 14.4 | 371.7 | 26.1 | 221.6 |
| 7.79 | 140.5 | 10363.8 | 6.1 | 5.8 | 305.2 | 22.2 | 209.4 |
| 7.8 | 152.1 | 10365.7 | 4.6 | 9.4 | 358 | 35.4 | 204.5 |
| 7.81 | 153.3 | 10390.9 | 5.9 | 6.5 | 375.1 | 16.2 | 201.2 |
| 7.82 | 142.9 | 10617.6 | 4.9 | 8.6 | 401.8 | 33.4 | 212.3 |
| 7.83 | 143.5 | 10407 | 4.5 | 10.9 | 351.2 | 19.6 | 222.6 |
| 7.84 | 149.3 | 10780 | 7.1 | 17.8 | 354.4 | 26.4 | 215.6 |
| 7.85 | 144.2 | 10178.7 | 0 | 9.5 | 326.9 | 20.2 | 210.7 |
| 7.86 | 152.5 | 9857.5 | 6 | 7.5 | 412.3 | 20.5 | 200 |
| 7.87 | 153.6 | 10928.6 | 5.9 | 8 | 329.7 | 17.8 | 221.8 |
| 7.88 | 141.8 | 10966.6 | 2.7 | 3.7 | 277.9 | 46.3 | 214.1 |
| 7.89 | 138.6 | 10940.6 | 4.4 | 8.9 | 277.8 | 15 | 211.1 |
| 7.9 | 145.9 | 10629.3 | 9 | 18.4 | 330.2 | 20 | 217 |
| 7.91 | 141.8 | 10982.6 | 5.7 | 12.1 | 273.2 | 20.6 | 223.5 |
| 7.92 | 131.4 | 10674.2 | 5.9 | 10.7 | 295.2 | 20 | 209.3 |
| 7.93 | 131.6 | 10156.1 | 6.3 | 14.2 | 312 | 14.2 | 204.2 |
| 7.94 | 143 | 9648.8 | 9.7 | 11.2 | 381.6 | 11.8 | 206.3 |
| 7.95 | 149.5 | 9869.3 | 5.9 | 8.9 | 384.1 | 13.8 | 201.5 |
| 7.96 | 149.6 | 10249.3 | 4.3 | 9.5 | 336.9 | 12.9 | 212.7 |
| 7.97 | 157.1 | 10700 | 3 | 7 | 281.9 | 41.5 | 214.7 |
| 7.98 | 148.4 | 10682.9 | 3.8 | 9.1 | 233.2 | 44.5 | 221.7 |
| 7.99 | 137.2 | 10876.4 | 4.5 | 6.4 | 220.7 | 27.1 | 228.5 |
| 8 | 132.1 | 10358.7 | 4.2 | 4.5 | 207.7 | 19.3 | 217.1 |
| 8.01 | 138.6 | 9963.1 | 2.8 | 5.3 | 215.6 | 22.4 | 222 |
| 8.02 | 144 | 10329.7 | 4.7 | 7.7 | 228 | 14.2 | 230.6 |
| 8.03 | 143 | 10405.4 | 5.1 | 12.4 | 281 | 21.4 | 220.7 |
| 8.04 | 140.1 | 10273.8 | 6.5 | 4 | 230.9 | 11 | 207.5 |
| 8.05 | 151.7 | 10706.3 | 3.3 | 9.7 | 237.6 | 21.4 | 224.5 |
| 8.06 | 138.5 | 9974.8 | 1.3 | 14.8 | 259.4 | 14.3 | 203.2 |
| 8.07 | 140.3 | 10852.8 | 2 | 9.6 | 239.5 | 20.5 | 223 |
| 8.08 | 143.1 | 10580.8 | 3.7 | 19.8 | 301.5 | 17.8 | 229.9 |
| 8.09 | 151.4 | 10573.1 | 1.7 | 9.3 | 282.6 | 45.3 | 218.1 |
| 8.1 | 143 | 10737.3 | 6.6 | 16.4 | 315.1 | 15.3 | 222.2 |
| 8.11 | 136.9 | 10402.8 | 4.1 | 17.1 | 306.6 | 19.8 | 220.6 |
| 8.12 | 132.8 | 10242.1 | 2.8 | 17.8 | 245.8 | 18.5 | 222.3 |
| 8.13 | 143.9 | 10302.6 | 2.6 | 10.1 | 254.8 | 15.5 | 225.7 |
| 8.14 | 133 | 10303.8 | 5.3 | 10.5 | 238 | 20.5 | 217.7 |
| 8.15 | 119.6 | 10277.5 | 3.6 | 11.5 | 163.1 | 18.5 | 240.9 |
| 8.16 | 130.1 | 10542.3 | 2 | 11.6 | 230.9 | 22.6 | 240.6 |
| 8.17 | 136.9 | 10720.4 | 2.5 | 7.3 | 165.8 | 14.8 | 243.2 |
| 8.18 | 124.7 | 10435.1 | 5.1 | 8.7 | 164.1 | 20 | 241.6 |
| 8.19 | 133.6 | 10503.3 | 1.8 | 7.7 | 197.8 | 10.3 | 223.9 |
| 8.2 | 154.3 | 10658.1 | 2.5 | 7.9 | 234.8 | 17.9 | 222.4 |
| 8.21 | 132 | 10713.1 | 3.2 | 8.4 | 232.1 | 22.9 | 212.7 |
| 8.22 | 135.7 | 10544 | 5.4 | 7.5 | 262.6 | 29.7 | 220.1 |

| Depth | K | Ca | Ti | Mn | Fe | Cu | Sr |
|-------|-------|---------|------|------|-------|------|-------|
| mbsf | cps | cps | cps | cps | cps | cps | cps |
| 8.23 | 154.2 | 11028.1 | 4.8 | 9.9 | 251.3 | 24.8 | 227.5 |
| 8.24 | 137.6 | 10734.5 | 0 | 8 | 258.3 | 18.5 | 227.6 |
| 8.25 | 148.2 | 10863.3 | 5.4 | 8.6 | 236 | 20.2 | 224.1 |
| 8.26 | 143.8 | 10803.3 | 3.3 | 8.5 | 250.4 | 31 | 220.9 |
| 8.27 | 142.3 | 10544.3 | 2.1 | 15.7 | 266.5 | 17.8 | 221.8 |
| 8.28 | 144.9 | 10575.1 | 1.5 | 14.3 | 259 | 17 | 229.9 |
| 8.29 | 130.5 | 9966.5 | 4.6 | 7.3 | 206.2 | 37.1 | 222.5 |
| 8.3 | 132.9 | 10272.2 | 0 | 8 | 228.3 | 23.7 | 216.6 |
| 8.31 | 145.9 | 10738.1 | 4.4 | 9.2 | 256.1 | 37.2 | 221.6 |
| 8.32 | 152.1 | 11044.4 | 3.4 | 6.1 | 211.4 | 29 | 226.6 |
| 8.33 | 151.2 | 10946.6 | 3.8 | 11.3 | 255.7 | 23.5 | 221.4 |
| 8.34 | 154.5 | 11099.6 | 4.5 | 7.3 | 260.9 | 27.2 | 218.1 |
| 8.35 | 145.1 | 11212.2 | 2.9 | 4 | 223.5 | 33 | 231.1 |
| 8.36 | 144.3 | 11376.1 | 1.8 | 20 | 296 | 15.3 | 234.4 |
| 8.37 | 147.1 | 11164.2 | 0 | 16.2 | 222.2 | 11.2 | 232.2 |
| 8.38 | 132.4 | 10632.1 | 6.7 | 9.7 | 185.6 | 14.8 | 232.1 |
| 8.39 | 131.4 | 10019.7 | 5.9 | 7.7 | 157 | 14.3 | 230.9 |
| 8.4 | 146.3 | 10773.3 | 3.9 | 10.8 | 197.1 | 12.5 | 228 |
| 8.41 | 140.1 | 10808.5 | 0 | 6 | 186.4 | 21.6 | 247.6 |
| 8.42 | 135.5 | 10402.2 | 4.9 | 15.6 | 248.8 | 19.5 | 233.9 |
| 8.43 | 132.2 | 10433.9 | 1.4 | 9.8 | 179.3 | 19.9 | 233.8 |
| 8.44 | 147.5 | 10987.5 | 0 | 8.9 | 156.8 | 26.5 | 240.4 |
| 8.45 | 153 | 11253.1 | 4.4 | 5.9 | 164 | 20.3 | 246 |
| 8.46 | 138.2 | 10752.4 | 0 | 9.3 | 134.9 | 20 | 246.8 |
| 8.47 | 133.2 | 10886.6 | 2.9 | 6.1 | 139.1 | 18.3 | 235.4 |
| 8.48 | 134.5 | 11015.7 | 4.1 | 5.2 | 149.8 | 12.8 | 250.3 |
| 8.49 | 129.2 | 10549.9 | 4.1 | 12.8 | 130.3 | 17.6 | 246.6 |
| 8.5 | 132.8 | 10375.8 | 1.8 | 5.4 | 115.3 | 15.5 | 256.5 |
| 8.51 | 125.3 | 10588.4 | 3 | 7.2 | 132.3 | 17.8 | 255.8 |
| 8.52 | 113.3 | 10143.4 | 4 | 6.7 | 124.1 | 9.7 | 253.7 |
| 8.53 | 120.8 | 10435.3 | 0 | 14.3 | 161.9 | 25.8 | 243.8 |
| 8.54 | 104.3 | 10753.5 | 3.2 | 2 | 127.6 | 16.4 | 247.9 |
| 8.55 | 139.2 | 10926 | 1.7 | 13.3 | 121.3 | 20.3 | 255.7 |
| 8.56 | 133.2 | 10518 | 5.9 | 5.5 | 117.7 | 17.1 | 250.3 |
| 8.57 | 124.7 | 10241.9 | 4.4 | 5.5 | 118 | 18 | 244.7 |
| 8.58 | 115.9 | 10184.3 | 2.9 | 8.1 | 105.7 | 17 | 256.7 |
| 8.59 | 131.5 | 10796.5 | 2.5 | 7.1 | 114 | 19.9 | 257.5 |
| 8.6 | 136.7 | 10860.7 | 4 | 6.6 | 97.9 | 12.9 | 257.4 |
| 8.61 | 129.7 | 10407.2 | 6.4 | 9.9 | 105.4 | 15.6 | 246.2 |
| 8.62 | 128.7 | 10537.9 | 0 | 7.6 | 116.8 | 28.1 | 258 |
| 8.63 | 129.4 | 10791.7 | 2.3 | 19.7 | 144.8 | 9.3 | 257.6 |
| 8.64 | 131.5 | 10537.8 | 5.2 | 4.5 | 97.8 | 13.3 | 250.6 |
| 8.65 | 114.9 | 10479.8 | 5.6 | 4.9 | 96 | 15.9 | 254.2 |
| 8.66 | 140.2 | 10643.7 | 0 | 8.9 | 122.7 | 18.1 | 251.8 |
| 8.67 | 130.6 | 10074.9 | 1.9 | 9.6 | 103 | 18 | 225.3 |
| 8.68 | 144.5 | 10890.6 | 2.5 | 2.8 | 116 | 22.8 | 247.5 |
| 8.69 | 140.2 | 11217.6 | 2.1 | 8.7 | 143.7 | 24.8 | 252.7 |

| Depth | K | Ca | Ti | Mn | Fe | Cu | Sr |
|---|---|---|---|---|---|---|---|
| mbsf | cps | cps | cps | cps | cps | cps | cps |
| 8.7 | 147.7 | 10915.5 | 0 | 8.2 | 137.2 | 21.7 | 254.9 |
| 8.71 | 134.3 | 10963.2 | 4 | 8.1 | 127.5 | 31.5 | 258.3 |
| 8.72 | 139.7 | 10802.8 | 2.7 | 6.3 | 124.4 | 18.4 | 253.1 |
| 8.73 | 150 | 10678.2 | 2.2 | 9.7 | 132.6 | 19.8 | 245.1 |
| 8.74 | 145 | 11355.7 | 0 | 18.1 | 194.2 | 16.3 | 255.2 |
| 8.75 | 158.6 | 11512.8 | 3.1 | 6.5 | 129.9 | 39 | 248.9 |
| 8.76 | 141.5 | 11132.5 | 2.5 | 20.2 | 173.2 | 34.4 | 250.7 |
| 8.77 | 151.6 | 11393.4 | 3.4 | 7.7 | 140.6 | 18.9 | 268 |
| 8.78 | 149.2 | 11974.5 | 0 | 17.3 | 210.4 | 25 | 262 |
| 8.79 | 147 | 11652.1 | 0 | 7.9 | 136.4 | 45.5 | 255.5 |
| 8.8 | 154.1 | 11041.2 | 0 | 7 | 135.4 | 23.5 | 251.6 |
| 8.81 | 136.2 | 10694.6 | 0 | 8.8 | 114 | 12.9 | 261.2 |
| 8.82 | 110.3 | 10342 | 2.2 | 11.4 | 125.3 | 11.2 | 259.7 |
| 8.83 | 114.2 | 9867.7 | 3.4 | 7.6 | 117.7 | 12.9 | 251.9 |
| 8.92 | 138.7 | 10629.2 | 0 | 19.8 | | 13.1 | 242.6 |
| 8.94 | 152.8 | 11749.5 | 3.9 | 12.7 | | 15.2 | 255 |
| 8.96 | 156.4 | 11592.2 | 2.9 | 7.6 | 139.4 | 26.2 | 250.6 |
| 8.98 | 151.8 | 11518.6 | 3 | 10.7 | 148.4 | 22 | 254.7 |
| 9 | 130.2 | 11085.3 | 0 | 4.1 | 132.1 | 25 | 247.8 |
| 9.02 | 127.7 | 10595.7 | 3 | 21.2 | 185.7 | 19.1 | 245.3 |
| 9.04 | 134.4 | 10889.2 | 1.6 | 9.5 | 168.8 | 24.5 | 257 |
| 9.06 | 159.9 | 12330.5 | 4.1 | 4.9 | 164.6 | 47.8 | 264.1 |
| 9.08 | 145.5 | 11158 | 4.2 | 13.8 | 168.3 | 42.4 | 241.9 |
| 9.1 | 148.7 | 11833.4 | 5.2 | 4.1 | 179.3 | 33.6 | 263.3 |
| 9.12 | 144.9 | 11209.2 | 3 | 4.7 | 159.4 | 23.8 | 249.5 |
| 9.14 | 133.2 | 11672.4 | 4.3 | 17.4 | 233.3 | 22.1 | 262.9 |
| 9.16 | 155.2 | 12537.6 | 5.5 | 3.7 | 154 | 57.8 | 258.1 |
| 9.18 | 147.2 | 12117 | 2.5 | 5.7 | 165 | 52.3 | 266.9 |
| 9.2 | 155.2 | 12353.2 | 2.6 | 4.8 | 145.5 | 41.1 | 268.1 |
| 9.22 | 165.6 | 12488.5 | 2.6 | 5.1 | 147.9 | 36.2 | 262.1 |
| 9.24 | 169.6 | 12401.6 | 1.7 | 5.3 | 163.1 | 74.1 | 267.2 |
| 9.26 | 149.4 | 11626.3 | 0 | 8.5 | 153.1 | 35.9 | 252 |
| 9.28 | 151.4 | 12489.7 | 0 | 8.5 | 141.1 | 26.2 | 271.5 |
| 9.3 | 156.3 | 12214.3 | 4.1 | 10.1 | 141.7 | 22.9 | 267.6 |
| 9.32 | 170.5 | 13167 | 2 | 5.5 | 133.1 | 26.7 | 267 |
| 9.34 | 161.4 | 11988.2 | 0 | 13 | 169.3 | 19.5 | 264.4 |
| 9.36 | 159.6 | 12567.2 | 2.8 | 8.6 | 143 | 39.2 | 269.9 |
| 9.38 | 155.3 | 12649.8 | 3.4 | 9.5 | 132.2 | 36.2 | 268.8 |
| 9.4 | 147.6 | 12178.2 | 3 | 6.5 | 123.3 | 40.6 | 277.7 |
| 9.42 | 165.4 | 12829.9 | 2.3 | 4.2 | 139 | 28.1 | 272 |
| 9.44 | 145.5 | 12360.7 | 2.5 | 8.9 | 123.3 | 54.6 | 263.7 |
| 9.46 | 154.5 | 12678.9 | 5.5 | 8.3 | 112.9 | 43.5 | 268.8 |
| 9.48 | 165.8 | 12640.1 | 6.5 | 9 | 131.7 | 33.8 | 261.2 |
| 9.5 | 162.3 | 13282.3 | 3.1 | 4.6 | 112.5 | 29.9 | 288.4 |
| 9.52 | 142 | 10520.8 | 2.2 | 9.8 | 112.7 | 24.4 | 225 |
| 9.54 | 159.9 | 12486 | 0 | 12.7 | 99 | 35.5 | 260.8 |
| df9.56 | 148.2 | 12945.4 | 4.1 | 8.1 | 108 | 20.7 | 269.4 |

| Depth | K | Ca | Ti | Mn | Fe | Cu | Sr |
|---|---|---|---|---|---|---|---|
| mbsf | cps | cps | cps | cps | cps | cps | cps |
| 9.58 | 140.5 | 11660.9 | 3.9 | 9.5 | 89.6 | 24.3 | 237.3 |
| 9.6 | 143.1 | 12008.1 | 3.4 | 9.1 | 89.5 | 26.7 | 251.7 |
| 9.62 | 128.2 | 11421.7 | 0 | 5.7 | 77.2 | 17.9 | 252.8 |
| 9.64 | 123.5 | 10605.2 | 2.1 | 7 | 61.4 | 20.8 | 225 |
| 9.66 | 141.6 | 11994.5 | 2.6 | 8.4 | 66.6 | 25.6 | 261.5 |
| 9.68 | 130.7 | 10490.7 | 2.2 | 8.1 | 59.9 | 18.1 | 234.3 |
| 9.7 | 134.9 | 11003.1 | 2.1 | 12.2 | 62.4 | 20.6 | 238.5 |
| 9.72 | 113.9 | 9329.3 | 0 | 10 | 73 | 11.1 | 229 |
| 9.74 | 137.8 | 10254.6 | 3.1 | 11.6 | 68.8 | 22 | 223.3 |
| 9.76 | 106.5 | 9261.4 | 1.8 | 5.1 | 59.4 | 12.7 | 222.8 |
| 9.8 | 102 | 9279.5 | 1.5 | 7.2 | 75.3 | 5.3 | 224.9 |
| 9.82 | 94.1 | 8087.6 | 4.2 | 4.2 | 54.1 | 6.9 | 201.7 |
| 9.84 | 92 | 8550.4 | 0 | 10.4 | 73.2 | 12.6 | 209.7 |

Irka Hajdas and George Bonani from the 14C-AMS facility at Hönggerberg are thanked for the efficient dating of our samples and Monica Sanchez Ramón for helping with the picking.

Ulla Röhl from Bremen University gave me the opportunity to measure the Site 1127 core on the 'magic' XRF scanner. Thank you Gerald Haug for initiatiation and organization of core transport.

Life as a graduate student within the Earth System Science group and at the Geological Institute was great fun. There was always someone to chat and socialize, to have a coffee and a break. I most enjoyed lunches, which usually started with the question: "Gömme go fooode?" and continued with near-exhausting discussions about lunch-time and choice of Mensa, often ended with a "Kappuch" at the BQM. Life in-between coffee- and lunch-breaks was not too hard, because the H34.1 office with Lemmie (Moritz Lehmann), Adi (Adi Gilli) and Burlas (Stefan Burla) was an entertaining place to be and well equipped in terms of coffee-machine, water kettle, soda star, not to forget the family-pack "Schoggi-Stengeli", cookies, Chewing-gum etc. Thanks guys for a helofalottafun.

Once out of the office, you sure ran into one of the H-floor gang in front of the elevator, in front of the printer (@##?!!!sh…!!!) or copy machine. Thank you to Jogi Graf, Daniela Schmidt, Michi Schnellman, Beno Brunner, Uli Heimhofer, Florian Kober, Patrick Meister, Yvonne van Lith, Katrin Monecke, Jorijntje Henderiks, Maria Theresa Galli, and Flavio Anselmetti for many fun hours in and out of the Institute.

For quite some time, the H42 became my second home, sitting at the microscope, listening to DRS3 and Radio Tropic while the seasons went by. Thank you Hans Thierstein for the use of this lab with a view, and for inviting me to the Leopoldina in Jena.

Thank you Daniela Schmidt for opening my eyes for the world of foraminifera. Thank you for all help and patience with the proper identification of foraminifera, with taking pictures under the light microscope, and for sharing many lunches, coffee and cigarette breaks.

Thank you Gerald Haug and Ralf Schiebel for your interest and patience with yet another paleoceanographic and micropaleontologic questions, for lending books, articles.

Thank you Rolf Warthmann for the search and hunt of Site 1127 bacteria.

Apart from my office and the H42 lab, most of my time was spent in the stable isotope lab on F-floor. Thank you Hilary Paul, Maureen Padden, and Bill Anderson for helping solve a lot of Prism problems. Thank you Cris for popping in from the Geomicro-lab for a brasilian hug and a chat.

A big thank you goes to the Prism, who does have a mind and will of its own, and who likes to be patted on the shoulder before starting a run.

Furthermore, I would like to thank Katrine Frese, from IMP for inter-institutional chats, lunches and Kondi. Thank you Tina van de Fliert, and Martin Frank from IGMR for also working in the Southern Ocean and thus borrowing the same books in the library and many discussions at Friday beer.

Dear Andi Baumeler, thank you for many philosophical soups in the Tannenbar, picnics in the garden of the university hospital and "die Löwenfreundschaft".

A sporty thank you goes to the ASVZ for keeping my brain body and soul in shape. Special thanks also to my friends of the Badminton instructor team – hard to beat a good game.

Dear Lisbeth and Fritz, thank you for oh so many good Birchermüeslis and Gschwellti and the never-ending supply of home-made jam.

Dear Mami, Papi, Sandra, Martial, and Arés – thank you for being my family and friends.

Lastly, because most importantly, I wish to thank Urs for being at my side through the rough and the tough –the happy and the fun hours of my everyday life as a PhD student.

Welcome to Miami!

Miriam S. Andres
Zurich, September 2002

# CURRICULUM VITAE

## MIRIAM SIMONE ANDRES

Date of Birth:      4th of August, 1972

Place of Birth:     Pretoria, Republic of South-Africa

Nationality:        Swiss

Education

1979-1986      German School Pretoria, Republic of South-Africa

1987-1988      Sekundarschule Turbenthal, Switzerland

1988-1992      Kantonsschule im Lee, Winterthur, Switzerland

1992-1997      Undergraduate Studies in Geology/Paleontology,
               University of Zurich, Switzerland

               Diploma Thesis:   Evolution of the Great Barrier Reef:
                                 A Chemostratigraphic Approach, at the Geological
                                 Institute, ETH-Zurich, Switzerland

1997-1998      Visiting Graduate Student at the Scripps Institution of Oceanography,
               San Diego, USA

1998-2002      Graduate Student at the Geological Institute, ETH-Zurich, Switzerland

               Dissertation:     Late Quaternary Paleoceaonography of the Great
                                 Australian Bight: a Geochemical and Sedimentological
                                 Study of Cool-Water Carbonates, Site 1127, ODP Leg 182

               Supervisors:      Prof. Dr. Judith A. McKenzie
                                 PD Dr. Stefano M. Bernasconi